SEISMIC FRAGILITY ASSESSMENT OF STEEL FRAMES IN THE CENTRAL AND EASTERN UNITED STATES

A Dissertation
Presented to
the Academic Faculty

By

KURSAT KINALI

In Partial Fulfillment
of the Requirements for the Degree
Doctor of Philosophy in the
School of Civil and Environmental Engineering

Georgia Institute of Technology
May, 2007

SEISMIC FRAGILITY ASSESSMENT OF STEEL FRAMES IN THE CENTRAL AND EASTERN UNITED STATES

Approved by:

Dr. Bruce R. Ellingwood, Advisor
School of Civil and Environmental Engineering
Georgia Institute of Technology

Dr. Abdul-Hamid Zureick
School of Civil and Environmental Engineering
Georgia Institute of Technology

Dr. Roberto T. Leon
School of Civil and Environmental Engineering
Georgia Institute of Technology

Dr. Kenneth M. Will
School of Civil and Environmental Engineering
Georgia Institute of Technology

Dr. Reginald DesRoches
School of Civil and Environmental Engineering
Georgia Institute of Technology

Dr. James I. Craig
Daniel Guggenheim School of Aerospace Engineering
Georgia Institute of Technology

Date Approved: March 6, 2007

To my present and future family...

ACKNOWLEDGMENTS

I dedicate my deepest gratitude to Dr. Bruce R. Ellingwood. It has been a great pleasure and honor to work with him. I admire his professionalism, dedication for excellence, expertise and wealth of knowledge. Thank you Dr. Ellingwood for everything. This dissertation would not be possible without your support and guidance.

I would like to express many thanks to Dr. Roberto T. Leon for his invaluable suggestions and guidance. Special thanks go to Dr. Abdul-Hamid Zureick for all his support for the last 5 years. I also feel indebted to Mr. Berk Taftali for all his help especially with OpenSees. Numerous discussions with him led to a fine piece of work.

The last but not the least, I am very grateful for the unconditional support of my family in Turkey, which made this work possible. I thank you all; mom, dad and my sister Sümbüle. You have always been by my side from thousands of miles away. You are great. Nothing would be meaningful without you.

This dissertation was conducted under the sponsorship of the Mid-America Earthquake Center, with additional support from the Georgia Institute of Technology. I gratefully acknowledge this support. The MAE Center is a National Science Foundation Engineering Research Center funded at the University of Illinois at Urbana-Champaign by Award No: EEC-9701785.

TABLE OF CONTENTS

LIST OF TABLES

LIST OF FIGURES

LIST OF ABBREVIATIONS

AISC	American Institute of Steel Construction
ASCE	American Society of Civil Engineers
ASTM	American Society for Testing and Materials
ATC	Applied Technology Council
BRB	Buckling-Restrained Brace
BRBF	Buckling-Restrained Braced-Frame
BSSC	Building Seismic Safety Council
CA	Clip Angle
CBF	Concentric Braced-Frame
CDF	Cumulative Distribution Function
CEUS	Central and Eastern United States
COV	Coefficient of Variation
CP	Collapse Prevention
CSM	Capacity Spectrum Method
EBF	Eccentric Braced-Frame
EOR	Engineer of Record
FEMA	Federal Emergency Management Agency
FR	Fully-Restrained
GM	Ground Motion
HAZUS	Hazards U.S.
IDA	Incremental Dynamic Analysis

IM	Intensity Measure
IO	Immediate Occupancy
ISDA	Interstory Drift Angle
KN	Krawinkler and Nassar (1992)
M_w	Moment Magnitude
MAE	Mid-America Earthquake
MCE	Maximum Considered Earthquake
MDOF	Multi Degree of Freedom
MTB	Memphis Test Bed
NBC	National Building Code
NEHRP	National Earthquake Hazard Reduction Program
NH	Newmark and Hall (1982)
NMSZ	New Madrid Seismic Zone
NSPA	Nonlinear Static Pushover Analysis
NTHA	Nonlinear Time History Analysis
OCBF	Ordinary Concentrically Braced Frame
PDF	Probability Density Function
PGA	Peak Ground Acceleration
PR	Partially-Restrained
R	Epicentral Distance
RDA	Roof Drift Angle
RM	Response Measure
S_a	Spectral Acceleration at Fundamental Period

SAC	Partnership of the Structural Engineers Association of California (**S**EAOC), the Applied Technology Council (**A**TC), and the California Universities for Research in Earthquake Engineering (**C**UREE)
SBC	Standard Building Code
SCBF	Special Concentrically Braced-Frame
SD	Structural Damage
SDOF	Single Degree of Freedom
SEAOC	Structural Engineers Association of California
SMRF	Steel Moment Resisting Frame
TS	T-Stub
UBC	Uniform Building Code
UHGM	Uniform Hazard Ground Motion
UHRS	Uniform Hazard Response Spectrum
USGS	United States Geological Survey
VFF	Vidic et al. (1994)
WUS	Western United States

SUMMARY

The main objective of this dissertation was to assess the seismic vulnerability of steel building frames typical of construction practices in the Central and Eastern United States (CEUS). Shelby Co., TN, which includes the city of Memphis and is a major urban population center near the New Madrid Seismic Zone (NMSZ), was selected to represent a region in the CEUS that is at substantial seismic risk. The Mid-America Earthquake (MAE) Center is currently engaged in a research program (the Memphis Testbed Project) to develop seismic risk reduction strategies for civil infrastructure in such regions. The research products of this dissertation contribute directly to that MAE Center program.

To represent the building stock in Shelby County, five code-compliant steel frames were identified. These frames had different lateral load resisting systems - rigid moment frame, partially-restrained (PR) moment frame and braced frame. They represented typical design and construction practices between 1950s and 1990s. The design of four of the frames was governed by wind loads, which is typical of the practice in the CEUS. Two concentrically-braced frames - a chevron braced frame and X-braced frame - represented typical braced-frames in the CEUS. Structure-specific performance limits were calculated and were used to define states of building performance.

Due to a lack of recorded accelerograms in the region of the NMSZ, seismicity was represented by two types of synthetic ground motions, e.g., uniform hazard and postulated scenario events. Using state-of-the-art performance assessment methods, building fragilities and performance state probabilities of all frames were evaluated for both a 2%/50 yr uniform hazard event and a rare scenario event with M_w=7.5, R=20 km.

Some of the frames behaved poorly under seismic events of this magnitude. The effect on building performance of seismic upgrades using feasible rehabilitation schemes also was considered. For one of the PR frames, the addition of brace members in one interior bay throughout the height of the frame was found to be sufficient. In the braced-frames, braces were converted to buckling-restrained braces. After rehabilitation, seismic performances of these frames were improved considerably.

The Capacity Spectrum Method (CSM) was investigated in detail with regard to its applicability to assessing performance of frames using response spectra from CEUS ground motions. It was found that the CSM can produce a unique performance point for some of the ground motion records but not for others. Smoothing of the actual response spectra using 6^{th} order polynomial functions was proposed and shown to greatly increase the convergence characteristics of the CSM solutions. When this approximation was applied to three of the frames, the estimated roof displacements were in good agreement with the results of nonlinear time history analyses for two of the three frames considered.

The steel building frames considered in this study performed better than might be expected for frames designed without strict seismic criteria, with the exception of the 5-story chevron frame which performed poorly prior to rehabilitation with buckling-restrained braces; following rehabilitation, it performed quite well. This can be attributed to the fact that the PR frames considered in this dissertation possessed good energy dissipation characteristics and thus performed quite well in comparison with rigid frames. The frame with X-bracing revealed good load-redistribution characteristics and more ductile behavior than the chevron-braced frame.

CHAPTER I

INTRODUCTION

1.1 Motivation

The Western United States (WUS) is known for its frequent seismicity, including such earthquakes as the 1906 San Francisco (M_w=7.7), 1933 Long Beach (M_w=6.4), 1952 Kern County (M_w=6.7), 1971 San Fernando (M_w=6.7), 1989 Loma Prieta (M_w=7.2) and 1994 Northridge (M_w=6.7). However, the largest earthquakes in recorded history in the contiguous United States occurred in the New Madrid Seismic Zone (NMSZ) in southeast Missouri. These occurred on December 16, 1811; January 23, 1812 and February 7, 1812 with estimated magnitudes of M_w=8.1, M_w=7.8 and M_w=8.0, respectively. The return period for such earthquakes in the NMSZ is estimated to be on the order of 500 – 1,000 years (e.g., Johnson, 1982). Sand blow deposits found in the region reveal that the region has been shaken previously by great earthquakes approximately every 500 years. Thus, the Central and Eastern United States (CEUS) (defined as the area east of the Rocky Mountains) is susceptible to infrequent earthquakes with high intensities and consequences.

In 1811-12, the population of the contiguous US was 7 million and the geographic center of population was 1,000 miles east of the NMSZ. Today, that population has grown to more than 280 million, with 219 million living in the CEUS. Furthermore, there are 75 million housing units, 3.5 million commercial buildings and 350,000 manufacturing establishments in the region. Over 25% of the energy consumed in the US is transported through the CEUS. The largest concentration of population near the NMSZ

is centered in and around Shelby County, Tennessee, with a population of nearly 900,000, which includes the city of Memphis (population approximately 650,000). The probable losses in the CEUS from a repeat of 1811-1812 earthquakes have been projected as being several thousand deaths and $200 billion in property damage (Beavers, 2002).

The differences in apparent seismicity between the WUS and CEUS are reflected in design, construction and building practices in these regions. Lateral force requirements for design in the CEUS are generally governed by wind, except in low-rise buildings or in certain critical facilities - identified as Building Category IV in *ASCE Standard 7-05* – (ASCE, 2005). The three steel moment frames designed and analyzed as part of the recent SAC Project[1] for Boston are typical of such designs (Gupta and Krawinkler, 2000; Yun, et al., 2002; Lee and Foutch, 2002). Only the design of the 3-story frame was governed by seismic requirements; designs of both 9-and 20-story frames were governed by wind loads. The perception of low seismicity in the CEUS was reflected in the building codes in use at the time (UBC, 1994). In contrast, the designs of all 3 SAC buildings (3-, 9- and 20-story) in Los Angeles were controlled by seismic effects. Engineers and decision-makers in the CEUS are more familiar with the damage potential of extreme winds and design of a building for wind does provide a lateral force-resisting system with some earthquake resistance as well. However, the structural actions from wind and earthquake are different and the philosophies underlying design for these two natural hazards (preventing damage versus allowing non life-threatening damage while preserving life safety) are not the same. Moreover, relative impacts of these hazards on public risk have yet to be quantified.

[1] The SAC Project was aimed at addressing both immediate and long-term needs related to solving performance problems with welded, steel moment-frame connections discovered following the 1994 Northridge, CA earthquake.

Earthquakes are highly uncertain in their occurrence and intensity, and in their impact on buildings and other structures, creating risk that must be addressed through codes, construction practices and possible rehabilitation of existing facilities. In recent years, probabilistic methods have been developed and applied to the quantification and analysis of earthquake risk. Buildings, in particular, are an essential part of the assessment of risk to human lives during an earthquake. A probabilistic assessment of seismic risk to building structures requires evaluation of their dynamic response to a spectrum of possible earthquakes. The results of such an evaluation can be displayed by the seismic fragility of the building, which measures the probability of failure to meet a pre-set performance limit expressed in terms of a building response parameter (e.g., maximum interstory drift angle, maximum story acceleration, etc.).

A seismic fragility assessment of a building structure involves stochastic ground motion models; complex structural analysis methods; practical or simplified two-dimensional (2-D) representations of the building; and definitions of limit or damage states that are consistent with the capabilities of the structural analysis. Because of modeling approximations and limited available supporting data (e.g., lack of recorded ground motion records, limited or no damage databases due to infrequent nature of substantial seismic events in the CEUS in recent history, etc.), the level of uncertainty in this assessment is very large. Some of these uncertainties stem from factors that are inherently random (or aleatoric); others are knowledge-based (or epistemic). All sources of uncertainty should be considered in risk assessment (Kinali and Ellingwood, 2007a).

Since most of the building inventory in regions of low-to-moderate seismicity, such as the CEUS, has not been designed to provide seismic resistance, seismic risk management policies that might be developed for that region would require individual buildings be assessed. Due to the infrequent occurrence of earthquakes, few designers or decision makers in the CEUS have experience dealing with their effects in building construction and may be reluctant to invest in seismic design of new buildings or in the retrofit of existing buildings. This reluctance makes comprehensive seismic assessments of individual buildings in support of policy decisions impractical.

The Mid-America Earthquake (MAE) Center at the University of Illinois at Urbana-Champaign is currently engaged in a broad-spectrum research program, i.e., Memphis Testbed (MTB) Project, to develop seismic risk reduction strategies for civil infrastructure in the CEUS. As part of this program, future seismic performance or, seismic vulnerability of current building stock in Shelby Co., TN is being investigated. This dissertation presents the results of the research study performed under this umbrella and aimed at providing insight to the seismic performance assessment of steel building portfolio in the region. Major sources of uncertainty in seismic demand and building response are taken into account to allow factors significant to risk assessment and to cost-benefit trade-offs be included in the decision model.

1.2 Objectives and Research Approach

The objective of this dissertation is to develop a reliability-based performance assessment procedure for steel frames that can be used to support the assessment of seismic risk in

regions of low-to-moderate seismicity such as the CEUS. This objective is accomplished through the following tasks:

- Identify scenario-based earthquakes from concurrent MAE Center research to characterize sources of seismic hazard in the CEUS and from the United States Geological Survey (USGS) seismic hazard deaggregation project.
- Identify and represent the inventory of steel frame buildings in the region by several code- compliant steel frames with the assistance of other MAE investigators and consulting structural engineers.
- Determine performance limits specific to each frame using available analysis tools and relate seismic response of the frames to performance levels by simulation-based nonlinear finite element reliability analysis.
- Develop fragilities of steel frames in the CEUS and assess their performances under possible future events.
- Apply feasible and economical rehabilitation schemes for frames performing less favorably and determine the benefits of rehabilitation in seismic performance.

Synthetic ground motion records simulated by other researchers are utilized in achieving these objectives. The dominant contributing events in the New Madrid Seismic Zone are obtained using the results of the USGS hazard deaggregation project for Mid-America, especially the city of Memphis, TN. The current steel building inventory of the city of Memphis is represented by five low-to mid-rise model frames. These frames include both moment resisting (fully-restrained (FR) and partially-restrained (PR)) and braced frames, reflect a range of structural systems and capacities, and represent typical

designs from the late 1940s to the early 1990s. Building heights range from 2-story (30 ft. or 9.14 m) to 6-story (80 ft. or 24.4 m). Different configurations of braced frames are employed to cover a variety of practices.

Seismic responses of these frames obtained from nonlinear time history analysis (NTHA) are related to building specific performance levels established in this study rather than generalized FEMA performance limits (FEMA 273/356, 1997/2000). The fragilities are developed by post-processing the results of these simulations. These fragilities display the current seismic risk on these frames (conditioned on ground motion intensity) which represent the steel building stock in Shelby Co., TN. Results of these assessments can be available for other purposes as well, such as providing tools needed by decision-makers in the region to assess the possible damage scenarios and determine appropriate rehabilitation techniques in the region for stipulated seismic events.

Performance state probabilities of model frames under both a uniform hazard event and a scenario event are determined. Depending on these results, rehabilitation strategies for the frames performing less favorably are suggested. The techniques are then applied on the frames and their performances are assessed again after rehabilitation. Capacity Spectrum Method (CSM), which is also the engine for seismic response analysis in the loss estimation methodology, HAZUS (FEMA, 2003), is investigated regarding its applicability to frames and the ground motion data in the CEUS. The results of the CSM are compared against those from NTHA of the same frames. Finally, suggestions for future research are made at the end of the dissertation.

1.3 Overview of Dissertation

This dissertation is composed of 8 chapters and a list of references at the end. The present chapter has provided the motivation for this research. Chapter 2 summarizes seismic performance assessment of steel structures with a broad literature review that describes the current state-of-the-art with regard to behavior of FR and PR moment frames as well as braced frames. Synthetic ground motions used in this study are described and discussed in Chapter 3. Both uniform hazard and scenario earthquakes representative of seismic events in the NMSZ are presented. In Chapter 4, the representative model frames of the current steel building inventory in Memphis, TN are described along with details of the modeling procedure utilized including hysteretic behavior of PR connections, compression behavior of brace members, and shear behavior of panel zones.

Chapter 5 summarizes current methods of seismic performance analysis and continues with the reported results of these methods for all of the frames. Chapter 6 deals with the uncertainty modeling and fragility assessment of the model frames. Also in this chapter are the suggested rehabilitation (or, strengthening) procedures for PR and braced frames. Chapter 7 presents the critiques for existing rapid performance assessment methods with their applications to model frames. The feasibility of these methods for CEUS practices are discussed in detail. Chapter 8 presents the main conclusions of this dissertation with suggestions for future research.

CHAPTER II

BACKGROUND AND LITERATURE REVIEW

Steel moment-resisting frames (SMRFs) have been used extensively in regions of high seismicity for many years. At one time, riveted connections were common in such frames; since the 1950's, however, connections have been fabricated using welds or high strength bolts (because they provide a more predictable clamping force and are easier to install). Fully-Restrained (FR) moment frames with welded connections were believed to be the best construction practice in highly seismic regions. However, the January 17, 1994 Northridge (U.S.) and January 17, 1995 Hyogo-Ken Nanbu (Kobe, Japan) earthquakes changed this belief (Maison and Bonowitz, 1999). The poor performance of welded steel beam-column connections led to numerous investigations, including the SAC Project (SAC, 1996). The SAC Joint Venture was formed by Structural Engineers Association of California (SEAOC), the Applied Technology Council (ATC), and the Consortium of Universities for Research in Earthquake Engineering (CUREe). The main purpose of this undertaking was the need for understanding of reasons for the occurrence of brittle fractures in welded connections during 1994 Northridge earthquake. Furthermore, the SAC project provided new guidelines for design to avoid such brittle behavior in future earthquakes.

Although no lives were lost in the Northridge earthquake as a result of poor performance of steel frame buildings, the subsequent inspection and repair of the steel buildings that were damaged was very costly. The Northridge earthquake was the

costliest earthquake in US history, resulting in $44 billion in damages[2]. In the wake of this event, earthquake-resistant design guidelines for steel frames in high-seismic regions changed significantly. In this dissertation, practices which were prevalent before 1994 will be referred to as pre-Northridge designs, and those after 1994 will be referred to as post-Northridge.

In the following sections, the literature on seismic performance assessment of steel structures is reviewed, describing the current state-of-the-art with regard to behavior of FR and PR moment frames and braced frames.

2.1 Fully-Restrained (FR) Moment Frames

2.1.1 Experimental Research on Connections in FR Frames

As part of the SAC project, Roeder and Foutch (1996) reviewed the results of experimental studies on steel moment frame connections dating back to the 1960s. Although there was considerable scatter in the results, they identified the key parameters governing connection performance: beam depth, beam length, panel zone yielding and the beam flange thickness. Riveted connections that were common prior to the 1950s were regarded as PR connections due to their rotational flexibility.

Popov and Pinkney (1969) performed tests of connections involving W8×20 beams and W8×48 columns. They investigated the effects of direct welding of beam and column flanges and the effects of column bending in weak axis. Later, Popov and Stephen (1970) experimented with W18 and W24 beams with bolted web angles and

[2] http://www.dis-inc.com/northrid.htm

welded flanges using both monotonic and cyclic loading schemes. The results of the above tests proved that fully welded flanges and bolted webs performed better than riveted connections under cyclic loading. The use of FR connection subsequently became common practice in seismic design. In later studies of connections, researchers attempted to simulate the FR frame behavior using subassemblages. Bertero et al. (1973) tested welded-flange and bolted-web connections and simulated their effects on overall frame behavior. The results revealed that panel zone yielding has a significant effect on frame deformation and provides additional energy dissipation capacity.

Rigid moment resisting frame design has evolved in the past several decades (Roeder and Foutch, 1996). At one time, FR connections were utilized for all connections in the moment frame, and because of the relatively high rotational stiffness provided; lighter structural members could be used. However, the increasing cost of designing and fabricating FR connections eventually led to systems in which only certain frames (especially those at the perimeter of the buildings) were designed to resist lateral loads; thus, only the connections in those frames were FR connections. This resulted in a smaller number of FR connections in the building frame but increased the size of the members and the connections in the perimeter framing system. Changes in building codes reflected the findings of the studies above. For example, the increase in the rated shear strength of the panel zones first appeared in the *Uniform Building Code*, 1988 edition (UBC, 1988). This step was taken due to the strain hardening that was observed in the panel zone after yielding initiated (Popov et al., 1986). However, this change made the structures designed according to the 1988 UBC more susceptible to yielding and larger

inelastic deformations in panel zones during an earthquake. The requirement for the welding of the beam web to the column flange first appeared in the UBC 1988, as well.

Rigid connections (and therefore rigid frame practices) continue to be widely used, especially in high-seismic regions. Also, the lack of detailed design aids in the codes favored the use of FR connections and made FR frames common practice among moment resisting frames throughout the U.S. In the following section, the performance of FR frames during recent earthquakes is appraised along, with changes suggested for future practice.

2.1.2 Behavior of FR Frames

Published research on earthquake-related performance of steel moment frames has focused mainly on building practices in high seismic regions. After each significant seismic event, the design codes in those regions have undergone significant changes or updates. Steel frames in low seismic areas, however, have received little attention. The amount of research done on the performance of such frames and the infrequent nature of such events in these regions has caused the public and policy-makers to be less aware of the danger to such frames posed by strong ground shaking. This can be attributed to the fact that the last seismic event of significance occurred nearly two centuries ago. Current seismic design concepts are still based on elastic analyses without any consideration to post-elastic response or to cyclic deformations. Design practices for lateral force resistance of steel frames have changed little during the last few decades in the CEUS.

During the 1994 Northridge earthquake, more than 100 steel moment-resisting frames were damaged from fractures in welded connections that usually initiated at or near the root of the weld connecting the bottom flange of the beam to the column flange and continued through the weld into the beam or column itself (Roeder, 2002). The way that these cracks propagated may be attributed to the greater beam depths and the panel zone yielding alluded to above (Roeder and Foutch, 1996). Studies in the aftermath of the earthquake showed that despite the damage or fracture in their connections, the model buildings would not collapse under another event of similar magnitude. In the following sections, the effects of beam depth and the panel zone yielding are reviewed along with changes in the provisions.

Following the Northridge earthquake, steel moment resisting frames were investigated in depth in the SAC project to better understand the performance of SMRFs under severe ground motion. For this purpose, steel buildings of three different heights (3-, 9-, and 20-story) for 3 cities in the U.S. (Los Angeles, CA; Seattle, WA and Boston, MA) were designed by three consulting firms using UBC 1994 for Los Angeles and Seattle; and the *National Building Code* (NBC) 1993 Edition for Boston. Perimeter SMRFs were chosen as main lateral load carrying system for all 9 buildings. Ensembles of ground motion records corresponding to three different return periods (Somerville et al., 1997) were used in dynamic assessment of these buildings. Analyses of these SMRFs by Gupta and Krawinkler (2000) revealed that these frames are very flexible, with fundamental periods (calculated from a "bare-frame" analysis) that are substantially larger than what one would calculate using the empirical equations in the building codes. The level of modeling complexity was found to play an important role in estimating the

response of such frames. For example, if the structure has weak panel zones, this feature should be modeled properly to obtain an accurate estimate of dynamic response.

Maison and Bonowitz (1999) evaluated the 9-story SMRF designed in the SAC Project for Los Angeles. They treated the plastic rotation capacity of the connections as a random variable, described by a probability density function that was modeled using previous experimental data. The variability in connection behavior (due to workmanship, weld quality, etc.) was vested in the plastic connection capacity, i.e., the rotation at which the connection fracture occurs and the moment capacity drops abruptly. In addition to this random variable model, deterministic brittle and ductile connection models were created and seismic responses were compared when these frames were subjected to five of the SAC ground motion records. A deterministic objective level of Life Safety[3], given the occurrence of an earthquake with a 10% probability being exceeded in 50 years (hereafter denoted as 10%/50 yr event), was targeted during this study. Results showed that the frames that incorporated the connection model with random capacity experienced 40% less connection damage than the frames with deterministic connection models. It also was found that the total number of connection fractures in the structural system is not necessarily a good indicator of global behavior; that the variability due to ground motion intensity is greater than that of the connection rotation capacity. Therefore, evaluations of pre-Northridge buildings using the deterministic connection model would lead to an overly conservative appraisal of the overall frame behavior.

Naeim et al. (2000) investigated the effects of hysteretic deterioration of connections on the seismic behavior of the SAC buildings. Three levels of deterioration

[3] The Life Safety (LS) level of deformation is often associated with a maximum interstory drift angle of 2.5% for ordinary steel frames (FEMA 356).

for different hysteretic characteristics (strength, stiffness, pinching deteriorations) were considered. They concluded that strength deterioration is by far the most important characteristic for describing hysteretic behavior of connections.

In short, the above investigations have shown that the behavior of FR frames designed prior to 1994, despite their apparent ductility, may not have fully measured up to their expected performance. In later chapters of this dissertation, partially-restrained (PR) frames will be investigated if they can be a solution for the shortcomings of FR frames from seismic performance perspective in moderately-seismic regions such as the CEUS.

2.2 Partially-Restrained (PR) Moment Frames

In conventional design office practice, beam-column connections of steel structures often have been assumed to be either fully-released (pinned) or fully-restrained (rigid) for structural design purposes. This greatly simplifies the structural analysis and design process for steel frames. However, connections that are assumed rigid in fact allow some relative rotation during any type of loading; conversely, connections that are assumed pinned provide some resistance against relative rotations. Numerous studies (e.g., Chen and Kishi, 1989) have revealed that stiffnesses of connections used in current practice fall somewhere between pinned and rigid. PR connections are also called "semi-rigid" connections for this reason. Although research has been conducted to understand and model the behavior of PR connections, practical design methods for including PR connection behavior remain limited for two main reasons. First, modeling the behavior of

PR connections is complex and can be difficult to implement in routine structural analysis. Second, the differences in the experimental procedures and substantial variations in the test results (Roeder and Foutch, 1996) hinder the acceptance of a general procedure suitable for different types of connections and capacities. PR connections reduce the lateral stiffness of the frames under monotonic lateral loading. However, as described later in this chapter, this does not necessarily mean that PR frames behave poorly under earthquake excitations.

The new *AISC Specification* (AISC, 2005) stipulates the connections into two categories; simple and moment connections. Simple connections are defined as that permitting shear transfer only. Moment connections are further divided into two groups; Fully-Restrained (FR) and Partially-Restrained (PR) connections. The FR connections transfer moment with only negligible amount of relative rotation and in analysis, they can be assumed to allow no relative rotation. PR connections, on the other hand, allow a substantial amount of relative rotation during moment transfer. Thus, in the analysis of such connections, moment-rotation characteristics of the connections should be taken into consideration.

2.2.1 Classification of PR Connections

Beam-column connections can be classified by three criteria, strength, stiffness and ductility. From the strength point of view, connections are classified as being either full strength or partial strength. From the standpoint of stiffness, they are grouped as FR, PR and simple (shear) connections. From the standpoint of ductility, they are classified as

brittle or ductile. Following the Northridge earthquake, a plastic rotation of 0.03 rad. under cyclic loading, with a loss of strength less than 20%, was been suggested as an acceptable rotation limit to differentiate between ductile and brittle connections for special moment-resisting frames (Swanson and Leon, 2000).

Several types of PR connections are common in steel frame design practice; some being very flexible and others being quite stiff. From least to most stiff, they can be ranked as: single web angle, double web angle, header plate, top and seat angle, top and seat angle with double web angle and T-stub (TS) connections.

2.2.2 Modeling PR Connections

The behavior of beam-column connections for structural analysis is characterized by the relation between the connection moment and the relative rotation of the beam and column. The contributions of axial load and shear force in the connection rotation are negligible as compared to that of the bending moment. The difficulty in modeling PR connections arises from the fact that their behavior is nonlinear even at very early stages of deformation.

Earlier attempts to model the behavior of PR connections date back to 1930s with simple linear models, e.g., Rathbun (1936). However, nonlinear behavior of PR connections restricted the use of linear models to a very limited deformation range. Bilinear and piecewise connection models emerged in the 1980s, e.g., Lui and Chen, 1986; Razzaq, 1983. Several databases were created for PR moment-rotation behavior from the experimental results starting in the 1980s, (e.g., Jones et al., 1980; Goverdhan,

1984; Kishi and Chen, 1986; Abdalla and Chen, 1995). Sudden changes in the slopes of these proposed models made their use in design difficult, and more recent research has proposed smooth functions to curve-fit the experimental results.

The models mentioned above have attempted to model the static backbone curve for the connections under investigation. This, in fact, is essential in estimating the hysteretic (cyclic) behavior of the connections which will allow analysts to better understand the dynamic behavior of frames under dynamic loading such as earthquakes. Cyclic models go one step beyond and represent the unloading and reverse loading behavior of the connections to some extent. However, PR connection behavior is difficult to be represented by a mathematical formulation due to such factors as strength degradation, stiffness degradation, pinching and bolt slippage. Therefore in this dissertation, beam-column connections are modeled using the experimental results of same or comparably sized specimens. This will later be elaborated in Chapter 4.

2.2.3 Behavior of PR Frames

Structural systems designed for earthquake forces should have enough stiffness and strength to resist inertial forces generated by the ground motion and should have the ability to dissipate energy through some means. Properly designed steel frames generally dissipate such energy by means of plastic hinges occurring at the beam ends. PR connections or frames are capable of adding considerable source of energy dissipation (Salazar and Haldar, 2001). The use of PR connections in lateral force-resisting systems of low-to-mid-rise steel frames in regions of low to moderate seismicity generally leads

to lighter beam and column sections and frames that transmit lateral forces more efficiently to interior bays (Maison and Kasai, 1999). This, in turn, increases the overall redundancy of the system against lateral loads.

Gao and Haldar (1995) used the 4-parameter Richard Model (Richard and Abbott, 1975) in their investigation of 1- and 2-story PR frames. To reflect the inherent scatter in the connection behavior, they treated the four parameters of the connection model as random variables. Results showed that as the connections became more and more flexible, the columns became safer and the beams became less safe due to increases in bending moment along the beam span. From a design perspective, PR connections cause the frames to become flexible enough that serviceability under static loading may become the governing criterion for design.

Nader and Astaneh-Asl (1996) demonstrated that frames with PR connections may behave almost as well as those with rigid connections at service level and moderate level earthquakes, and do not necessarily sustain higher deformations. Furthermore, the PR connections add ductility to the system and enhance its seismic performance. However, for larger earthquakes the top and bottom seat angles may yield and bolts may slip. It was also shown that the catenary forces that develop in the top and bottom seat angles may increase the plastic moment capacity of the PR connections significantly.

Foley and Vinnakota (1997) compared the monotonic behavior of four different frame configurations (all are strong-beam, weak-column; 2 to 3 stories in height; designed with no seismic considerations) using both FR and PR connections. Their study indicated that when the connections are changed from FR to PR, the ultimate base shear capacity of the frame decreases and roof displacement at the ultimate increases. It was

also shown that as the connection stiffness decreases, the spread of yielding occurs along the length of the column; this finding favors the use of spread plasticity elements rather than plastic hinge elements in frame modeling.

Elnashai et al. (1998) demonstrated that PR connections can perform as well as FR connections under dynamic loading. Bolted PR frames may attract lower loads due to their longer periods and due to higher energy dissipation capacity, they usually have higher damping values. As a result, they may undergo lower displacements than FR frames. The influence of connection stiffness on the overall frame response has also been studied and within the range of frames investigated (2-story); it was shown that a 50-60% reduction in connection stiffness yielded approximately a 25% decrease in the frame stiffness. A similar trend was observed when the effect of connection capacity on the overall frame capacity was investigated. It was also shown that PR connections provided significant ductility and stable hysteretic behavior.

Swanson and Leon (2000) tested 48 T-Stub and 10 Clip Angle (CA) connections. They tested individual T-stubs rather than full connections for the sake of efficiency. The components were subjected to axial loads based on expected beam flange forces in actual connections. The axial loading is a simplification of the actual conditions, since both localized bending and shear forces present in the actual connection were missing in the component tests. This study showed that the major contributions to the overall deformation of T-Stub components were made by the flange deformation, tension bolt elongation, stem deformation, and relative slip. Energy dissipation capacity was due mainly to flange yielding and connection slip.

Salazar and Haldar (2001) examined the energy dissipation at PR connections, and demonstrated that PR connections not only add flexibility to the overall lateral force resisting system but also add a major source of energy dissipation under cyclic loading, which is sometimes higher than that from viscous damping. Under dynamic loading, it was observed that as the connection stiffness increases, the maximum total base shear also increases. Furthermore, it was revealed that maximum lateral roof displacement does not necessarily increase as the connections get weaker. The response under earthquake loading depends mainly on the structure and frequency content of the excitation rather than the initial stiffness of the structure. The role of PR connections in energy dissipation becomes more important as the height of the frame increases.

The review above shows that seismic performance of PR frames can be comparable to, or even at some instances better than, that of FR frames. The advantages of PR frames include the following:

- Their flexibility lengthens the structural period and hence attracts less inertial forces under earthquakes.
- They have higher damping, which helps controlling excessive deformations.
- They possess superior energy dissipation characteristics.
- The use of PR connections leads to beams that are weaker, in a relative sense, than the columns into which they frame.
- PR construction practice results in better distribution of lateral force resistance throughout the frame.

The disadvantages of the PR connections are due in part to difficulties in assuring desired performance using current design tools. Bolt slip, pinching, strength and stiffness degradation also hamper the acceptable overall behavior of PR frames under severe earthquakes.

2.3 Braced Frames

In a braced frame, the lateral load-resisting system is provided by the braces which act as axial load members in a vertical truss arrangement. The connections in this type of frame are generally designed as simple connections. Braced frames are especially common in low-rise (1-2 stories) industrial structures. Braced frames are divided into two categories with respect to their geometry: Concentric Braced Frames (CBFs) and Eccentric Braced-Frames (EBFs). With respect to their behavior, these two fall into the category of buckling- permitted braced frames. Another type is the Buckling Restrained Braced-Frame (BRBF). The current steel building stock in the CEUS indicates the substantial presence of only CBF practice for braced frames; therefore, EBF practice will not be discussed in this dissertation.

2.3.1 Concentrically Braced Frames

CBFs are systems where braces are placed as diagonals or as Vees (or inverted Vees, also referred to as chevron bracing) so that their points of action coincide (Fig. 2.1). The main advantage of CBFs comes from the complete truss action they can undergo, which gives these systems very high initial stiffness. However, they behave as brittle systems beyond

the linear-elastic range because once buckling of the compression braces occurs and is followed by yielding of the tension braces at the same story level, the result is a soft-story effect in the structure.

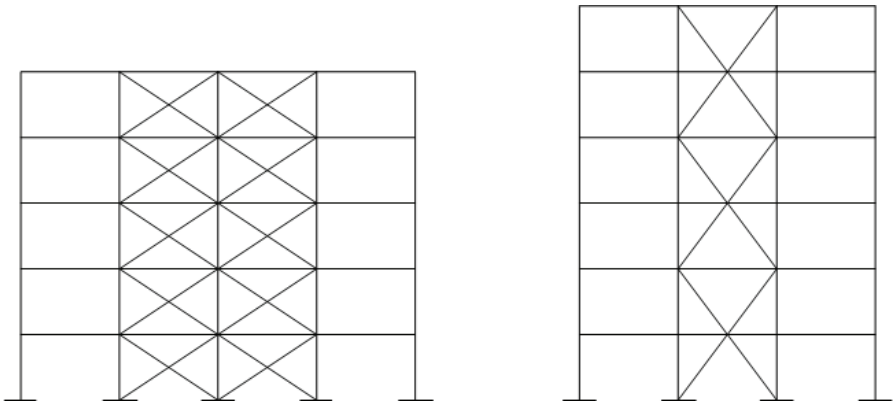

(a)

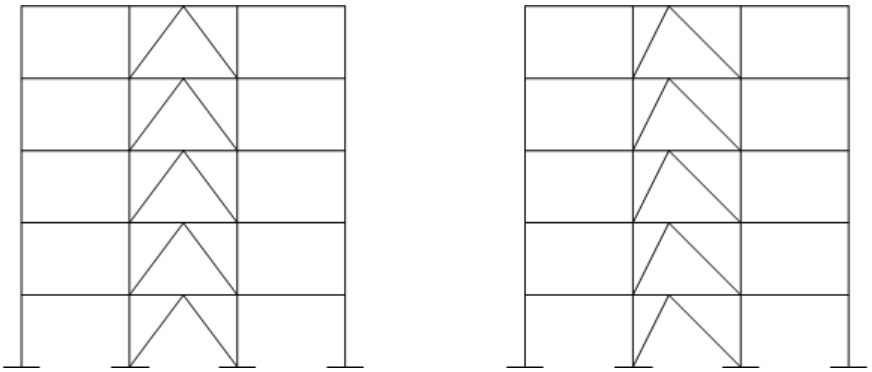

(b)

Figure 2.1 Typical layouts for CBFs. a) X bracing; b) Chevron bracing.

The International Building Code (IBC, 2003) further separates CBFs into ordinary concentric braced frames (OCBFs) and special concentric braced frames (SCBFs) (Kim and Choi, 2005). The main difference between these two classes of frames is that the

floor beams of SCBFs intersected by the bracing members are designed to carry all the gravity loads assuming no bracing is present. OCBFs are considered as strong brace-weak beam type structures whereas SCBFs are considered as strong beam-weak brace type structures. Complete truss action can only be achieved in SCBFs. However, the moments imposed due to unbalanced vertical load on the floor beams can be quite large, resulting in very heavy sections and uneconomical beam designs. Another type of CBF application is that braces are placed to form an X either in a single story or in multiple stories. This eliminates the consideration of unbalanced vertical loads imposed on the floor beams in V or chevron bracing systems.

2.3.2 Buckling-Restrained Braced Frames

Buckling-Restrained Braced Frame (BRBF) systems allow the braces to yield in both tension and compression by preventing buckling. This system emerged in the United States as a result of the unfavorable performance of CBF systems during the 1994 Northridge and 1995 Kobe earthquakes. BRBF systems avoid the following drawbacks of the conventional CBF (Sabelli et al., 2003):

- Compression and tension capacities of the brace members are quite different, which results in high unbalanced forces in the floor beams,
- Brace capacity degrades under compressive and/or cyclic loading.

To overcome these drawbacks, brace members (usually selected from rectangular or circular solid cross-sections) are encased in a steel tube which then is filled by a

material (usually mortar) to provide continuous lateral support to inhibit buckling. The mortar is unbonded to the steel member (a layer of separating material is applied on the surface of the inner core member) inside so that it does not carry any compressive or tensile force. This restraint of buckling allows the brace members to undergo considerable inelastic deformations during large load reversals. The hysteretic behavior of the buckling-restrained brace members is generally stable with very little post-yield stiffness. This can be approximated as elastic-perfectly plastic behavior. During design, the tension capacity of these members is calculated for yielding and 110% of this value is taken as the compression capacity of the members (Sabelli et al., 2003). BRBF systems also have superior ductile performance. Since the unbalanced forces in the braces are lower, the beams are lighter. Clark et al. (1999) reported that BRBF systems save 50% of the steel used in braced frames in which buckling otherwise can occur and behave better than ordinary braced frames under monotonic loading. They also possess stable energy dissipating characteristics.

However, BRBF systems have their own shortcomings. Most importantly, the issue of permanent drift is of significant concern due to their low post-yield stiffness (Uang and Kiggins, 2003), and the possibility of permanent drifts under moderate seismic events hinders the use of these systems as the sole lateral force resisting system in a building.

2.3.3 Brace Member Modeling

Procedures for modeling braces have evolved in the last two decades. Earlier models were limited to elastic behavior in tension and compression, tension only, and tension yielding-compression elastic buckling. None considered the energy dissipation capacity of the brace in the post-buckling region (Jain et al., 1980). Two of the main issues in modeling brace behavior are: predicting the reduction in compressive strength and increase in member length during cyclic loading.

Experimental studies performed to date showed, conclusively, that the capacity of brace members under cyclic compression decreases steadily after the first buckling cycle (Fig. 2.2). This amount of decrease is related to the effective slenderness ratio of the member. The reduction increases as the slenderness ratio of the brace increases. The ratio of post-buckling compressive load to critical buckling load is referred as factor *c* in FEMA-273. In the literature, values around 0.1-0.3 have been reported (Jain et al., 1980; Tremblay, 2002; Goggins et al., 2006). FEMA-273 provides values for factor *c* between 0.2 and 0.4.

The behavior of a brace member also is dependent on the loading history. If it is loaded in tension first and yields, then the member generally buckles at higher compressive loads than it would if it was loaded in compression first due to strain hardening and Bauschinger effect. The tensile capacity of the braces also undergoes a reduction during repeated cycling loading. However, this reduction is substantially less than the reduction that occurs in compression capacity.

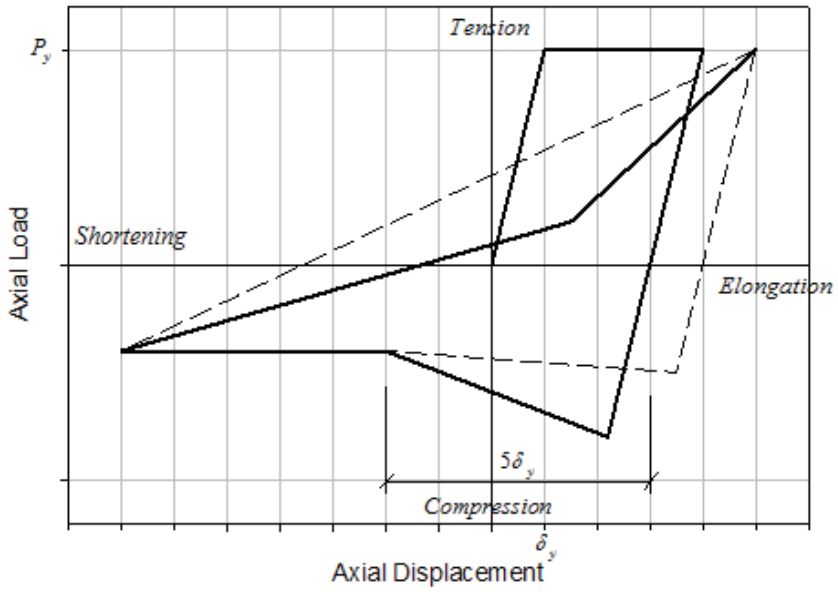

Figure 2.2 Idealized brace behavior by Jain and Goel (1979).

2.3.4 Seismic Performance of Braced Frames

Braced Frames, especially CBF systems, are generally perceived as performing poorly under earthquakes. Considerable damage was found to have occurred to CBF systems following both the Northridge and the Kobe earthquakes. The brittle post-buckling behavior of braces, which reduces the ability of the structural system to dissipate energy during an excitation, and the tendency of multiple braces to buckle within the same story levels are responsible for the poor performance of these systems under severe seismic events. CBF systems seldom are used in high-seismic regions. Seismic design codes or provisions tend to penalize the use of CBF systems through the stipulation of lower response modification factors, enforcing the use of low slenderness ratios for braces,

neglecting compression capacity of braces, etc. However, the stricter rules for designing moment resisting frames in high-seismic regions put into effect in the aftermath of the 1994 Northridge earthquake has made the use of braced frames in low-to-medium rise structures more attractive.

From the seismic performance point of view, BRBF systems are superior to the use of CBF systems alone. BRBF systems also are both very ductile and stiff; however under cycling loading they may undergo considerable permanent drift. Martinelli et al., (1998) proposed a design method which uses CBF systems along with moment resisting frames. In this composite system, the structure benefits from the stiffness of the CBF system to meet strict interstory drift limits (which often govern the design and result in bulkier sections), while moment resisting frames are responsible for the ductile behavior and the energy dissipation. In this resisting frame-stiffening brace method, the structure is first designed as moment frame for the ultimate limit state seismic actions without checking the serviceability requirements which are then fulfilled by the CBF. The results reported in that study suggest that this methodology can be applied in seismic design of steel structures. However, premature failure of braces in the earlier stages of excitation may result in unpredictable overall dynamic behavior.

2.4 Summary

In this chapter, seismic response of steel buildings was reviewed. Steel moment frames were classified as partially-restrained (PR) and fully-restrained (FR) frames. The ease of construction, greater redundancy, lighter member sizes and more economical connection

detailing are points in favor of PR frames, while the lack of initial stiffness and the lack of well established seismic design codes are their main drawbacks. The shortcomings of FR frames designed prior to 1994 were given in relation to their poor performance in 1994 Northridge and 1995 Kobe earthquakes. Seismic performance of PR frames can be quite satisfactory, especially if the panel zones and connections are detailed properly.

Current design practice and the current steel building inventory in the CEUS, particularly in Shelby Co., TN, suggests that the emphasis in fragility assessment should be given to the CBF systems. Chapter 4 describes how the current building stock in Memphis is represented by five frames; three moment frames and two CBFs (one X-braced and one chevron braced). BRBF system characteristics will be revisited in Chapter 6 when possible rehabilitation or seismic improvement schemes are being appraised for two braced frame models.

CHAPTER III

SEISMICITY AND GROUND MOTIONS IN THE CEUS

The Central and Eastern U.S. (CEUS) is defined as the area east of the Rocky Mountains. The seismicity in that region can be described, in general, by events which are infrequent in nature but may have high consequences for civil infrastructure and urban populations. The dominant contributor to seismic risk in the region is the New Madrid Seismic Zone (NMSZ) in the central Mississippi Valley extending from northeast Arkansas, through southeast Missouri, western Tennessee, and western Kentucky to southern Illinois. The last major earthquake occurred in the NMSZ nearly two centuries ago. In a 3-month period (December 1811 to February 1812), a sequence of three very powerful quakes with magnitudes ranging from M_W=7.8 to M_W=8.1 occurred. Thousands of aftershocks followed these great earthquakes throughout the spring and remainder of 1812. It was reported, by eyewitness accounts, that the settlement of New Madrid, MO was totally destroyed. These earthquakes were felt throughout much of the CEUS.

The largest populated area near the NMSZ is centered around the city of Memphis in Shelby County, Tennessee, with a population of nearly 900,000 in the metropolitan Memphis area. Most building structures in Shelby County have not been designed and constructed to withstand severe earthquake shaking, as they have been in more seismically active areas like the Western US (WUS).[4] Research during the last two decades has revealed that the region has previously been struck by at least two earthquakes of comparable magnitude. Sand blow deposits and other findings suggest that the previous shakings occurred at intervals of approximately once in every 500 years

[4] The City of Memphis recently adopted the 2003 edition of the *International Building Code* (ICC, 2003).

(USGS, 2002a). Figure 3.1 shows the seismicity of the region with recorded events since 1974. The NMSZ averages about two to three earthquakes a week, but most of these tremors are never felt. Usually one or two earthquakes that are large enough to be noticed by people living in the area occur per year. The probability of an earthquake with magnitude 6 or greater in the near future is considered significant; the chance of such an earthquake occurring in the next 50 years has been estimated as 90%, while the odds of magnitude 8 event within 50 years have been estimated as being 7 to 10 percent (USGS, 2002a). The probable losses from a repeat of 1811-1812 earthquakes have been projected as being several thousand deaths and $200 billion in property damage (Beavers, 2002).

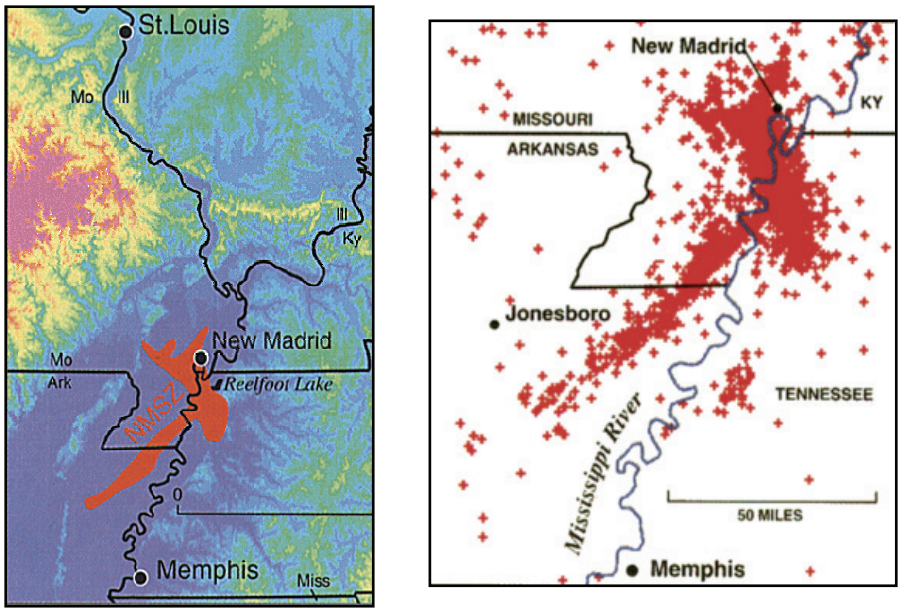

(a) (b)

Figure 3.1 a) Location of the NMSZ in the Central Mississippi Valley[5] and b) the recorded seismicity since 1974[6].

[5] USGS, "http://quake.wr.usgs.gov/prepare/factsheets/HiddenHazs/NMSZBig.gif" (3/07)
[6] "http://upload.wikimedia.org/wikipedia/en/b/b5/New_Madrid_quakes.png" (3/07)

3.1 Seismic Hazard in the CEUS

A significant component of the uncertainty in response of buildings, bridges and other civil infrastructure to strong earthquake ground motion is due to the inherent randomness in the ground motion itself: peak intensity, time-varying amplitude, strong-motion duration, and frequency content. Seismic hazard curves for sites in the CEUS are available from the USGS website[7] and are expressed as (tabulated) complementary cumulative distribution functions describing the maximum 5% damped spectral accelerations to occur in 50 years at structural periods of 0.2, 0.3, and 1.0 sec. These hazard curves for sites in the CEUS are determined, in part, from postulated seismic source zones and ground motion attenuation models, and thus are generally interpreted as *mean* seismic hazard curves, since they are averaged from a number of alternate sources and ground motion models.

Modern probabilistic seismic hazard analysis (e.g., McGuire, 2004) has shown that over a limited range of seismic intensities or return periods, the seismic hazard can be described by:

$$H(S_a) = k_o \cdot S_a^{-k} \tag{3.1}$$

where k_o and k are site-dependent parameters, the latter parameter being the slope of the hazard curve on a log-log plot (hazard decay). This information is sufficient to construct a uniform hazard response spectrum for any return period of interest. The mean hazard curves for Memphis, TN (35.117^{o}N, 90.083^{o}W) constructed using data from the USGS website is given in Figure 3.2 for structures with fundamental periods of 1 and 2 seconds; this period range spans the periods of most of the frames considered in this dissertation.

[7] USGS, "http://earthquake.usgs.gov/research/hazmaps/products_data/2002/ceus2002.php" (3/07)

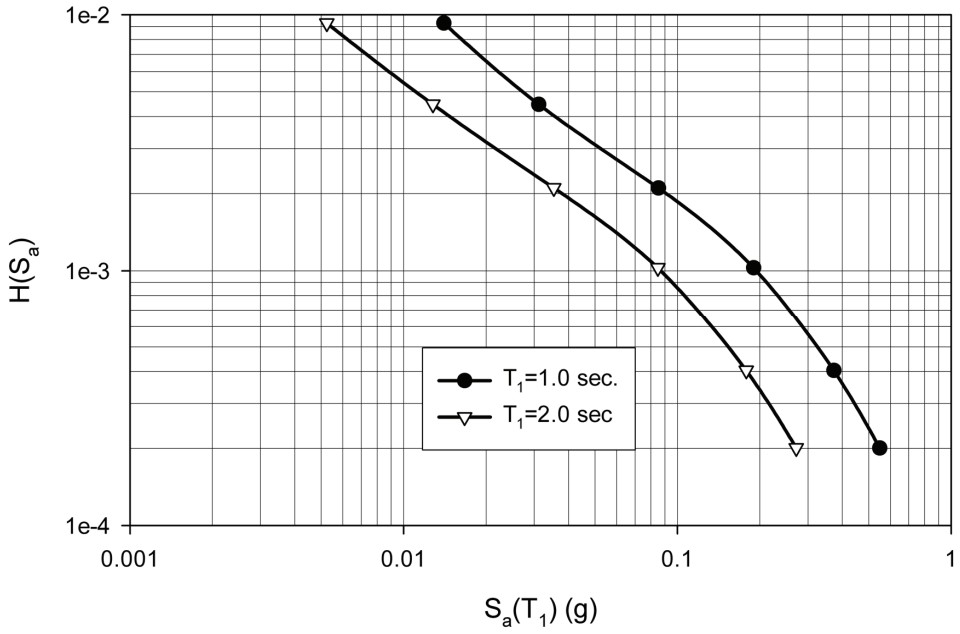

Figure 3.2 Seismic hazard curves for Memphis, TN.

3.2 Comparison of Seismic Hazard: CEUS vs. Western U.S.

The WUS is known for its active seismic faults and frequent seismicity. However, the seismic hazard in the CEUS is less well known due to its different seismotectonic features. Unlike the WUS, which has active plate boundaries, the NMSZ is thousands of kilometers away from known seismic plate boundaries. There are striking differences in the seismic hazard plots of two regions. In the CEUS, the hazard curve is very flat (the Coefficient of Variation (COV) in annual extreme or 50-yr maximum spectral acceleration is in excess of 100%) and the factor *k* typically is on the order of 1 to 2. In contrast, the hazard curve in the WUS is much steeper and *k* is around 3 to 4. Figure 3.3 shows the seismic hazard curves for Memphis, TN and Los Angeles, CA for a structure with 1 sec. fundamental period. For a return period of 475 year event (designated a 10%/50 yr hazard), the spectral accelerations are 0.085g and 0.41g for Memphis and Los Angeles,

respectively; for a return period of 2,475 years (2%/50 yr hazard), the corresponding spectral accelerations are closer: 0.37g and 0.72g. The 2%/50 yr hazard defines the Maximum Considered Earthquake (MCE) stipulated in the *BSSC/NEHRP Recommended Provisions* (BSSC, 2003) and in *ASCE Standard 7-05* (ASCE, 2005).

In addition to differences in the occurrence and frequency of the seismic events in the CEUS and WUS, the seismic wave propagation characteristics are also different. The waves attenuate much faster in the WUS than in the CEUS (USGS, 2002a). The WUS is mostly rock with relatively shallower soil depths. Thus, large events in the NMSZ would be felt much further away than events of comparable magnitude in the WUS. Figure 3.4 compares the affected areas of two similar magnitude events: the 1895 Charleston, MO, earthquake and the 1994 Northridge earthquake. The area of structural damage is indicated in red, while yellow indicates area where shaking was felt.

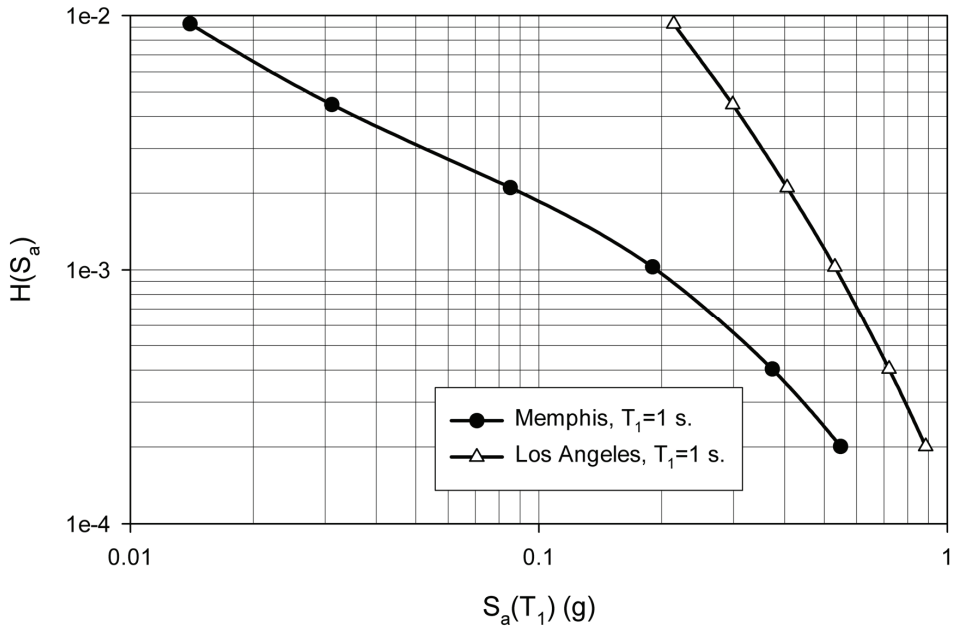

Figure 3.3 Comparison of the seismic hazard for Memphis and Los Angeles.

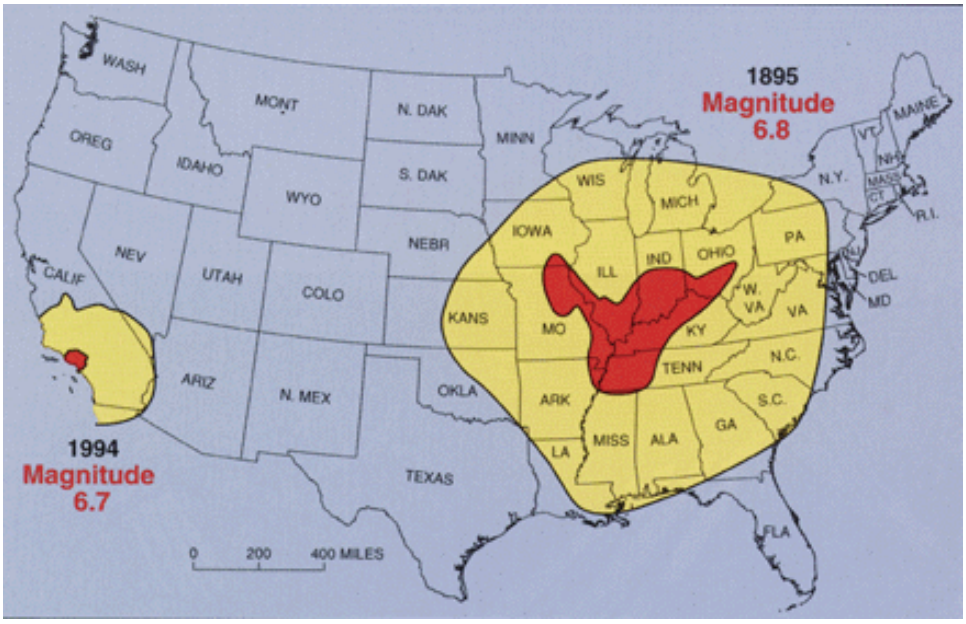

Figure 3.4 Comparison of the affected areas for two comparable magnitude events[8].

3. 3 Deaggregation of Seismic Hazard in the CEUS

The seismic hazard at any site in the United States is deaggregated by the USGS to determine the contribution of regional seismic events to the overall hazard at that site. An example of this deaggregation for Memphis, TN is depicted in Figure 3.5 for a ground motion with a probability of 2% of being exceeded in 50 years or, equivalently, a return period of 2,475 years. The height of each bar in this figure represents the percent contribution of earthquakes in that magnitude and distance bin to the annual rate of exceeding the ground motion corresponding to the specified return period. The probabilistic hazard corresponding to a 2,475-year return period event is the integrated effect of earthquakes at all of these magnitudes and distance bins. Such plots are useful

[8] USGS "http://quake.wr.usgs.gov/prepare/factsheets/NewMadrid/Charleston1895.gif" (3/07)

for specifying scenario earthquakes. The deaggregation results are often described in terms of the mean magnitude $\overline{M}$ and mean distance $\overline{D}$. It has been suggested that $\overline{M}$ and $\overline{D}$ be used to specify a scenario earthquake (USGS, 2002b). Figure 3.5 shows that the dominant contributor to the seismic hazard for the Memphis area is a M_w=7.8 event at an epicentral distance R=40 km; there also is a significant contribution from a M_w=7.8 event at a distance R=70 km.

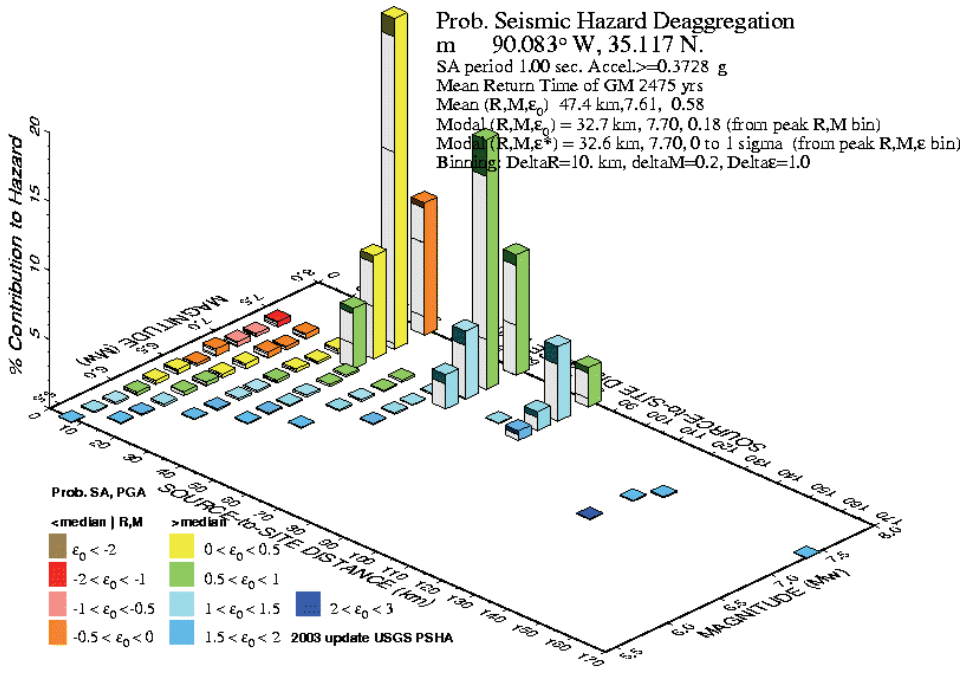

Figure 3.5 Deaggregation plot of seismic hazard for Memphis, TN (USGS, 2002b).

3.4 Natural vs. Synthetic Ground Motions

Uncertainties in seismic demand on a structural system are characterized by simulating nonlinear structural response to an ensemble of ground motions that are consistent with

the specified seismic hazard. In the recently completed SAC Project (Gupta and Krawinkler, 2000; Yun et al., 2002; Lee and Foutch, 2002) and in ongoing research in the Pacific Earthquake Engineering Research Center addressing building performance in regions of high seismicity (Shome and Cornell, 1998; Giovenale et al., 2004), it has been possible to develop ensembles for this purpose from natural (recorded) ground motions that are appropriately scaled. In contrast, there are few recorded ground motions for sites in the CEUS, and there are none that correspond to the large earthquakes that are likely to challenge modern civil infrastructure in that region. Accordingly, seismic vulnerability and risk assessment of buildings in the CEUS must rely mainly on ensembles of synthetic ground motions. There are several alternative models for generating synthetic ground motions in the CEUS (e.g., Atkinson and Boore, 1995; Frankel et al., 1996), each of which is judged plausible in the seismological community.

Three sets of synthetic ground motions that have been developed in research sponsored by the MAE Center were used to evaluate the dynamic response of the steel building frames in this dissertation. Two of the sets are "uniform hazard" ground motions and the third ground motion set corresponds to a specific earthquake scenario. Uniform hazard ground motion records and scenario-based simulated records are fundamentally different in the way they portray the underlying seismic hazard. The former aims to generate suites of records whose spectral amplitudes best match a target response spectrum corresponding to a stipulated probability or return period for a specific region over a pre-defined range of periods. Scenario earthquakes, on the other hand, can be identified from the deaggregation of the seismic hazard at a site at a particular return period (e.g., 2,475 years in Figure 3.5) but the ensembles cannot be associated with a

specific (probabilistic) level of seismic hazard (unless the return period event is due to only one magnitude/distance pair). Rather, they represent ground motions from stipulated events with specific epicentral distances and magnitudes.

3.4.1 Wen-Wu Uniform Hazard Ground Motions

Wen and Wu (2001) generated suites of ground motions corresponding to 2% and 10% probability of exceedance in 50 years (denoted as 2%/50 yr and 10%/50 yr hereafter), corresponding to return periods of 2,475 and 475 years, respectively, for three sites in the CEUS (Carbondale, IL; Memphis, TN; and St. Louis, MO). These sites were intended to represent the primary urban areas at risk from events in the NMSZ. The bedrock ground motion records were synthesized by using a point source model by Atkinson and Boore (1998) was used along with finite fault model by Beresnev and Atkinson (1998) which was utilized for high magnitude events. Earthquake occurrences were modeled by a Poisson process. In generating records for soil sites however, local soil conditions were not considered in detail and a generic soil profile was assumed for all three sites. Soil amplification is modeled by the quarter wavelength method which overestimates the ground motion intensity at low periods.

Constant aleatoric uncertainty of 75% was assumed for the standard deviation of natural logarithms of peak ground acceleration values. A large number of accelerograms was generated to obtain uniform hazard response spectra at the 10%/50 yr and 2%/50 yr probability levels. Then, ensembles of 10 ground motions were selected so that the response spectra of those accelerograms best match the uniform hazard response spectra

for all period range in a least-squares sense. With three sites, two soil conditions/site, and two probability levels, there are 12 ensembles with a total of 120 accelerograms. These ground motions will be denoted Wen-Wu GMs in subsequent analyses. Figures 3.6 through 3.8 show the Uniform Hazard Response Spectra (UHRS) for 3 sites, 2%/50 yr hazard level, soil conditions and 5% damping. Figures 3.9 through 3.11 depict the UHRS for the 10%/50 yr hazard level. The thick line in each plot represents the median response spectra for that ensemble.

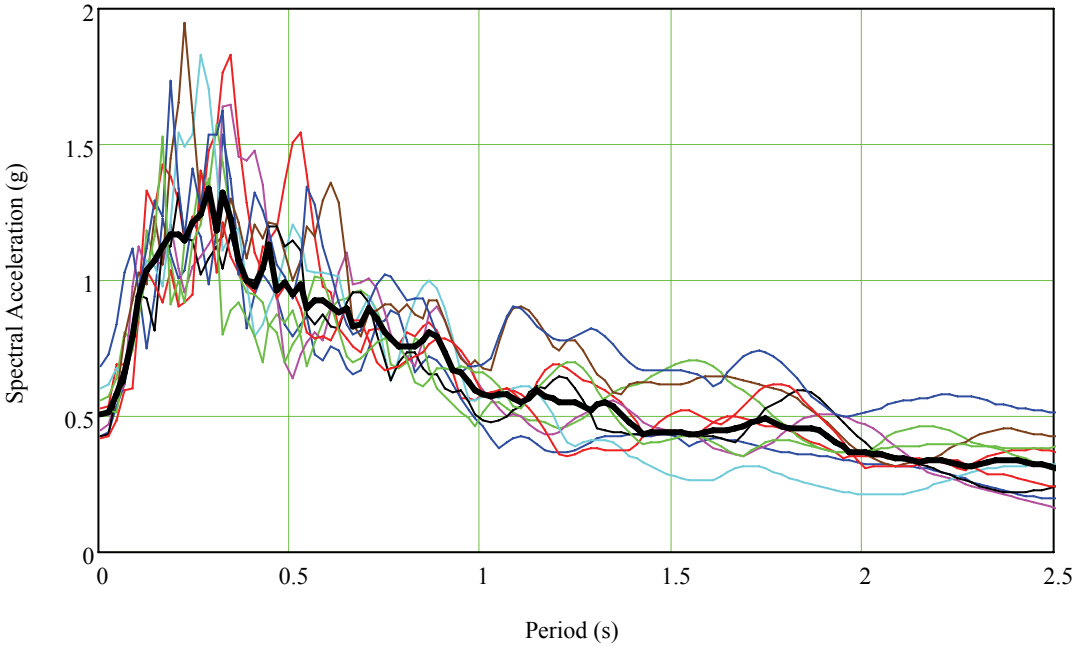

Figure 3.6 UHRS for Carbondale soil profile; 2%/50 yr hazard level, 5% damping.

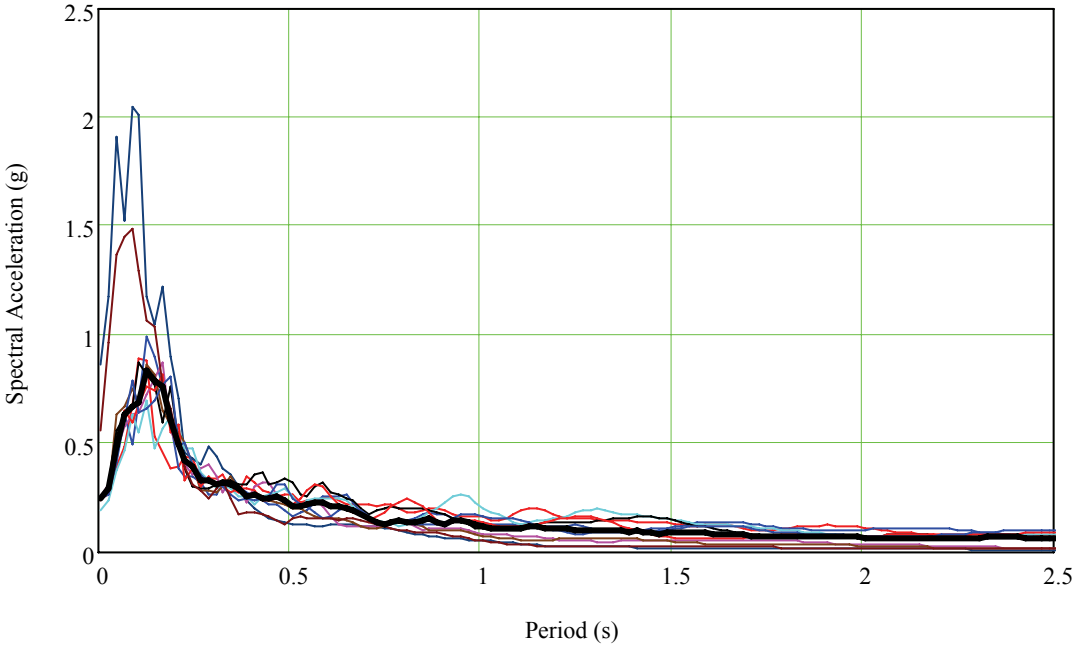

Figure 3.7 UHRS for St. Louis soil profile; 2%/50 yr hazard level, 5% damping.

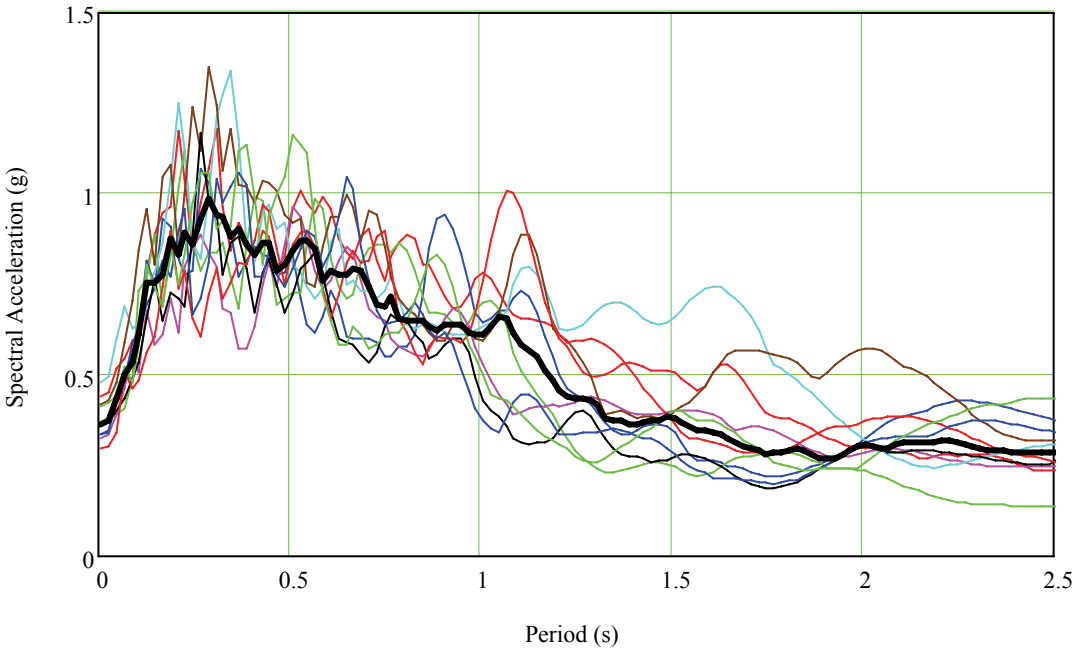

Figure 3.8 UHRS for Memphis soil profile; 2%/50 yr hazard level, 5% damping.

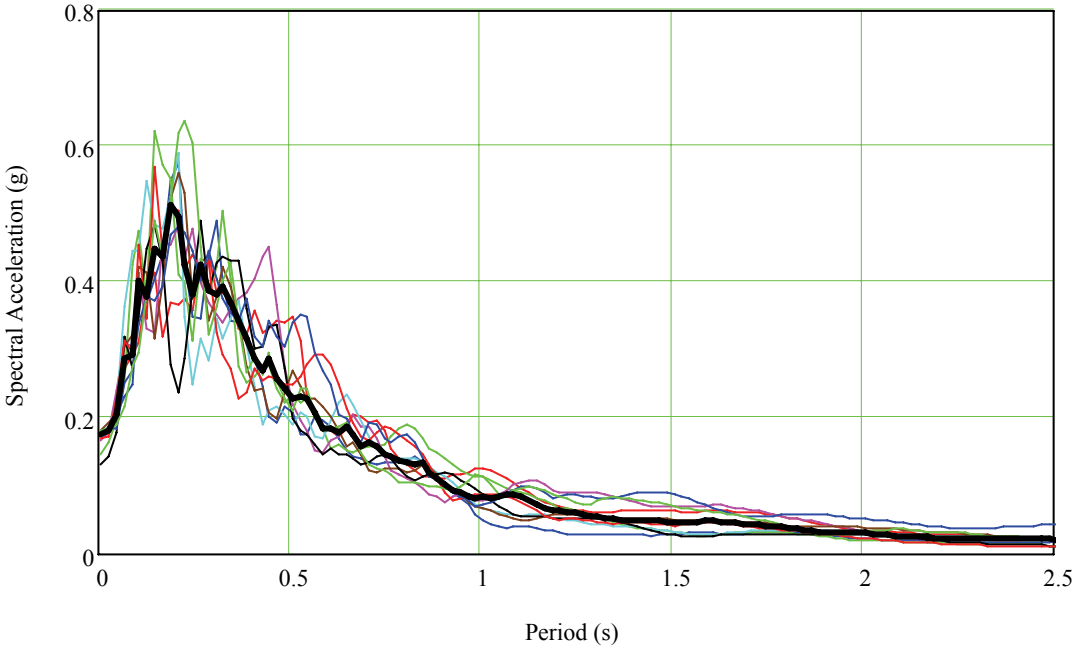

Figure 3.9 UHRS for Carbondale soil profile; 10%/50 yr hazard level, 5% damping.

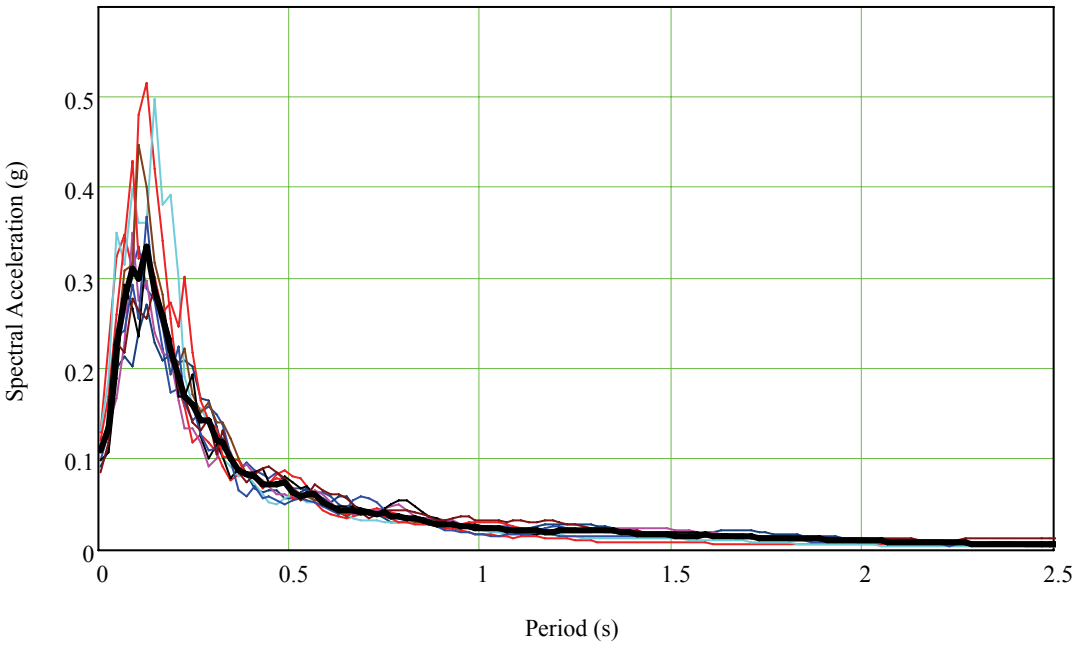

Figure 3.10 UHRS for St. Louis soil profile; 10%/50 yr hazard level, 5% damping.

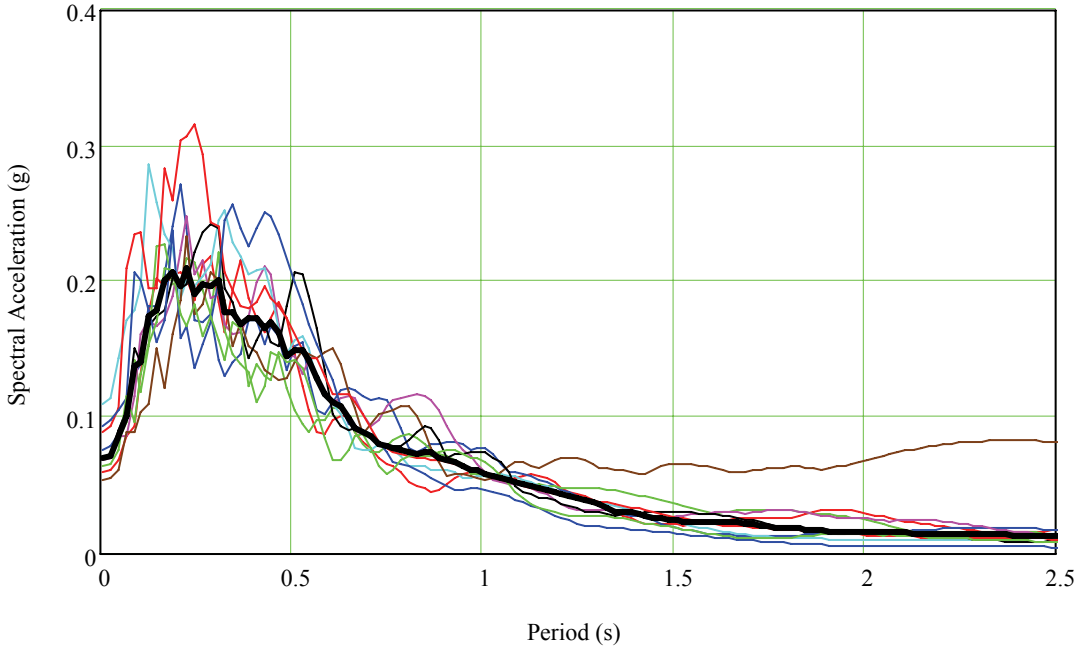

Figure 3.11 UHRS for Memphis soil profile; 10%/50 yr hazard level, 5% damping.

3.4.2 Rix-Fernandez Uniform Hazard Ground Motions

Fernandez and Rix (2006) generated Uniform Hazard Ground Motions (UHGMs) for seven sites within the Upper Mississippi Embayment and for three different levels of hazard, i.e., 10%/50 yr, 5%/50 yr, and 2%/50 yr (corresponding to return periods of 475, 975 and 2475 years, respectively). The sites are: Memphis, TN; Jackson, TN; Jonesboro, AR; Blytheville, AR; Little Rock, AR; Paducah, KY; and Cape Girardeau, MO. These accelerograms will be noted as Rix-Fernandez GMs. Effects of epistemic and aleatory uncertainties due to source, path and source processes were accounted for in the attenuation relationships. Three different point source models (Atkinson and Boore,

1995; Frankel et al., 1996; and Silva et al., 2003) and three stress drop values were used to represent the epistemic uncertainty in the process. Aleatory uncertainty, on the other hand, was handled by treating attenuation parameters as random variables with appropriate medians, standard deviations and probability distributions. A Monte Carlo simulation technique was employed to generate attenuation relationships. Nonlinear site response was incorporated in the accelerograms generated. Ten accelerograms were generated for each site and for each hazard level. For Memphis, TN, however, sets were synthesized separately for lower and upper regions of the city: lowlands and uplands, respectively. Figures 3.12 - 3.14 show the UHRS for Memphis, Uplands soil conditions and all three hazard levels with assumed 5% damping.

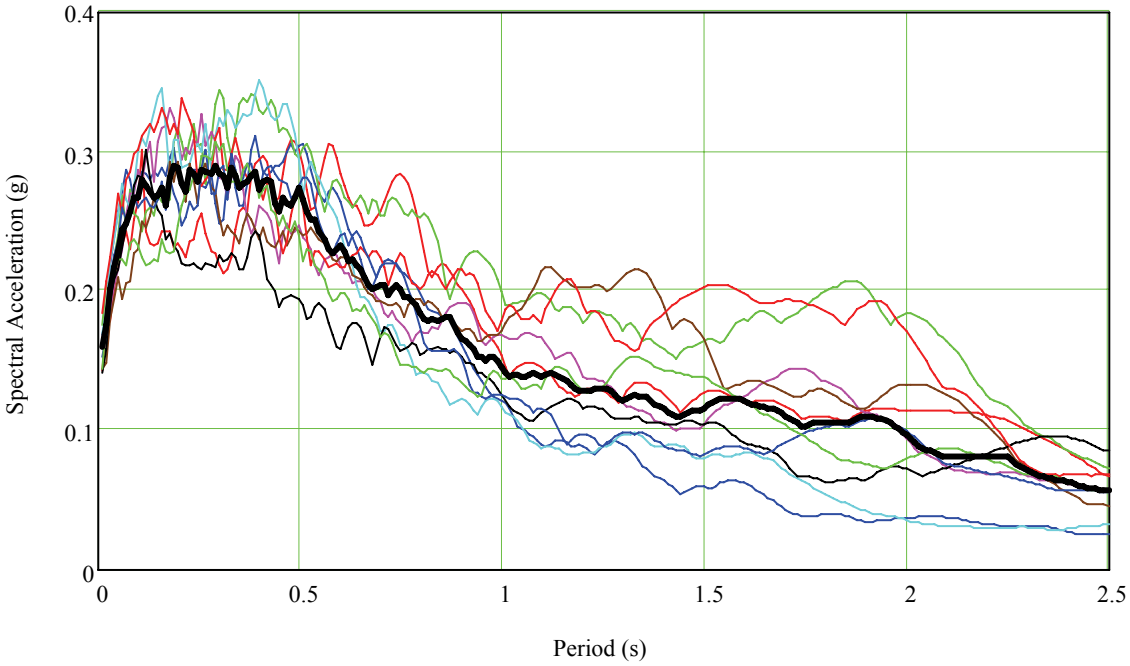

Figure 3.12 UHRS for Memphis Uplands; 10%/50 yr hazard level, 5% damping.

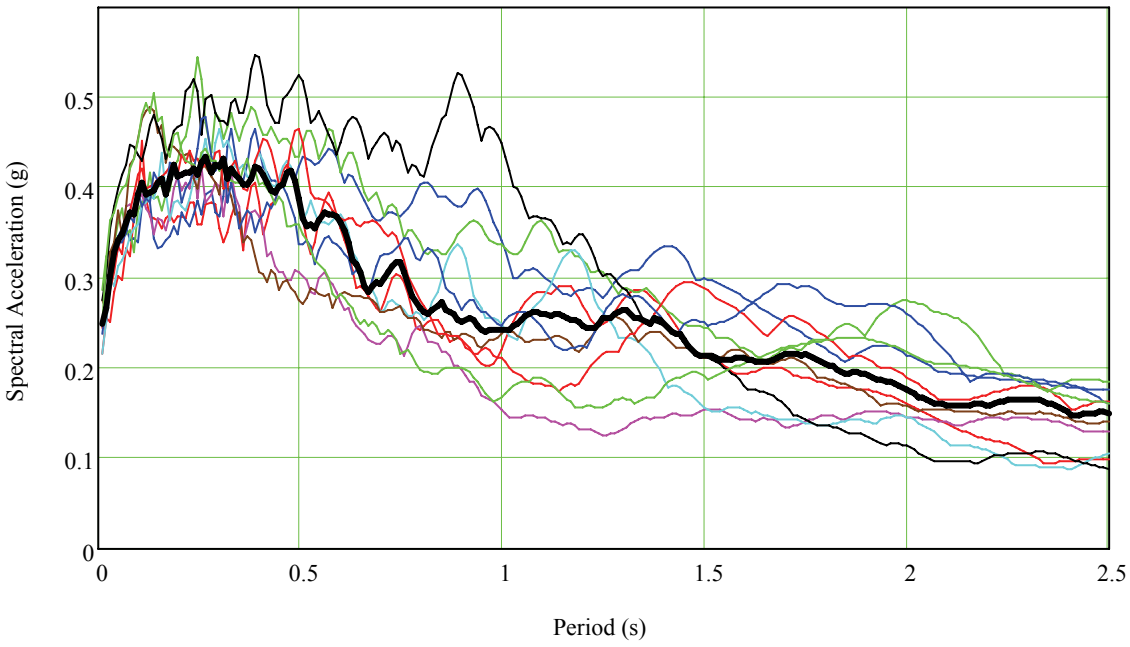

Figure 3.13 UHRS for Memphis Uplands; 5%/50 yr hazard level, 5% damping.

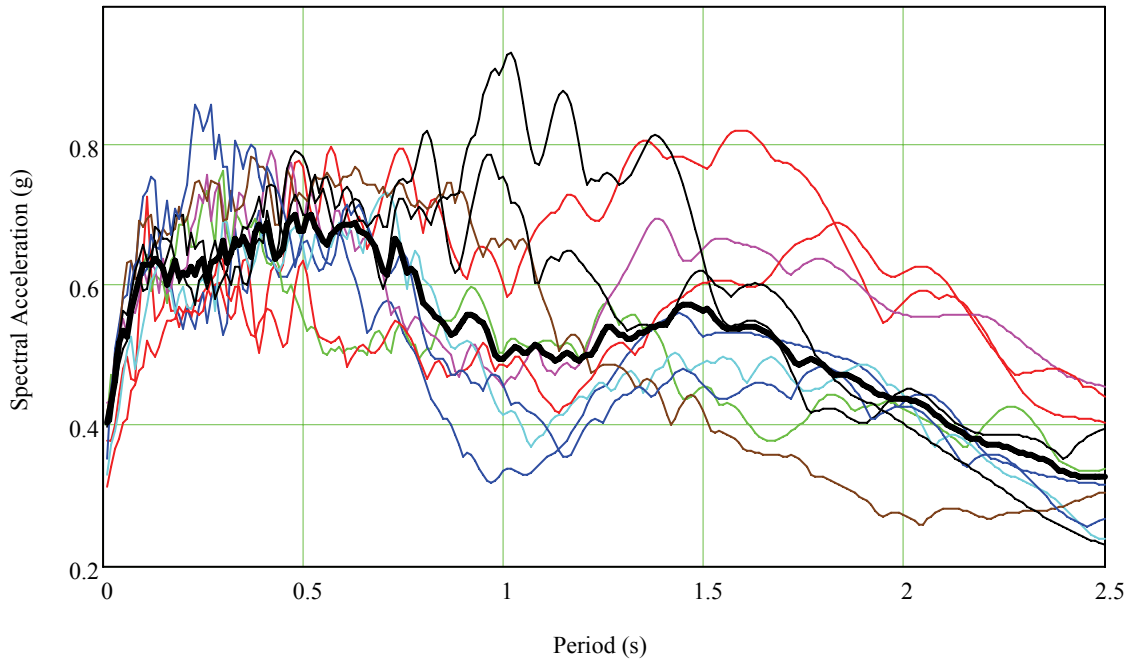

Figure 3.14 UHRS for Memphis Uplands; 2%/50 yr hazard level, 5% damping.

3.4.3 Rix-Fernandez Scenario Ground Motions

Rix and Fernandez (2005)[9] also generated ensembles of ground motions for Memphis, TN corresponding to scenario events occurring in the NMSZ. The sets were synthesized for three earthquake magnitudes (M_w=7.5, 6.5 and 5.5) and four epicentral distances, (R=10, 20, 50 and 100 km), omitting the M_w=7.5 and R=10 km combination, using both the Frankel et al. (1996) and Atkinson and Boore (1995) point source models. These events and distances span the range indicated in the deaggregation plot for Memphis in Figure 3.5. Seismic hazard deaggregation and scenario earthquakes such as these can be used together to assess the seismic demand on the building inventory in a specific area. The 5% damped response spectra for the M_w=7.5, R=20 km ensemble using the Frankel et al. model is presented in Figure 3.15. The thick line indicates the median response spectra. Note that the ground motion ensembles from all of these studies are consistent with the recommendation that a minimum of 3 to 7 records should be used to determine the median and logarithmic standard deviation in seismic demand (SEAOC, 1999).

[9] Rix, G.J., Fernandez, J.A. (2005) Personal Communication.

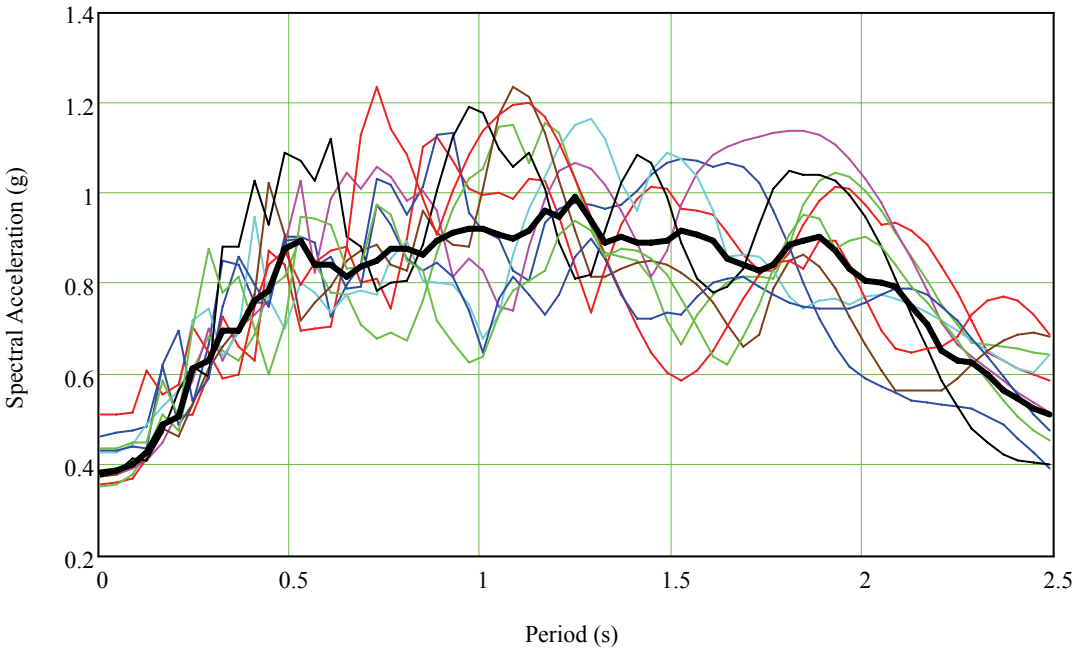

Figure 3.15 Response spectra for M_w=7.5, R=20km ensemble (Records 1-10).

3.5 Comparison of Uniform Hazard GMs (Wen-Wu vs. Rix-Fernandez)

The following differences between Wen-Wu and Rix-Fernandez GMs should be noted:

- The Wen-Wu GMs are based on a generic soil profile, and changes in soil profile in the area are ignored. The Rix-Fernandez GMs were generated using site-specific soil profiles. Soil depth (which is important in regions like the CEUS) was taken into consideration using soil attenuation relationships developed for the Upper Mississippi Embayment.
- The Wen-Wu GMs were created using a single point source model. In contrast, the Rix-Fernandez ensembles were created using three different attenuation models to account for the epistemic uncertainty in ground motion modeling.

- Aleatory uncertainties were incorporated in Rix-Fernandez GMs by treating attenuation parameters as random variables. Wen-Wu GMs, on the other hand, were generated using deterministic parameters.
- The record-to-record variability in the 5% damped response spectra is higher for Rix-Fernandez GMs than Wen-Wu GMs, as can be seen by comparing Figures 3.11 and 3.12.
- For the 2%/50 yr hazard level and Memphis site, Rix-Fernandez GMs predict higher spectral acceleration values for structures having periods longer than 1.2 seconds (cf Figs. 3.8 and 3.14). For structures with shorter periods, Wen-Wu GMs produce higher accelerations (mainly due to the use of quarter wave length method to model soil amplification).
- For the 10%/50 yr hazard level, Rix-Fernandez GMs yield higher spectral accelerations for the whole range of periods (Figs. 3.11 and 3.12).

3.6 Summary

Seismicity in two different regions of the United States was compared. In the WUS, analysts have large databases of natural ground motion records because of the frequency of occurrence of large earthquakes. This is not the case in the CEUS where the records strong enough to threaten the current building stock are scarce. Synthetic ground motions must be relied on for simulations of structural behavior. Two different approaches of generating synthetic GMs were summarized; uniform hazard ground motions (UHGMs) and scenario ground motions. Two plausible sets of UHGMs generated especially for the

CEUS and for Shelby County, TN were compared and their differences were presented. Finally, effects of uncertainty in generating these ensembles were discussed in detail. The impact of the synthetic ground motion ensemble selected for seismic demand analysis on the fragility of steel frames will be considered subsequently in Chapters 5 and 6.

CHAPTER IV

DESCRIPTIONS AND FINITE ELEMENT MODELING OF STEEL FRAMES

4.1 General Modeling Concepts

The level of structural modeling in dynamic simulations of the response of steel frames to earthquakes is of great importance. The complexity of real structures makes modeling a nontrivial task. Stairwells, partition walls, cladding, composite action in floor systems, large openings in elevator areas and complex material behavior are some of the challenges of representing the structural system. As the complexity of a model increases, so does the computational time and effort. The level of modeling should be sufficiently refined to obtain accurate estimates of responses of interest, such as the interstory drift demands, and finally the seismic fragilities. On the other hand, using too refined modeling would not be justified if the uncertainties in seismic demand and limitations in modeling are considered. In this dissertation, fiber sections (divided into 10 sections in direction of bending) and beam-column members with distributed plasticity were utilized. All frame members were divided into 7 elements.

Analytical modeling of all frames in this dissertation has been conducted using OpenSees (Open System for Earthquake Engineering Simulation) program. OpenSees, developed and maintained at the University of California at Berkeley, is an open source software framework for simulating the seismic response of structural systems. It has advanced non-linear modeling capabilities such as distributed plasticity beam-column elements, fiber sections, link elements, etc (Mazzoni at al., 2005).

4.1.1 Modeling Assumptions

The structures modeled and analyzed in this dissertation are reasonably regular in their geometry (no soft stories, re-entrant corners, or torsional eccentricities) and are biaxially symmetric in plan. Under these circumstances, they can be modeled as two-dimensional or planar in nature. One (or two) of the lateral load carrying frames are identified and analyzed assuming that they carry their respective portions of lateral and gravity loads. An inherent assumption here is that contributions from the rest of the structure can be neglected. Another assumption that can be made is that relative rotations of beams and columns in fully-restrained connections can be neglected and can be modeled as perfectly rigid. In all analyses, the structural steel is modeled using a bilinear force-deformation relationship (linear up to the point of yielding with 3% strain-hardening beyond that point).

The beam-column joint region must be modeled to account for the deformations accumulating in that area. Panel zones are formed in these joints. They are neglected in centerline dimensions, however, when actual dimensions are considered, they need to be modeled explicitly. This important aspect of frame modeling is discussed below.

4.1.2 Panel Zone Modeling

Panel zones have good energy dissipation characteristics when designed to sustain stable hysteretic behavior under cyclic inelastic straining (Bertero et al., 1972; Krawinkler et al., 1975). Schneider and Amidi (1998) demonstrated that frame models that do not include

panel zone deformations could underestimate the drift by as much as 10% and could overestimate base shear capacity by 30%. Panel zones that are not properly designed can greatly reduce the overall capacity of the connection (Gupta and Krawinkler, 2000). They may lead to premature shear yielding and prevent the joint from reaching the full strength of the beams or columns that frame into it.

The simplest approach to modeling panel zone behavior is the so-called *scissors* model first proposed by Krawinkler (1978). The portions of the beams and columns within the panel zone are modeled with rigid elements. A rotational spring with an appropriate moment-rotation relationship is placed at the intersection of the beam and column centerlines (Fig 4.1). There are two drawbacks inherent in this approach. First, the shear forces in the panel zone and the moment at the center of the panel zone are related through the beam moments at the face of the column. Second, the panel zone boundaries do not remain orthogonal to the adjacent beams and columns under cyclic deformation which, in turn, results in erroneous estimates of frame deflections.

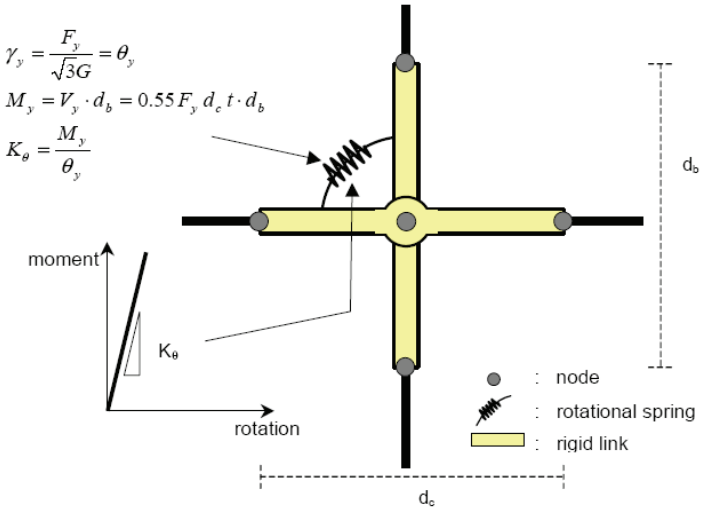

Figure 4.1 Scissors model for panel zone modeling (FEMA 355-F).

A more refined approach is to create a panel zone model with rigid boundary elements and springs (FEMA 355-C). These elements create a panel zone that deforms into a parallelogram. The strength and stiffness contributions of the column web and the column flanges are modeled using two bilinear rotational springs connected in parallel, resulting in a trilinear moment-rotation model of behavior. The resistance after the yielding of the panel zone is due to the bending resistance of the column flanges at the panel zone corners, shown by the stiffness term K_p in Figure 4.2. This model avoids the drawbacks of the scissors model but requires eight rigid members for each panel zone in the analytical model (Fig. 4.3). However, because of the importance of the panel zone model to frame behavior, this refined approach has been utilized in all frames analyzed in this dissertation.

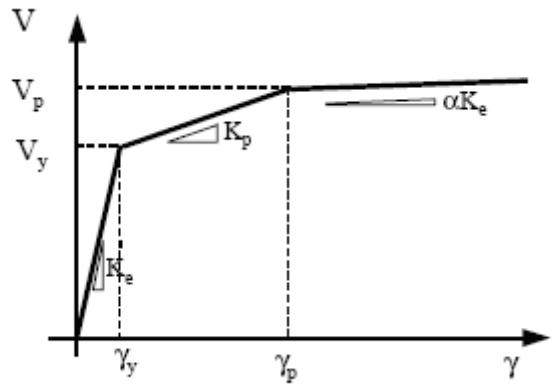

Figure 4.2 Tri-linear force-deformation relationship of panel zone (FEMA 355C).

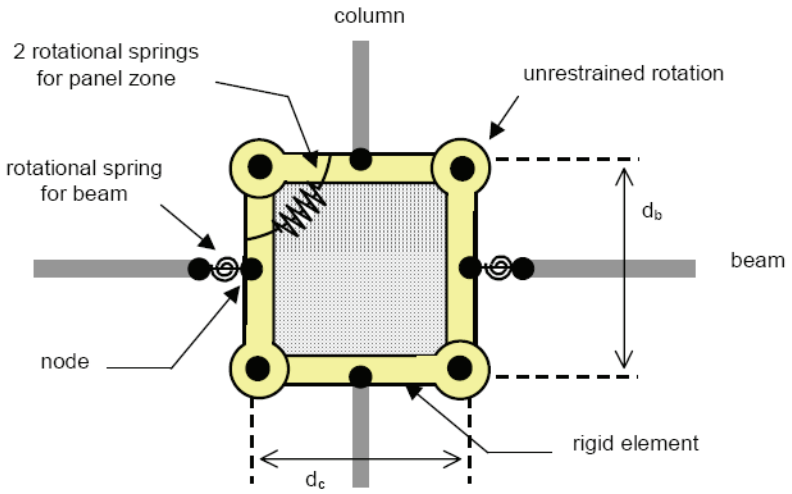

Figure 4.3 Rigid boundary model for panel zone modeling (FEMA 355-F).

The forces and deformations necessary to define the backbone curve of the panel zone model (Fig. 4.2) are summarized below:

$$\gamma_y = \frac{F_y}{\sqrt{3} \cdot G} \tag{4.1}$$

$$\gamma_p = 4 \cdot \gamma_y \tag{4.2}$$

$$V_y = 0.55 \cdot F_y \cdot d_c \cdot t \tag{4.3}$$

$$K_e = \frac{V_y}{\gamma_y} \tag{4.4}$$

$$V_p = V_y \left[1 + \frac{3 \cdot K_p}{K_e} \right] = 0.55 \cdot F_y \cdot d_c \cdot t \left[1 + \frac{3 \cdot b_c \cdot t_{cf}^{\,2}}{d_b \cdot d_c \cdot t} \right] \tag{4.5}$$

$$V = \left[\frac{\Delta M}{d_c} - V_{col} \right] \tag{4.6}$$

where:

γ_y = Yield shear deformation of the panel zone.

F_y = Yield strength of the column.

G = Shear modulus, i.e., $G = E / 2(1+\upsilon)$.

γ_p = Plastic shear deformation of the panel zone.

V_y = Yield shear force demand on the panel zone.

d_c = Depth of column.

t = column web thickness plus thickness of any doubler plates if present.

V_p= Plastic shear force demand on the panel zone.

b_c = Column flange width.

t_{cf}= Column flange thickness.

d_b = Depth of beam.

α = Strain hardening ratio.

Figure 4.4 depicts the application of these formulae using a cyclic load in which the amplitude is increasing linearly.

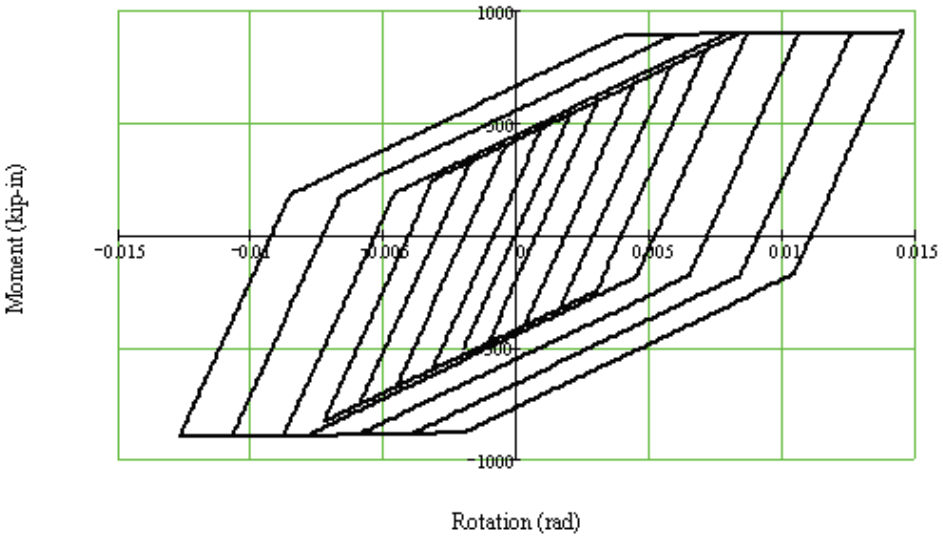

Figure 4.4 Representation of trilinear behavior in OpenSees.

4.2 Steel Building Inventory of Shelby Co., TN and Representative Model Frames

The Mid-America Earthquake (MAE) Center[10] initiated the Memphis Test Bed (MTB) Project as a demonstration project to illustrate the assessment of seismic risk for civil infrastructure in Shelby County, TN, including the city of Memphis. This project is being conducted in collaboration with regional stakeholders who are responsible for anticipating and meeting the needs of the businesses and communities that might be adversely affected by future earthquakes in the NMSZ.

In one of the main thrusts of the project, the current building stock of Shelby County was surveyed and summarized for risk assessment purposes. This part of the project was performed by French and Olshansky (2001). Considering essential buildings

[10] http://mae.ce.uiuc.edu (March 2007)

(schools, fire stations, police stations and hospitals), steel frames comprise one-third of the inventory[11]. Table 4.1 summarizes these data on essential facilities.

Table 4.1 Essential Facilities in Shelby, Co., TN (French and Olshansky, 2001).

Type	Police	Fire	Hospital	School	Total
Steel	21 (16%)	50 (29%)	76 (54%)	171 (27%)	318 (30%)
Concrete	26 (20%)	33 (19%)	33 (24%)	77 (12%)	169 (16%)

To cover the range of steel building structures identified by French and Olshansky (2001), seismic fragilities for five frames of different heights and ages were analyzed in this dissertation. These frames are 2 to 6 stories in height and are typical of design practices from the late 1940s to the 1990s. Further details regarding their construction are provided later in this chapter. The following convention is used throughout this dissertation to designate the frame being analyzed: the first three characters provide information regarding number of stories, e.g., 3ST, 5ST, etc. The fourth character (hyphen) is a separator, and the last two characters define the type of frame i.e., FR for fully-restrained moment frame, PR for partially-restrained moment frame, CB for chevron braced frame, XB for X-braced frame. Table 4.2 summarizes the frames analyzed and their designators.

[11] Approximately 95% of the buildings in the region are wood construction but the majority of these are residential buildings.

Table 4.2 Notation of each frame in this dissertation.

Frame Name	Number of Stories	Lateral Force Resisting System
2ST-PR	2	PR moment frame
3ST-FR	3	FR moment frame
4ST-PR	4	PR moment frame
5ST-CB	5	concentric chevron braced frame
6ST-XB	6	concentric X-Braced frame

4.3 Frame 2ST-PR

4.3.1 Description of Frame

Frame 2ST-PR is a two-story, four-bay partially restrained (PR) moment resisting frame previously analyzed by Barakat and Chen (1991). This frame is very similar to one designed by Lindsey (1987) except for the height of the second story. Its dimensions and member sizes are given in Figure 4.5. The frame is a strong beam-weak column frame, and was designed without any seismic considerations. It was designed using the AISC Specification, 1989 Edition. Two load combinations were considered for strength design: (1.2D+1.6L) and (1.2D+0.5L+1.3W). Serviceability, then, was checked under the un-factored combination (D+L+W). Wind load deflections governed the design of the frame. All members bend around their strong axes. This frame is intended to represent one interior frame of a series of frames which are placed 25 feet (7.62 m) apart. Design dead loads are 68 psf (3.3 kPa) for floor and 20 psf (0.96 kPa) for the roof. Design live loads are 40 psf (1.9 kPa) for floor and 12 psf (0.57 kPa) for the roof. The nominal wind pressure was taken as 20 psf (0.96 kPa). Grade A36 steel was used for all members.

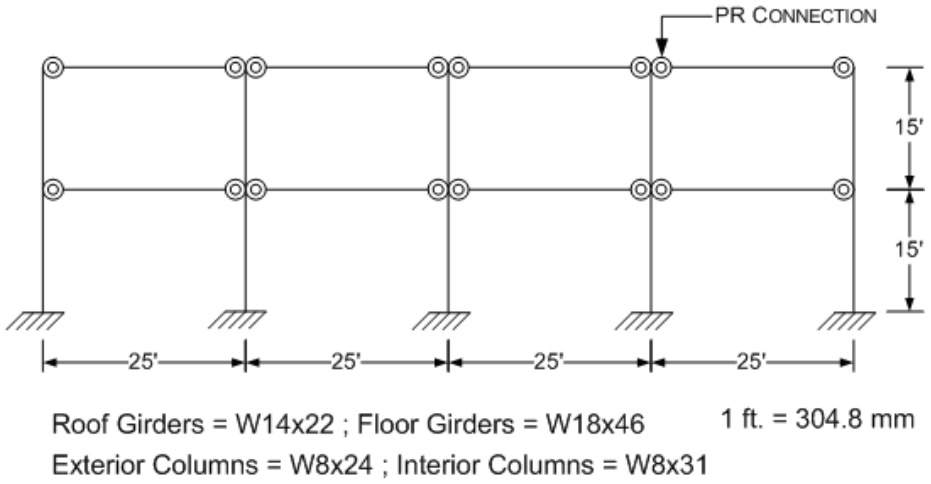

Figure 4.5 Elevation view for Frame 2ST-PR (Barakat and Chen, 1991).

In the structural response analysis of this frame that follows, the mean yield strength of 40 ksi (276 MPa) was adopted for all members, based on the test results performed by Azizinamini et al. (1985) and collected by Kishi and Chen (1986). The clear dimensions of this frame were used in the structural model, i.e., panel zones were modeled explicitly. Material nonlinearity in the beams and columns was taken into account using spread plasticity elements having bilinear behavior with 3% strain hardening. Since the frame is one of several lateral force resisting frames in the building, it is required to carry only its tributary gravity load.

4.3.2 PR Connection Modeling

The connections in Frame 2ST-PR were modeled using rotational springs with moment-rotation relationships adjusted to fit the results of a series of experimental tests discussed in the previous paragraph. The results used as a benchmark in this dissertation were

obtained from a test which used W12×96 column, W14×38 beam, L6×4×5/8 top and seat angles, and L4×3½×1/4 double web angles. The results of this test were normalized by the plastic moment capacity of the joining beam (Fig. 4.6) and the connection behaviors for this study were determined by scaling the backbone curve to match the plastic moment capacity of the joining beam for each connection. Connection backbone curves were modeled with a significant drop in connection strength after relative rotation of 0.04 rad to account for bolt slippage and seat angle failure. Hysteretic model for the cyclic behavior of the connection did not exhibit pinching during the tests. The hysteresis behavior of a typical first story connection is shown in Figure 4.7.

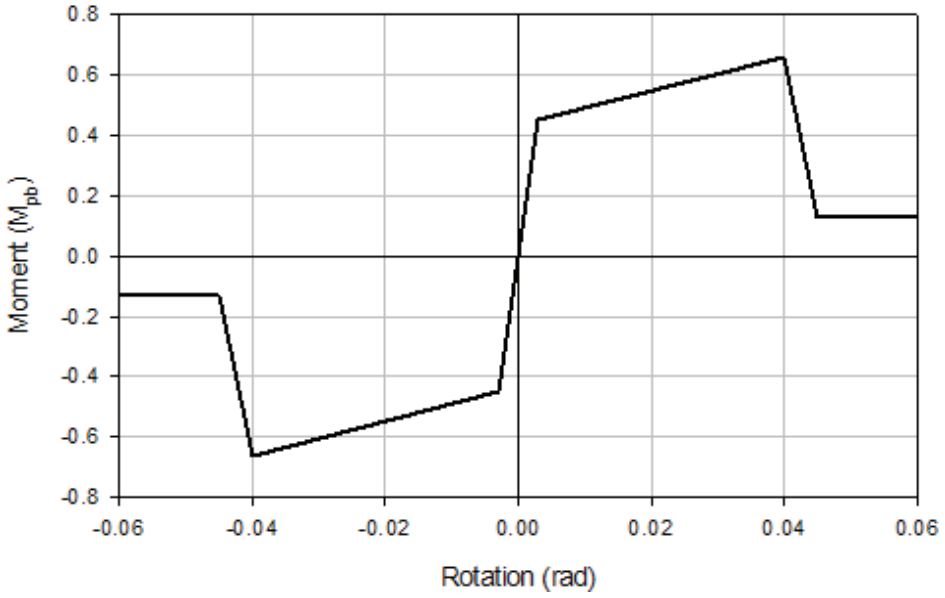

Figure 4.6 Typical moment-rotation envelope for PR connections in Frame 2ST-PR.

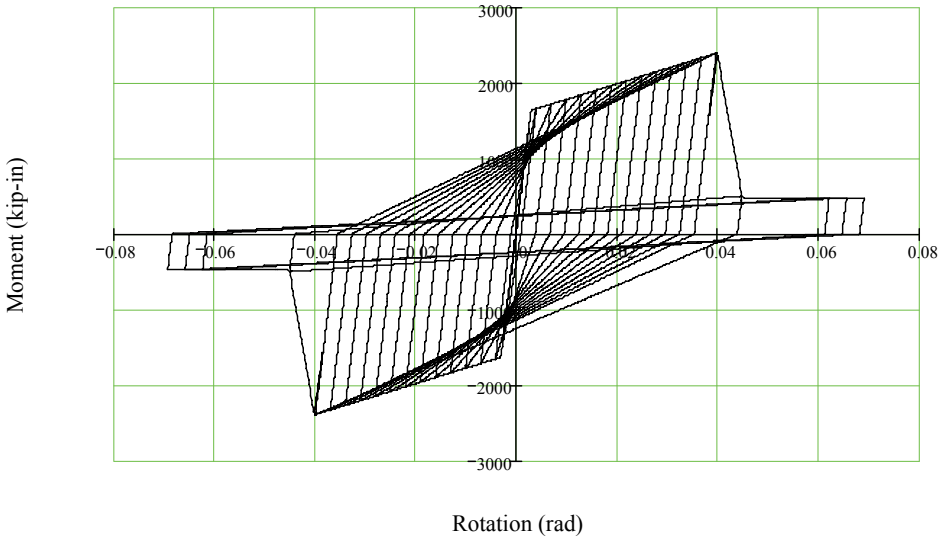

Figure 4.7 First story connection hysteresis behavior as modeled for Frame 2ST-PR.

4.4 Frame 3ST-FR

Frame 3ST-FR (Fig. 4.8) is one of the two four-bay perimeter moment-resisting frames of the three-story Pre-Northridge steel building designed for Boston as part of the recently completed SAC Project. It would be typical of a moment frame in a region of moderate seismicity in the CEUS. It was designed by a consulting structural engineering firm using NBC 1993 Edition. The design of the lateral force resisting system is governed by seismic loads. All beams and columns are A572 Grade 50 steel. Member sizes are given in Table 4.3. Frame 3ST-FR is located in the N-S direction of the building and represents one-half of the lateral load carrying capacity of the building in this direction.

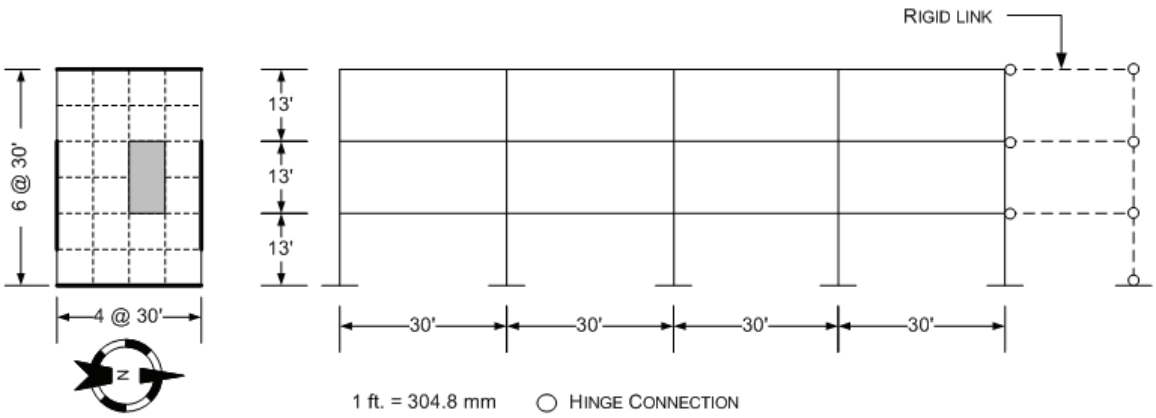

Figure 4.8 Floor plan (FEMA 355-C) and analytical model for Frame 3ST-FR.

Table 4.3 Member sizes for Frame 3ST-FR.

Story	Columns		Girders
	Exterior	Interior	
1	W14×74	W14×99	W21×62
2	W14×74	W14×99	W21×57
3	W14×74	W14×99	W18×35

The following dead and live loads were considered in the analysis of this frame:

Floor dead load for weight calculations: 96 psf (4.6 kPa),

Floor dead load for mass calculations: 86 psf (4.1 kPa),

Roof dead load excluding penthouse: 83 psf (4.0 kPa),

Penthouse dead load: 116 psf (5.6 kPa),

Reduced live load per floor and for roof: 20 psf (0.96 kPa).

The seismic weight carried by Frame 3ST-FR (for the half building) is 1140 kips (5071 kN) for the top floor and 1054 kips (4688 kN) for the other two floors. The maximum interstory drift under nominal wind forces specified in ASCE 7-05 (ASCE,

2005) is roughly equal to $h/700$ (assuming exposure B), in which h = story height. Since common design office practice is to limit the interstory drifts to $h/500$ - $h/400$ under nominal wind load, this frame would be considered overly stiff if wind alone were the governing design consideration. Clear dimensions of this frame were used in the structural model, i.e., panel zones were modeled explicitly to account for the contribution of beam-column panel zones to seismic demand. Material nonlinearities in beams and columns were included in the model using distributed plasticity elements having bilinear behavior with 3% strain hardening. The mean yield strength was assumed to be 57.6 ksi (397 MPa) for all members. The possibility of cracking or deterioration in the connections was not considered. Song and Ellingwood (1999) observed that cracking of welds in frame connections has a significant impact on building response only at larger intensities of ground motion, particularly if the connection deterioration is concentrated at one story. For details of this frame see FEMA 355-C, Appendix B.

In Frame 3ST-FR, two frames in N-S direction represent the lateral strength of the whole structure (Fig. 4.8), and the remaining frames carry only gravity loads. The effects of P-Δ moments (i.e., the overturning moments due to gravitational loads) on these perimeter frames need to be taken into account (Foutch and Yun, 2002). Due to symmetry, each perimeter frame is assumed to carry one-half of the lateral loads; one-half the total structural weight contributes to the P-Δ effect acting on the perimeter columns. First the frame is loaded with distributed loads coming from its tributary area, (half of the first bay in E-W direction); subsequently, the gravity loads on the remaining area of the half-structure are applied to the fictitious column at each story level (see Fig. 4.8). This column is connected to the moment frame using rigid links with pinned-ends. Thus, any stiffness

contribution of the interior columns to the lateral stiffness of the frame is neglected in this model while accounting for the effects of additional overturning moments that develop in the structure. Foutch and Yun (2002) found out that the contribution of gravity loads coming from the interior frames can be quite large, especially for perimeter frames. This method is conservative since it accounts for detrimental P-Δ effects while neglecting any stiffness contribution from interior frames.

4.5 Frame 4ST-PR

4.5.1 Description of Frame

Frame 4ST-PR is taken from a 4-story, 3-bay building (Fig. 4.9) in which both perimeter and interior frames have PR moment connections. The building was designed for the CEUS according to practices in the 1950s using the 1948 Joint Committee Recommendations of San Francisco for lateral loads and the 1952 AISC Steel Construction manual for gravity loads (Leon and Kim, 2004). A36 grade steel has been used for all members. Member sizes are given in Table 4.4.

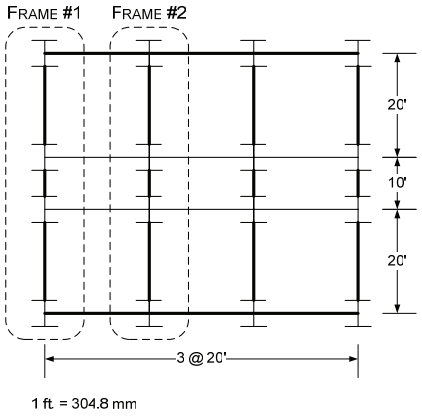

(a) Floor plan

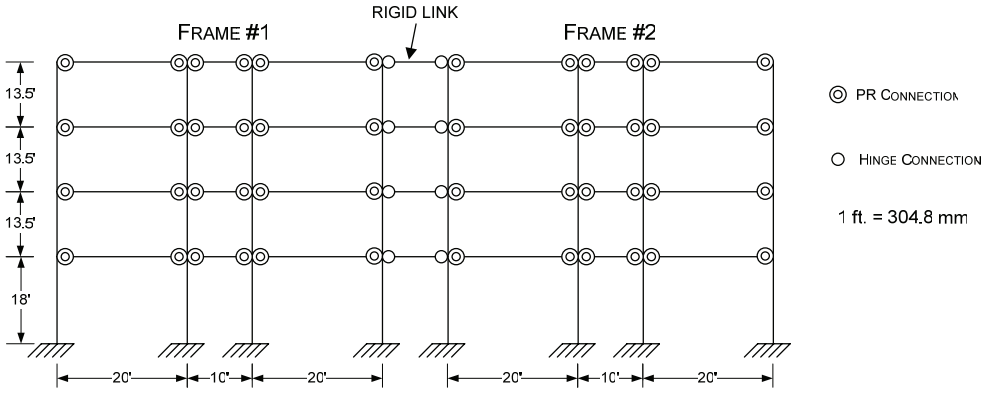

(b) Analytical model

Figure 4.9 Floor plan and analytical model for Frame 4ST-PR (Leon and Kim, 2004).

Table 4.4 Member sizes for Frame 4ST-PR.

Story	Columns		Beams	
	Exterior	Interior	Exterior	Center
1	W10×49	W10×60	W18×50	W12×26
2	W10×49	W10×60	W18×50	W12×26
3	W10×33	W10×39	W18×50	W12×26
4	W10×33	W10×39	W16×50	W8×21

Nominal loads used to design this frame are as follows:

Dead Load: 80 psf (3.8 kPa),

Live Load: 60 psf (2.9 kPa),

Wind Pressure: 20 psf (0.96 kPa).

The wind load combination (D+L+W) governed the design of the lateral force-resisting system of Frame 4ST-PR. In order to investigate the effects of connection stiffness and cyclic behavior on the older steel moment resisting frames, two different connection types were studied using this frame: Clip Angle (CA) and T-Stub (TS) connections. For details of this frame, the reader is referred to Kim (2003). Frame 4ST-PR with CA and TS connections are denoted in this study as 4ST-PR(CA) and 4ST-PR(TS), respectively.

The lateral force-resisting system was modeled by two moment-resisting frames connected with rigid links (Fig. 4.9b). The connected frames represent one exterior and one interior frame. The mean value of the yield strength of Grade A36 steel manufactured in the 1950's - 1960s is approximately 40 ksi (276 MPa) (Galambos and Ravindra, 1978). This value has been used in the analyses of this frame. Material nonlinearities were included in the model using distributed plasticity elements having bilinear behavior with 3% strain hardening. The structural model of Frame 4ST-PR also includes the explicit modeling of beam-column panel zone behavior (See Section 4.1.2). One-half of the whole building is represented in the analytical model and their tributary areas cover the area of the half building, leaving no additional overturning effects; therefore, there is no need for a fictitious P-Δ column in modeling Frame 4ST-PR.

4.5.2 CA and TS Connection Modeling

Clip angle and T-Stub connections were modeled using the results of experimental tests of connections, utilizing rotational springs with moment-rotation relationships adjusted to fit the experimental results. The cyclic behavior of the CA connection, which is relatively stable with no degradation, was derived from the test results by Altman et al. (1982), as summarized in Figure 4.10. This is a relatively weak connection; the beam used in this experiment has plastic moment capacity of 2184 k-in (247 kN-m). In other words, the connection can develop only 40% of the beam plastic moment. The capacity of each connection in the frame was adjusted depending on the plastic moment capacities of their joining beams. Frame 4ST-PR(TS) was modeled in a similar way using the results of the tests performed by Forcier (1994). The beam used in the experiment had a plastic moment capacity of 4646 k-in (525 kN-m). In contrast to the CA connections, the TS connections exhibited pinching behavior and were modeled accordingly. This connection is stiffer and stronger than the CA, and develops 65% of the beam capacity. Figure 4.11 shows a typical connection hysteresis in Frame 4ST-PR(TS) along with the mathematical representation in OpenSees, used in this dissertation.

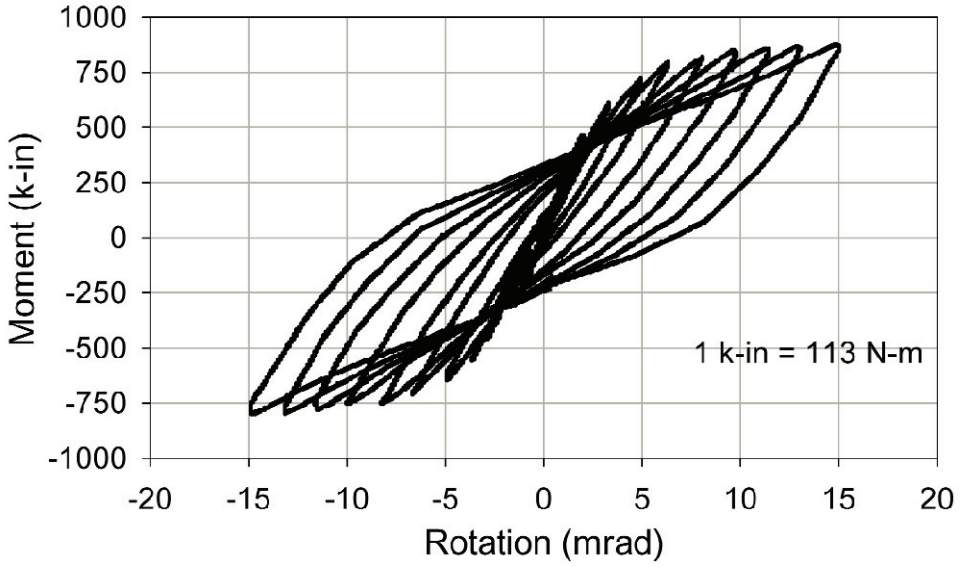

Figure 4.10 Hysteretic behavior of the CA connection (Altman et al., 1982).

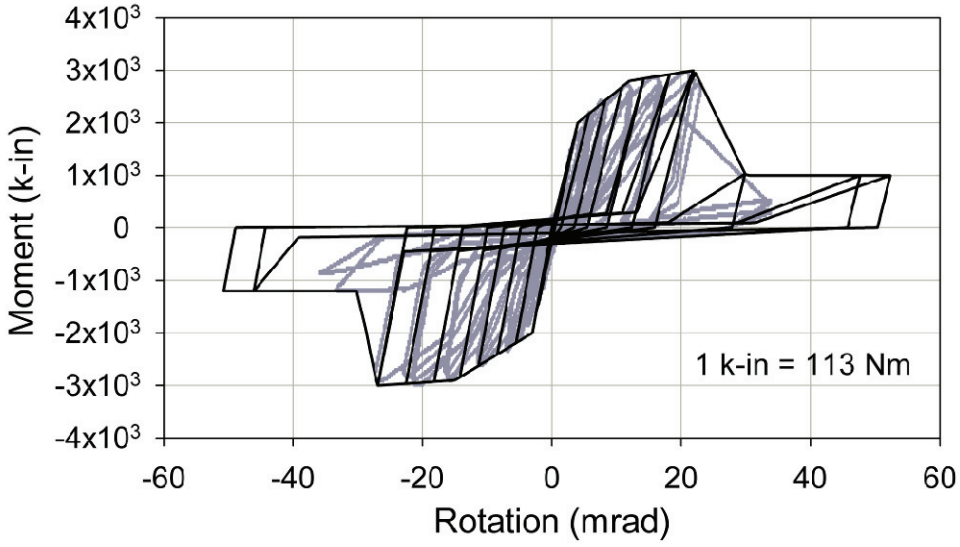

Figure 4.11 Experimental hysteretic behavior for the T-Stub connection (Forcier, 1994) and its mathematical representation.

4.6 Frame 5ST-CB

4.6.1 Description of Frame

Frame 5ST-CB is a 3-bay interior chevron-braced frame of a 5-story steel building designed for and constructed in Memphis, TN (Fig. 4.12). It was designed by a consulting firm in the southeast using the Standard Building Code (SBC) 1988 Edition and the AISC 1989 specification for allowable stress design. A572 Grade 50 steel was used for all members except the exterior columns, which are A36 steel, and the brace members, which are ASTM A500 Grade B steel. The configuration of the chevron braces is such that they are not symmetric, i.e., they do not meet in the midpoint of the floor beams, they are not of the same length and the bracing sections are different in 4 out of 5 stories. Beams of the exterior bays are identical as well as the exterior columns; however, the interior columns are not identical. The frame has a uniform story height of 12'-8" (3.86 m) and a uniform bay width of 30 ft (9.14 m). Since the loading information was not provided by the Engineer of Record (EOR), same loading information used in Frame 3ST-FR above was utilized in this frame. All beam-column connections are shear connections. Exterior columns in the frame are oriented in their weak-axis directions, while the interior columns are loaded in strong-axis bending. The columns are spliced at the second floor level. The weight of the frame is 1350 kips (6,005 kN). Member sizes are given in Table 4.5.

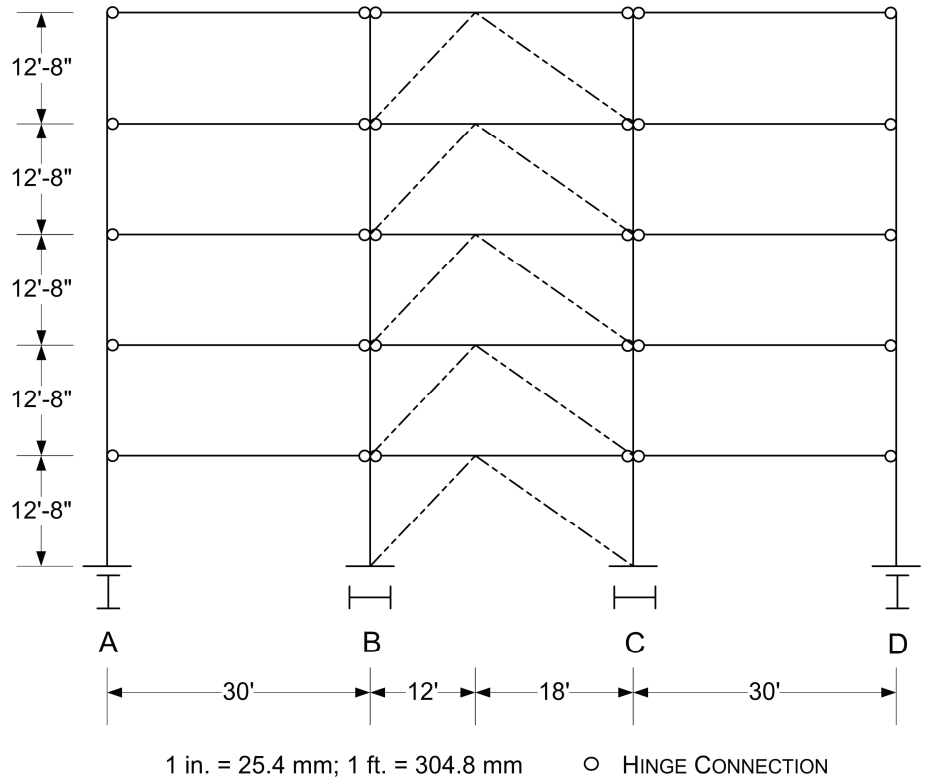

Figure 4.12 Analytical model for Frame 5ST-CB.

Table 4.5 Member sizes for Frame 5ST-CB.

Story	Columns			Beams		Braces	
	Line B	Line C	A&D	Interior	Exterior	Short	Long
1	W12×136	W12×120	W12×96	W18×50	W16×26	TS8×8×5/16	TS8×8×1/2
2	W12×136	W12×120	W12×96	W18×50	W16×26	TS8×8×5/16	TS8×8×1/2
3	W12×72	W12×58	W12×65	W18×50	W16×26	TS8×8×5/16	TS8×8×3/8
4	W12×72	W12×58	W12×65	W18×50	W16×26	TS8×8×1/4	TS8×8×5/16
5	W12×72	W12×58	W12×65	W16×36	W16×26	TS8×8×1/4	TS8×8×1/4

All beams and columns were modeled using nonlinear beam-column elements with distributed plasticity. Panel zones were modeled for the interior beam-column joint regions but not for the exterior columns since they were oriented in their weak-axis direction. All beam-column connections are simple connections. Both material and geometric nonlinearities were taken into consideration. Brace members were modeled as

axially-loaded members. All bracing connections were idealized as pinned connections. The bilinear force-deformation relation for all beam and column members included 3% strain hardening. Details of brace member modeling are presented below.

4.6.2 Brace Member Modeling

The behavior of a brace member is dependent on three factors: its buckling load (P_{cr}), post-buckling residual strength and its tension yield capacity (P_y). A typical constitutive model (axial load vs. axial displacement) is presented in Figure 4.13. Post-buckling compressive load carrying capacity, $P_{residual}$, is a factor, *c*, times P_{cr}. The value of *c* is still a topic for research, with values around 0.2-0.4 being reported in the literature (Jain et al., 1980; Tremblay, 2002; Goggins et al., 2006). The value of axial displacement at which $P_{residual}$ is reached can be assumed to be $5\Delta_y$, a value originally proposed by Jain and Goel (1978) and adopted in FEMA-274.

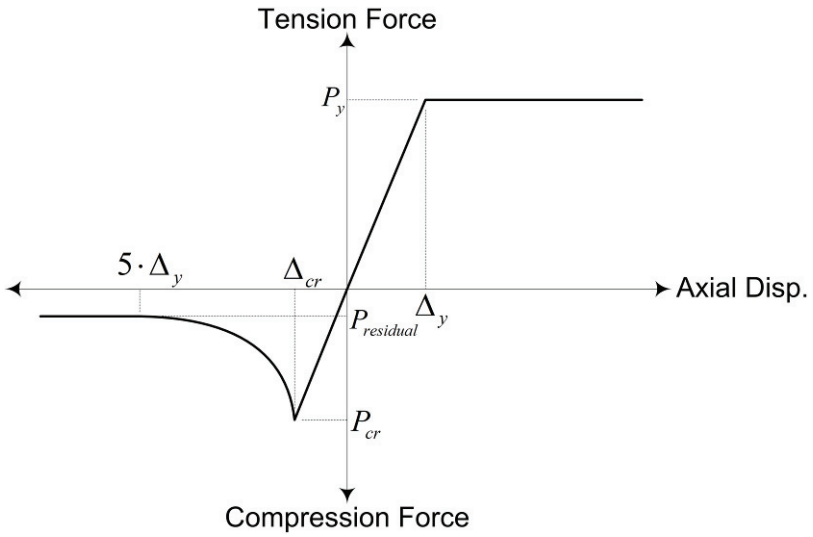

Figure 4.13 The constitutive relationship for typical brace behavior.

The expected strengths of braces were calculated using effective length factor k = 0.8 for in-plane buckling and k = 1.0 for out-of-plane buckling. These values were taken from FEMA-274. Frame 5ST-CB has square tubular sections as bracing members; therefore, out-of-plane buckling always controlled with k = 1.0. The nominal yield strength for ASTM A500 Grade B steel is 46 ksi (317 MPa). No data could be located to define the mean value for this grade of steel. Accordingly, it was assumed that ratio of mean value to nominal value is 1.07, a value typical for similar carbon steels (Galambos and Ravindra, 1978). Thus, the mean value for the yield strength of the braces was assumed to be 46 ksi ×1.07 = 49.2 ksi (339 MPa). The AISC Manual of Steel Construction LRFD, Second Edition (AISC, 1994) has been used to calculate the buckling loads of bracing members (Table 4.6). The values were adjusted in order to reflect the expected yield strength of the steel used in these members, i.e., F_y = 49.2 ksi (339 MPa). The tabulated values in the manual are for design purposes, already multiplied by factor 0.85 and are for nominal yield strength, F_y = 46 ksi (317 MPa). Therefore, a factor has been used to adjust the buckling load of the members;

$$\text{Strength ratio} = \frac{1}{0.85} \cdot \frac{49.2}{46.0} = 1.26 . \tag{4.7}$$

Table 4.6 summarizes the results of the calculations for all braces in the system. The capacity of the bracing elements was governed by the capacity of the braces, not by the fracture of the connecting elements i.e., gusset plates. The typical cyclic behavior of one of the braces is illustrated in Figure 4.14.

Table 4.6 Brace properties for Frame 5-ST-CB.

Member	Section	A (in^2)	P_{cr} (kips) [Manual]	Strength Ratio	P_y (kips)	Pcr (kips)	Δ_y (in)	Δ_{cr} (in)
S.1-SH.[a]	TS 8×8×5/16	9.36	271	1.26	460.5	341.5	0.355	0.263
S.1-LO.[b]	TS 8×8×1/2	14.4	338	1.26	708.5	425.9	0.448	0.269
S.2-SH.	TS 8×8×5/16	9.36	271	1.26	460.5	341.5	0.355	0.263
S.2-LO.	TS 8×8×1/2	14.4	338	1.26	708.5	425.9	0.448	0.269
S.3-SH.	TS 8×8×5/16	9.36	271	1.26	460.5	341.5	0.355	0.263
S.3-LO.	TS 8×8×3/8	11.1	266	1.26	546.1	335.2	0.448	0.275
S.4-SH.	TS 8×8×1/4	7.59	220	1.26	373.4	277.2	0.355	0.264
S.4-LO.	TS 8×8×5/16	9.36	226	1.26	460.5	284.8	0.448	0.277
S.5-SH.	TS 8×8×1/4	7.59	220	1.26	373.4	277.2	0.355	0.264
S.5-LO.	TS 8×8×1/4	7.59	185	1.26	373.4	233.1	0.448	0.280

[a] Story-1, short bracing member.
[b] Story-1, long bracing member.
1 kip = 4.45 kN; 1 in = 25.4 mm.

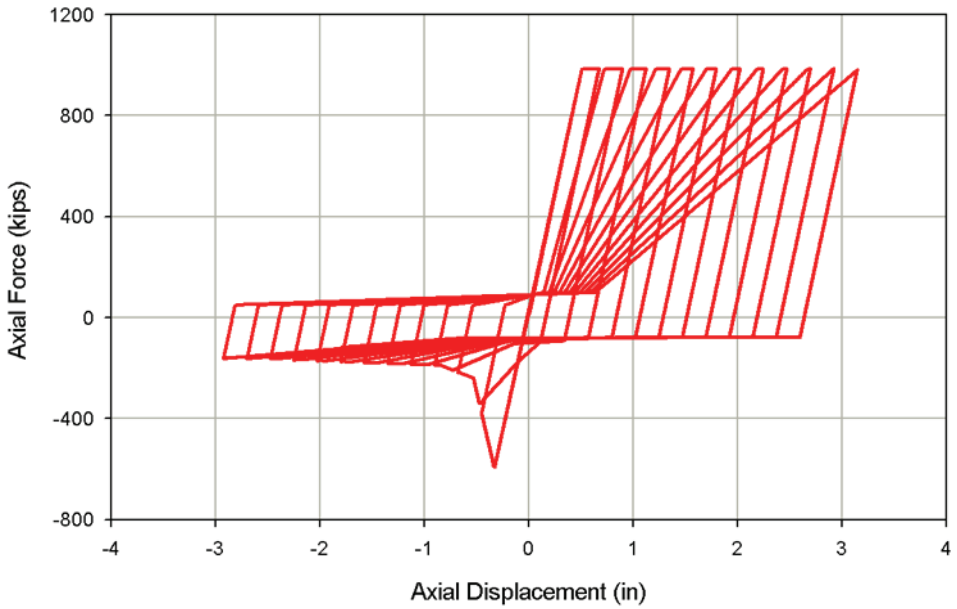

Figure 4.14 Typical cyclic behavior of a brace.

4.7 Frame 6ST-XB

4.7.1 Description of Frame

Frame 6ST-XB (Fig. 4.15) is a 3-bay X-braced interior frame of a 6-story steel building designed for and constructed in Memphis, TN. It was designed by a consulting firm using the SBC 1991 Edition and the AISC 1989 Specification for allowable stress design. The building is regular in plan, with three bays, of which two exterior bays are identical. It was framed with A572 Grade 50 steel for all beams and columns. The braces are of ASTM A500 Grade B steel. Loading information was assumed to be the same as for Frame 3ST-FR in Section 4.4 due to the lack of sufficient information from the EOR. All beam-to-column connections in this frame are shear connections; therefore the lateral stiffness of the frame is dependent solely on the truss action in the diagonal bracing system. Columns are spliced at every second floor level. Exterior columns are oriented to bend around their strong axes, while the interior columns bend around their weak axes. The weight of the frame is 2,245 kips (9,986 kN). Member sizes are given in Table 4.7.

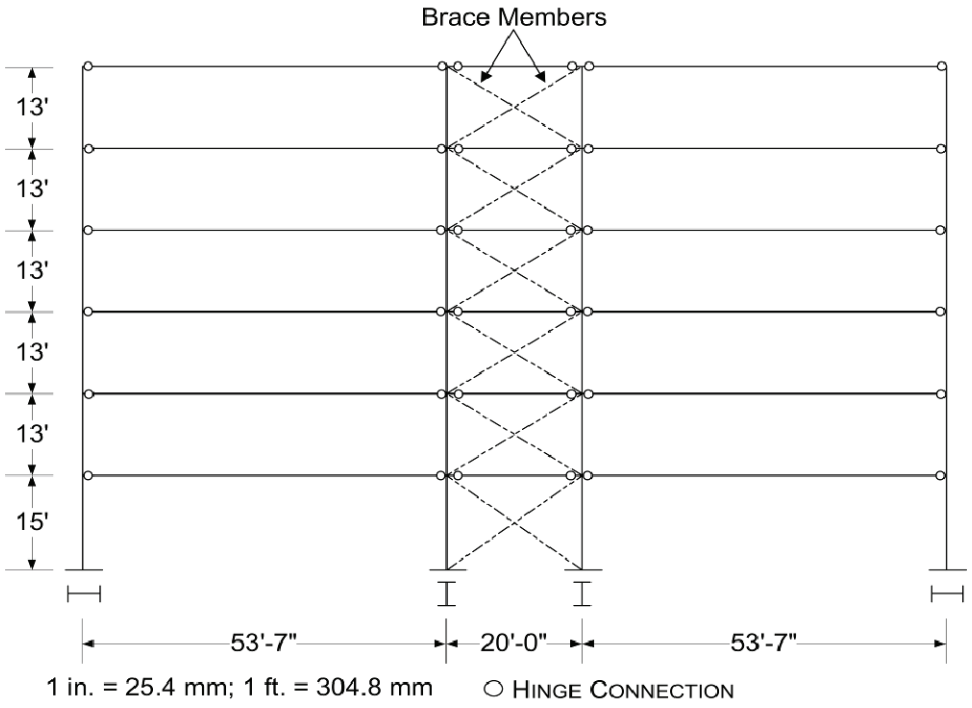

Figure 4.15 Analytical model for Frame 6ST-XB.

Table 4.7 Member sizes for Frame 6ST-XB.

Story	Columns		Beams		Braces
	Interior	Exterior	Interior	Exterior	
1	W12×170	W14×145	W16×36	W21×57	TS8×8×1/2
2	W12×170	W14×145	W16×36	W21×57	TS8×8×3/8
3	W12×106	W12×72	W16×36	W21×57	TS8×8×5/16
4	W12×106	W12×72	W16×36	W21×57	TS8×8×1/4
5	W12×58	W12×72	W16×36	W21×57	TS8×8×1/4
6	W12×58	W12×72	W24×62	W24×62	TS7×7×1/4

All beams and columns were modeled using nonlinear beam-column elements with spread plasticity. Both material and geometric nonlinearities were taken into consideration. The force-deformation relation for all beams and columns was bi-linear, with 3% strain hardening. The panel zones were modeled for the exterior beam-column

joint regions but not for the interior columns since they were oriented in their weak-axis. All connections were idealized as pinned connections.

4.7.2 Brace Member Modeling

Brace members in Frame 6ST-XB were modeled in the same way as those in Frame 5ST-CB, with a similar axial force-axial deformation relationship (Fig. 4.14). Buckling loads are, in general, smaller than those in the previous frame due to their lengths. Results of brace calculations for this frame are given in Table 4.8. As with Frame 5ST-CB, the capacity of the bracing elements was governed by the capacity of the members rather than by the fracture strength of the gusset plates.

Table 4.8 Brace properties for Frame 6ST-XB.

Story	Section	A (in^2)	P_{cr} (kips) [Manual]	Strength Ratio	P_y (kips)	P_{cr} (kips)	Δ_y (in)	Δ_{cr} (in)
1	TS 8×8×1/2	14.4	291	1.26	708.5	366.7	0.509	0.263
2	TS 8×8×3/8	11.1	243	1.26	546.1	306.2	0.486	0.273
3	TS 8×8×5/16	9.36	207	1.26	460.5	260.8	0.486	0.276
4	TS 8×8×1/4	7.59	170	1.26	373.4	214.2	0.486	0.279
5	TS 8×8×1/4	7.59	170	1.26	373.4	214.2	0.486	0.279
6	TS 7×7×1/4	6.59	124	1.26	324.2	156.2	0.486	0.234

1 kip = 4.45 kN; 1 in = 25.4 mm.

4.8 Summary

Five steel frames ranging from 2 to 6 stories in height were assumed to represent the steel building inventory of Shelby Co., TN. The frames included designs from late 1940s through early 1990s. Out of 5 model frames, one is rigid frame (3-story), two of them are

PR moment frames (2- and 4-stories) and remaining two are braced frames (5- and 6-stories). General finite element modeling issues were discussed. Details of the frames used in this dissertation are summarized in Table 4.9.

Table 4.9 Details of the model frames.

Frame	# of stories	Height	Type	Code Year
2ST-PR	2	30’	PR MRF[a]	1989
3ST-FR	3	39’	FR MRF[b]	1993
4ST-PR	4	58’-6”	PR MRF	1948
5ST-CB	5	63’-4”	Chevron Braced Frame	1988
6ST-XB	6	80’	X-Braced Frame	1989

[a] Partially Restrained Moment Resisting Frame.
[b] Fully Restrained Moment Resisting Frame.

CHAPTER V

SEISMIC PERFORMANCE ASSESSMENT OF FRAMES

5.1 General Analysis Methods

Central to the development of quantitative seismic risk assessment tools to evaluate the performance of steel buildings is a finite element model of the structure that represents its strength and stiffness characteristics. This model is the basis for an analysis to predict the values of various seismic response parameters when the steel building frame is subjected to earthquake ground motion. Analysis procedures that have evolved in the past decade are reviewed below, with regard to their advantages and shortcomings for fragility analysis of steel frames.

5.1.1 Nonlinear Static Pushover Analysis

A Nonlinear Static Pushover Analysis (NSPA) estimates the strength and deformation demands on a structural system subjected to an earthquake through a relatively efficient static analysis (Krawinkler and Seneviratna, 1998). A static predetermined force pattern is applied laterally to the structure at floor levels over the height in increasing intensity until a predefined response at a target point is reached. This method predicts inelastic seismic deformation demands while accounting for the redistribution of internal forces in the inelastic range of the structural behavior, highlighting the importance of nonlinear behavior by using both material and geometric nonlinearities.

Two important issues in NSPA are the target displacement limit and the applied lateral load pattern. The target displacement represents the response that system must sustain in a design (or performance assessment level) earthquake. Generally, the roof displacement is chosen to be the control variable and the system is displaced until either a predetermined level of deformation at the roof level is reached or instability occurs, manifested by ill-conditioning of the stiffness matrix. This level often is estimated from displacement spectra, using an equivalent SDOF system to obtain the displacement demand, and transforming it to the roof displacement of the MDOF structure by using an appropriate shape vector (FEMA-355C). The analysis is terminated once a global drift of 10% is reached, since the results obtained from most finite element programs used for building response predictions become questionable after that point. The gravity loads are applied to appropriate elements of the model during the analysis. Due to the degrading nature of some systems (plastic hinging at the columns, brace buckling, etc.), zero or, even negative lateral stiffness can be encountered.

The lateral load pattern applied to the system is intended to model the vertical distribution of lateral inertial forces during an earthquake. However, inertial forces vary from record to record and with time during the excitation. Krawinkler and Seneviratna (1998) noted that the assumptions made in the NSPA are reasonable if the structure is first mode dominant and has a single yielding mechanism that can be detected by an invariant lateral load pattern. For a better understanding of the response of a system, multiple load patterns such as uniform, linear and quadratic distributions can be employed. This enables analysts to understand the behavior of the system rather accurately and to identify any soft story mechanisms, yielding patterns, etc. However, the

invariance in the inertial force distribution in the system during the course of excitation is a major drawback for this method. Mwafy and Elnashai (2001) argued that pushover analysis is more dependable for low-rise structures with short first-mode periods due to the increasing importance of higher modes in taller structures.

The results of a NSPA are highly dependent on the distribution of the lateral forces. The distribution of lateral forces is calculated as follows:

$$V_i = \frac{w_i \cdot h_i^{\ k}}{\sum_{i=1}^{n} w_i \cdot h_i^{\ k}} \tag{5.1}$$

where V_i = force at i^{th} level; w = floor weight; h = floor height from the base level; n = number of stories; and k = factor related to the shape of the fundamental mode. In the SAC program, pushover analyses of moment frames were performed assuming that $k = 2$. The accuracy of the NSPA depends on the validity of the assumption that the response of a multi degree-of-freedom (MDOF) system can be approximated by that of a SDOF system. In other words, it is assumed that the response of the building system is strongly dependent on the first mode and furthermore, that the shape of this mode remains constant during the time history of the excitation. Studies have shown that for single-mode governed systems, maximum seismic response can be estimated rather accurately by NSPA.

5.1.2 Nonlinear Time History Analysis

In a Nonlinear Time History Analysis (NTHA), the response of the structure to a suite of ground motion time histories is determined through numerical integration of the

equations of motion for the structure. The structural stiffness is altered during the analysis to conform to the nonlinear hysteretic models of the structural components. Both material nonlinearity and geometric (P-Δ) effects are taken into consideration. NTHA avoids many of the assumptions made in the NSPA. It accounts for higher mode effects and for shifts in inertial load patterns as structural softening occurs. Furthermore, for a given ground motion record, it yields the maximum global displacement demand produced by the record, eliminating the need for estimating it from empirical relationships, (e.g., Equation 3.11 of FEMA-273).

However, this approach requires much more numerical effort than the NSPA and is highly sensitive to the particular earthquake record used. Two ground motion records sampled from the same normalized set of records may yield drastically different results. To overcome this sensitivity, the response of the system to an ensemble of accelerograms is determined and the results are post-processed statistically. A sufficient number of accelerograms must be utilized in each ensemble to draw healthy conclusions from the statistical analyses. In the present study, sets of at least 10 records form an ensemble, which is more than suggested minimum number of 3-7 records by the Structural Engineers Association of California (SEAOC). NTHA generally would be impractical for rapid assessment of complex structural systems.

5.1.3 Incremental Dynamic Analysis

Incremental Dynamic Analysis (IDA) method is a sequential form of NTHA. Shome et al. (1998) demonstrated that scaling ground motion records to a target spectral acceleration

at the first mode period of the structure is an efficient way of characterizing seismic demand at that particular intensity level. An IDA involves multiple nonlinear dynamic analyses of a structure subjected to ensembles of earthquake records which are scaled upward from the elastic range to reveal the behavior of the structure under very large demands up to the verge of collapse. The results of the IDA produce a plot of Response Measure (RM) (described subsequently) vs. Intensity Measure (IM, generally measured by $S_a(T_1)$), which terminates at the point beyond which the analysis does not converge or, where the slope of the line connecting discrete points drops below a certain percent, often 20% (Vamvatsikos and Cornell, 2002) of the initial slope, whichever occurs first. Generally, a single IDA plot involves 20 to 30 increments of ground motion intensity, and thus represents a considerable computational effort.

In this dissertation, different ground motion intensity increments were used to assess the seismic performance of the various frames considered. The braced frames were most sensitive to small increments in ground motion intensity since the buckling of a brace is almost instantaneous. Thus, the increments of 0.02g were utilized for braced frames not to miss the points of successive brace buckling. Conversely, the largest increment, i.e., 0.1g, was used in Frame 3ST-FR since it is a low-rise rigid frame with regular geometry. For the PR frames, however, a finer increment of 0.05g was employed to capture the effects of connection failure better.

5.2 Structural Response Measures

A Response Measure (RM) is a positive scalar quantity that describes the response of a structure to a static lateral force, a dynamic loading from ground motion, or other demand parameter. When the demand and response are dynamic, an envelope of damage, i.e., the maximum response during the excitation, is recorded and used. There are many possible choices for RM such as; roof displacements, interstory drift angle (ISDA, defined as the relative story drift divided by story height), joint rotations, floor accelerations, etc. Which RM to choose depends on type of structure, type of analysis and the performance level of interest. For instance, floor accelerations are suitable for expressing damages to non-structural building contents. Interstory displacements, on the other hand, relate closely to nonstructural partition or cladding damage and provide insight regarding the potential for local or global instability or collapse of the structure under gravity loads. Maximum interstory drift angle has been related to several structural response levels of steel frames by FEMA-273 and other sources.

Shome and Cornell (1999) suggested a relation between maximum interstory drift angle, (θ) and first mode spectral acceleration, (S_a) having the following simple form;

$$\theta = a \cdot S_a^{\,b} \cdot \varepsilon \tag{5.2}$$

where ε = random variable with *median = 1* and logarithmic standard deviation, $\sigma_{ln\varepsilon}$, that describes the uncertainty in the relationship. Estimates of these model constants (*a* and *b*) and the standard error can be determined by performing nonlinear dynamic analyses of the building frame using an appropriate ensemble of ground motions, determining the resulting maximum ISDAs, and performing a linear regression analysis of $ln\ \theta$ on $ln\ S_a$ to

determine constants a, b and $\sigma_{ln\varepsilon}$. Studies (e.g., Cornell et al., 2002) have suggested that $b \approx 1$ may be an appropriate value for steel frames. The value $b = 1$ is also consistent with the well-known equal displacement rule (Veletsos and Newmark, 1960) for frames with fundamental periods greater than 0.5 sec.

5.3 Structural Performance Levels

Performance based structural engineering requires structures to meet pre-defined performance levels with certain confidence. This, in turn, requires the identification of quantitative performance limits expressed in terms of response measures such as interstory drifts, floor accelerations, joint rotations, etc. Three different levels of performance are considered in this dissertation: Immediate Occupancy (IO), Structural Damage (SD) and Collapse Prevention (CP). These levels are related to appropriate RMs in the buildings. Although FEMA-273 contains recommended performance levels for several construction technologies, most of the suggested limits are based on professional judgment and are believed to apply mainly to building construction in high-seismic zones. Only steel moment-resisting frames governed by seismic design requirements have been studied in detail in the recent SAC Project (Yun et al., 2002; Lee and Foutch, 2002).

5.3.1 Immediate Occupancy (IO)

The Immediate Occupancy (IO) level is the state at which the building is safe to be occupied immediately following the earthquake with little or no repair. This requires that

the structure remains essentially in the elastic range during the earthquake and that non-structural components of the building are not damaged significantly. The elastic range of the structure is determined from the NSPA curve. In steel structures, unlike reinforced concrete buildings, there is a clear region of linearity in the early stages of the NSPA. The level of deformation beyond which the curve becomes nonlinear can be considered as the limit of the IO level. Generally, this level corresponds to approximately 0.8-1.0 % interstory or roof drift for buildings with steel moment-resisting frames (Song and Ellingwood, 1999; Kinali and Ellingwood, 2007a).

5.3.2 Structural Damage (SD)

In FEMA 273/356 (FEMA, 1997/2000), the intermediate damage state is identified as Life Safety. Relating this performance level to a response measure determined from structural analyses has proved to be problematic, as there is no obvious way of quantifying the ISDA or floor acceleration that threatens life safety; these limits clearly would depend on details of building construction. While the life safety limit would generally be expected to fall between IO and CP limits, it also depends on the building occupancy. For instance, floor accelerations only slightly above the IO level may well be dangerous for some occupants due to the unwanted movement of heavy objects and some non-structural components. As defined in FEMA-273 and FEMA-302, the life safety level is a performance state in which "significant" damage has been sustained, although some margin remains against either partial or total building collapse. In FEMA-302, this

margin is taken as 50%, a figure that is based on professional judgment and dates back to the ATC 3 project conducted in the 1970's (ATC 3-06, 1978).

In this dissertation, then, the intermediate level of performance is denoted Structural Damage (SD) rather than life safety, and is identified with a response level where significant damage to structural or nonstructural elements may occur but where overall instability of a redundant structural system would be unlikely. Identification of this limit will be made by using the results of a NSPA to ensure a consistent measure across several categories of frames. Specifically it will be assumed to correspond to roof drift angle (RDA, defined as the roof drift divided by building height) at which the secant slope of the NSPA curve drops to half of its initial value as demonstrated in Figure 5.1. It is assumed that the frame possesses no soft-story mechanism, so the RDA is, in approximation, equal to maximum ISDA. In frames where story mechanism is of concern, however, this RDA needs to be converted to maximum ISDA at that level of deformation. This can be done by examining individual story drifts during the course of the NSPA.

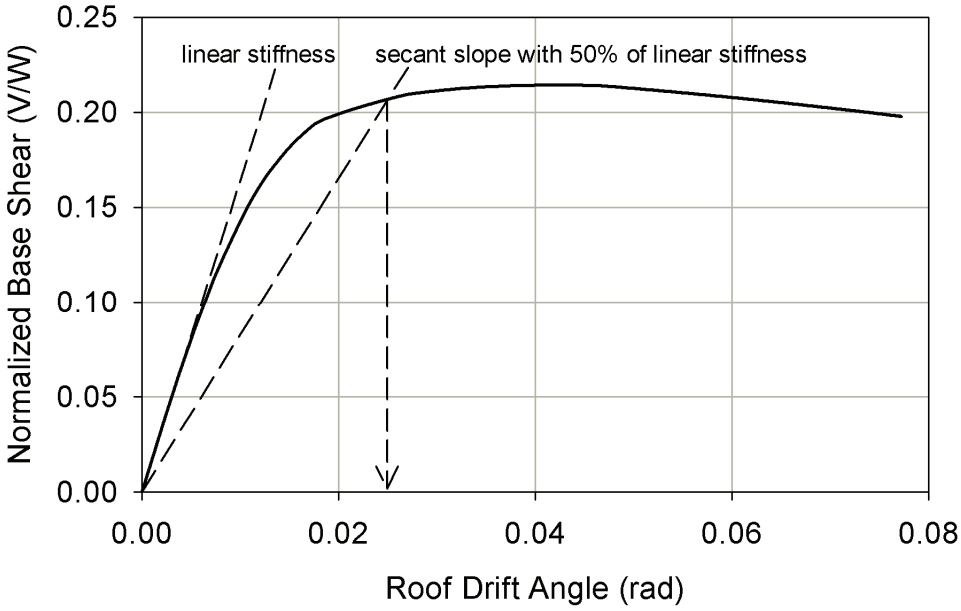

Figure 5.1 Illustration of SD limit point calculation.

5.3.3 Collapse Prevention (CP)

The Collapse Prevention (CP) level is the point at which the structure can no longer support its own weight due to large P-Δ effects. This is accompanied by large interstory drifts and is manifested by non-convergence of the analytical model. For reasons described earlier, the analysis was terminated at 10% ISDA unless non-convergence occurred prior to this point. Subject to these limitations, the CP limit can be identified using the IDA method. Previous IDAs conducted in the SAC Steel Project have shown that steel structures with moment resisting frames designed for Los Angeles typically lose their lateral stability under gravity load at around 8-10% maximum interstory drift (FEMA-351). This is substantially higher than the recommended limit of 5% for CP in FEMA-273/356. Corresponding limits for steel moment frames which are not governed

by seismic considerations, steel braced frames and other types of construction have yet to be determined. These limits are identified subsequently in this dissertation.

5.4 Ground Motion Intensity Measures

A ground motion Intensity Measure (IM) connects the results of nonlinear dynamic structural analysis, embodied in the seismic fragility, to the seismic hazard curves or seismic demands from a scenario earthquake. Traditional IMs are Peak Ground Acceleration (PGA) and Spectral Acceleration at the fundamental period of the structure (S_a). Vamvatsikos and Cornell (2002) showed that S_a is an appropriate intensity measure for moderate-period structures where the first mode dominates the response in the Western United States (WUS). This is because S_a reflects the frequency content of the ground motion near the first-mode frequency at which many structures are sensitive. There has been little investigation of the suitability of alternate intensity measures for buildings in regions of moderate seismicity, where the lateral force-resisting system is governed by wind effects.

Luco and Cornell (2001) defined two criteria for the selection of most suitable IM. These are "efficiency" and "sufficiency". An "efficient" IM is one that results in a relatively low scatter of structural demand measure (generally taken as maximum interstory drift angle), given the IM, with the sole purpose of reducing the required number of ground motion records to be used to achieve a given level of confidence in estimating the seismic demand. A "sufficient" IM, on the other hand, assures that the structural response measure, given the IM, is independent of the magnitude and distance

of the excitation. In addition, the IM also should be compatible with the manner in which the seismic hazard is specified. The main driving factor in the use of spectral acceleration S_a is the widely availability of seismic hazard curves in terms of S_a (see Chapter 3). Luco and Cornell (2001) showed that the same set of ground motions results in smaller conditional dispersion when S_a is used as the IM rather than PGA; further, if the dispersion from a set of records can be reduced by half using an efficient IM, the number of required earthquake records to achieve same amount of precision drops to one fourth. Two main drawbacks of S_a as an IM are that it does not account for higher mode effects and does not take into consideration the period elongation in the inelastic response range of the structure.

5.5 Seismic Performance Assessment of Model Frames

The seismic behavior and performance of the five model frames described in Chapter 4 were assessed. The general procedure followed involves the following aspects:

- Eigenvalue extraction to determine the dynamic characteristics of the system such as fundamental period, mode shapes, modal participation factors, etc;
- NSPAs with different lateral loading schemes to identify general characteristics of system behavior, i.e., presence of any soft-story mechanisms, locations of plastic hinging, and overall system ductility;
- NTHAs to determine the system response to sets of ground motions and to assess the uncertainties in the system response; and finally,

- IDAs to determine the capacities of the frames to withstand increasing levels of ground motion.

There are some common assumptions and steps taken in the analyses of these five frames. Unless otherwise stated, they were applied to all frames considered. These are:

- Eigenvalue extraction was utilized to determine the dynamic and modal characteristics of the frames.
- Seismic mass was calculated using dead load plus 25% of live load.
- Seismic mass was distributed at floor levels as lumped masses at column lines.
- Viscous modal damping of 2% was assumed in dynamic analyses.
- NSPAs were performed using three different lateral load distributions. These three candidate shapes are:
    - Fundamental mode shape of the frame,
    - Linear lateral load shape, i.e., k=1 shape using Equation (5.1),
    - Parabolic lateral load shape, i.e., k=2 shape using Equation (5.1).

5.5.1 Assessment of Frame 2ST-PR

The modal characteristics of Frame 2ST-PR were determined by an eigenvalue analysis. The fundamental period of the frame was calculated to be 1.07 s, while the second mode period is 0.42 s. Modal participation factors are 96% and 4% for the first and second modes, respectively. Mode shapes are given in Figure 5.2.

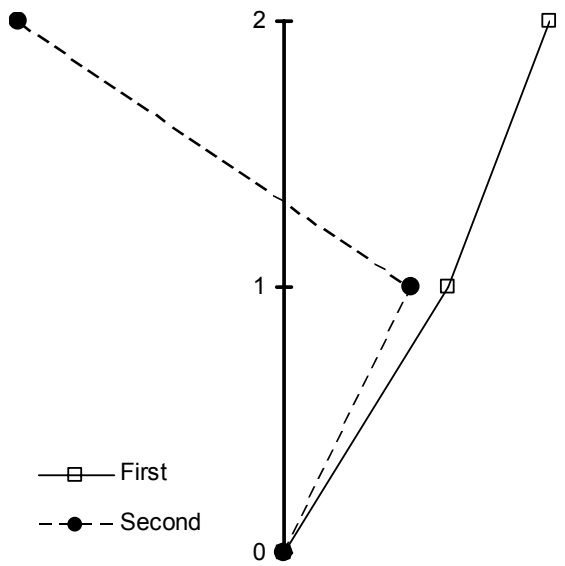

Figure 5.2 Mode shapes for Frame 2ST-PR.

A NSPA of Frame 2ST-PR was performed using the three different lateral force distributions described previously over its height. The resulting NSPA curves are depicted in Figure 5.3. Lateral force multipliers in these three cases are presented in Table 5.1. It can be observed that first-mode-shape lateral loading gives both the smallest initial stiffness and the ultimate capacity. Therefore, it reflects a more conservative behavior of the system.

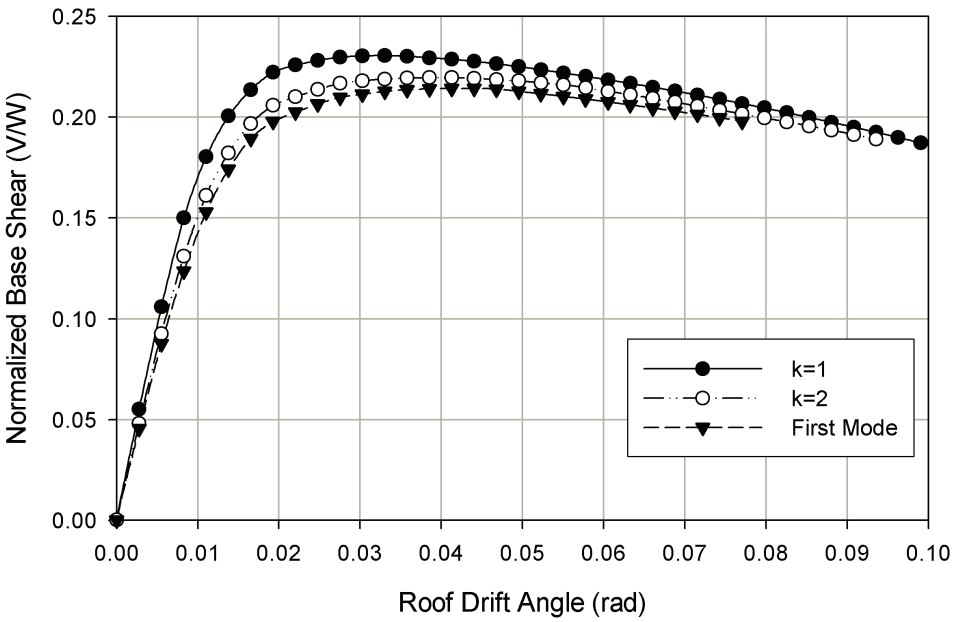

Figure 5.3 NSPA curves for Frame 2ST-PR using three lateral loading schemes.

Table 5.1 Lateral load distributions for three cases of NSPA for Frame 2ST-PR.

Story Level	First Mode Shape	*k*=1 Shape	*k*=2 Shape
2	0.618	0.372	0.542
1	0.382	0.628	0.458
Summation	1.000	1.000	1.000

After choosing the lateral loading scheme, the PR connections in the frame were replaced by rigid connections to determine the effects of PR connections on the overall system behavior. The NSPA was conducted using lateral forces proportional to the first mode. The results are shown in Figure 5.4. The results for the frames with two different connection rigidities are surprisingly similar. This can be attributed to the fact that it is a low-rise light frame with strong beam-weak column design. It can be observed from Figure 5.4 that:

- Nonlinear action initiated at around 0.7% roof drift angle (RDA) for both models; thus, the IO performance limit was chosen as 0.007 maximum interstory drift angle (ISDA) for this frame.
- The secant slope drops to half of the initial stiffness at 2.5% RDA.
- At around 0.08 RDA the upper story exterior connections in the frame with PR connections suffered significant strength loss, reaching a rotation of 40 mrad, and the finite element model failed to converge.
- When all the connections were assumed rigid, the frame remained stable until well beyond 8% RDA.
- Using rigid connections in this particular frame would not affect the monotonic static behavior appreciably since both initial stiffness and the ultimate base shear capacities are close in these two cases.

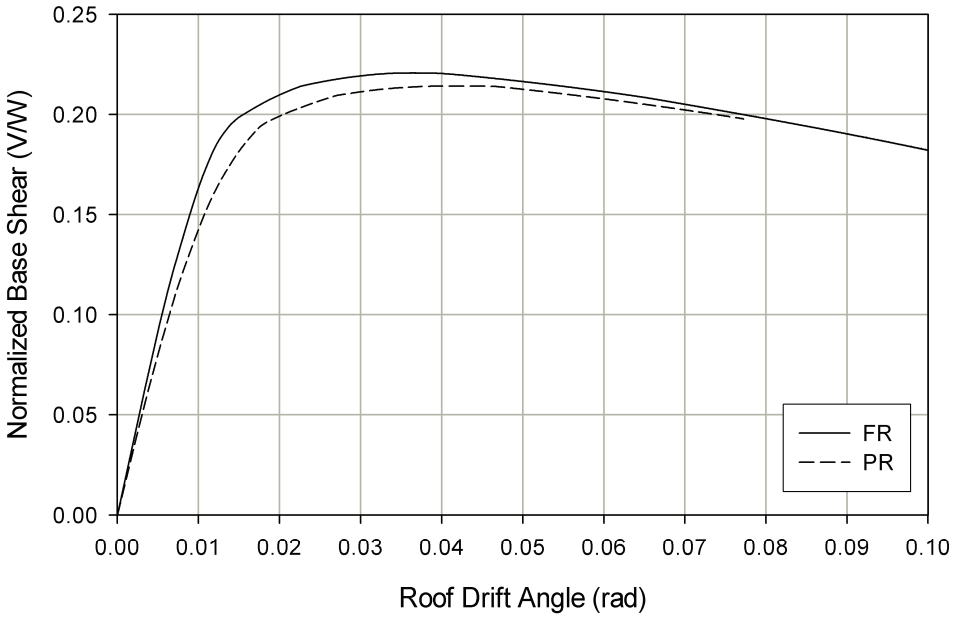

Figure 5.4 NSPA curves for Frame 2ST-PR, comparing behavior with PR and FR connections.

The CP performance limit will be identified later using an IDA of this frame, since capacities calculated from static methods are generally overly conservative. The maximum ISDAs under design wind loads are 1/370 and 1/400 for the frames with PR and FR connections, respectively. To investigate the possible presence of any soft-story mechanisms, a conventional NSPA curve (using first mode shape lateral load distribution) was plotted in the same figure with the first and second story interstory drift angles, as shown in Figure 5.5. This figure shows that although the interstory drift angle at the first story level is more critical than the roof drift angle, there are no dominant story mechanisms and the roof drift is quite close to the maximum interstory drift. At the 2.5% RDA deformation level, the maximum ISDA occurs in the first story with a value 2.7%. This can be observed in Figure 5.5 by entering from X-axis at 0.0245 rad until intersecting "*Roof Drift*" line and going parallel to the right and intersecting "*story 1*" line. The deformation limit defining SD, therefore, was chosen to be 0.027 rad ISDA. The occurrence of the maximum ISDA will be determined for each record and results will be compared to see if first story dominates the overall behavior of this frame.

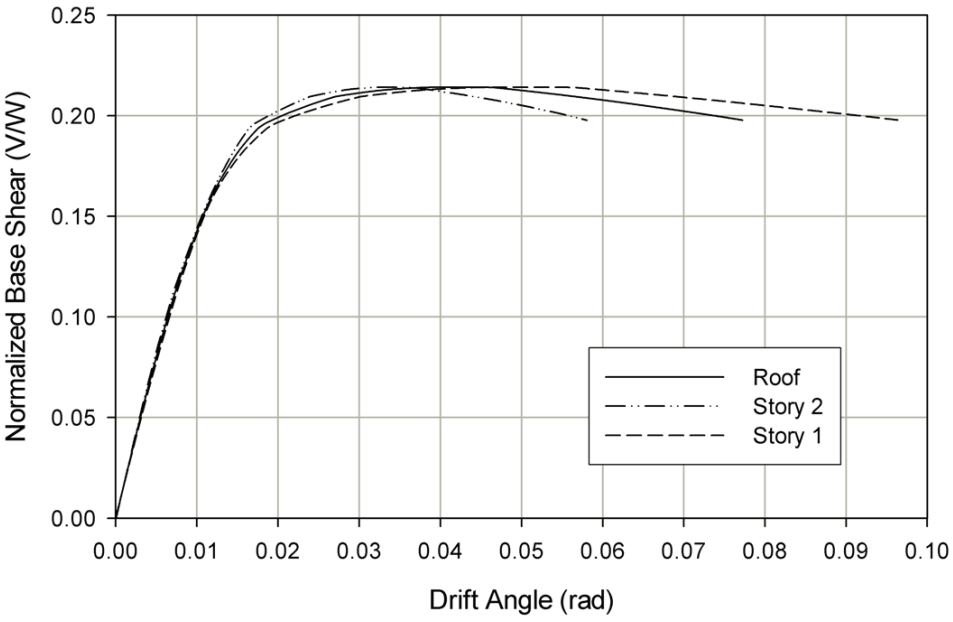

Figure 5.5 Comparison of roof drift against ISDAs for Frame 2ST-PR.

The seismic demand on frame 2ST-PR was examined using two sets of ground motion records. The first suite consists of the Wen-Wu 2%/50 yr ground motion records. The second suite of ground motion records consists of the Rix-Fernandez Memphis (upland soil profile) UHGMs for three ensembles (2%/50 yr, 5%/50 yr and 10%/50 yr). Each ensemble consists of 10 accelerograms. The seismic demands on this frame were determined by NTHA, and were post-processed by regression analysis. The statistical analysis of demands from the Wen-Wu accelerograms (as shown in Fig. 5.6) produced the following median seismic demand relationship and logarithmic standard deviation:

$$\hat{\theta}_{\max} = 0.0509 \cdot S_a^{\,0.913}, \ \beta_{D|S_a} = 0.19 \tag{5.4}$$

The Rix-Fernandez suite yielded similar seismic demand statistics (Fig. 5.7):

$$\hat{\theta}_{\max} = 0.0492 \cdot S_a^{\,0.804}, \ \beta_{D|S_a} = 0.16 \tag{5.5}$$

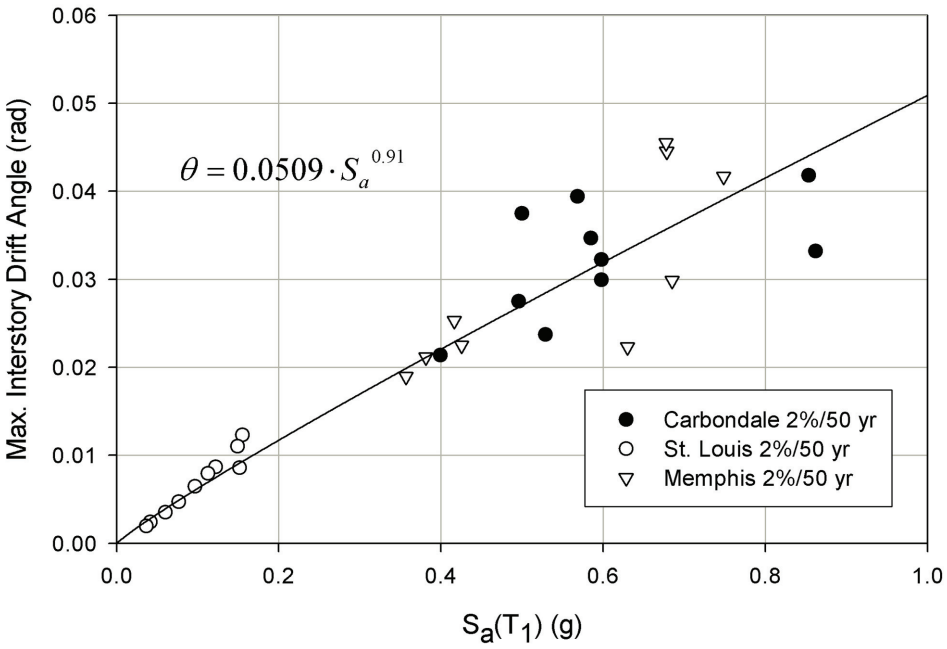

Figure 5.6 NTHA results for Frame 2ST-PR using Wen-Wu 2%/50 yr GMs.

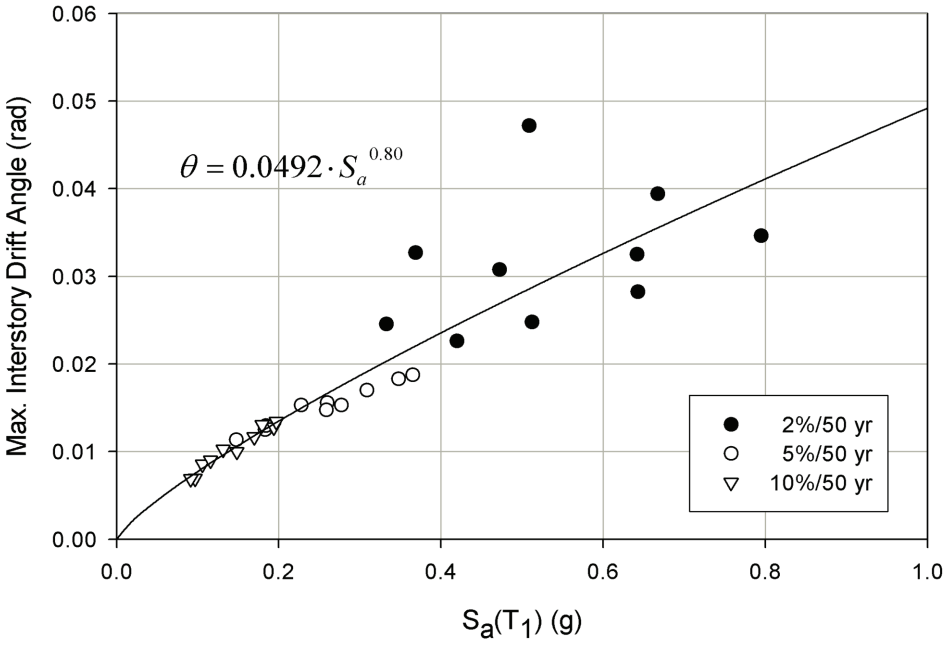

Figure 5.7 NTHA results for Frame 2ST-PR using Rix-Fernandez UHGMs.

The median relationships produced by two different ensembles of accelerograms are compared in Figure 5.8. The median seismic demands are virtually independent of the ensemble used to produce them (recall that the ensembles do not include near-field ground motions). A total of 60 NTHA were performed, and it was found that the maximum ISDA always occurred in the first story. This finding is consistent with the results of the NSPA, which indicated that the first-story drift is more critical than second story and roof drifts in this particular frame.

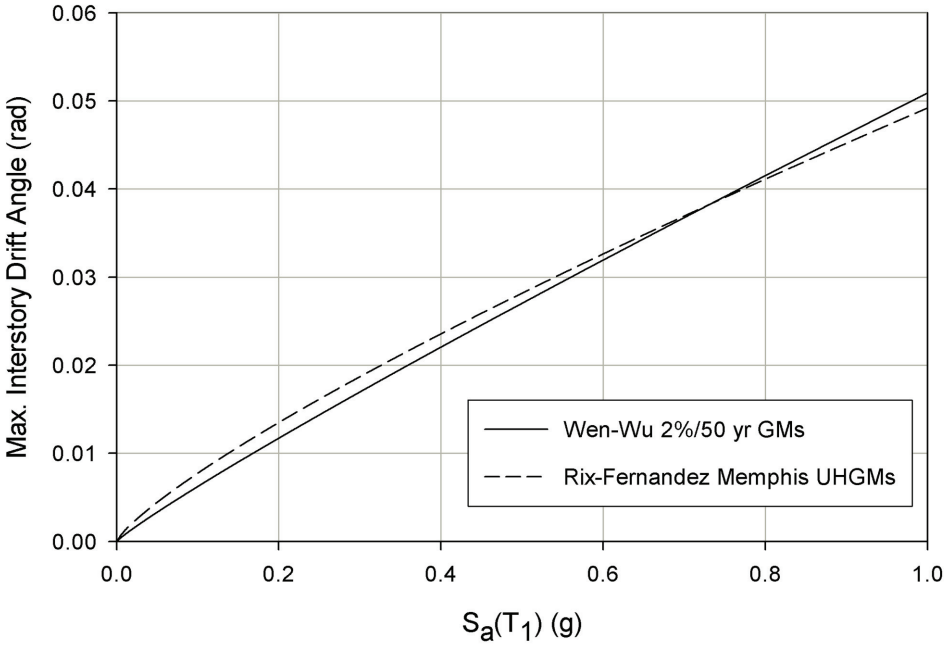

Figure 5.8 Comparison of two median relationships obtained from different suites of GMs.

The 30 Wen-Wu accelerograms were scaled in increasing intensity to perform the IDA of frame 2ST-PR. The frame withstood interstory drifts of up to 0.10[1] for 28 out of 30 records prior to reaching a state of non-convergence or a decrease in slope to less than 20% of that of the initial elastic slope. This shows that the P-Δ moments in this frame are not significant. This result can be attributed to the height and weight of the frame; it is a low-rise and relatively light frame. Therefore, the deformation limit of this frame associated with the CP performance level is assumed to be 0.10. Figure 5.9 depicts the results of two IDA sets (Memphis ensemble shown; Carbondale and St. Louis ensembles are not presented for brevity).

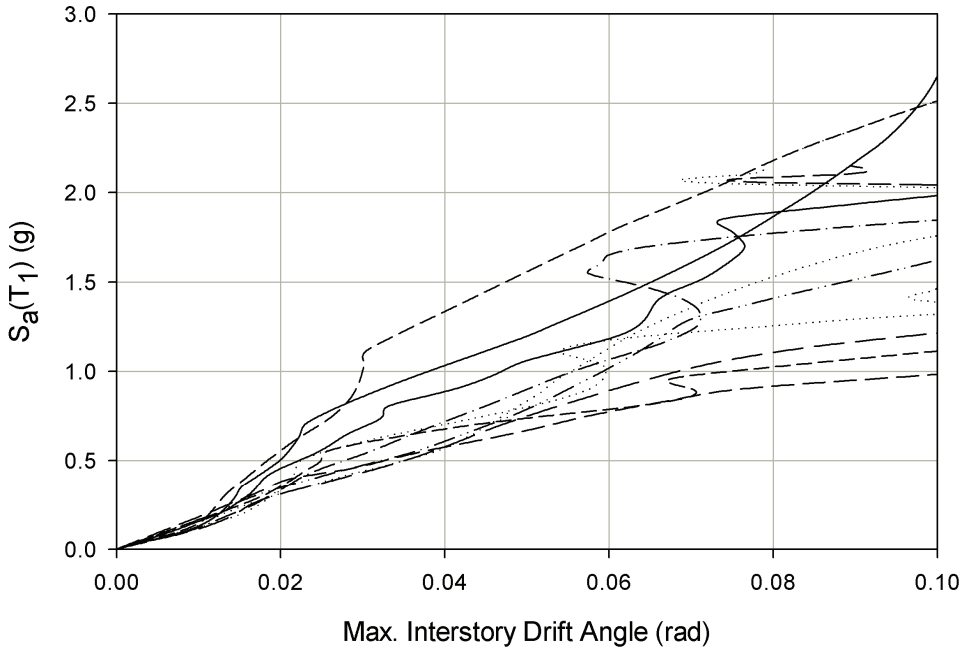

Figure 5.9 IDA results for Frame 2ST-PR using Wen-Wu 2%/50 yr sets for Memphis and Carbondale.

[1] In the opinion of the author, the analyses at structural deformations beyond 10% maximum interstory drift angle become questionable.

5.5.2 Assessment of Frame 3ST-FR

The modal properties of Frame 3ST-FR were examined using an eigenvalue extraction. The fundamental period of this frame is 2.01 sec, while the second and third mode periods are 0.51 and 0.25 sec, respectively. The first three mode shapes are given in Figure 5.10. The frame is first-mode dominant and the modal participation factors are 84%, 13%, and 4% for the first three modes, respectively.

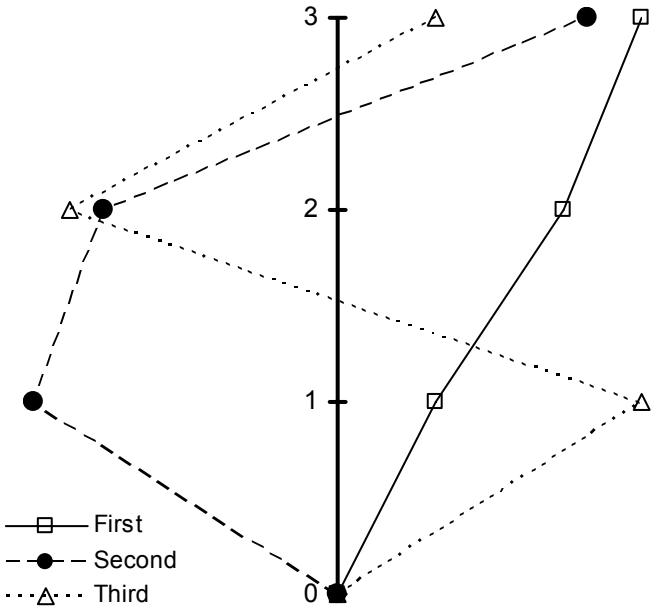

Figure 5.10 Mode shapes for Frame 3ST-FR.

A NSPA was performed using the same general approach taken with the previous frame. The corresponding lateral load multipliers for three distributions are given in Table 5.2, and the results of the NSPA are depicted in Figure 5.11. The outcome of this

comparison is different than that of Frame 2ST-PR. The most critical lateral loading is achieved with the distribution associated with k=2, which produces the smallest elastic stiffness and lateral load carrying capacity. Therefore, the NSPA result for this frame is assumed to be given by k=2 distribution for conservatism.

Table 5.2 Lateral load distributions for three cases of NSPA for Frame 3ST-FR.

Story Level	First Mode Shape	k=1 Shape	k=2 Shape
3	0.48	0.52	0.66
2	0.36	0.32	0.27
1	0.16	0.16	0.07
Summation	1.00	1.00	1.00

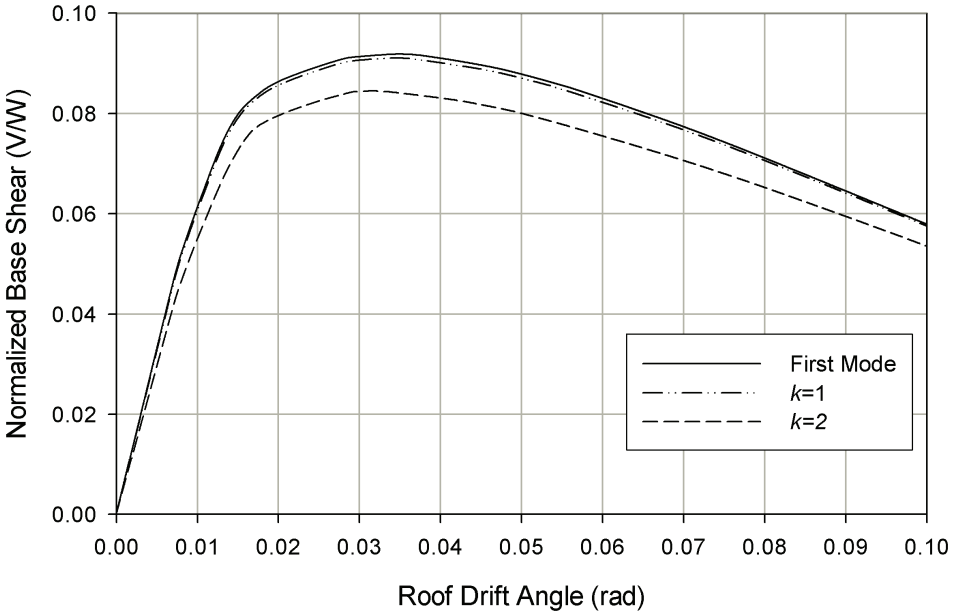

Figure 5.11 NSPA curves for Frame 3ST-FR using three lateral loading schemes.

The following conclusions can be drawn from the NSPA results summarized in Figure 5.11:

- Linear behavior extends to approximately 0.008 RDA; thus, the IO performance limit was chosen as 0.8% ISDA for this frame.
- The secant slope of the curve corresponding to the lateral force distribution with k=2 drops by 50% at 2.8% RDA.
- When deformations exceed a RDA of approximately 0.03, the frame is subjected to large P-Δ moments and gradually loses strength.

To investigate the possible presence of any soft-story mechanisms, the conventional NSPA curve (using the k=2 shape lateral load distribution) was plotted in the same figure with the ISDAs for the most critical level. It was found that the second story ISDAs are larger than the roof drift angle at all base shear levels. A comparison of this drift with the roof drift angle, presented in Figure 5.12, indicates that the 2nd story experiences 10% ISDA when the global drift reaches 9%. Accordingly, using the roof drift as target displacement in a NSPA may be misleading for this particular frame. In support of this observation, the secant slope approach yielded a RDA limit of 2.8% limit for SD. If this value is entered in Figure 5.12, one finds out that it corresponds to 3.4% ISDA in the 2nd story. The difference is larger than that observed for Frame 2ST-PR. This is, however, expected since in taller frames, story mechanisms are more likely to occur and maximum ISDA is somewhat larger than RDA. Therefore, the SD limit for Frame 3ST-FR was chosen to be 3.4% ISDA.

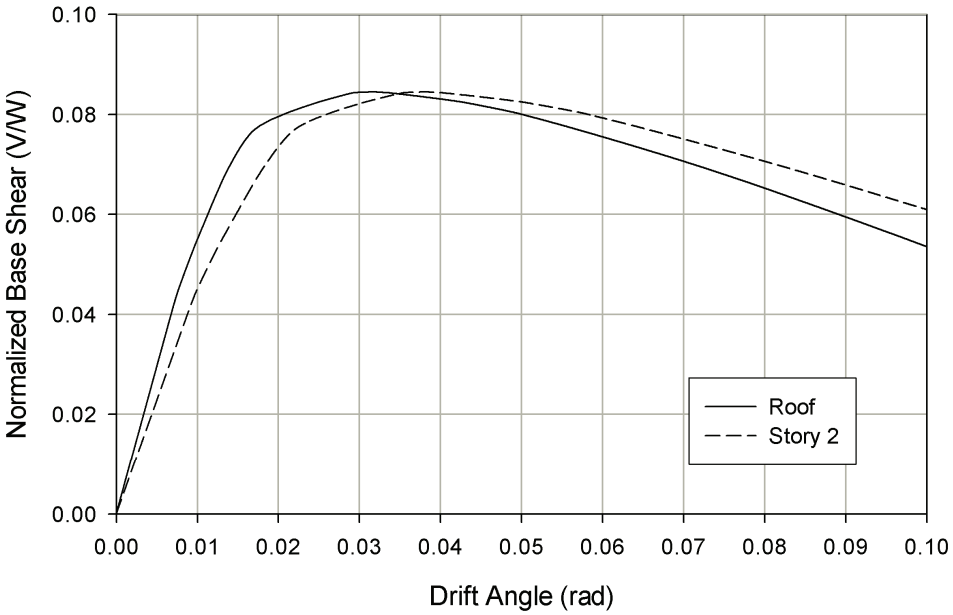

Figure 5.12 Comparison of roof drift angle against second story ISDA for Frame 3ST-FR.

The seismic demand on Frame 3ST-FR was examined using three sets of accelerograms. The first suite consists of the Wen-Wu 2%/50 yr ground motion records (30 records in total, 10 for each of three sites). The second suite of ground motion records is made up of two Rix-Fernandez scenario earthquake ensembles: M_w=7.5, R=20 and 50 km, each containing 20 records. The third suite of accelerograms is Rix-Fernandez Memphis (upland soil profile) UHGMs with three ensembles (2%/50 yr, 5%/50 yr and 10%/50 yr), each of which consists of 10 accelerograms. The seismic demands from these three sets are illustrated in Figures 5.13 – 5.15. The statistical analysis of results for the first suite produced the following seismic demand statistics (median and logarithmic standard deviation):

$$\hat{\theta}_{\max} = 0.0924 \cdot S_a^{0.78},\ \beta_{D|S_a} = 0.25 \tag{5.6}$$

The second suite yielded following seismic demand statistics:

$$\hat{\theta}_{\max} = 0.0795 \cdot S_a^{0.70},\ \beta_{D|S_a} = 0.20 \tag{5.7}$$

The third suite gave the median seismic demand statistics:

$$\hat{\theta}_{\max} = 0.0969 \cdot S_a^{0.80},\ \beta_{D|S_a} = 0.19 \tag{5.8}$$

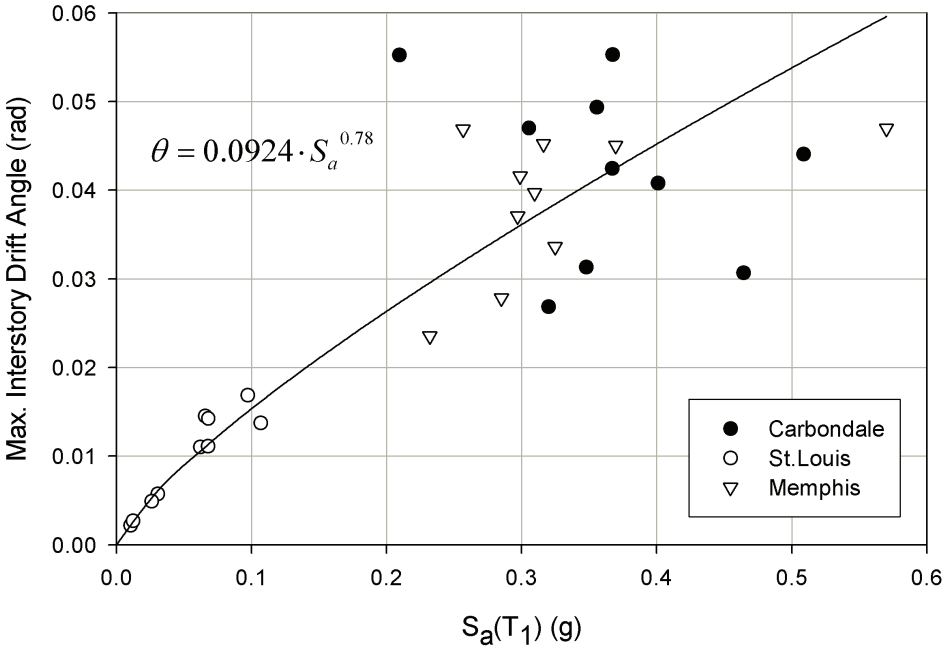

Figure 5.13 NTHA results for Frame 3ST-FR using Wen-Wu 2%/50 yr GMs.

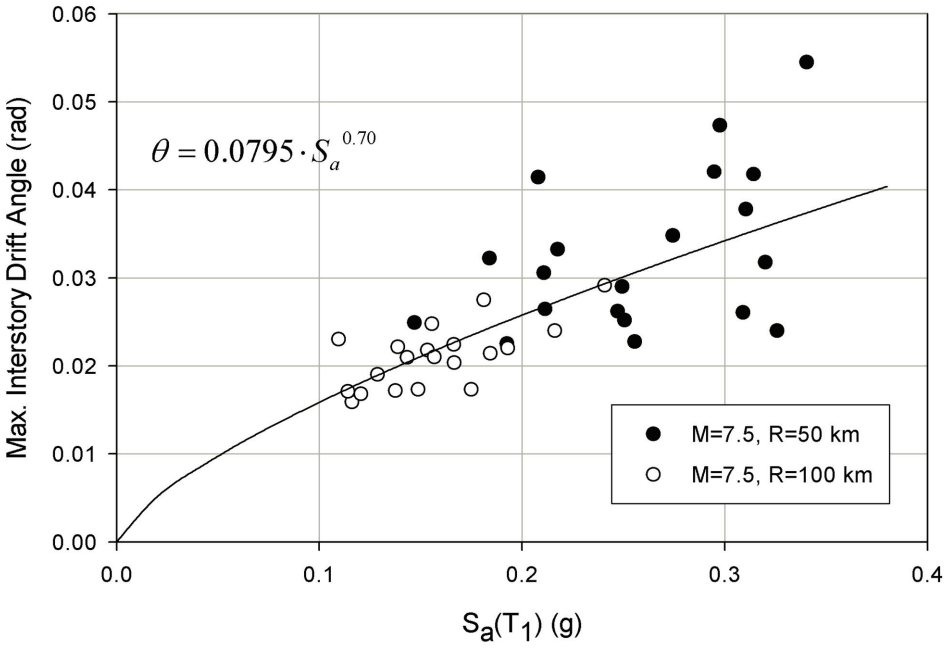

Figure 5.14 NTHA results for Frame 3ST-FR using Rix-Fernandez scenario GMs.

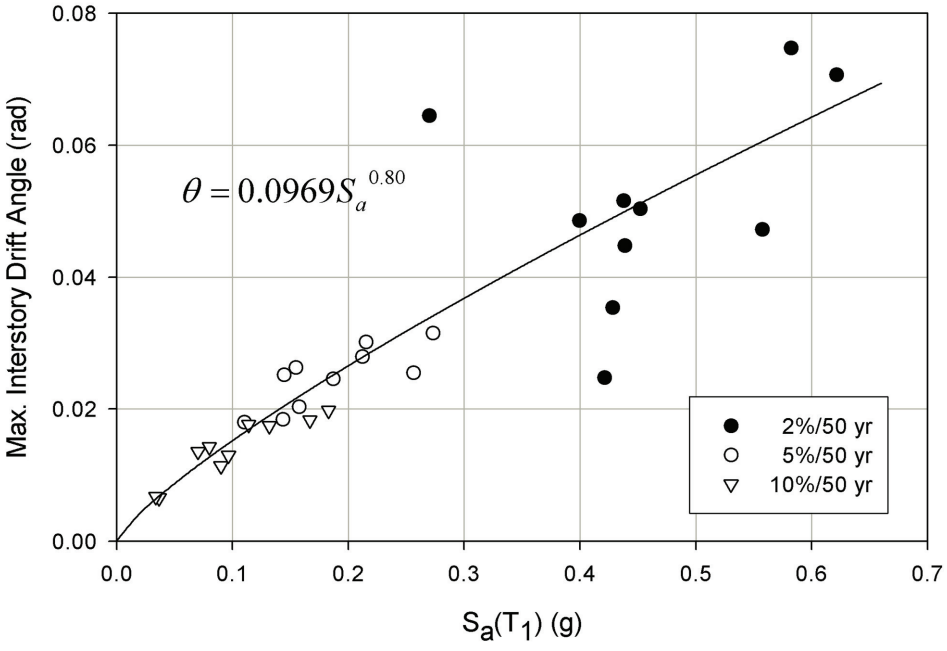

Figure 5.15 NTHA results for Frame 3ST-FR using Rix-Fernandez UHGMs.

In contrast to the similarity in median demands produced by different earthquake ensembles on Frame 2ST-PR (Fig. 5.8), the median seismic demand relationships produced by these three suites of accelerograms acting on Frame 3ST-PR differ from one another especially in the higher spectral acceleration region, as illustrated in Figure 5.16. Moreover, as the intensity (in terms of S_a) of the ground motions increases, the maximum ISDAs tend to accumulate in the lower stories of this frame, mainly at the first two stories. About 60% of the accelerograms resulted in maximum ISDAs in the second story, while 35% led to maximum ISDAs in the first story. This is shown in Table 5.3 for two suites of accelerograms. Recall from Figures 3.6 thru 3.8 that the intensity of Memphis and Carbondale ensembles in Wen-Wu 2%/50 yr suite is higher than that of St. Louis ensemble.

The outcome of the NTHA supports the results of the NSPA in the sense that they both predict the second story as being the most critical of all three. The statistical analysis of story levels at which the maximum ISDAs occurred clearly indicates that lower stories suffer higher interstory drifts as the ground motion intensity increases. This is mainly because of the higher P-Δ moments in the lower stories as the frame deforms into the inelastic range.

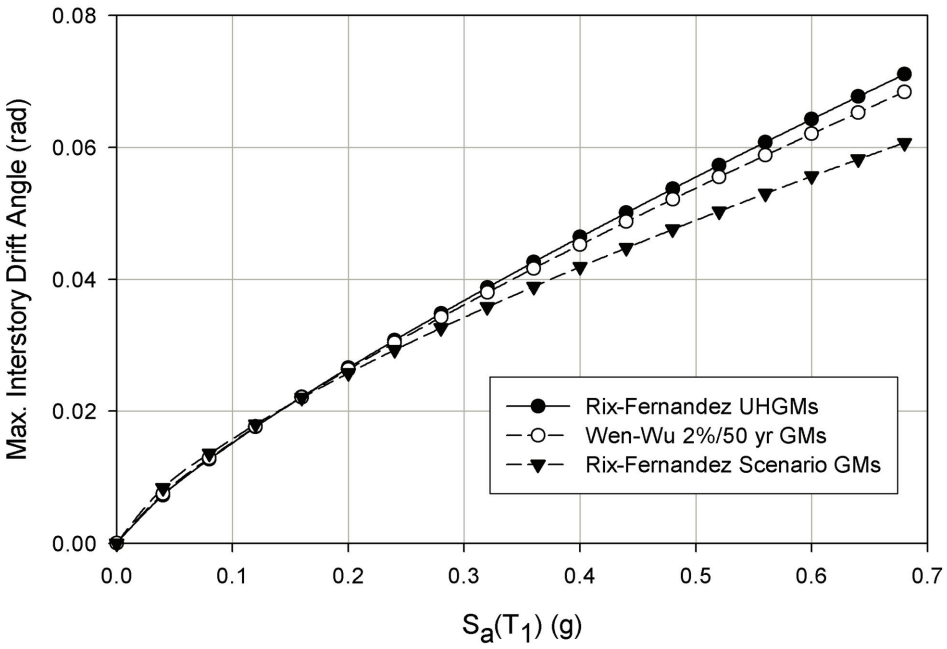

Figure 5.16 Comparison of median relationships obtained from different suites of GMs.

Table 5.3 Story levels at which maximum ISDAs observed in Frame 3ST-FR.

GM #	Rix-Fernandez UHGMs			Wen-Wu 2%/50 yr GMs		
	10%/50 yr	5%/50 yr	2%/50 yr	St. Louis	Carbondale	Memphis
1	2	2	2	2	2	1
2	2	2	2	2	2	1
3	2	2	NC[a]	3	1	2
4	2	2	NC	2	1	1
5	3	2	1	2	1	2
6	2	2	1	3	1	1
7	2	2	2	2	1	1
8	2	1	2	2	2	1
9	2	2	1	2	1	1
10	2	2	1	3	1	1

[a] Non-Convergence of analytical model.

The capacity of Frame 3ST-FR against increasing levels of ground motion intensity was assessed through an IDA that involved scaling the 30 Wen-Wu 2%/50 yr accelerograms upward (Fig. 5.17). The failure point (as defined in Section 5.1.3) for each

record was calculated, as summarized in Figure 5.18. Eight out of 30 records did not cause failure of the system prior to reaching 10% maximum ISDA. The mean value of the 30 maximum ISDAs achieved by this frame is 8.6%, while the coefficient of variation (COV) is 16%. The very same frame modeled without explicit consideration of the beam-to-column panel zone behavior yielded a mean maximum ISDA of 8.8% and a COV of 23%. These values defining the CP point did not change appreciably for IDAs performed using the different ground motion ensembles described above, suggesting that the point of collapse depends mainly on the structural system characteristics. Thus, the CP deformation limit for Frame 3ST-FR is assumed to be 0.086. It is interesting to note that the drift limit defining the CP performance level of this frame is approximately the same as the drift limit defining the CP level for special moment frames designed for high-seismic regions investigated in recent SAC steel project.

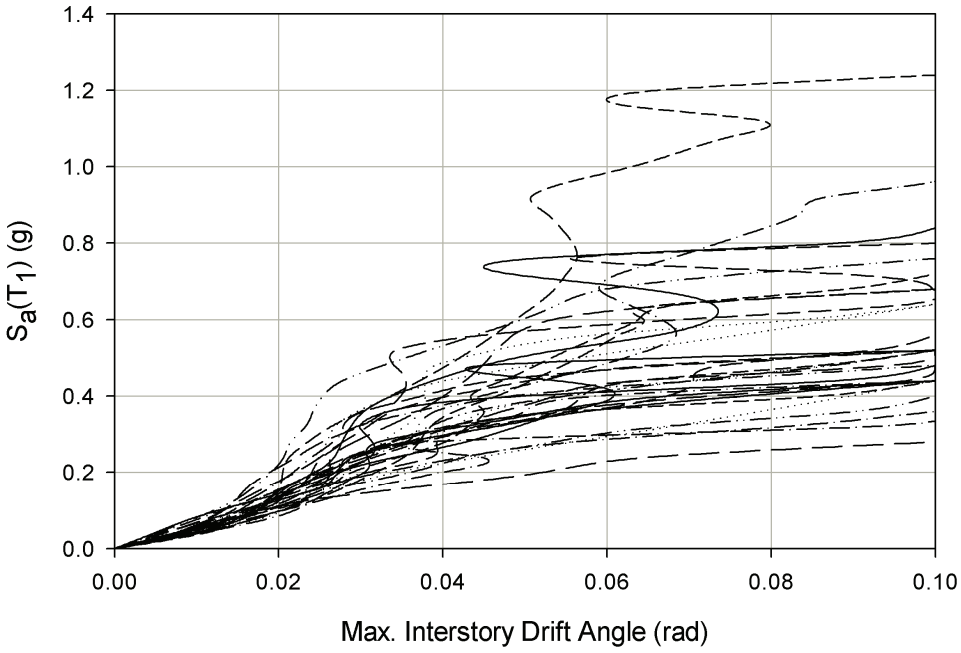

Figure 5.17 IDA results for Frame 3ST-FR using Wen-Wu 2%/50 yr GMs.

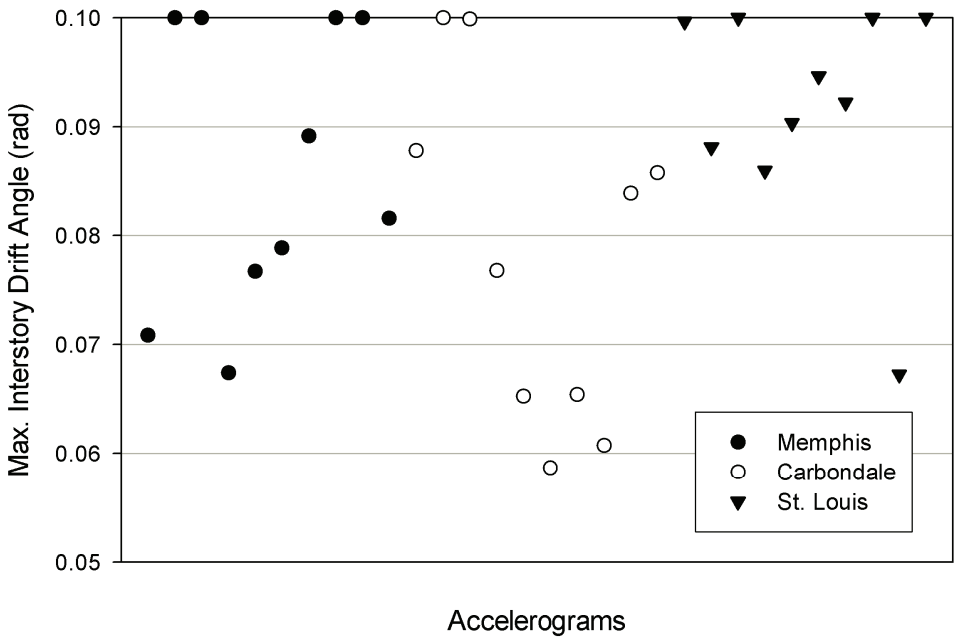

Figure 5.18 Record by record ISDA values after IDAs on Frame 3ST-FR.

5.5.3 Assessment of Frame 4ST-PR

The dynamic characteristics of Frame 4ST-PR were determined by an eigenvalue analysis. The periods and modal participation factors are summarized in Table 5.4 for the three models described in detail in Chapter 4; CA connections, TS connections and rigid connections. The mode shapes are very close to one another; thus, only the TS model mode shapes are illustrated in Figure 5.19.

Table 5.4 Periods and modal participation factors for three models of Frame 4ST-PR.

Mode #	CA Model		TS Model		Rigid Model	
	Period (s)	MPF[a] (%)	Period (s)	MPF (%)	Period (s)	MPF (%)
1	1.40	89	1.34	90	1.20	91
2	0.45	9	0.43	8	0.40	7.5
3	0.24	1	0.23	1	0.22	1

[a] Modal participation factor.

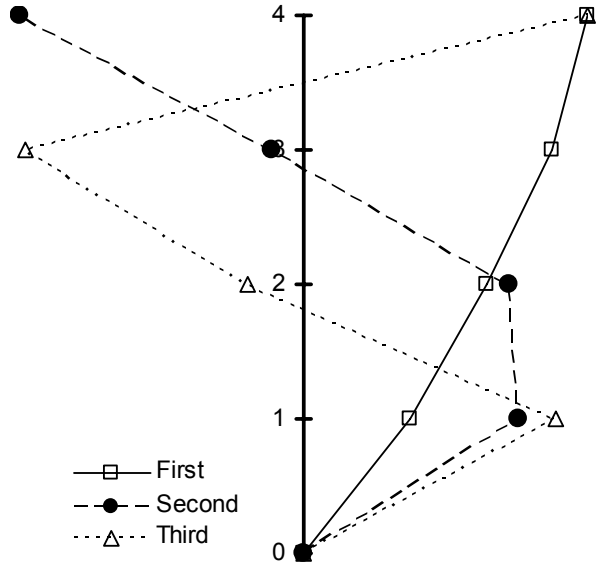

Figure 5.19 First three mode shapes for Frame 4ST-PR (TS).

The NSPA was performed on Frame 4ST-PR for three models: 4ST-PR(CA), 4ST-PR(TS) and the frame modeled with rigid connections [identified in the following as 4ST-PR(R)], a rigid frame representation of the original PR frame. Lateral forces proportional to the first mode shape were assumed in all three analyses. The results of the NSPAs are presented in Figure 5.20. The ultimate capacity of Frame 4ST-PR(TS) under monotonic lateral loading is very close to that of the rigid model although their initial

behaviors are different. On the other hand, the initial lateral stiffnesses of the two PR frames are quite close, although their ultimate capacities are considerably different. Frame 4ST-PR(CA) starts losing its capacity at a RDA around 4%, the point at which some of the lower story connections lose most of their capacities. In contrast, Frame 4ST-PR(TS) is stable until an RDA of 6% is reached, at which point some of the connections attain 0.03 rad. relative rotations and lose their strengths, as modeled explicitly in Figure 4.11. The elastic region extends further for the TS model than for the CA model. Nonlinear action initiates at about 0.7% RDA in both CA and TS models. These limits were assumed to define the IO limits for these frames. SD limits were calculated using the same approach as done for the other frames. Secant slopes of NSPA curves for Frames 4ST-PR(CA) and 4ST-PR(TS) drop to half of their initial values at 2.3% and 2.4% RDAs, respectively.

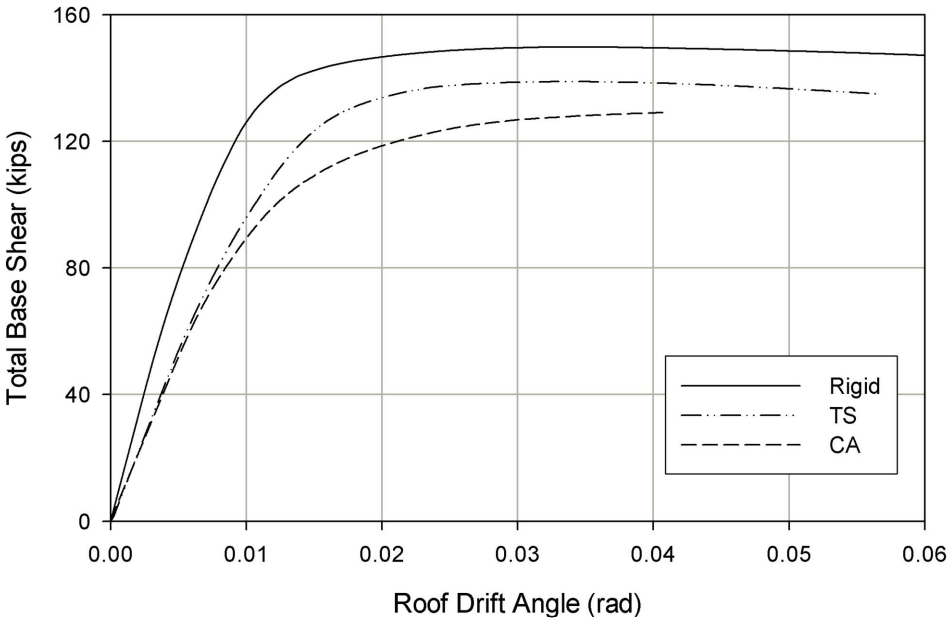

Figure 5.20 NSPA curves for Frame 4ST-PR with different models of connections.

The NSPA of the relatively weaker model, Frame 4ST-PR(CA), was performed using the same procedure as for the frame with TS connections. Lateral load multipliers for three cases are presented in Table 5.5. The first mode shapes for Frames 4ST-PR(CA) and 4ST-PR(TS) differ only in the third decimal point, and therefore are assumed to be the same. Moreover, lateral forces for k=1 and k=2 do not depend on the frame's period and are the same for both frames. In other words, the load multipliers in Table 5.5 are valid for both frames. The resulting NSPA curves for the different lateral force distributions are given in Figure 5.21. The first-mode and k=1 loadings are coincident since their distributions are very close. On the other hand, the k=2 loading pattern yields larger roof drift angles at all base shears, indicating that the frame is more vulnerable if lateral loads are applied at those proportions.

Table 5.5 Lateral load distributions for three cases of NSPA for Frame 4ST-PR.

Story Level	First Mode Shape	k=1 Shape	k=2 Shape
4	0.346	0.346	0.467
3	0.302	0.311	0.323
2	0.223	0.218	0.158
1	0.129	0.125	0.052
Summation	1.000	1.000	1.000

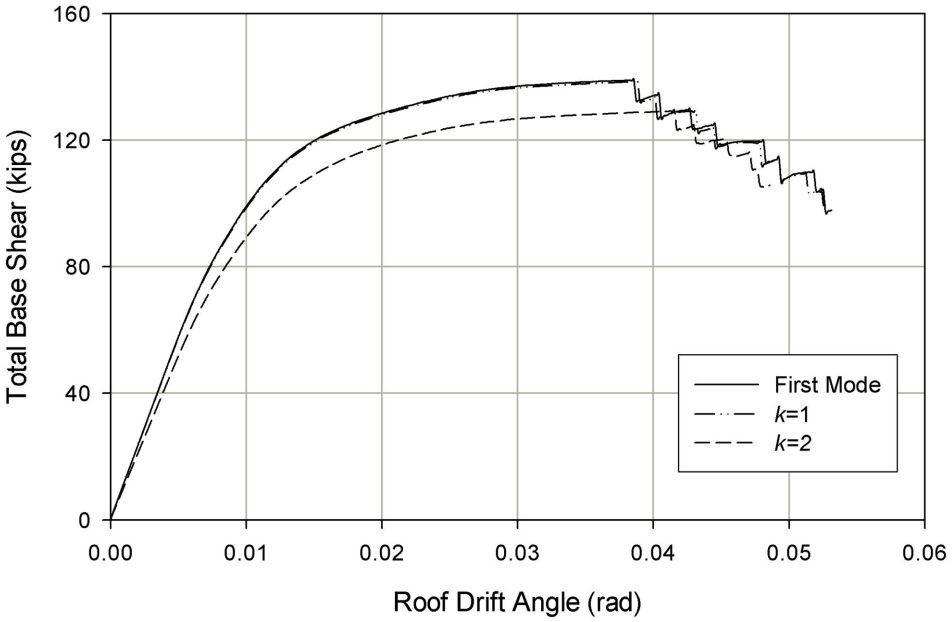

Figure 5.21 NSPA curves for Frame 4ST-PR(CA) using different loading schemes.

The relative strength or weakness of individual stories in Frame 4ST-PR(CA) was investigated using the *k*=2 lateral force pattern, as illustrated in Figure 5.22. The ISDA in the 2nd story is the largest at all points in the NSPA and shows the potential for a soft story mechanism. The calculation of SD limit at a RDA of 2.3% yields a maximum ISDA of 3.0% at 2nd story level (Fig. 5.22). This value was adopted to be the SD limit for Frame 4ST-PR(CA).

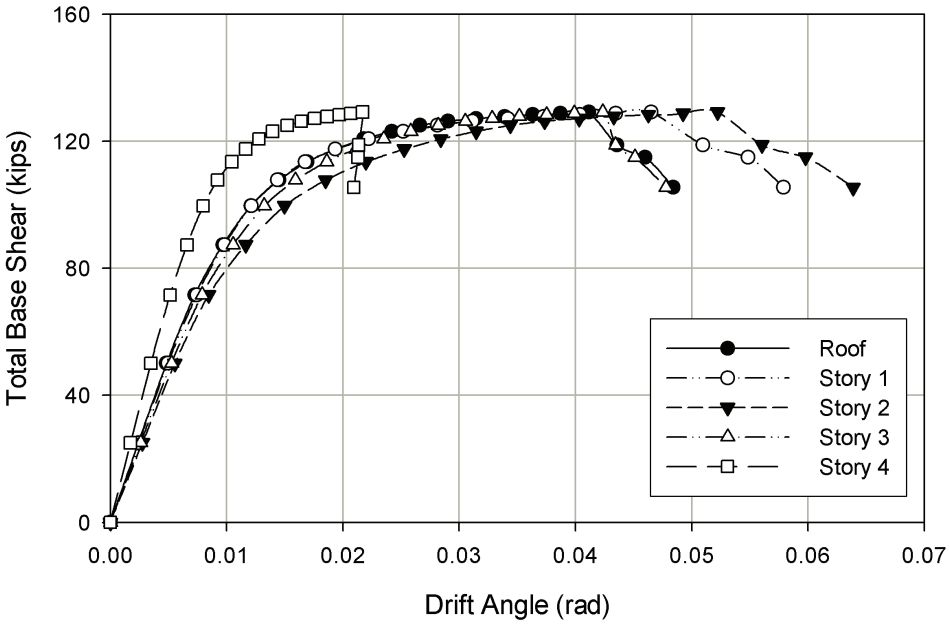

Figure 5.22 Comparison of roof drift angle against ISDAs for Frame 4ST-PR(CA).

The relatively stronger frame with T-stub connections, Frame 4ST-PR(TS), also was assessed using the NSPA under three load distributions, as summarized in Figure 5.23. As with the frame with the clip-angle (CA) connections, the k=2 loading pattern is the most critical lateral force pattern. Figure 5.24 shows that, as with the weaker frame, the most flexible story in Frame 4ST-PR(TS) is the second story. Similarly, the SD limit was calculated to be 3.0% for this frame using Figure 5.24.

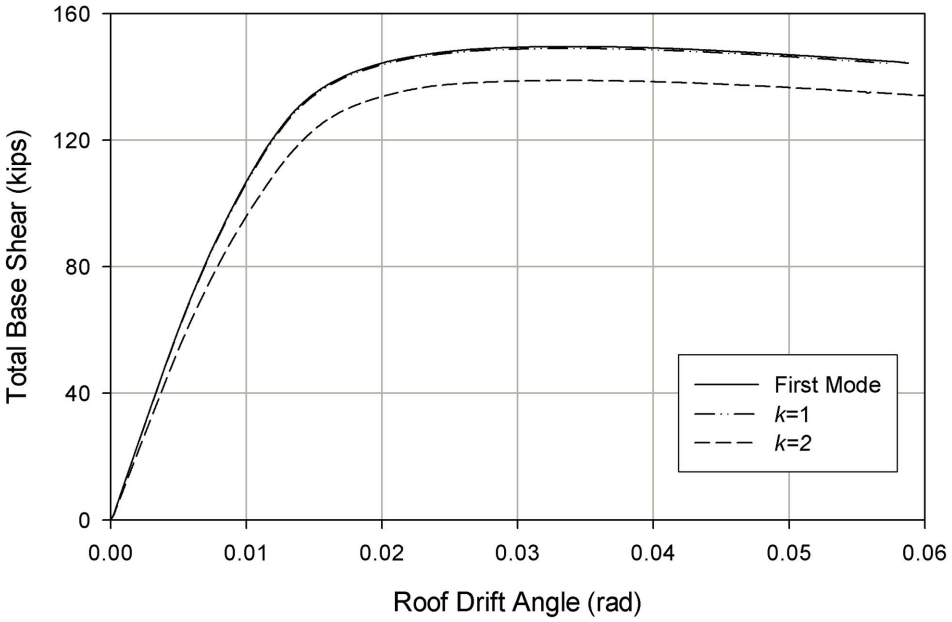

Figure 5.23 NSPA curves for Frame 4ST-PR(TS) using different loading schemes.

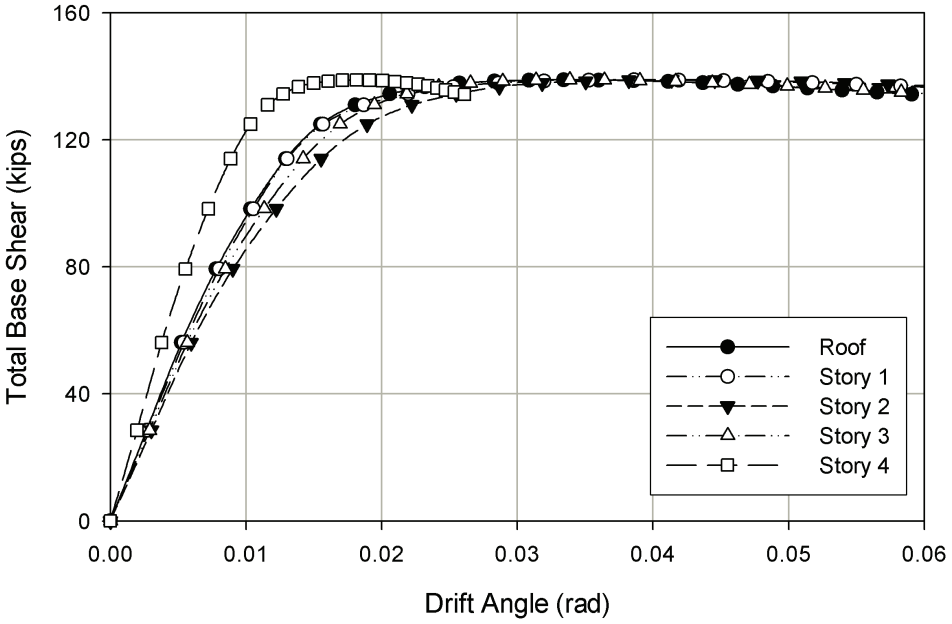

Figure 5.24 Comparison of roof drift angle against ISDAs for Frame 4ST-PR(TS).

The dynamic response characteristics of Frames 4ST-PR(CA) and 4ST-PR(TS) were evaluated using two suites of ground motions. The first suite consists of the Rix-Fernandez Scenario accelerograms for events of M_w=7.5, R=50, and 100 km for CA model[2]; and R=20, and 50km for the TS model. The second set is composed of Wen-Wu Memphis accelerograms for 2%/50 yr and 10%/50 yr hazard levels. The results of these NTHAs are summarized in Figures 5.25 through 5.28. Statistical analysis of the seismic demands from the Rix-Fernandez accelerograms on Frame 4ST-PR(CA) produced the following seismic demand statistics:

$$\hat{\theta}_{\max} = 0.0484 \cdot S_a^{0.85}, \ \beta_{D|S_a} = 0.13 \tag{5.9}$$

These same records yielded the following seismic demand relationship for TS model:

$$\hat{\theta}_{\max} = 0.0555 \cdot S_a^{1.10}, \ \beta_{D|S_a} = 0.25 \tag{5.10}$$

The Wen-Wu suite produced following statistics for the CA model:

$$\hat{\theta}_{\max} = 0.0459 \cdot S_a^{0.86}, \ \beta_{D|S_a} = 0.18 \tag{5.11}$$

These same records yielded similar results for the TS model:

$$\hat{\theta}_{\max} = 0.0461 \cdot S_a^{0.88}, \ \beta_{D|S_a} = 0.19 \tag{5.12}$$

[2] The CA model failed repeatedly to converge for M_W= 7.5 and R = 20 km ensemble.

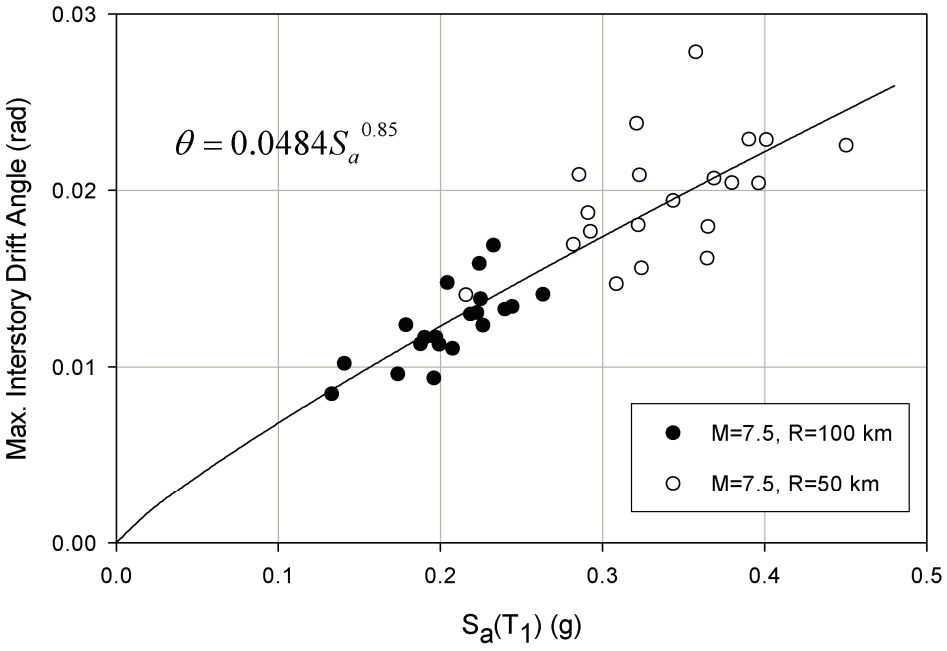

Figure 5.25 NTHA results for Frame 4ST-PR(CA) using Rix-Fernandez scenario GMs.

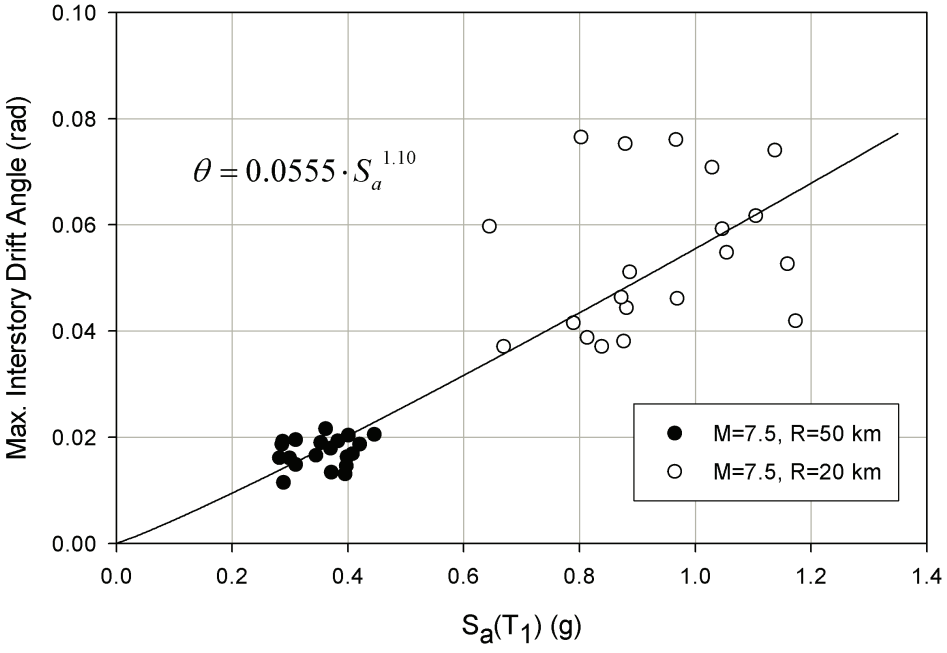

Figure 5.26 NTHA results for Frame 4ST-PR(TS) using Rix-Fernandez scenario GMs.

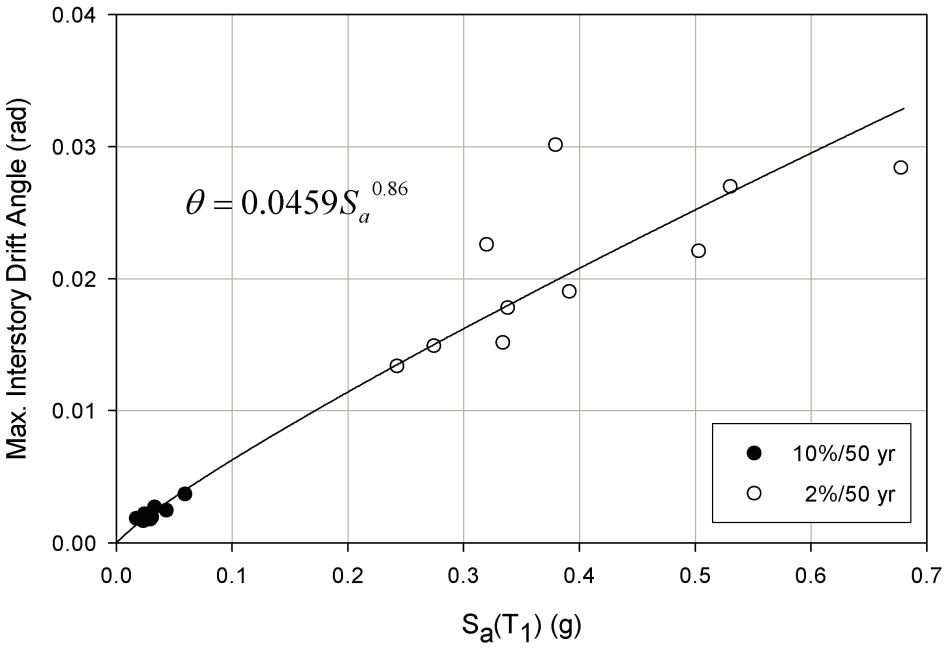

Figure 5.27 NTHA results for Frame 4ST-PR(CA) using Wen-Wu Memphis GMs.

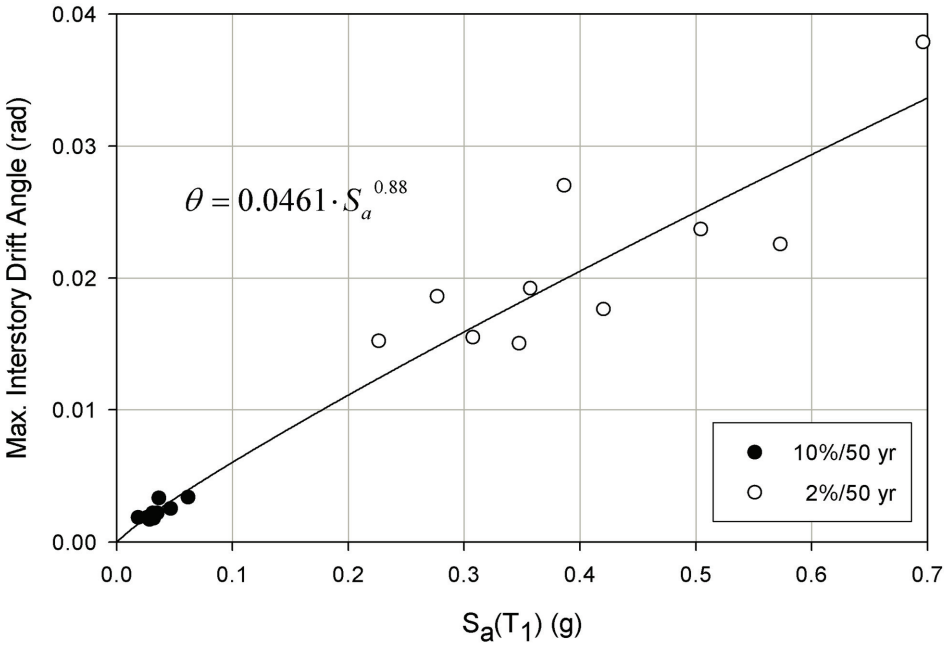

Figure 5.28 NTHA results for Frame 4ST-PR(TS) using Wen-Wu Memphis GMs.

A comparison of the median seismic demand relationships for these two cases is plotted in Figures 5.29 and 5.30 for CA and TS models, respectively. The variation in median seismic demand from ensemble to ensemble is quite small, indicating that seismic demand is more dependent on the characteristics of the structural system than on the ground motion ensembles chosen for the analyses. This supports the use of fewer ensembles in seismic fragility assessments. Structural Engineers Association of California (SEAOC, 1999) suggests the use of at least 7 records to be used in an ensemble. The NTHA results were examined in detail to identify where the maximum ISDA occurs during each accelerogram (Table 5.6). Especially in Frame 4ST-PR(CA), more than 90% of the records produced the maximum ISDA at the second story level. This is in good agreement with the findings from the NSPA.

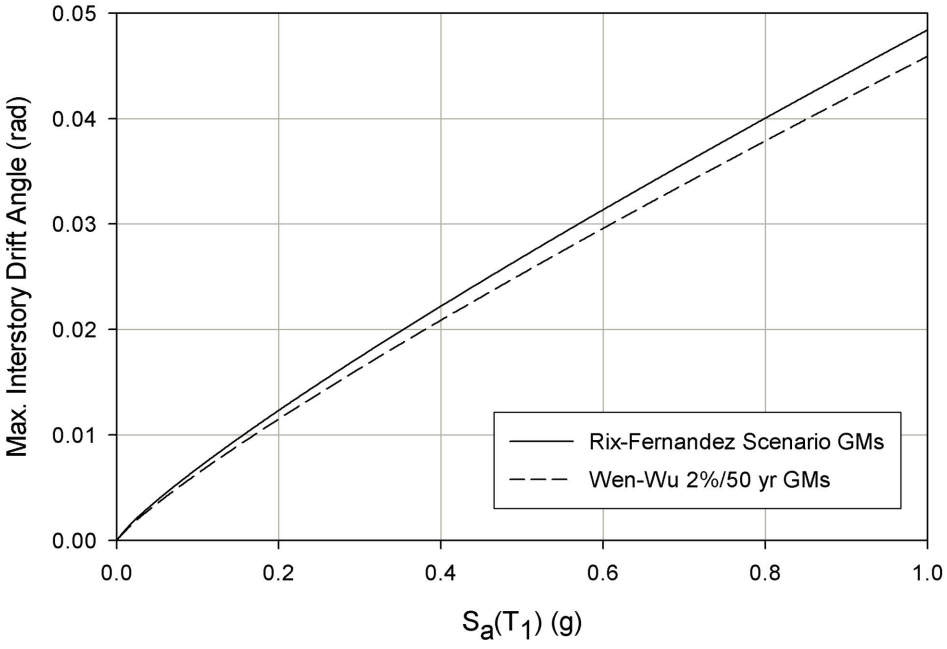

Figure 5.29 Comparison of median relationships for Frame 4ST-PR(CA).

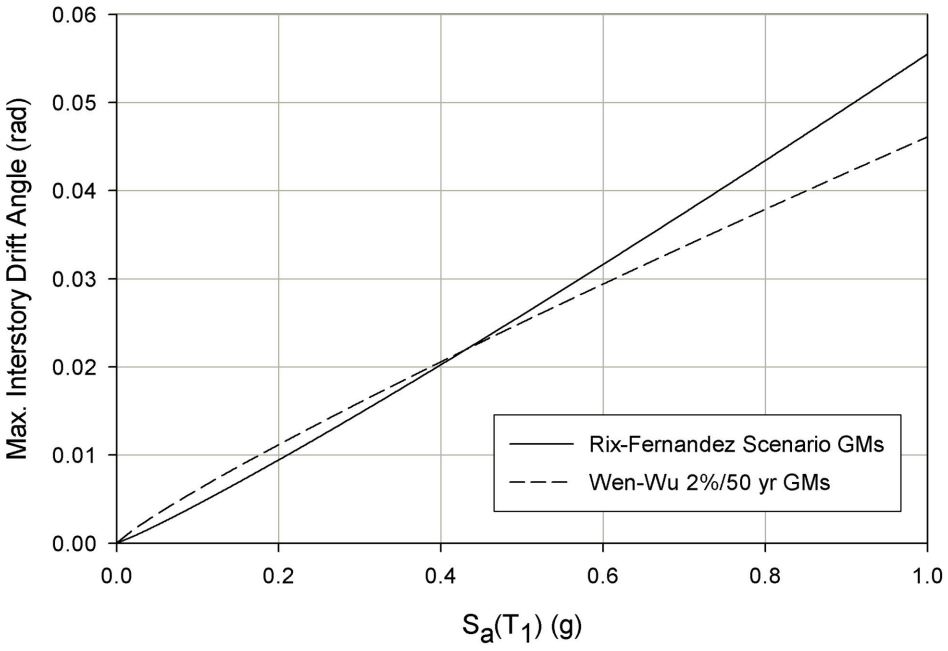

Figure 5.30 Comparison of median relationships for Frame 4ST-PR(TS).

Table 5.6 Story levels at which maximum ISDAs observed in Frame 4ST-PR.

Rix-Fernandez Scenario GMs (M_w=7.5, R=50 km)						Wen-Wu Memphis 2%/50 yr		
GM #	CA[a]	TS[b]	GM #	CA	TS	GM #	CA	TS
1	2	2	11	2	1	1	2	2
2	2	1	12	2	2	2	3	2
3	2	1	13	2	2	3	3	3
4	2	1	14	2	1	4	2	1
5	2	2	15	2	2	5	2	1
6	2	1	16	2	1	6	2	2
7	2	2	17	2	2	7	2	3
8	2	2	18	2	2	8	2	2
9	2	2	19	2	2	9	2	2
10	2	2	20	2	2	10	2	1

[a] Frame 4ST-PR(CA)
[b] Frame 4ST-PR(TS)

The capacities of Frames 4ST-PR(CA) and 4ST-PR(TS) with regard to overall stability were investigated using the IDA method with Wen-Wu 2%/50 yr ensembles. The maximum ISDA and the corresponding S_a values for each accelerogram in three ensembles are given in Table 5.7. The dynamic capacity of CA model is lower than TS model by 30% (Fig. 5.31). It might be noted that the COV values are quite low, 13 and 19% (similarly, the COV was 16% in Frame 3ST-PR). These consistently low COVs indicate that the responses of frames become less sensitive to the particular time history as the capacity of the frames is approached. Mean ISDA values of 4.7 and 6.7% were assumed to define the collapse prevention limits for the CA and TS models, respectively, as suggested by the results in Table 5.7.

Table 5.7 ISDA and S_a limits obtained from IDA method in Frame 4ST-PR.

Ground Motion	Frame 4ST-PR(CA)		Frame 4ST-PR(TS)	
	Max. ISDA (rad)	Max. $S_a(T_1)$ (g)	Max. ISDA (rad)	Max. $S_a(T_1)$ (g)
St. Louis_01	0.0477	1.40	0.0679	1.90
St. Louis_02	0.0488	0.80	0.0806	1.10
St. Louis_03	0.0570	0.90	0.0274	0.50
St. Louis_04	0.0379	0.70	0.0673	0.90
St. Louis_05	0.0487	1.20	0.0672	1.50
St. Louis_06	0.0611	2.30	0.0329	1.10
St. Louis_07	0.0478	1.40	0.0672	2.00
St. Louis_08	0.0308	0.70	0.0726	1.70
St. Louis_09	0.0458	0.80	0.0711	1.60
St. Louis_10	0.0521	1.30	0.0351	0.70
Carbondale_01	0.0495	1.30	0.0755	1.80
Carbondale_02	0.0516	1.30	0.0714	1.50
Carbondale_03	0.0480	0.90	0.0689	1.80
Carbondale_04	0.0492	1.40	0.0759	1.30
Carbondale_05	0.0454	0.70	0.0583	1.00
Carbondale_06	0.0465	1.10	0.0658	1.30
Carbondale_07	0.0503	1.10	0.0761	1.40
Carbondale_08	0.0503	0.80	0.0669	0.80
Carbondale_09	0.0481	1.10	0.0688	0.50
Carbondale_10	0.0416	0.70	0.0724	1.40
Memphis_01	0.0510	1.50	0.0750	1.30
Memphis_02	0.0389	0.60	0.0713	0.90
Memphis_03	0.0425	0.70	0.0662	0.90
Memphis_04	0.0380	0.90	0.0723	1.90
Memphis_05	0.0464	1.20	0.0772	1.60
Memphis_06	0.0458	0.70	0.0739	1.10
Memphis_07	0.0367	0.60	0.0616	0.90
Memphis_08	0.0470	1.20	0.0778	1.70
Memphis_09	0.0481	0.90	0.0756	1.40
Memphis_10	0.0436	0.60	0.0717	1.10
MEAN	0.0465	1.03	0.0671	1.29
MEDIAN	0.0478	0.90	0.0712	1.30
COV	13.0%	36.2%	19.3%	32.6%

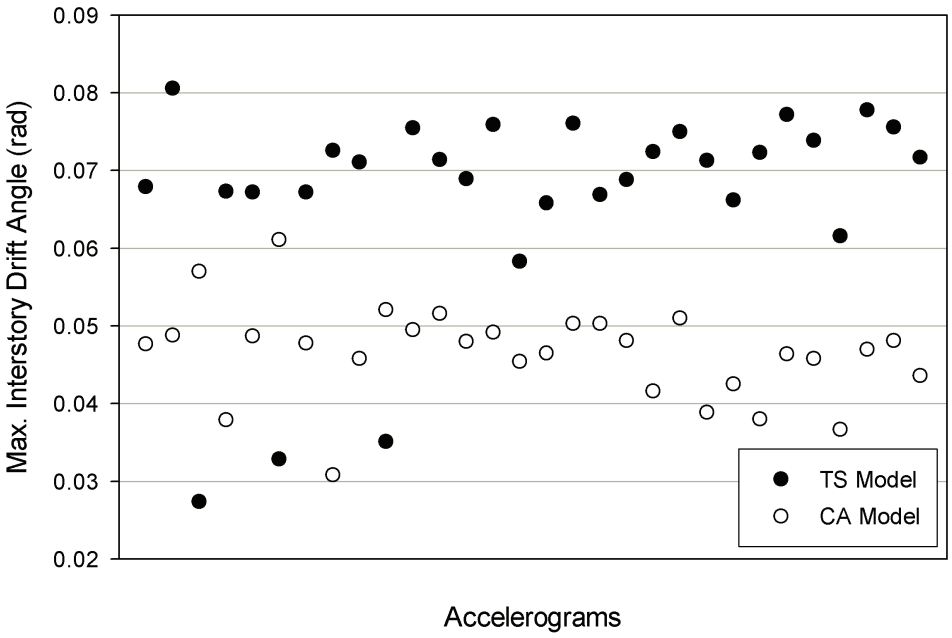

Figure 5.31 Record by record maximum ISDA values attained on Frame 4ST-PR.

5.5.4 Assessment of Frame 5ST-CB

The dynamic properties of Frame 5ST-CB (chevron braced frame) were examined by eigenvalue extraction. The fundamental period of the frame is 0.59 seconds (an analysis of an alternate frame model in which panel zone dimensions were neglected indicated a fundamental period of 0.61 seconds). Modeling the panel zones explicitly made the frame somewhat stiffer mainly due to shortening of the member lengths. The second and third mode periods are 0.22 and 0.14 seconds, respectively. The first three mode shapes are given in Figure 5.32. Higher mode effects are not negligible in this frame; modal participation factors are 80%, 14%, and 3% for the first three modes, respectively.

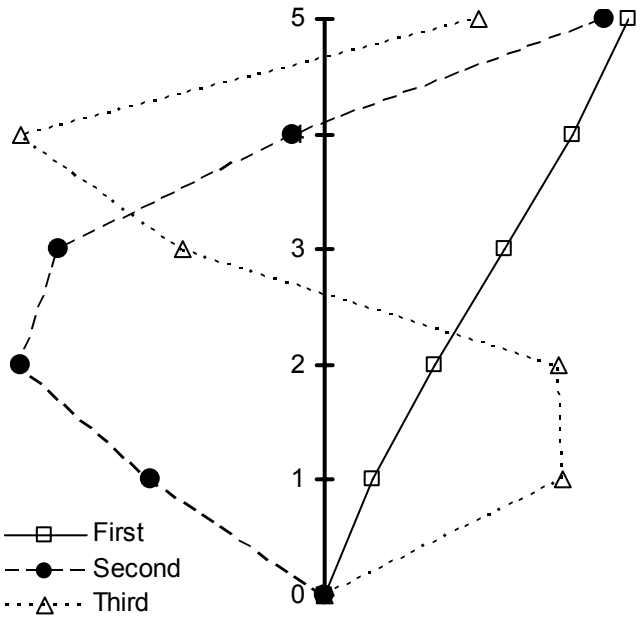

Figure 5.32 First three mode shapes for Frame 5ST-CB.

The static behavior of the braced frame was evaluated with a NSPA employing three different lateral loading schemes. The corresponding lateral load multipliers are given in Table 5.8. The results of the first-mode and k=1 loading are almost same since the first mode shape of the frame is almost linear. However, the k=2 load pattern yields a lower capacity and thus is more critical (Fig. 5.33). The sudden drops in this figure are due to buckling of the compression braces. Under all three loading schemes, the first brace to buckle (3rd story compression brace) does so at a 0.35% RDA and the frame loses more than half of its lateral strength at that point.

Table 5.8 Lateral load distributions for three cases of NSPA for Frame 5ST-CB.

Story Level	First Mode Shape	*k*=1 Shape	*k*=2 Shape
5	0.342	0.350	0.474
4	0.278	0.260	0.280
3	0.202	0.195	0.158
2	0.125	0.130	0.070
1	0.053	0.065	0.018
Summation	1.000	1.000	1.000

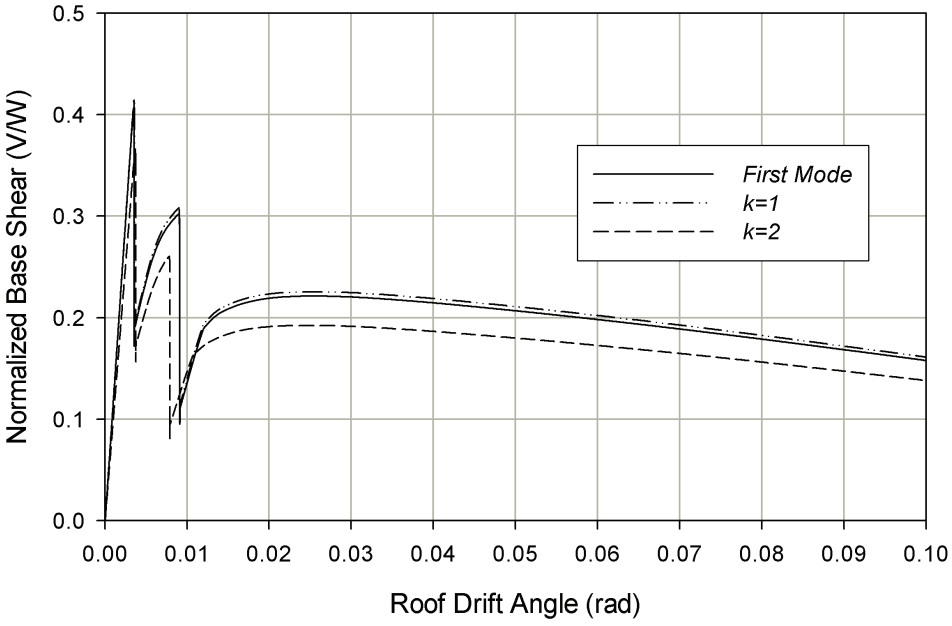

Figure 5.33 NSPA curves for Frame 5ST-CB using different loading schemes.

After buckling occurs, the tension brace at the 3rd story and braces at other stories pick up some of the lost stiffness and the frame is able to withstand increasing lateral loads. At around 0.8% RDA for *k*=2 loading pattern, and 0.9% RDA for the other two patterns, the compression brace at the 4th story buckles. Following buckling of this second brace, the frame strength decreases to one–third of its initial strength at that point. Following load redistribution among the remaining braces, especially those in tension,

the frame capacity increases substantially, but not to the level where buckling of the bracing system initiated. Finally, the capacity of the frame reaches a local maximum at around 2% RDA, remains stable until deformed to approximately 3% RDA, and then gradually decreases due to P-Δ effects which become progressively more are more pronounced at these levels of deformation.

The deformation limit defining the IO performance level was chosen as the point at which the first brace buckles in compression and a sudden drop in strength occurs, i.e., at approximately 0.35% maximum ISDA. The SD limit was identified using the same general approach taken for other frames at the point at which the secant slope of the NSPA curve decreases by 50% at 0.38% RDA. This value will be later used to find the maximum ISDA sustained at that level. None of the tension braces reach their yielding limits during the course of the NSPA. Thus, the frame responds to buckling of its braces in a brittle fashion. The response of the system is affected significantly by the loss of one of the compression braces. It is typical of the behavior of ordinary chevron braced frames where no special consideration was given to the design of the floor beam on which the braces meet (Kim and Choi, 2005).

To determine the possibility of any soft-story behavior, the conventional NSPA curve (k=2 distribution) was plotted in the same figure with the ISDAs for the two most critical stories (Fig. 5.34). This figure shows that at lower levels of deformation, i.e., before the first brace buckles, the maximum ISDA occurs at the 4th story. However, after buckling of the 3rd story compression brace, the 3rd story ISDA governs the maximum interstory drifts until the end of the analysis. At 0.38 RDA, maximum ISDA occurs at 3rd story with a value of 0.5%. This ISDA is chosen to define the SD limit for Frame 5ST-

CB. The ISDA at the 3rd story reaches 10% when the RDA reaches only 4.5%. Thus, the 3rd story behavior is the most critical of all and earlier buckling at this level determines the behavior of the frame at later stages of deformation. This, in turn, shows that the use of a NSPA using the roof drift as target displacement is unconservative for such frames.

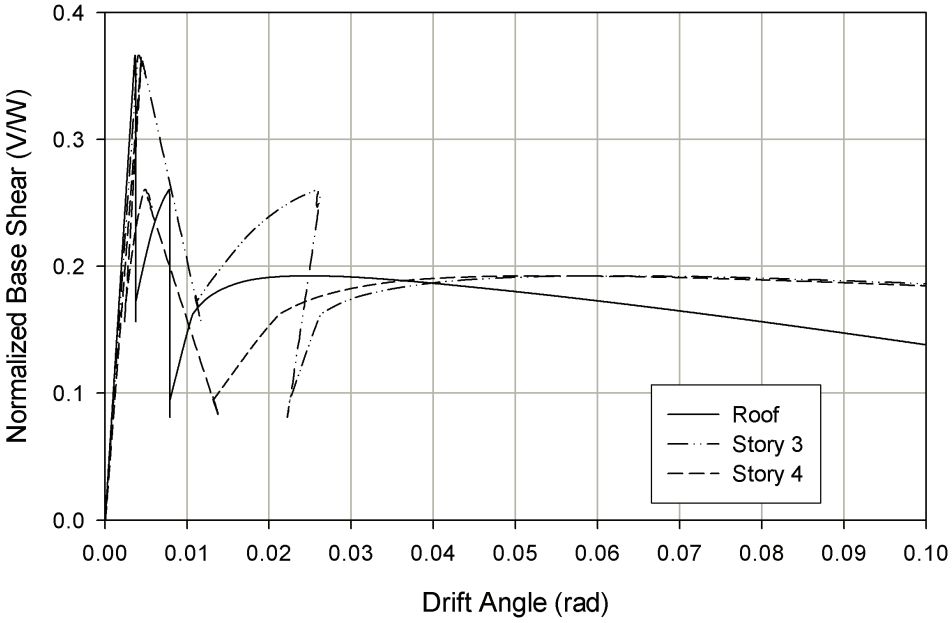

Figure 5.34 Comparison of roof drift angle against ISDAs for Frame 5ST-CB.

The seismic demand on Frame 5ST-CB was examined using three sets of ground motions. The first set is the Rix-Fernandez 10%/50 yr UHGM ensemble for Memphis; the second is the 5%/50 yr ensemble; and the third is Wen-Wu 10%/50 yr ensemble for Memphis. The intensity of the sets increase from Wen-Wu 10%/50 yr to Rix-Fernandez 10%/50 yr, and Rix-Fernandez 5%/50 yr is the highest. The results of the NTHAs are summarized in Figure 5.35. Statistical analysis of results produced by these NTHAs leads to the following median and logarithmic standard deviation in seismic demand:

$$\hat{\theta}_{\max} = 0.0619 \cdot S_a^{1.38},\ \beta_{D|S_a} = 0.33. \tag{5.13}$$

In contrast to the moment frames considered previously, the demand relationship in Eq. (5.13) indicates substantial structural softening since the power of S_a is larger than unity. Out of the 30 accelerograms, the finite element model failed to converge for 6 of them due to instabilities caused by the buckling of braces. The occurrences of maximum ISDA by story are given in Table 5.9, which indicates that the maximum ISDAs tend to occur in the 3rd story, particularly as the intensity of records increases. This is due to the buckling of 3rd story brace. This finding is consistent with the results of detailed NSPA in this section where 3rd story was identified as the weakest story.

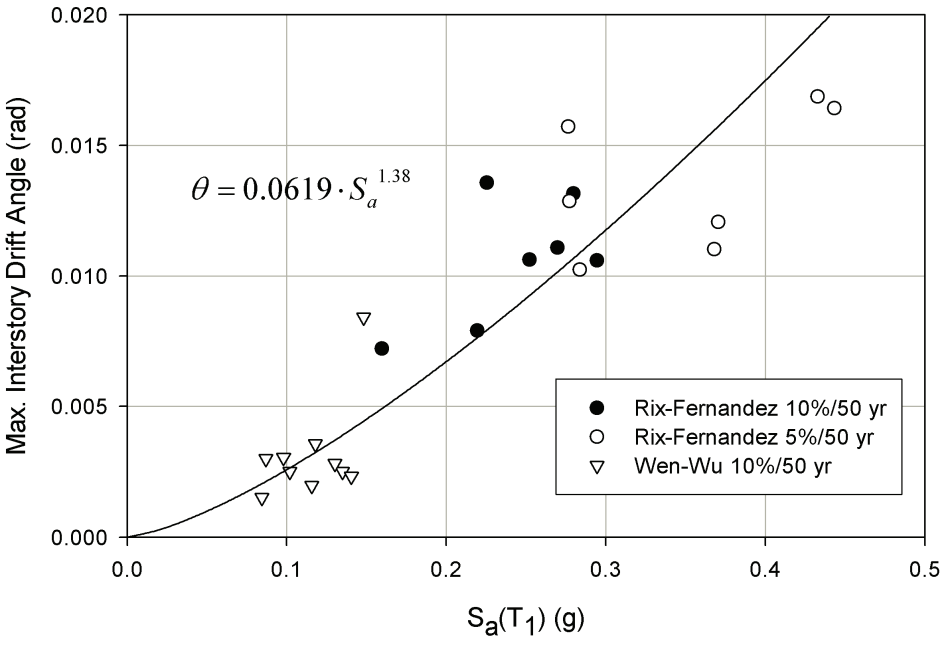

Figure 5.35 NTHA results for Frame 5ST-CB using three ensembles.

Table 5.9 Maximum ISDA occurrence statistics for Frame 5ST-CB.

Ensemble	3rd story	4th story	5th story	Total
Wen-Wu 10%/50 yr	0	4	6	10
Rix-Fernandez 10%/50 yr	2	3	2	7
Rix-Fernandez 5%/50 yr	4	2	1	7

The point of dynamic instability of the frame against increasing levels of ground motion intensity was assessed through an IDA using 10%/50 yr Rix-Fernandez Memphis (upland profile) UHGMs. The results of the IDA are summarized in Figure 5.36 and the ISDA values at incipient instability are listed in Table 5.10. In all cases, the failure was governed by the point at which the slope of the individual curves decreased below 20% of initial slope. As can be seen in Figure 5.36, the slope of the IDA curves change abruptly at around 0.4% maximum ISDA for all ground motions considered. In all cases, this sudden change coincides with the buckling of one or more of the chevron braces. Although no analytical convergence problems were encountered, the story at which buckling was experienced undergoes large deformations with little increments in ground motion intensity (0.02g intervals were utilized in IDAs). The mean value of the ISDA at defining the CP performance level is 0.4% with 15% COV.

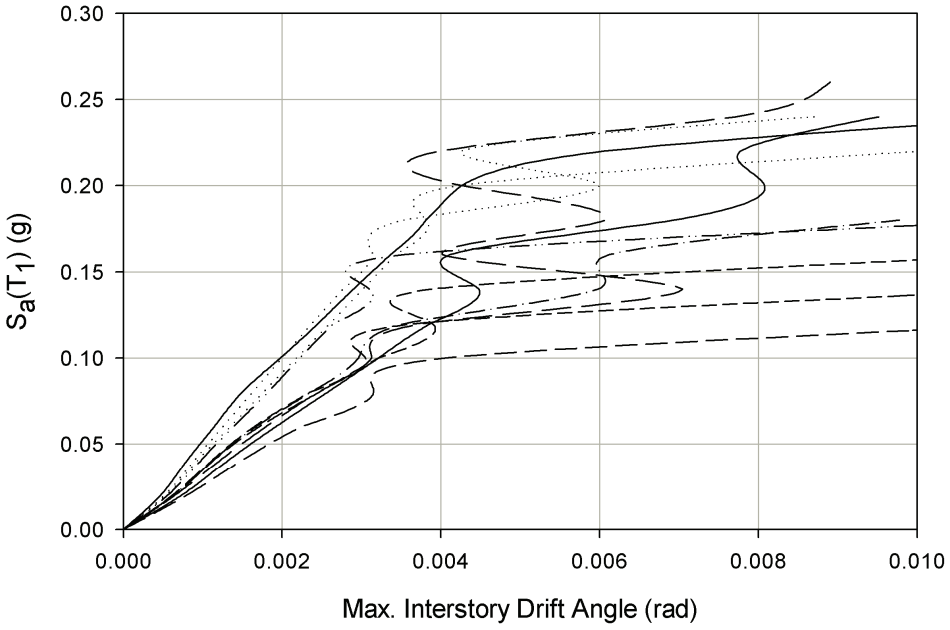

Figure 5.36 IDA results for Frame 5ST-CB using 10%/50 yr Rix-Fernandez UHGMs.

Table 5.10 ISDA and S_a limits obtained from IDA method in Frame 5ST-CB.

GM #	Maximum ISDA (rad)	Corresponding $S_a(T_1)$ (g)
1	0.0055	0.215
2	0.0042	0.200
3	0.0037	0.120
4	0.0036	0.160
5	0.0040	0.120
6	0.0045	0.130
7	0.0040	0.100
8	0.0050	0.170
9	0.0035	0.180
10	0.0040	0.140
MEAN	0.0042	0.1535
COV	15.1%	24.6%

If the failure criteria for individual IDAs are relaxed by permitting the capacity to be defined by the highest ISDA that the frame can sustain under a given accelerogram without losing stability, rather than the point beyond which the slope of the IDA curve drops below 20% of that of the initial slope, then the mean value of ISDA at this limit

increases to 2.1% with 36% COV (Table 5.11). This higher 2.1% capacity for Frame 5ST-CB can be justified in the light of the NSPA results considered earlier. In Figure 5.33, it was shown that the frame still possess some reserve strength after buckling of even two adjacent story braces (3^{rd} and 4^{th}) and attains a local maximum strength at around 2% RDA. Therefore, the capacity or CP deformation limit, in terms of ISDA, was defined as 2.1% for Frame 5ST-CB.

Table 5.11 ISDA and S_a limits obtained from IDA method in Frame 5ST-CB.

GM #	Maximum ISDA (rad)	Corresponding $S_a(T_1)$ (g)
1	0.0182	0.50
2	0.0203	0.48
3	0.0191	0.44
4	0.0188	0.48
5	0.0190	0.50
6	0.0391	0.50
7	0.0162	0.30
8	0.0299	0.42
9	0.0160	0.40
10	0.0145	0.30
MEAN	0.0211	0.432
COV	35.9%	18.0%

5.5.5 Assessment of Frame 6ST-XB

The dynamic characteristics of Frame 6ST-XB (X-braced frame) were determined by an eigenvalue analysis. The fundamental period of the frame is 1.04 sec, while the second and third mode periods are 0.31 and 0.18 sec, respectively. The first three mode shapes are given in Figure 5.37. As with the chevron-braced frame, the higher mode effects are substantial in this frame as well, with modal participation factors of 73%, 19%, and 4% for the first three modes, respectively.

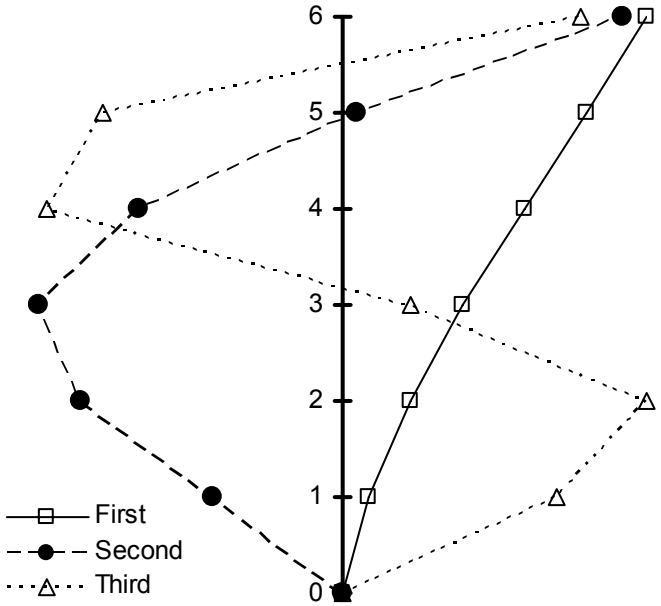

Figure 5.37 First three mode shapes for Frame 6ST-XB.

A NSPA was performed on Frame 6ST-XB using three different lateral force distributions over its height to determine which of the three yields the most critical behavior of the system so that the capacity of the frame is not overestimated. Lateral load multipliers for three cases are presented in Table 5.12. The results of the NSPA are depicted in Figure 5.38, from which it can be observed that the k=2 lateral loading yields both the least initial stiffness and the least ultimate capacity. Therefore, this pattern reflects the most critical behavior of the system. Greater load multipliers at the higher story levels make the frame more vulnerable overall.

Table 5.12 Lateral load distributions for three cases of NSPA for Frame 6ST-XB.

Story Level	First Mode Shape	*k*=1 Shape	*k*=2 Shape
6	0.322	0.297	0.407
5	0.259	0.23	0.264
4	0.193	0.185	0.171
3	0.126	0.141	0.099
2	0.072	0.096	0.046
1	0.028	0.051	0.013
Summation	1.000	1.000	1.000

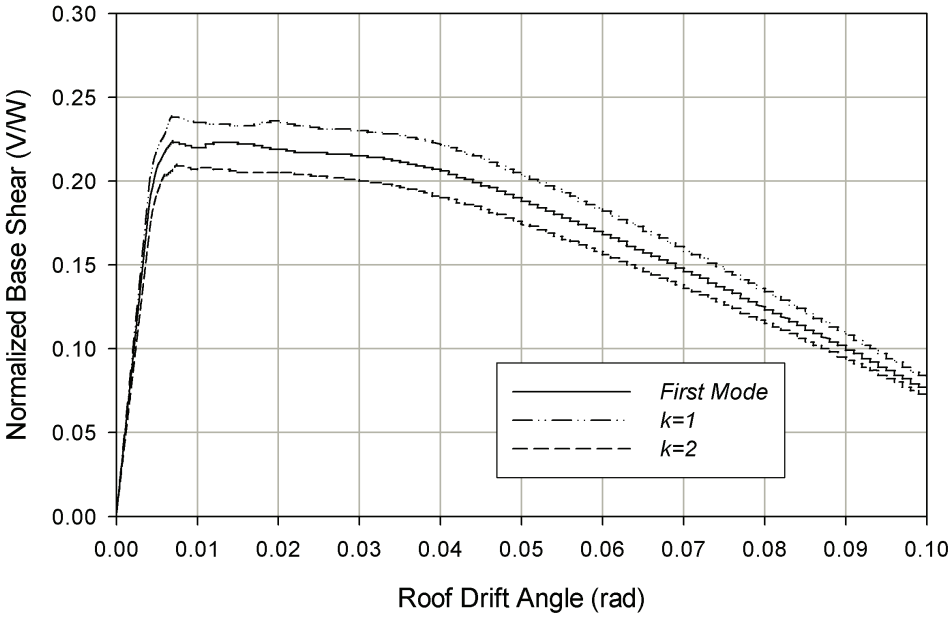

Figure 5.38 NSPA curves for Frame 6ST-XB using different loading schemes.

The brace buckling and yielding sequence for this frame are summarized in Table 5.13 for a NSPA with a lateral load pattern associated with *k*=2. The first brace to buckle is the compression brace at the 4th story. This takes place at 0.4% RDA, which is close to the value of 0.5%, a typical value for braced frames (FEMA-273). Buckling of the 3rd story brace follows immediately because the buckling of the 4th story brace leads to

additional axial force on the latter. Other stories at which compression braces buckle are the 2nd, 5th, and 1st stories in that order of occurrence. The 6th story compression brace is subjected to low gravity forces and does not experience buckling. The last of the 5 braces buckles at 0.6% RDA; immediately thereafter, the tension braces in the frame yield in the same sequence by story as they buckle, i.e., 4th, 3rd, 2nd, and 5th. First yielding occurs at 0.6% RDA and the 5th story (last story to experience yielding) yields at 1.6% RDA. The first story tension brace does not experience yielding during the course of NSPA. The first occurrence of buckling at the 4th story indicates that this story may be the weakest of the five, dictating the overall response. Accordingly, the IO deformation limit was chosen as the point of occurrence of first buckling, i.e., at an ISDA equal to 0.4%. Secant slope of the NSPA curve drops by half at 1.1% RDA for k=2 loading (Fig. 5.38). This will later be used for SD limit calculation.

Table 5.13 Buckling and yielding sequence of braces in Frame 6ST-XB.

Story Level	Buckling		Yielding	
	Roof Drift (in)	RDA (% rad)	Roof Drift (in)	RDA (% rad)
4	3.89	0.41	5.88	0.61
3	4.04	0.42	6.65	0.69
2	4.73	0.49	11.39	1.19
5	4.98	0.52	15.68	1.63
1	5.70	0.59	N/A	N/A

The NSPA suggests that this frame is not as sensitive as Frame 5ST-CB to brace buckling. In particular, it does not show any abrupt drops in strength as the braces buckle and the frame responds mildly to buckling of the braces. In this sense, it is more ductile

than the chevron-braced frame which lost half of its lateral load carrying capacity around 3% RDA. Frame 6ST-XB, on the other hand, has lost only 10% of its maximum capacity at the same RDA level. This can be attributed to the fact that the braces meet at the intersections of floor beams and columns. Therefore, there is much less demand on the floor beam. On the other hand, buckling of braces takes place in a relatively short time frame, indicating less redundancy. The frame response in the inelastic range (after about 0.4-0.5% RDA) is dictated solely by the capacity of the tension members. To examine the relative story stiffnesses and calculating the SD limit, the ISDAs recorded at each story level from a NSPA using the k=2 lateral load distribution were plotted in Figure 5.39.

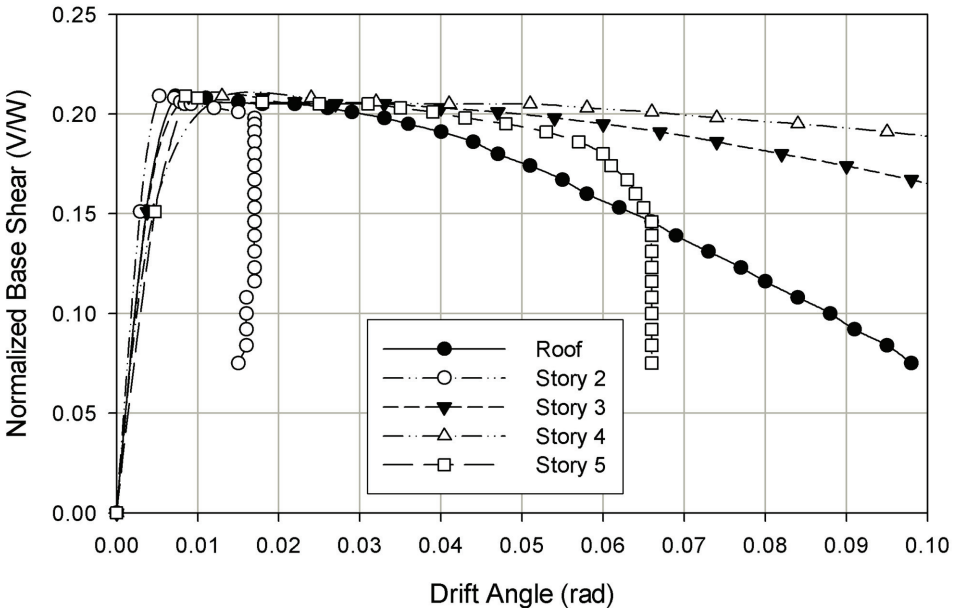

Figure 5.39 Comparison of roof drift angle against ISDAs for Frame 6ST-XB.

This plot reveals that the 4th story ISDA is the highest at all points during the course of NSPA. Moreover, the difference between the 4th story ISDA and the other story drifts becomes more pronounced as the frame deformation increases. At 1.1% RDA where the secant slope is 50% of the initial, maximum ISDA of 1.3% occurs at 4th story level. This value was chosen to represent the SD limit for Frame 6ST-XB. The 4th story ISDA reaches 10% when the roof drift angle reaches only 4%. Therefore, it can be stated that the 4th story is the most critical of the stories and earlier buckling at this level has a significant impact on the behavior of the frame at later stages of deformation. This indicates that using the NSPA with the roof drift as target displacement as a basis for performance assessment is unconservative; this conclusion also was reached for the chevron-braced frame.

The seismic demand on Frame 6ST-XB was examined using five ensembles of accelerograms. Three of these ensembles come from the Rix-Fernandez UHGMs for Memphis (upland soil profile): 10%/50 yr, 5%/50 yr, and 2%/50 yr. The remaining two ensembles are from the Wen-Wu Memphis GMs (10%/50 yr and 2%/50 yr). There are 10 accelerograms in each ensemble. The seismic demands from the NTHA of Frame 6ST-XB are illustrated in Figure 5.40. A statistical analysis of the results for these 50 accelerograms produced the following median seismic demand statistics:

$$\hat{\theta}_{\max} = 0.0338 \cdot S_a^{\,0.98},\ \beta_{D|S_a} = 0.26. \tag{5.14}$$

The relative weakness of the 4th story identified during the NSPA is also apparent in the NTHA. The 4th story produces most of the maximum ISDA values during the NTHAs; in particular, for the records of 5%/50 yr or higher hazard values, almost all of the maximum ISDAs are attributed to the 4th story. These statistics are given in Table 5.14.

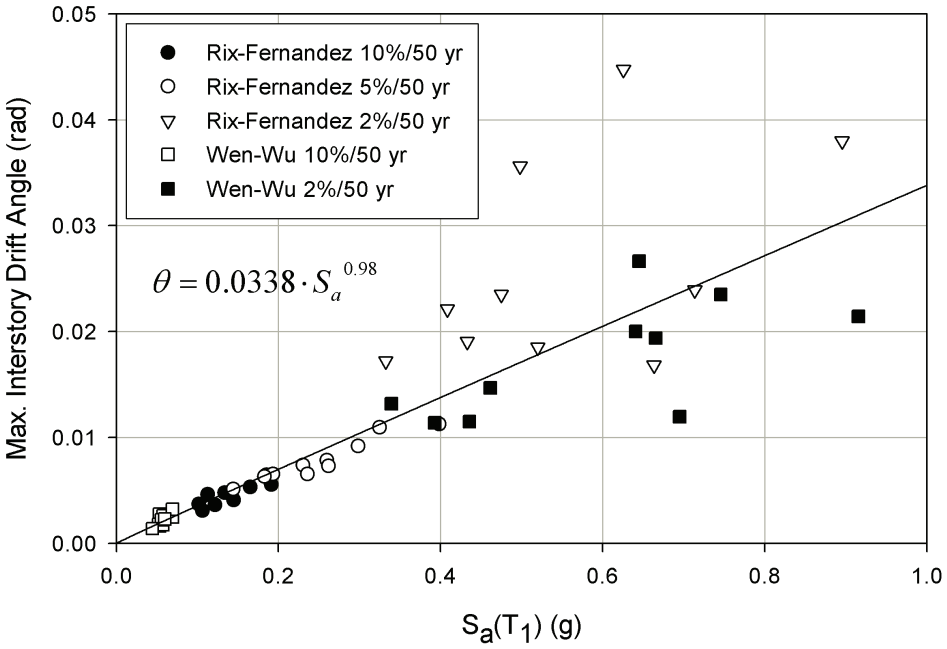

Figure 5.40 NTHA results for Frame 6ST-XB using five ensembles.

Table 5.14 Story levels at which maximum ISDAs observed in Frame 6ST-XB.

GM #	Rix-Fernandez UHGMs			Wen-Wu GMs	
	10%/50 yr	5%/50 yr	2%/50 yr	10%/50 yr	2%/50 yr
1	5	4	4	6	4
2	6	4	4	6	4
3	5	4	4	6	4
4	6	5	4	6	4
5	4	4	4	6	3
6	4	4	4	6	4
7	6	4	4	6	4
8	4	4	4	6	4
9	6	4	4	6	4
10	5	6	4	6	4

The capacity of Frame 6ST-XB at the point of instability was investigated by performing IDAs with two different ensembles, scaled in increasing intensity. The first of these is the Wen-Wu Memphis 2%/50 yr set, while the second is the 10%/50 yr set of Rix-Fernandez UHGMs for Memphis (upland profile). Nine out of 10 accelerograms

from the first set were unable to make the frame fail (according to the prior definition of failure) before an ISDA of 10% had been reached (Fig. 5.41). The remaining accelerogram caused the frame to fail at approximately 7% ISDA. With the second ensemble, the frame withstood ISDAs of up to 10% without failure for 7 of 10 records (Fig. 5.42) and produced a mean capacity of 9.2% ISDA. This can be attributed to the fact that diagonally placed braces allow for redistribution of forces to the tension braces following buckling of their compression counterparts. However, once the ISDAs exceeded approximately 1%, the majority of the braces buckled and by 3% most had yielded in tension, as well. Because of this, the median CP deformation limit for Frame 6ST-XB was chosen to be 5% ISDA, despite the fact that it apparently could maintain its stability at higher ISDA levels.

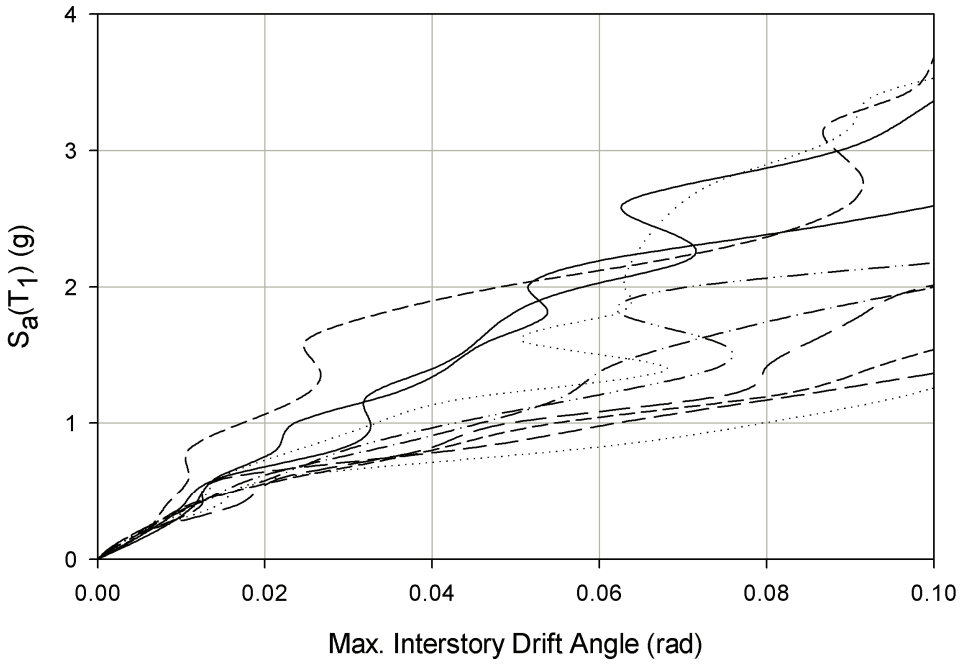

Figure 5.41 IDA results for Frame 6ST-XB using Wen-Wu 2%/50 yr GMs for Memphis.

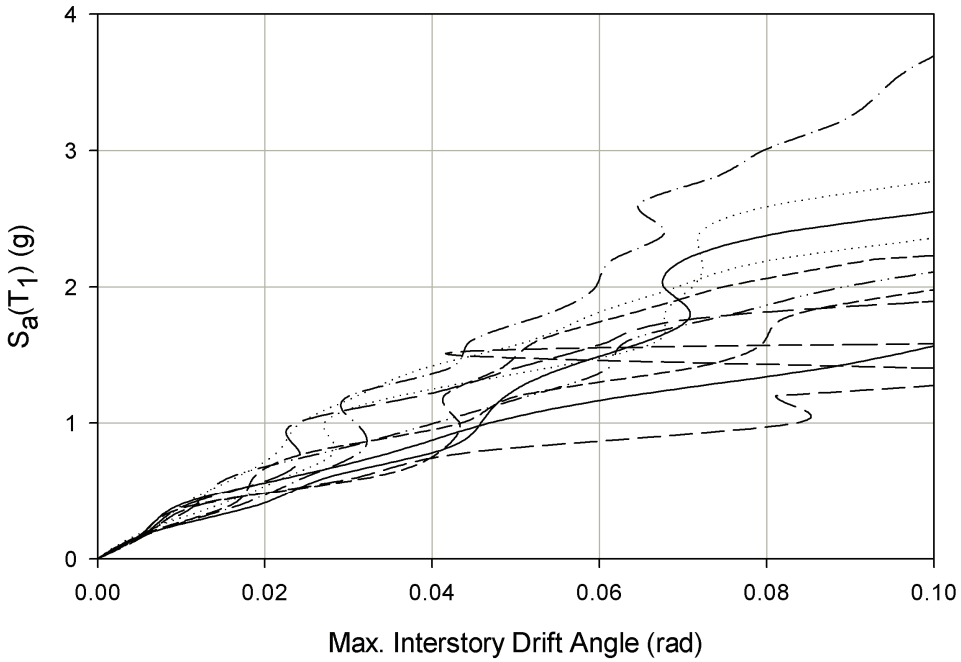

Figure 5.42 IDA results for Frame 6ST-XB using Rix-Fernandez 10%/50 yr set for Memphis.

5.6 Alternative Response Indices and Seismic Intensity Measures

The interstory drift angle was the main response measure considered in this dissertation, but other response indices were also investigated. Among these were the relative connection rotations (for PR frames) and panel zone shear deformations. In all frames, the panel zones are weaker than the adjoining beams, i.e., panel zone strength is less than plastic moment capacity of the beams in that joint. The only exception to this occurs at the top story joints of Frame 3ST-FR. In Frame 2ST-PR, the panel zone strength is larger than the connection capacity at the top floor, but less at the first floor. In Frame 4ST-PR, the connection capacities are larger than the panel zone strengths in the exterior bays at all story levels, but lower in the interior bay at all levels.

Tables 5.15 and 5.16 summarize the results of the statistical analyses for connection rotations and panel zone deformations. The Wen-Wu Memphis 2%/50 yr GM ensemble was utilized for this purpose. The maximum value for each of the indices attained during the time history of 10 ground motion records was calculated. In other words, the tables depict the mean, median, maximum and COV of maximum rotation and deformation attained in any joint of the frames during the course of the excitation. It is worth noting that as the connection capacity increases, deformations move from connections to the panel zone region as expected. This can easily be seen by comparing the last two lines in Tables 5.15 and 5.16.

Table 5.15 Statistical analysis of connection rotations in moment frames.

Frame	Relative Connection Rotation			
	Mean (milirad)	Median (milirad)	Maximum (milirad)	COV (%)
2ST-PR	8.4	7.7	13.1	27
3ST-FR	---	---	---	---
4ST-PR(CA)	17.1	16.3	25.4	32
4ST-PR(TS)	9.8	9.5	13.6	27

Table 5.16 Statistical analysis of panel zone deformations in moment frames.

Frame	Panel Zone Shear Deformation			
	Mean (milirad)	Median (milirad)	Maximum (milirad)	COV (%)
2ST-PR	16.9	17.4	26.5	35
3ST-FR	29.5	32.2	39.2	29
4ST-PR(CA)	7.8	8.1	11.7	22
4ST-PR(TS)	16.5	14.4	35.2	52

An alternative ground motion intensity measure, i.e., peak ground acceleration, PGA, also was evaluated with regard to its "*efficiency*" as discussed in Section 5.4. Multiple sets of ground motion records were used in NTHAs to determine the scatter in the response and were compared to the previous results with S_a used as the seismic intensity measure. The ground motions used were the same in both sets of analyses. In all cases, the scatter in maximum ISDA plotted against PGA was substantially higher than the scatter when S_a was the control variable. An example of this comparison is shown in Figures 5.43 and 5.44 for Frame 2ST-PR. Three sets of Wen-Wu Memphis 2%/50 yr GMs were used in both cases, with 30 records in total.

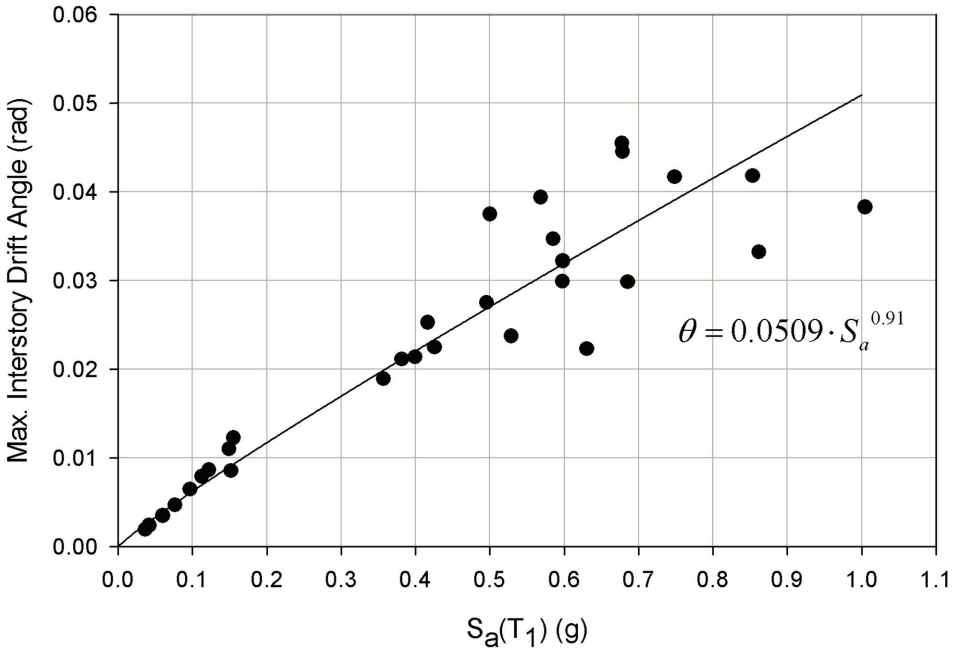

Figure 5.43 NTHA results for Frame 2ST-PR using S_a as the intensity measure.

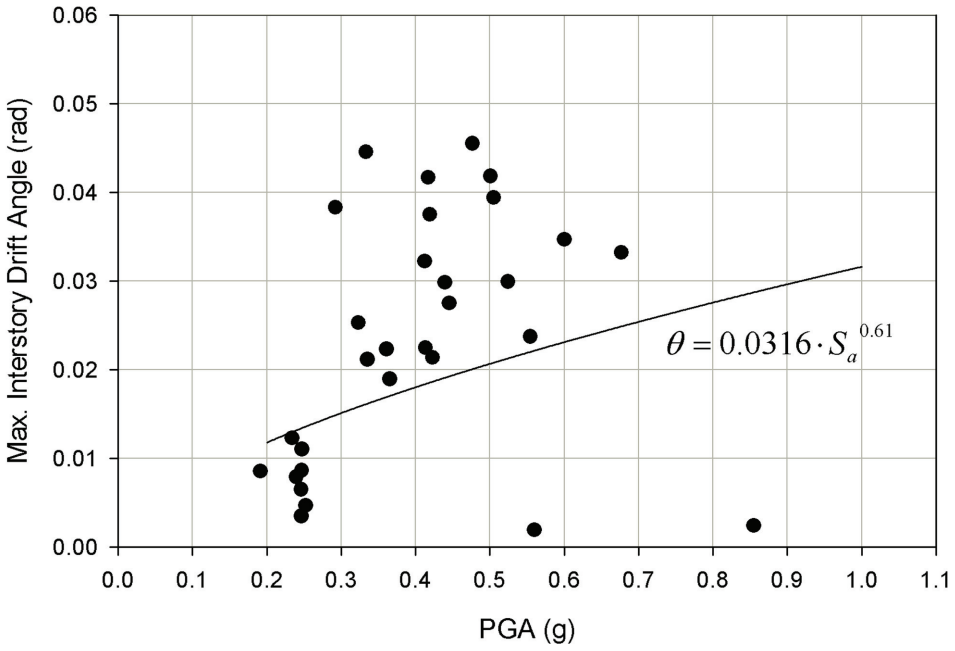

Figure 5.44 NTHA results for Frame 2ST-PR using PGA as the intensity measure.

The scatter for each frame and each seismic intensity measure was calculated using the following formula:

$$COV = \sqrt{\frac{1}{n-2}\sum_{i=1}^{n}(\ln\theta_i - \ln\hat{\theta})^2} \tag{5.15}$$

where n = number of records, θ_i = maximum ISDA produced by record #i, $\hat{\theta}$ = median ISDA value from the best fit curve. The parameter COV estimates the logarithmic standard deviation of the residual of the regression. Similar trends were observed for all frames, as summarized in Table 5.17. The table reveals that PGA is a relatively inefficient measure of seismic intensity for the frames considered in this dissertation. This finding is consistent with a study reported by Giovenale et al. (2004) for frames designed for high-seismic regions.

Table 5.17 The efficiency comparison for two seismic intensity measures.

Frame	Period (s)	# of GM records	COV with S_a (%)	COV with PGA (%)
2ST-PR	1.07	20	19	89
3ST-FR	2.01	30	25	90
4ST-PR(CA)	1.40	20	18	32
4ST-PR(TS)	1.34	20	19	35
6ST-XB	1.04	20	22	33

5.7 Appraisal of Seismic Performance of Model Frames

The seismic performance of several moment frames and braced frames has been investigated in detail. Frame 3ST-FR is the most flexible of the frames analyzed; its fundamental period is higher than one would calculate using the empirical formulas in the literature (FEMA-273/356). Higher-mode effects are important in Frames 5ST-CB and 6ST-XB, where first mode participation factors are 80 and 73%, respectively. Fundamental periods calculated for these braced frames are in good agreement with the results of a recent study by Tremblay (2005), in which it was suggested (after a review of 7,254 reference buildings) that the fundamental periods of the braced frames are between two straight lines; $T = 0.025 \cdot h_n$ and $T = 0.09 \cdot h_n$; where h_n is the height of the frame in meters and T is the fundamental period in seconds. The best fit expression to the data yielded the following expression:

$$T = 0.056 \cdot h_n^{0.90} \quad . \tag{5.15}$$

Using this formula, the fundamental periods of Frames 5ST-CB and 6ST-XB would be calculated as 0.80 s. and 0.99 s., respectively, which differ by 27% for Frame 5ST-CB

and 5% for Frame 6ST-XB from the periods determined by the eigenvalue extractions performed for these frames.

The NSPA method was employed to assess the inelastic behavior of the system under increasing static loading. The use of multiple lateral load patterns identified which distribution made the system appear more vulnerable and which distribution yielded a more conservative prediction of its behavior. A lateral load distribution with k=2 shape produced the least initial stiffness and the least capacity for all frames except Frame 2ST-PR. This loading scheme was also used throughout the SAC Project, as it was believed to be consistent with Western U.S. practices. Identification of weak or, soft stories using the NSPA was confirmed in all frames by the NTHA. The maximum ISDA occurrence statistics agreed very well with the soft story of the frames found by the NSPA, especially at higher magnitudes of seismic demands.

The NTHA method was used to determine the seismic demand relationships for each frame to be used later in fragility assessment (see Chapter 6). Different suites of ground motion records produced relationships which are quite close to each other. These similarities suggest that the seismic demands are more dependent on the characteristics of the frame rather than on the ensembles used to create them. The NTHAs also indicated that maximum drifts tend to occur in the lower stories as the intensity of the accelerograms increase. The capacity of each frame was determined using the IDA method. Some frames did not experience failure or non-convergence prior to reaching 10% maximum ISDA; others showed relatively early failures under certain accelerograms.

A summary of the ISDAs that define the three performance levels used subsequently in fragility assessments is presented in Table 5.18.

Table 5.18 Fundamental periods and performance limits for all frames.

Frame	Fundamental Period (s)	Performance Limit ISDA (rad)		
		IO	SD	CP
2ST-PR	1.07	0.0070	0.0270	0.1000
3ST-FR	2.01	0.0080	0.0340	0.0860
4ST-PR (CA)	1.40	0.0070	0.0300	0.0465
4ST-PR (TS)	1.34	0.0070	0.0300	0.0670
5ST-CB	0.59	0.0035	0.0046	0.0210
6ST-XB	1.04	0.0040	0.0130	0.0500

CHAPTER VI

FRAGILITY ASSESSMENT AND REHABILITATION STRATEGIES FOR STEEL FRAMES

Most risk-informed decision methods require an estimate of the limit state or damage state probability for the system of concern. In the simplest formulation, it is assumed that the uncertainties in demand, Q, and capacity, R, can be modeled by treating R and Q as random variables with known probability distributions. The margin of safety, M, is defined as $M=R–Q$, where clearly R and Q must be expressed in dimensionally consistent units – forces, deformations, accelerations, etc. The limit state (or, damage state) occurs if R is less than Q. The probability of this event is:

$$P_{LS} = P[R < Q] = \int_0^\infty F_R(x) \cdot f_Q(x)\, dx \tag{6.1}$$

in which $F_R(x)$ = cumulative distribution function (CDF) of R and $f_Q(x)$ = probability density function (PDF) of Q. Equation (6.1) is an expression of the theorem of total probability, which can be rewritten as,

$$P_{LS} = \sum_x P[LS \mid Q = x] \cdot P[Q = x] \tag{6.2}$$

in which the term LS represents a state of unsatisfactory performance. Equation (6.2) is a useful alternative representation for seismic risk analysis purposes, as it clearly identifies the two essential ingredients of seismic risk assessment: the fragility, $P[LS|Q=x]$ and the seismic hazard, $P[Q=x]$. If the risk assessment is based on a scenario earthquake (for example, a M_w=7.5 earthquake 50 km from the site) rather than a fully-coupled analysis,

then, the event $P[Q=x]$ and the summation in Equation (6.2) are unnecessary and the conditional probability is replaced with $P[LS|Scenario]$.

If the probability distributions (or, densities) for the terms in *LS* can be established with near-certainty, the risk assessment becomes a simple application of applied probability. Unfortunately, sources of demand and capacity data are limited in seismic risk assessment. Both *R* and *Q* are functions of many random variables. The capacity and demand represent models of reality rather than the reality, regardless of their sophistication. A number of seismic fragility studies of buildings and bridges conducted during the past decade (Ellingwood, 1990; Singhal and Kiremidjian, 1996; Shinozuka et al., 2000) have confirmed that the fragility term in Equation (6.2) can be modeled by a lognormal distribution. The limit state probabilities calculated from such models based on limited data may not be correct in a relative frequency sense. On the other hand, what is of interest is the comparison of P_{LS} for two (or, more) competing alternatives, and a comparative analysis of several alternatives is likely to give a correct ordinal ranking of decision preferences provided that the uncertainties are modeled consistently. With the lognormal distribution modeling of the uncertainties in demand and capacity, we have:

$$F_R(x) = \Phi[\ln(x / m_C) / \beta_R] \tag{6.3}$$

in which, fragility parameters m_C = median capacity, β_R = logarithmic standard deviation (approximately the coefficient of variation when COV < 0.30) in capacity. The seismic hazard can be represented, in approximation, by:

$$H(S_a) = k_o \cdot S_a^{-k} \tag{6.4}$$

where k_o is related to the characteristic extreme of the distribution (Benjamin and Cornell, 1970), and *k* is the slope of the hazard curve on a log-log plot. Substitution of Equations

(6.3) and (6.4) into Eq. (6.1) and numerically integrating leads to a point estimate, P_{LS}. Equations (6.3) and (6.4) describe the fragility and the hazard, respectively when the state of knowledge is essentially perfect, at least within the bounds of normal seismology and structural engineering. Parameters m_C and β_R measure inherent randomness (or, aleatory uncertainty) in system capacity. Similarly, k_o and k measure uncertainty in the basic seismic hazard. Such uncertainties are essentially irreducible under current engineering analysis procedures. This inherent variability is a characteristic of inherent (or aleatory) uncertainty; additional data or other information does not change the probabilistic model in any significant way. Similarly, parameters k_o and k in Equation (6.4) define the basic stochastic nature of ground motions at a particular site. Its existence is known and it is quantified by a probability distribution. Examples of this type of uncertainty would be the future occurrence of a seismic event on a fault, its intensity and frequency content, compressive strength of concrete, or properties of structural steel.

6.1 Uncertainty Modeling

Performance assessment of civil engineering structures subjected to earthquakes should account for all sources of uncertainty in the estimated seismic forces, or demands and the nonlinear behavioral characteristics and capacities of these relatively complex facilities. Recent advances in computing power have made it possible to predict the behaviors of large and complex structural systems relatively accurately, provided that their demand and capacity characteristics are known (Wen et al., 2003).

In addition to the factors that are inherently random as noted above, additional sources of uncertainty in capacity and demand arise from the assumptions and approximations made in specifying the hazard, modeling the strength and stiffness of structural materials and components, and modeling the structural system by finite element methods, and limitations in the supporting databases. In contrast to the aleatory uncertainties, these knowledge-based (or, epistemic) uncertainties depend on the quality of the analysis and supporting databases. Sources of epistemic uncertainty in seismic hazard include representing 3-D structures with 2-D frames, using centerline models of frames instead of models that include finite connection sizes, limitations in available databases (which invariably are restricted to small samples), ignoring the contributions from non-structural elements, etc. It is generally understood that the seismic hazard curves provided by the USGS represent the *mean* seismic hazard at a site, inasmuch as the values represent an average of values obtained from several alternate plausible ground motion models.

The presence of epistemic uncertainty in hazard and fragility is displayed by a family of curves, reflecting incomplete knowledge regarding the parameters used to model the aleatory uncertainty in Equations (6.3) and (6.4): m_C, β_R, k_o and k. The choice of CDF is also a source of epistemic uncertainty, but the CDFs, have been specified, as noted above, with the idea of developing a risk tool that results in decisions that ranked correctly in an ordinal sense. To first order, it is assumed that these epistemic uncertainties can be modeled by treating the estimates of m_C and k_o, as bayesian random variables This is customary in modeling epistemic uncertainty in seismic probabilistic risk assessment of critical facilities. Studies to date have shown that the contribution of uncertainty in the variance or

coefficient of variation is of secondary importance in comparison to that of uncertainty in the mean or median (here, k_o and m_C).

If the epistemic uncertainties are small, the probability density function will be centered on the point estimate P_{LS} with small dispersion; conversely, if the epistemic uncertainties are large, the PDF of P_{LS} will be broad. As depicted in Figure 6.1, higher epistemic uncertainty leads to greater variation from the median to achieve the same level of confidence, e.g., 95%. The width of the confidence interval gives some idea of how the uncertainty in the estimate of the parameters affects the performance metric, such as P_{LS}. A very wide interval may indicate that more data should be collected or, a more refined model should be used before making definitive conclusions.

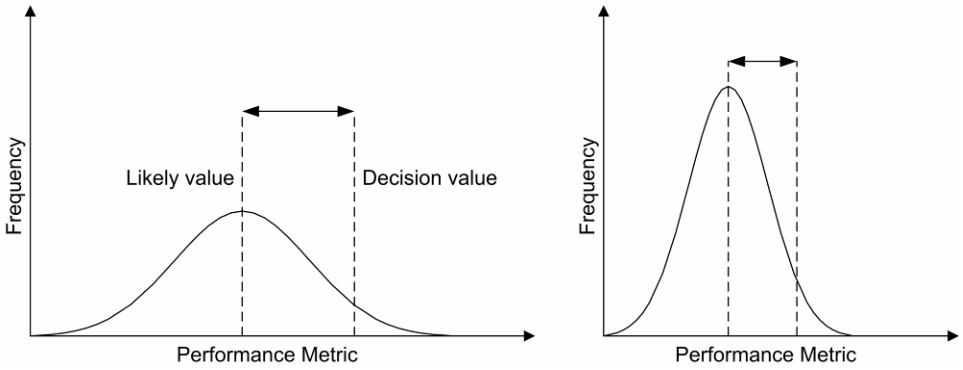

(a) (b)

Figure 6.1 Representations of (a) high and (b) low epistemic uncertainties.

It is important to distinguish the epistemic uncertainties from the aleatoric uncertainties, if at all possible. The epistemic uncertainty is required for the decision-maker to assert a "degree of confidence" in the results of the risk assessment. Using the results above, it is possible to construct a statement, such as "I am 95% confident that the

damage state probability is between p_1 and p_2" or "I am 90% confident that the damage state probability is less than p_2." Such statements convey a sense of the confidence of the analyst in his/her risk assessment. The point estimate P_{LS} is not informative as to this confidence level, i.e., two alternative analyses, one made with limited data and a second made with comprehensive effort, would lead to the same P_{LS} if the estimates of the aleatory uncertainty were the same. With the presence of epistemic uncertainties in the nature of the process, the fragility equation now becomes mean fragility by replacing β_R in Equation (6.3) by β_C as follows:

$$F_R(x) = \Phi[\ln(x / m_C) / \beta_C] \tag{6.5a}$$

where

$$\beta_C = \sqrt{\beta_R{}^2 + \beta_U{}^2} \tag{6.5b}$$

$$\beta_R = \sqrt{\beta_{D\backslash S_a}{}^2 + \beta_{SC}{}^2} \tag{6.5c}$$

Seismic fragilities in this dissertation were calculated using Equation (6.5a), where total uncertainty, β_C, is divided into two distinct groups, i.e., aleatoric uncertainty, β_R and epistemic uncertainty in modeling, β_U. Aleatoric uncertainty, β_R is further divided into two; $\beta_{D\backslash S_a}$ = uncertainty in seismic demand, β_{SC} = uncertainty in structural capacity. The term β_{SC} reflects three levels of structural performance. For the CP level, it is calculated from the IDA and is equal to the COV of the limiting ISDA value. For the frames considered, this COV was less than 15% in nearly all cases; therefore this value was assumed for the CP level. For the higher performance levels (IO and SD), it is assumed to be 25% since it has been observed that lower levels of excitation tend to

produce larger variability (Kinali and Ellingwood, 2007a). Modeling uncertainty, β_U, is assumed to be 20%, consistent with the typical prediction uncertainty associated with nonlinear finite element analysis platforms. The uncertainty in seismic demand is assumed to be equal to $\sigma_{ln\varepsilon}$ obtained from corresponding demand relationships, which were later used in the fragility calculations. The three performance levels (IO, SD, and CP) define the boundaries separating four damage states: continued occupancy, impaired occupancy, structural damage and structural collapse, as seen in Figure 6.2. These damage probabilities can be related to the expected economic losses in a seismic vulnerability or loss assessment (Ellingwood and Wen, 2005).

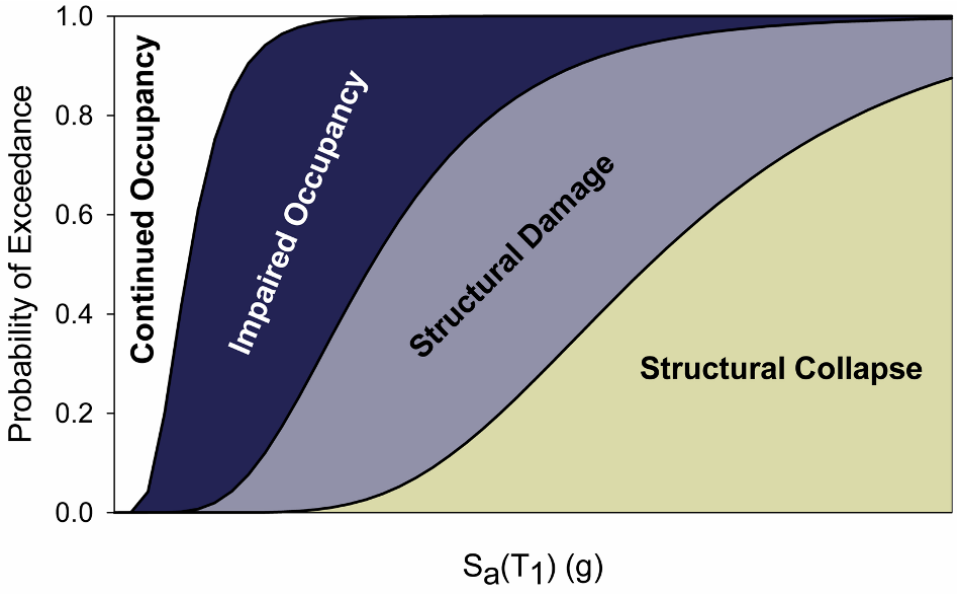

Figure 6.2 Four performance states used throughout this dissertation.

6.2 Fragility Assessment of Steel Frames

The fragility analysis of steel frames requires a system reliability approach involving Monte Carlo simulation and repeated nonlinear finite element analyses of the frames in the time domain. Because of the cost of performing such analyses, the number of simulations, *N*, necessary to model the frame, propagate the uncertainties and construct the fragility must be kept to a minimum. Although it is not difficult to model randomness in beam and column stiffness and ultimate strength using an efficient random sampling plan such as Latin Hypercube sampling, it has been found that the variability in seismic demand dominates the overall response variability of steel frames (Song and Ellingwood, 1999). In this dissertation, the yield strength, the ultimate strength, and the modulus of elasticity of the steel beams and columns were modeled as deterministic and were set equal to their respective mean values. The uncertainty in seismic demand thus is dependent on the ground motions, modeled by suites of appropriately scaled synthetic ground motions.

The seismic fragilities of all steel frames were calculated for three performance levels: IO, SD and CP. These limits were calculated for each frame in Chapter 5 and given in Table 5.18. Maximum interstory drift angle was used as the corresponding response measure. The procedure adopted in fragility calculation is shown in Figure 6.3 as a flowchart. Fragilities were calculated using median seismic demand relationships obtained from different sources of synthetic ground motion records. These results are presented in Figures 6.4 thru 6.11. For the 2- and 3-story frames, two fragility plots were provided; each was calculated using demand results of different ground motion sets. The results illustrate the relative insensitivity of frame fragilities to the selection of GM ensembles.

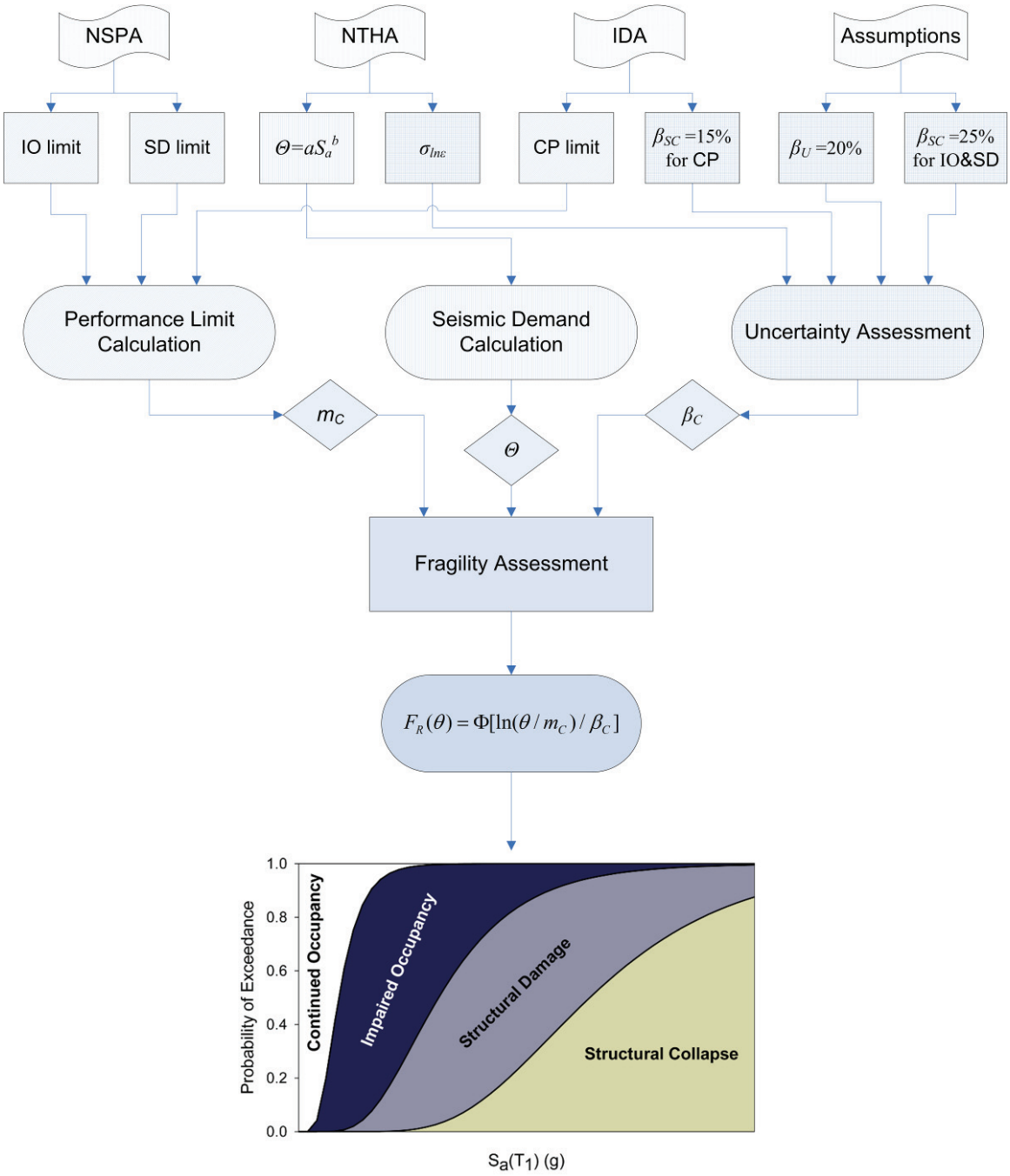

Figure 6.3 Flowchart describing the general fragility assessment procedure used in this dissertation.

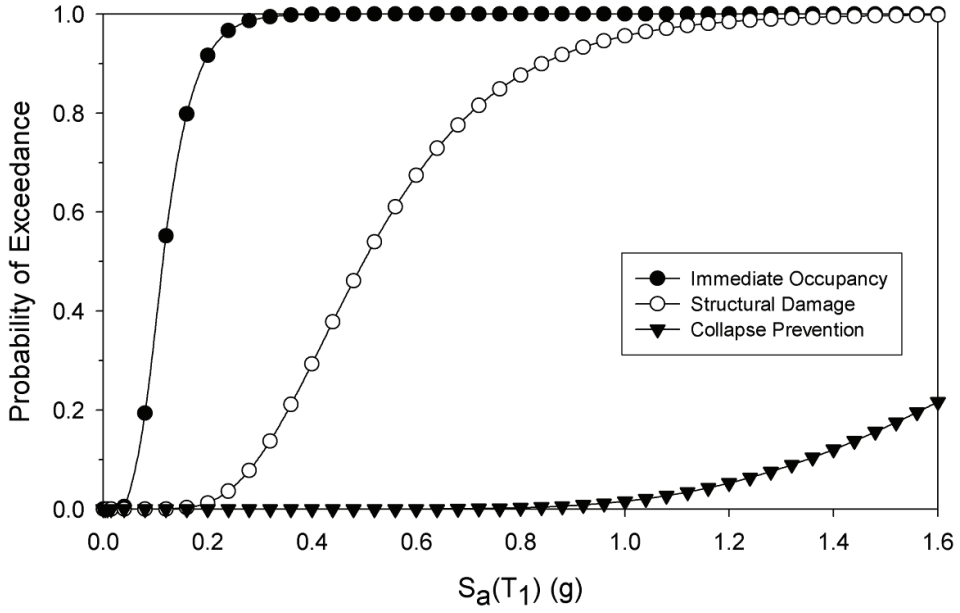

Figure 6.4 Seismic fragilities for Frame 2ST-PR using Wen-Wu demand statistics.

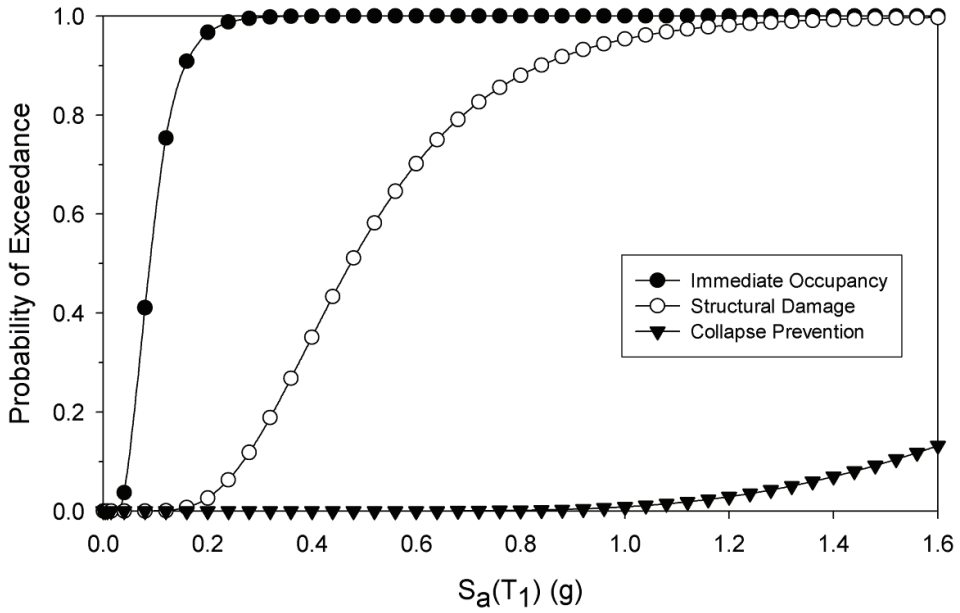

Figure 6.5 Seismic fragilities for Frame 2ST-PR using Rix-Fernandez demand statistics.

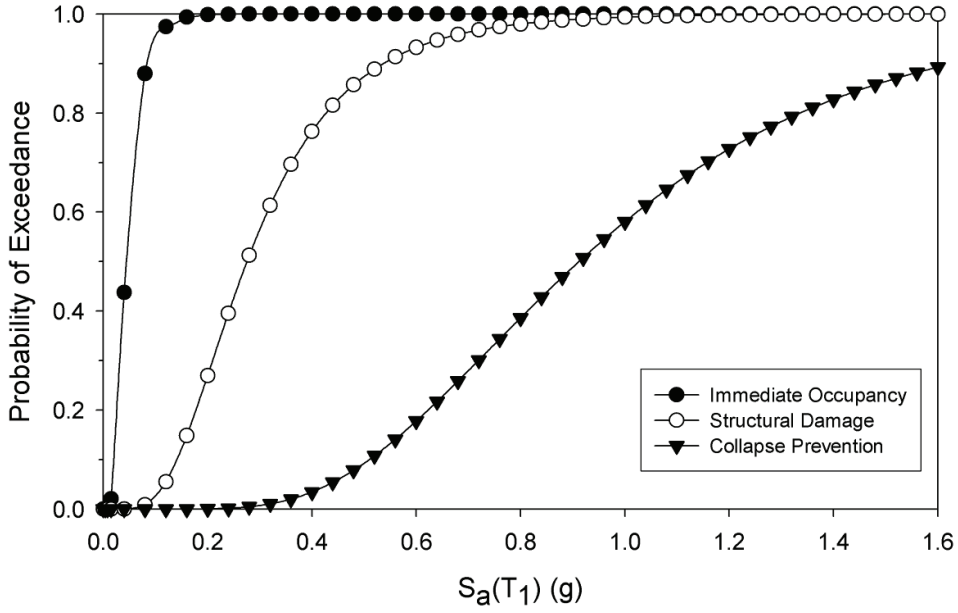

Figure 6.6 Seismic fragilities for Frame 3ST-FR using Wen-Wu demand statistics.

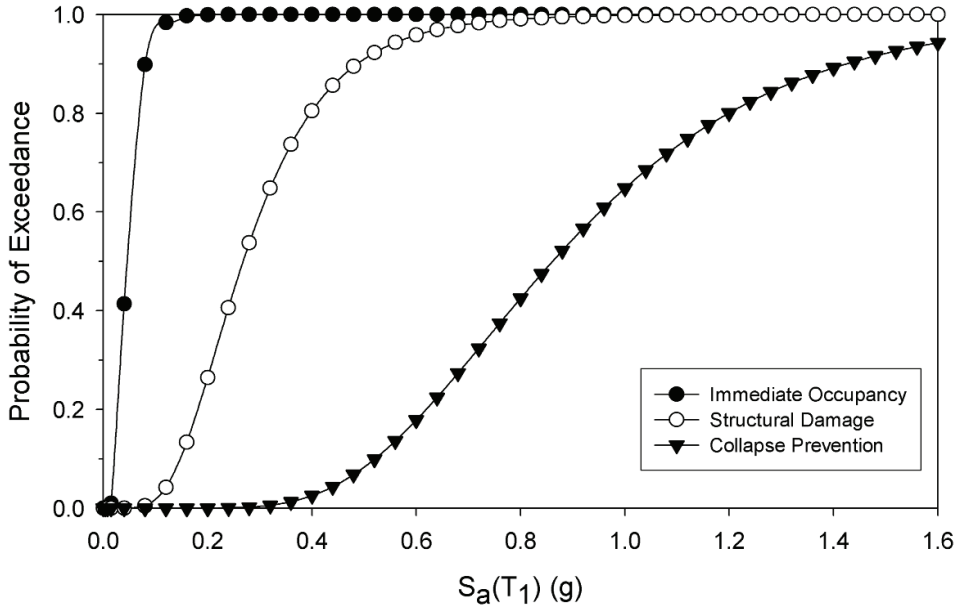

Figure 6.7 Seismic fragilities for Frame 3ST-FR using Rix-Fernandez UHGM demand statistics.

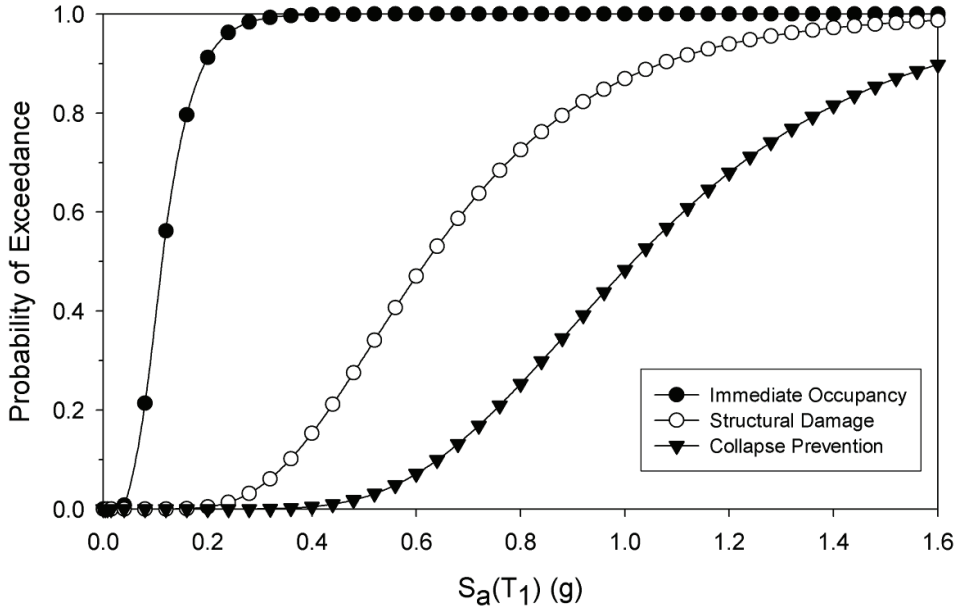

Figure 6.8 Seismic fragilities for Frame 4ST-PR(CA) using Wen-Wu demand statistics.

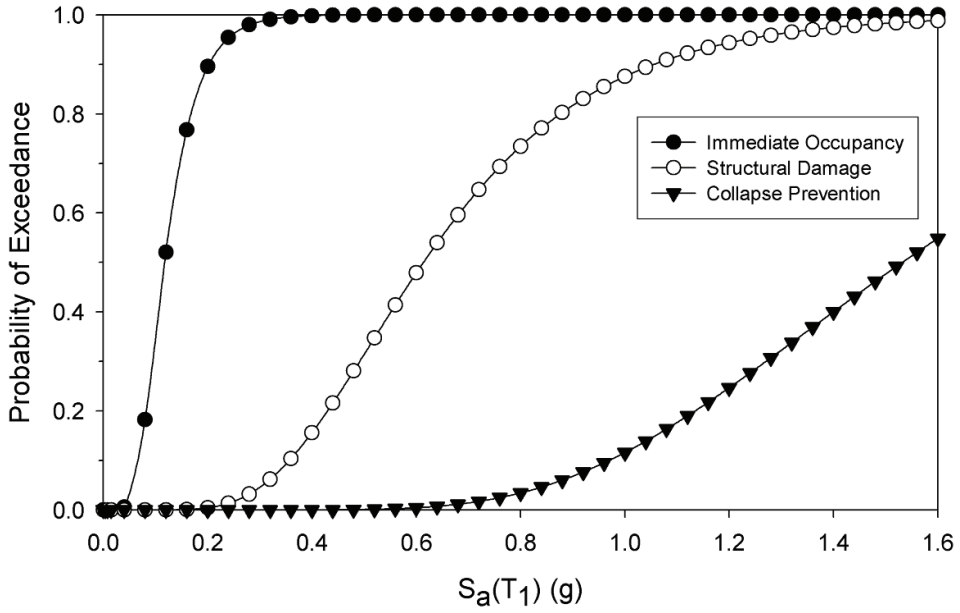

Figure 6.9 Seismic fragilities for Frame 4ST-PR(TS) using Wen-Wu demand statistics.

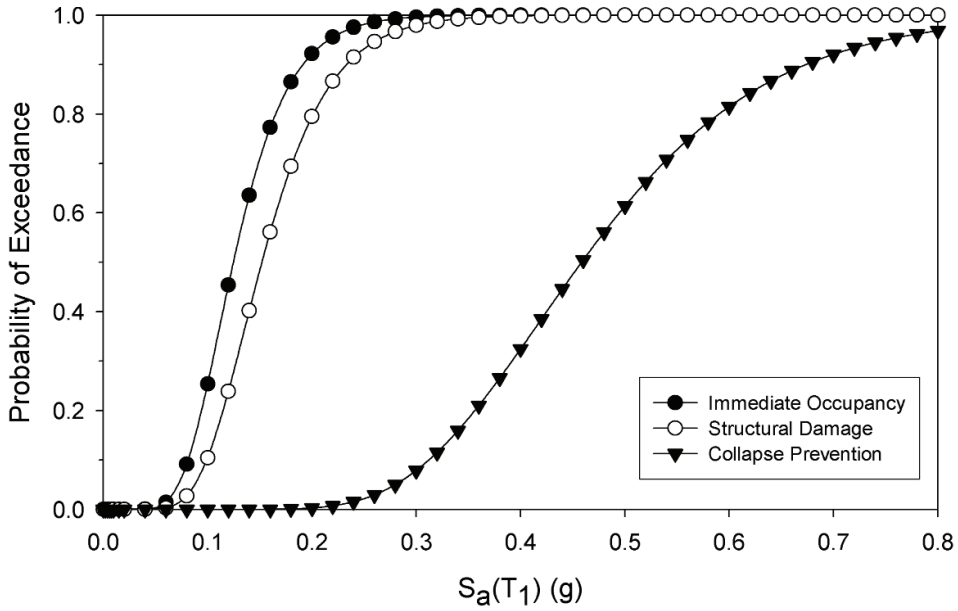

Figure 6.10 Seismic fragilities for Frame 5ST-CB.

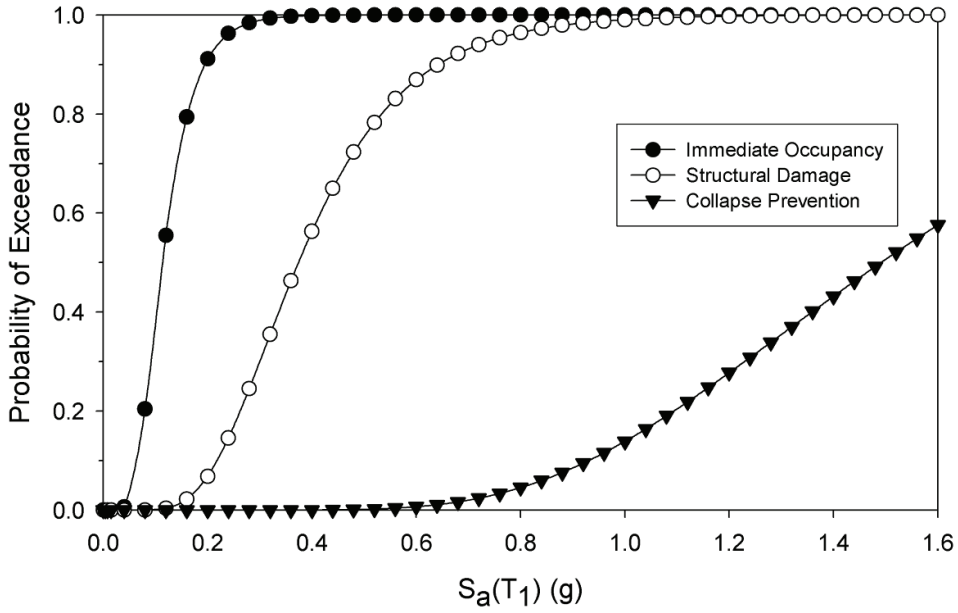

Figure 6.11 Seismic fragilities for Frame 6ST-XB.

To interpret these fragilities from an engineering perspective, the 2%/50 yr uniform hazard mean spectral accelerations were identified from the USGS website for each frame, adjusted appropriately for building period, and damage state probabilities were calculated. If there are two demand relationships for a particular frame, the Wen-Wu motions were used to generate the fragilities. The results are provided in Table 6.1.

Table 6.1 Performance state probabilities using 2%/50 yr mean hazard in Memphis, TN.

Frame	Spectral Acceleration (g)	Return Period (yrs)	Continued Occupancy (%)	Impaired Occupancy (%)	Structural Damage (%)	Structural Collapse (%)
2ST-PR	0.34	2,475	0	82	18	0
3ST-FR	0.18	2,475	0	79	21	0
4ST-PR(CA)	0.27	2,475	2	95	3	0
4ST-PR(TS)	0.28	2,475	2	95	3	0
5ST-CB	0.55	2,475	0	0	27	73
6ST-XB	0.35	2,475	0	56	44	0

[a] 2%/50yr mean spectral acceleration for Memphis, TN.

A different perspective on frame fragility is obtained when performance probabilities are assessed based on a scenario event of M_w=7.5 and R=20 km, that, according to the USGS deaggregation of seismic risk for Memphis (Fig. 3.5) represents a possible threat to the frames considered. Here, the median spectral acceleration values were calculated using the corresponding Rix-Fernandez scenario ground motion ensemble; these spectral accelerations have return periods that are much longer than 2,475 years. The results are presented in Table 6.2 and discussed in the following sections.

Table 6.2 Performance state probabilities in the scenario event of M_w=7.5, R=20 km.

Frame	Spectral Acceleration (g)	Appr. Return Period (yrs)	Continued Occupancy (%)	Impaired Occupancy (%)	Structural Damage (%)	Structural Collapse (%)
2ST-PR	0.91	6,400	0	7	92	1
3ST-FR	0.81	10,500	0	2	58	40
4ST-PR(CA)	0.90	7,500	0	19	44	37
4ST-PR(TS)	0.89	7,200	0	19	75	6
5ST-CB	0.86	4,900	0	0	2	98
6ST-XB	0.90	6,200	0	2	90	8

[a] Median spectral acceleration of M_W=7.5, R=20 km ensemble.

The following inferences can be made from the results presented in Tables 6.1 and 6.2:

- The probability of reaching the collapse state (measured in terms of deformation) under the 2%/50 yr event is zero for all but Frame 5ST-CB, which has the lowest CP level capacity of all frames considered, i.e., ISDA of 2.1%.
- All frames except 4ST-PR sustain damages at or beyond the impaired occupancy state under 2%/50 yr event.
- Frame 5ST-CB sustains the most damage and Frame 4ST-PR experiences the least damage under the 2%/50 yr event.
- For Frame 4ST-PR, connection capacity plays no role under the 2%/50 yr event.
- Frames 2ST-PR and 3ST-FR experience similar damage under the 2%/50 yr event.
- Under a severe scenario event (M_w=7.5, R=20 km), Frame 3ST-FR experiences more damage than Frame 2ST-PR. This difference can be attributed to the fact that the CP limit is less for the FR frame than that for the PR frame.
- The effect of connection capacity is significant under the severe scenario event, the 4-story model with TS connections behaving favorably in comparison with the CA model.

- The chevron-braced frame (5ST-CB) experiences almost certain collapse under the severe scenario event.
- Frame 2ST-PR has almost zero probability of collapse under both 2%/50 yr and severe scenario events mainly due to low P-Δ and high CP limit.
- In both cases, the X-braced frame behaves more favorably than the chevron-braced frame.
- The X-braced frame and PR frames, i.e., 2ST-PR and 4ST-PR(TS), experience less damages than the frames with rigid or, weak PR connections or, chevron-bracing.

In the following sections, possible seismic rehabilitation schemes are investigated for selected PR and braced frames.

6.3 Rehabilitation of Steel Frames for Seismic Performance

Seismic upgrade of existing buildings is of great concern if building portfolio in a region does not possess adequate design details with regard to current seismic hazard. Not all buildings in a portfolio are expected to be retrofitted due to feasibility concerns. Sometimes, it is more economical to demolish and rebuild a new structure reflecting the latest seismic design criteria in the region. However, due to excessive costs incurred in this process, such as interruption of business and the labor costs involved, it is more feasible for some structures to be seismically upgraded. As mentioned in earlier chapters, current building stock of Shelby Co., TN does not reflect the latest seismic design

requirements. Due to low perception of seismic risk, most building designs were governed by wind requirements. Seismic performance of the steel building stock of the region is crucial since more than one third of essential buildings have steel frames.

In the literature, different rehabilitation techniques were suggested for different types of frames. FEMA-273 lists possible strengthening methods for steel frames. For moment resisting frames following techniques are suggested:

1. Adding braces to one or more bays of each story,
2. Attaching new steel frames to the exterior of the building,
3. Strengthening the joint region to move hinge locations away from that area,
4. Adding damping devices.

Of these four possible schemes, the third is not likely to work for the frames considered in this dissertation, since, in all of them beams are stronger than the connecting columns. Further strengthening of the joint region through use of doubler plates to strengthen the panel zone region, or strengthening the PR connections would impose higher demands on vertical members. This method will be employed for two PR frames considered later in this chapter. Also, a more viable option for strengthening PR frames, i.e., addition of brace members to one of the bays of each story, will be employed for Frame 4ST-PR, as well, later in this chapter.

For braced frames, suggested rehabilitation techniques include the following (FEMA 273/356):

1. Increasing capacity of brace members,
2. Converting braces to buckling-restrained braces,

3. Adding damping devices.

In addition to these, for chevron braced frames, increasing the size of floor beams on which the braces meet is also suggested. Second technique will be utilized for two braced-frames in the following sections.

6.4 Rehabilitation of Braced-Frames by Buckling-Restrained Braces

As discussed previously in Chapter 2, the response of braced frames is mainly dictated by the behavior of the individual braces. Buckling-restrained braced-frames (BRBFs) have superior characteristics for responding to dynamic loads over the conventional braced-frames (Section 2.3.2). The two braced-frames previously considered (5ST-CB and 6ST-XB) were modified using this approach. These frames are denoted as BR-5ST-CB and BR-6ST-XB, respectively. The general practice in BRBFs is that brace members are encased in a steel tube filled with a solid medium like mortar. This provides continuous lateral support, preventing the brace from buckling. Since a separating material is placed between the member and the mortar, this medium does not carry any axial load either in tension or in compression, producing the symmetrical behavior under axial loading illustrated by the constitutive model in Figure 6.12. Previous studies have shown that these members possess almost ideal bilinear behavior (e.g., Sabelli et al., 2003). The additional mass of the medium used can be neglected as compared to the whole mass of the frame itself and the modal characteristics of the frames remain unchanged. In other words, both periods and mode shapes of Frame BR-5ST-CB are the same as those of

Frame 5ST-CB and not presented here again. Reader can refer to Chapter 5 for these details. The seismic performance of these modified Frames 5ST-CB and 6ST-XB was assessed using the same general procedure as in Chapter 5.

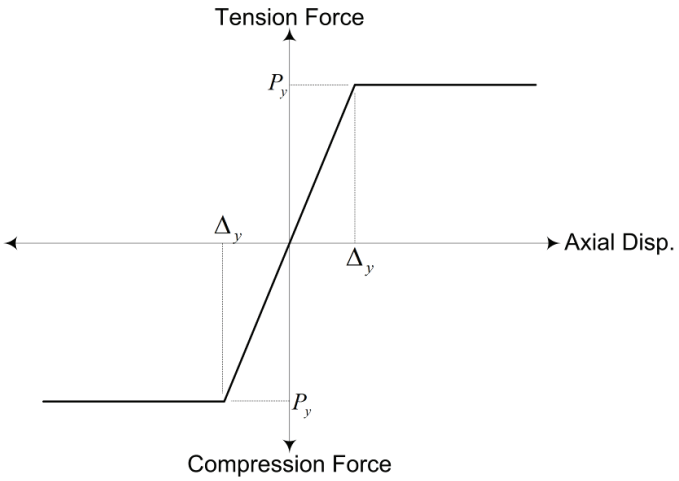

Figure 6.12 The constitutive relationship for a typical buckling-restrained brace.

6.4.1 Rehabilitation of Frame 5ST-CB

A NSPA was performed for Frame BR-5ST-CB using the same lateral loading distribution as in the original case. The results are compared in Figure 6.13 with the original case for k=2 loading. The difference is significant; capacity is more than doubled. The rehabilitated frame behaves during the NSPA like a moment resisting frame, since there is no capacity lost due to buckling of a brace. Due to this difference, the IO limit (onset of inelastic action) shifts from 0.35% to 0.5% ISDA.

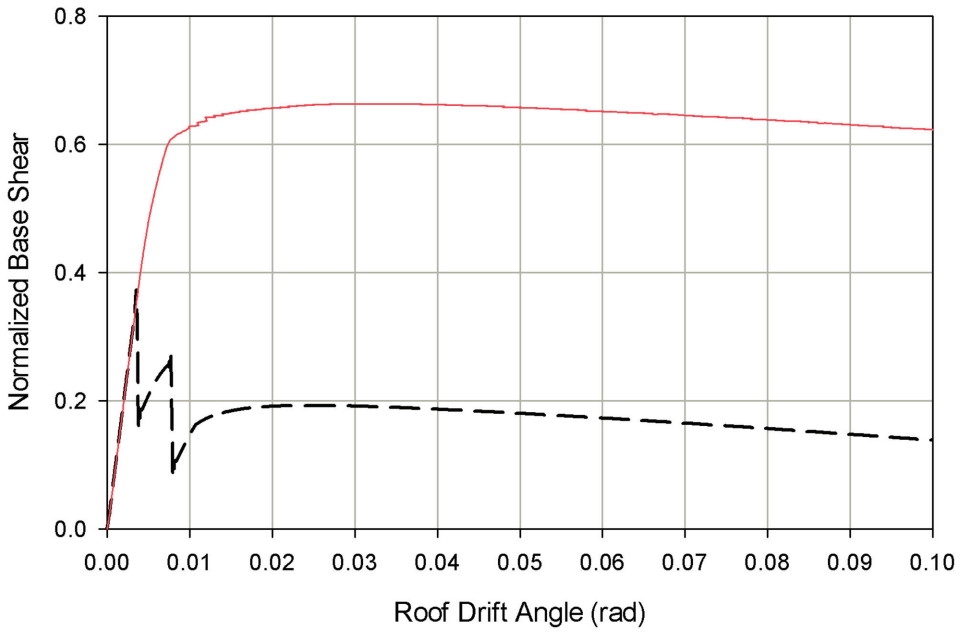

Figure 6.13 The NSPA comparison of the original and rehabilitated models of five-story chevron-braced frame.

The SD limit was calculated using the same general approach as in the original case. The slope of the secant line drops to half of initial stiffness at 1.2% RDA. This corresponds to a maximum 1.7% ISDA; this value was assumed to be the SD limit for the rehabilitated version of the frame. The seismic demand on the modified frame was assessed using both Rix-Fernandez and Wen-Wu Memphis UHGMs as shown in Figure 6.14. Statistical analysis of the results produced the following demand relationship:

$$\hat{\theta}_{\max} = 0.013 \cdot S_a^{\,0.66}, \ \beta_{D|S_a} = 0.24 \tag{6.6}$$

indicating an apparent hardening in the modified structural system in contrast to the softening observed in the original system. This difference in the median seismic demand relationships is depicted in Figure 6.15. The effect of rehabilitation on seismic demand is substantial, solves the problem of apparent weak behavior of the original frame.

Occurrences of the maximum ISDAs follow the same trend as the original model. As the intensity of GMs increase, the deformations tend to accumulate in the lower levels, however, this time; the second story has the highest number of occurrences.

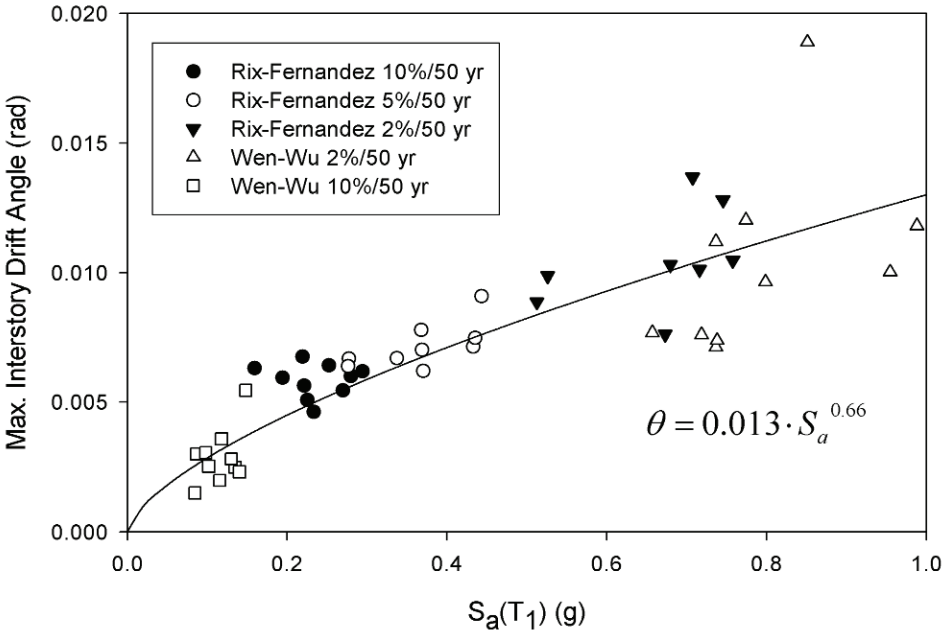

Figure 6.14 NTHA results for Frame BR-5ST-CB with 50 records.

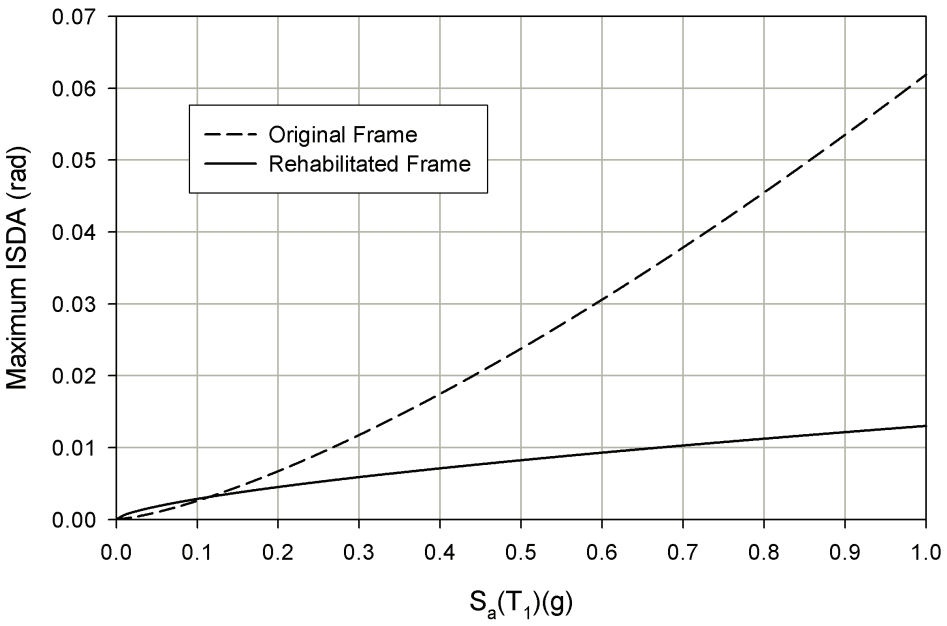

Figure 6.15 Comparison of median seismic demand relationships for original and rehabilitated Frame 5ST-CB.

The capacity of Frame 5ST-CB was evaluated using the 10%/50 yr ensemble of Rix-Fernandez UHGMs. Results indicated a mean capacity of 3.9% ISDA with 24% COV, representing an increase of more than 80% as compared to the original case. This value was adopted as the CP limit for this frame. The three performance limits for the rehabilitated frame are 0.5, 1.7 and 3.9% ISDA for the IO, SD and CP levels, respectively.

Rehabilitation of Frame 5ST-CB using buckling-restrained braces had a significant effect on the seismic fragility of the frame, as depicted in Figure 6.16. The biggest impact is seen at the higher levels of damage, i.e., structural damage and structural collapse regions. The performance state probabilities of this frame were calculated for the same two seismic hazard levels (2%/50 yr UHGM vs. severe scenario) as done in the previous section. The frame behaves very favorably under both situations as seen in Table 6.3 where the results are compared against those of the original case. The

probability of collapse drops to zero in both cases. At 2%/50 yr hazard level event, it drops from 73% to 0%; similarly, for the scenario event considered, it decreases by 98%. Some of these gains are due to higher CP limit (3.9% ISDA), however, for the most part, the structural stiffening of the frame indicated in the demand equation is responsible for this performance enhancement.

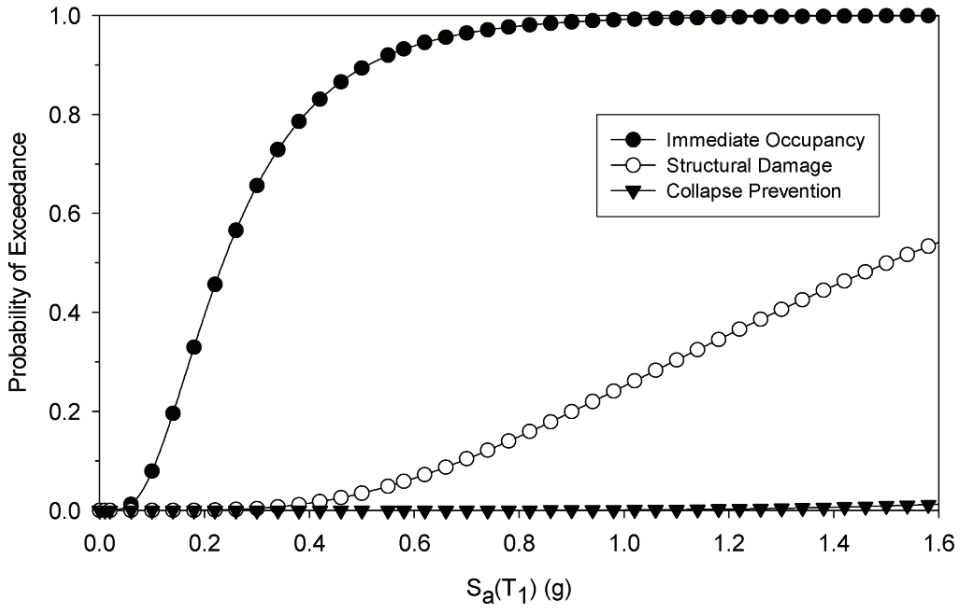

Figure 6.16 Seismic fragilities for Frame BR-5ST-CB.

Table 6.3 Performance state probabilities for Frame 5ST-CB.

Perspective	Model	Spect. Accel. (g)	Continued Occupancy (%)	Impaired Occupancy (%)	Structural Damage (%)	Structural Collapse (%)
2%/50 yr UH	Original	0.55[a]	0	0	27	73
	Retrofitted	0.55[a]	8	87	5	0
M_w=7.5, R=20 km scenario	Original	0.86[b]	0	0	2	98
	Retrofitted	0.86[b]	2	81	17	0

[a] 2%/50yr mean spectral acceleration for Memphis, TN.
[b] Median spectral acceleration of M_W=7.5, R=20 km ensemble.

6.4.2 Rehabilitation of Frame 6ST-XB

Frame 6ST-XB was modified using the same BRBF approach and the new frame was denoted as BR-6ST-XB. The dynamic characteristics of this frame are same as those of the original frame presented in Chapter 5. The NSPA was performed for Frame BR-6ST-XB using the k=2 lateral loading distribution. The results are compared with the original case in Figure 6.17. The capacity differs almost by 80%. Due to the extended linear region, the IO limit shifts from 0.4% to 0.8%. This is adopted as the new IO limit for this frame. The SD limit was determined from the same pushover curve as the point at which the secant stiffness of the curve drops to its half. This occurs at 1.7% RDA, which corresponds to 3.4% ISDA at 4th story level.

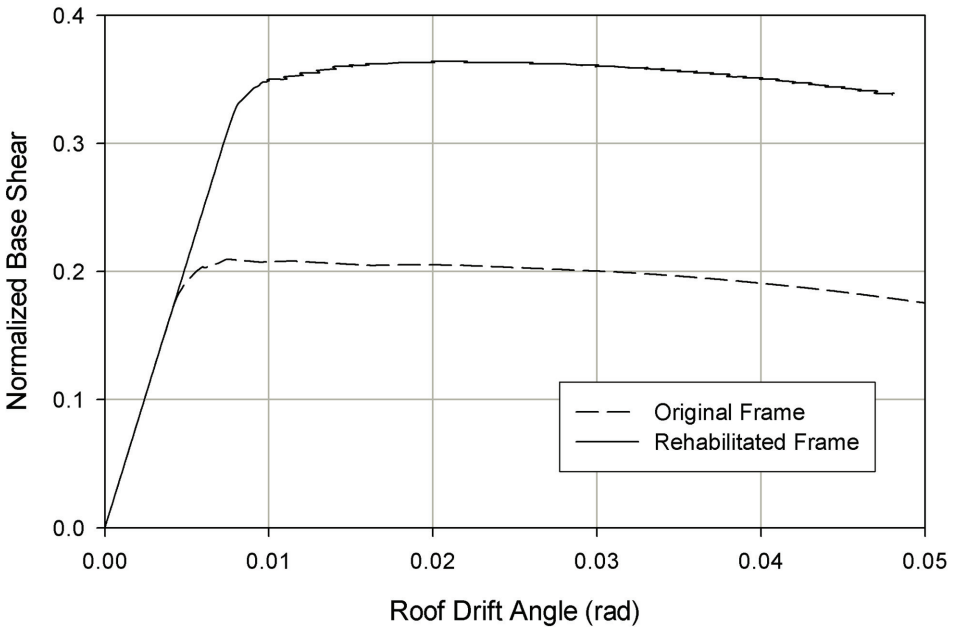

Figure 6.17 NSPA comparison of the original and the rehabilitated models.

To be consistent with the analysis of the original frame, the seismic demand on the frame was determined by NTHA, utilizing both Rix-Fernandez and Wen-Wu Memphis UHGMs. The results are shown in Figure 6.18. A statistical analysis of the results produced the following seismic demand relationship:

$$\hat{\theta}_{\max} = 0.0278 \cdot S_a^{0.90}, \beta_{D|S_a} = 0.20. \tag{6.7}$$

The resulting median demand relationship is compared to the relationship obtained from the original case in Figure 6.19, where it can be seen that the rehabilitated frame undergoes smaller interstory drifts for the same level of seismic excitation. Although the difference becomes larger as the intensity of ground motions increases, it is much less than the difference indicated in Figure 6.15 for the chevron-braced frame. The smaller gain can be attributed to the fact that the original X-braced frame performed relatively well in comparison to the chevron-braced frame. The capacity of Frame 6ST-XB was calculated using the IDA approach. The calculated mean maximum ISDA was 4.0%, and this value was taken to define the CP limit for this frame.

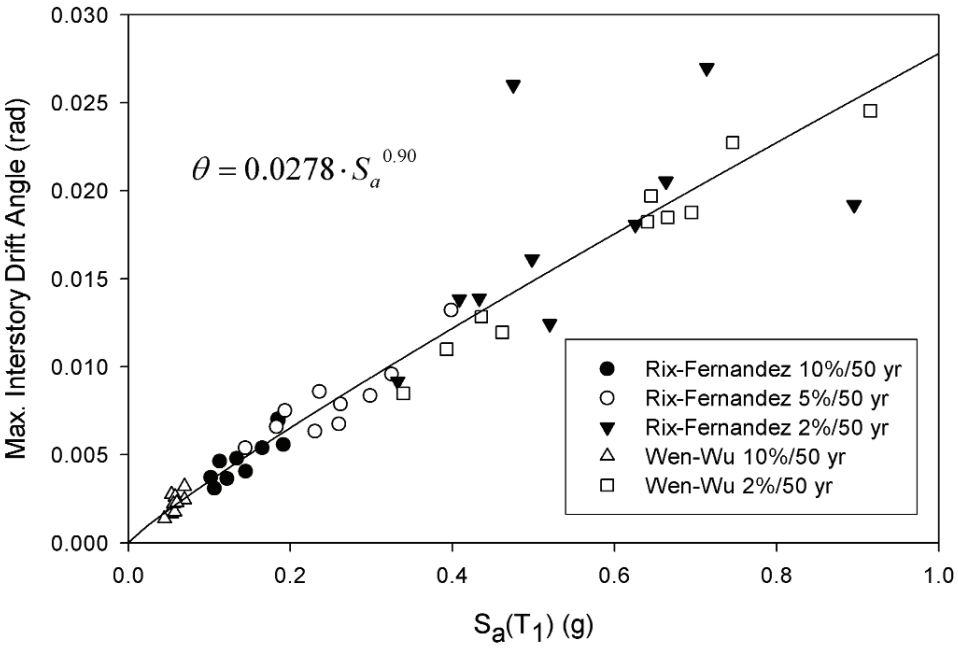

Figure 6.18 NTHA results for Frame BR-6ST-XB with 50 records.

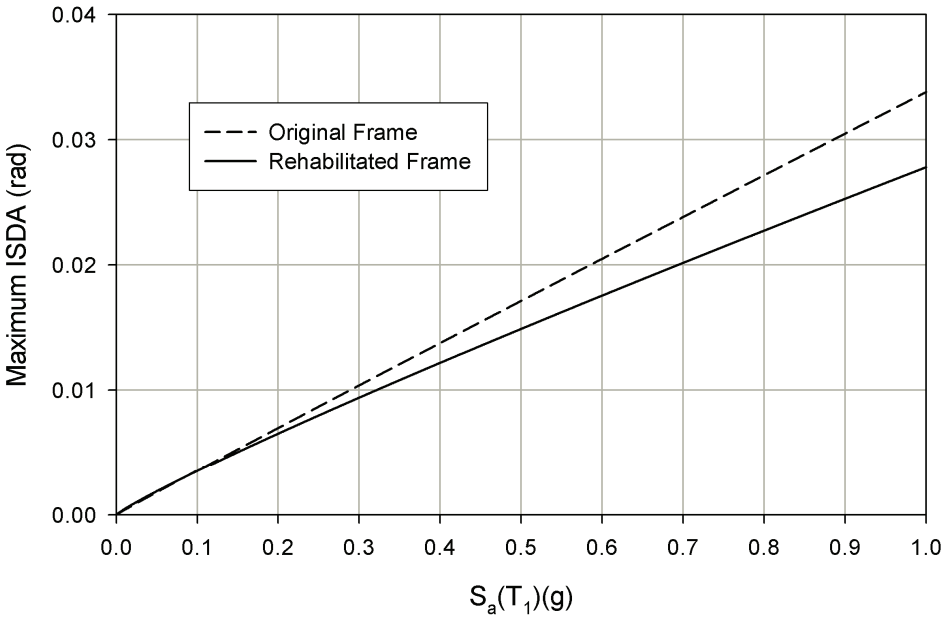

Figure 6.19 Comparison of seismic demand relationships for original and rehabilitated Frame 6ST-XB.

The fragilities for this modified frame are depicted in Figure 6.20. The rehabilitation of this frame had a pronounced effect on the frame performance state probabilities. Performance state probabilities calculated for two perspectives are given in Table 6.4 where they are compared against the results of the original case. The probability of structural damage under the 2%/50 yr event drops to zero from 44%. Under scenario event, similarly, structural damage probability decreases from 90% to 15%, with a slight improvement in the collapse probability. For these reasons, it can be concluded that rehabilitation through the use of buckling-restrained braces would be an effective and feasible risk management strategy for this frame.

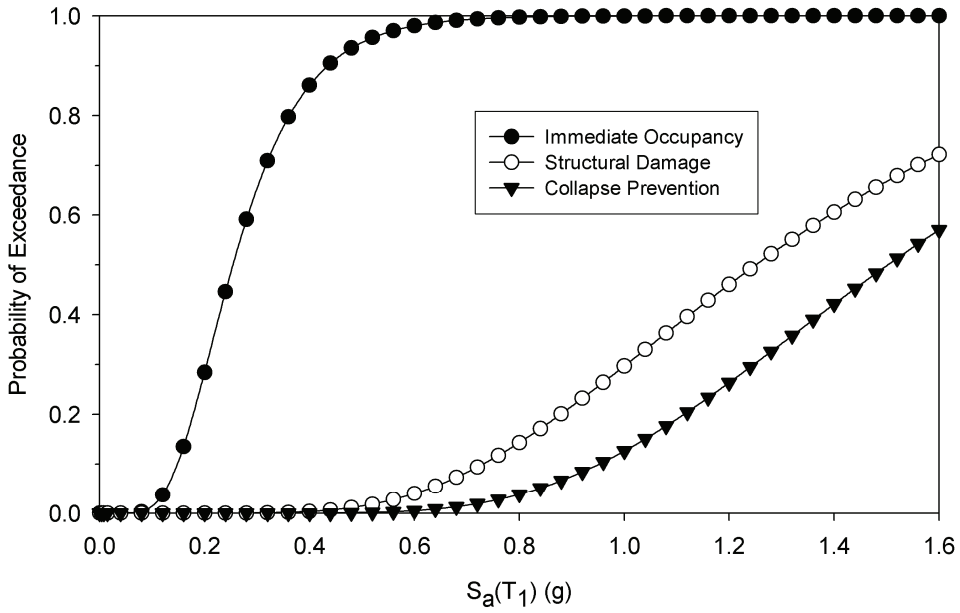

Figure 6.20 Seismic fragilities for Frame BR-6ST-XB.

Table 6.4 Performance state probabilities for Frame 6ST-XB.

Perspective	Model	Spect. Accel. (g)	Continued Occupancy (%)	Impaired Occupancy (%)	Structural Damage (%)	Structural Collapse (%)
2%/50 yr UH	Original	0.35[a]	0	56	44	0
	Retrofitted	0.35[a]	22	78	0	0
M_w=7.5, R=20 km scenario	Original	0.90[b]	0	2	90	8
	Retrofitted	0.90[b]	0	78	15	7

[a] 2%/50yr mean spectral acceleration for Memphis, TN.
[b] Median spectral acceleration of M_W=7.5, R=20 km ensemble.

6.5 Rehabilitation of PR Moment Frames with FR Connections

The two and four-story PR moment frames were retrofitted by strengthening the connections, as suggested in FEMA 273/356. The idea behind this approach is to see the relative superiority of FR frames over PR frames in their seismic performance. This approach allows the full moments on the beam ends to be transferred to columns through FR connections. This increases the risk of column hinging by taking some of the moments away from the beam and putting them on the columns. This procedure also stiffens the frames and results in shorter natural periods. This may cause the frames to attract more seismic loads depending on their fundamental periods. In this section, the impact of such modifications in seismic performance enhancement will be investigated.

6.5.1 Rehabilitation of Frame 4ST-PR

The modified four-story frame is designated as R-4ST-PR (R stands for Rigid). The general approach in the frame analysis is the same as in Chapter 5 for the original frames.

The dynamic characteristics of the frame were determined by modal analysis. The periods of the frame decrease to 1.20 s, 0.40 s, and 0.22 s for the first three modes. Mass participation ratios are 91%, 7.5%, and 1%, respectively. This was discussed briefly in Section 5.5.3 of Chapter 5. The NSPA results were presented in Figure 5.20 for both the original and the rigid connection model using the first mode shape lateral loading. However, after the assessment of two original PR frames, it was shown that k=2 lateral loading yields lower base shear capacity. In Figure 6.21, therefore, the NSPA results are shown for this loading scheme. It can be observed from the figure that the inelastic behavior initiates at 0.6% RDA.

SD performance limit was determined as the point of deformation at which the secant slope of the NSPA curve decreases by 50%, producing 1.85% RDA. The corresponding maximum ISDA is 2.3%, occurring at the 2nd story. These interstory drift limits, i.e., 0.6% and 2.3%, were adopted to define the IO and SD performance levels, respectively. The dynamic response characteristics of the rehabilitated frame were evaluated using two ensembles of Wen-Wu Memphis UHGMs (Fig. 6.22) producing the following demand relationship:

$$\hat{\theta}_{\max} = 0.0318 \cdot S_a^{\,0.86},\ \beta_{D|S_a} = 0.16. \tag{6.8}$$

When compared to the original two models, i.e., CA and TS, the rigid connection model yields a lower seismic demand as depicted in Figure 6.23. However, it should be kept in mind that the rehabilitated frame has a shorter fundamental period, so attracts higher inertial forces. For example, at 2%/50 yr hazard level, this frame undergoes 0.32g spectral acceleration as opposed to 0.27g and 0.28g for CA and TS models, respectively. However, the rigid frame still experiences lower ISDAs than the original models.

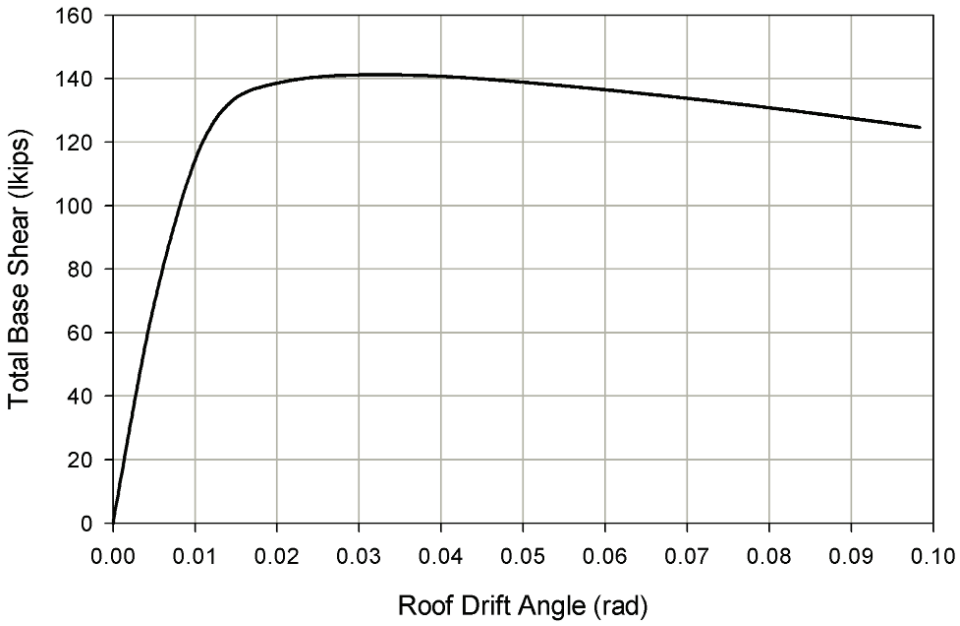

Figure 6.21 NSPA results for Frame R-4ST-PR.

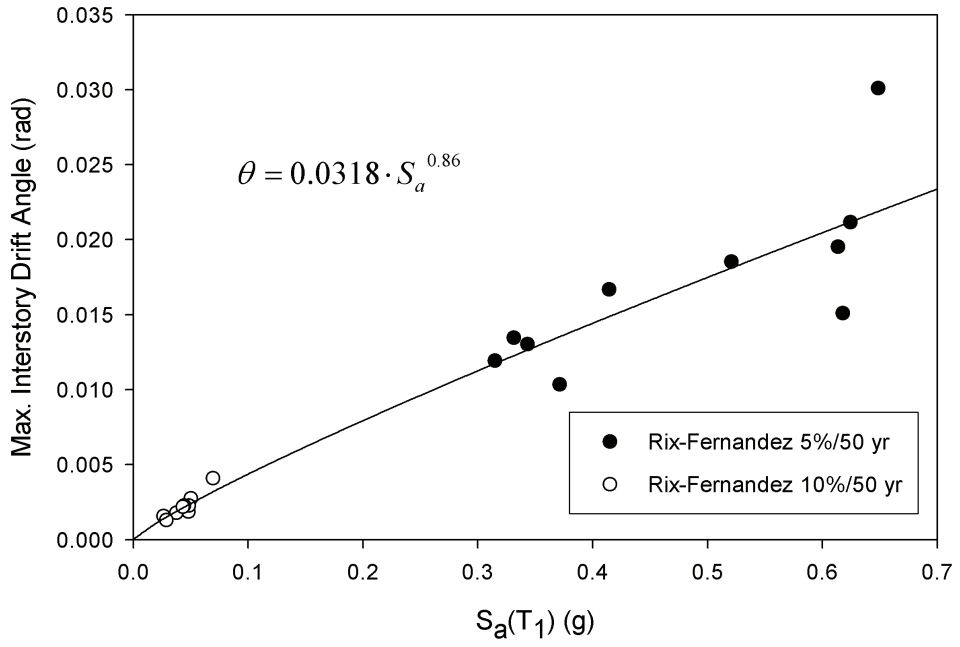

Figure 6.22 NTHA results for Frame R-4ST-PR.

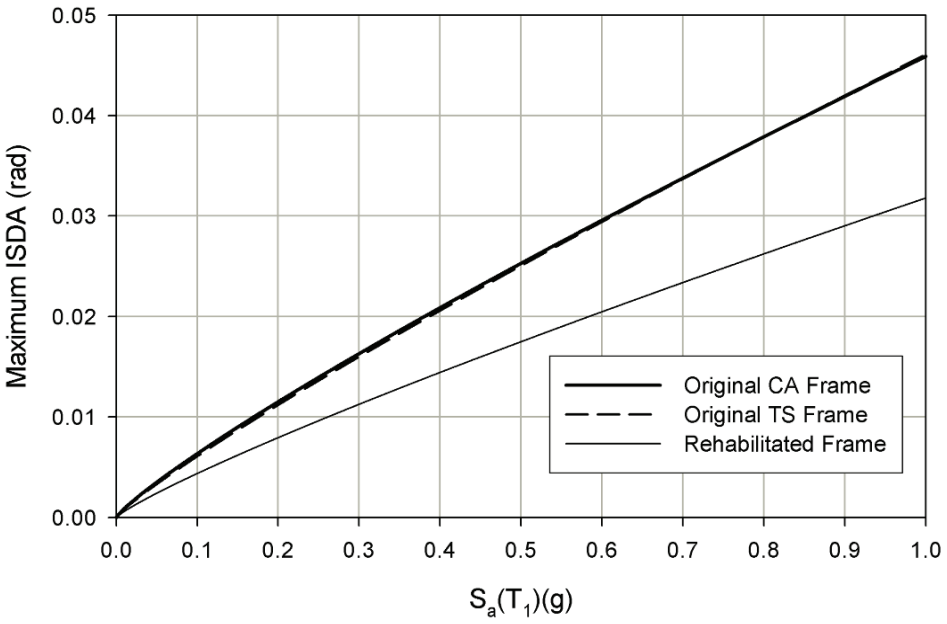

Figure 6.23 Comparison of seismic demand relationships for original and rehabilitated Frame 4ST-PR.

The ultimate capacity of Frame R-4ST-PR was assessed using the same ground motion records (Wen-Wu 2%/50 yr ensembles for three sites) as the original model. The frame withstood up to 10% maximum ISDA in all records. Thus, this drift was adopted as the CP limit for the rehabilitated frame. This indicates a considerable increase in the capacity of the frame. In the NSPA, this frame showed only a small increase in capacity (Fig. 5.20). The fundamental difference between NSPA and IDA is that the reversals of and lack of coherence in the inertial forces in the dominant modes help the frame withstand and make it more likely to survive. The lower median seismic demand relationship depicted in Figure 6.23 and higher CP limit obtained from IDAs have a beneficial effect on the fragilities for this frame with respect to the structural collapse damage state. Fragilities for rehabilitated frames were plotted in Figure 6.24.

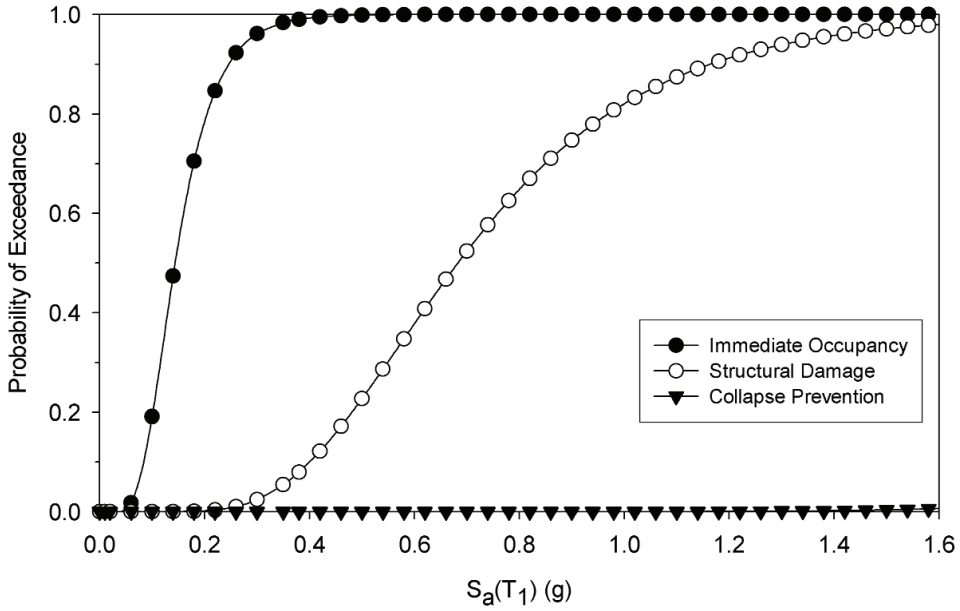

Figure 6.24 Seismic fragilities for Frame R-4ST-PR.

The overall effect of the rehabilitation was determined through the resulting fragilities and performance state probabilities derived from them, as shown in Table 6.5. The results are compared against the original case. The resulting fragilities do not change appreciably for the 2%/50 yr event. However, the difference is more pronounced under the scenario event especially if the performance of the original frame with CA connections is considered.

Table 6.5 Performance state probabilities for Frame 4ST-PR.

Perspective	Model	Spect. Accel. (g)	Continued Occupancy (%)	Impaired Occupancy (%)	Structural Damage (%)	Structural Collapse (%)
2%/50 yr UH	Original	0.27[a]	2	95	3	0
	Retrofitted	0.32[a]	3	94	3	0
M_w=7.5, R=20 km scenario	Original	0.90[b]	0	19	44	37
	Retrofitted	0.95[b]	0	21	79	0

[a] 2%/50yr mean spectral acceleration for Memphis, TN.
[b] Median spectral acceleration of M_W=7.5, R=20 km ensemble.

6.5.2 Rehabilitation of Frame 2ST-PR

The natural periods of this rehabilitated frame did not change significantly. The first two mode periods are 1.03 and 0.40 seconds with 97% and 3% mass participation ratios, respectively. In Figure 6.25, the NSPA results are shown for k=2 lateral loading pattern. It can be observed that inelastic behavior initiates at 0.7% RDA. SD limit was determined from the pushover curve as the point of deformation where the secant slope of the curve is half of the initial stiffness. It gave the limiting point as 2.3% RDA. This corresponds to a maximum ISDA of 2.7%, occurring at the first story. These limits, i.e., 0.7% and 2.7%, were adopted as the IO and SD limits, respectively, for this modified frame.

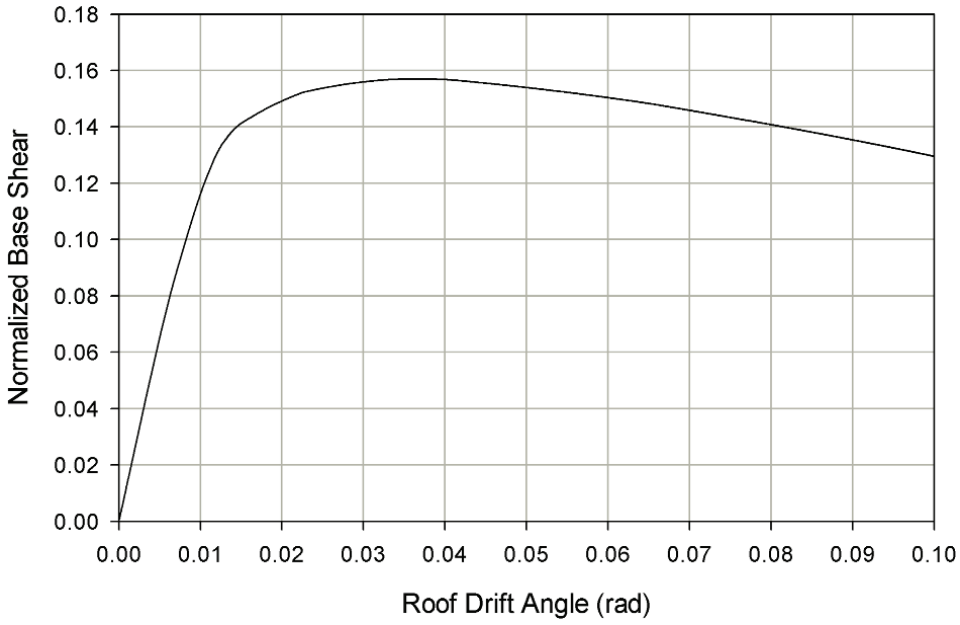

Figure 6.25 NSPA results for Frame R-2ST-PR.

The dynamic response characteristics of the rehabilitated frame were evaluated using the combination of 6 ensembles, 3 from the Rix-Fernandez and 3 from the Wen-Wu UHGMs, as illustrated in Figure 6.26. Analyses of these data produced the following demand relationship which is not significantly different from the original model:

$$\hat{\theta}_{\max} = 0.0511 \cdot S_a^{0.90},\ \beta_{D|S_a} = 0.19. \tag{6.9}$$

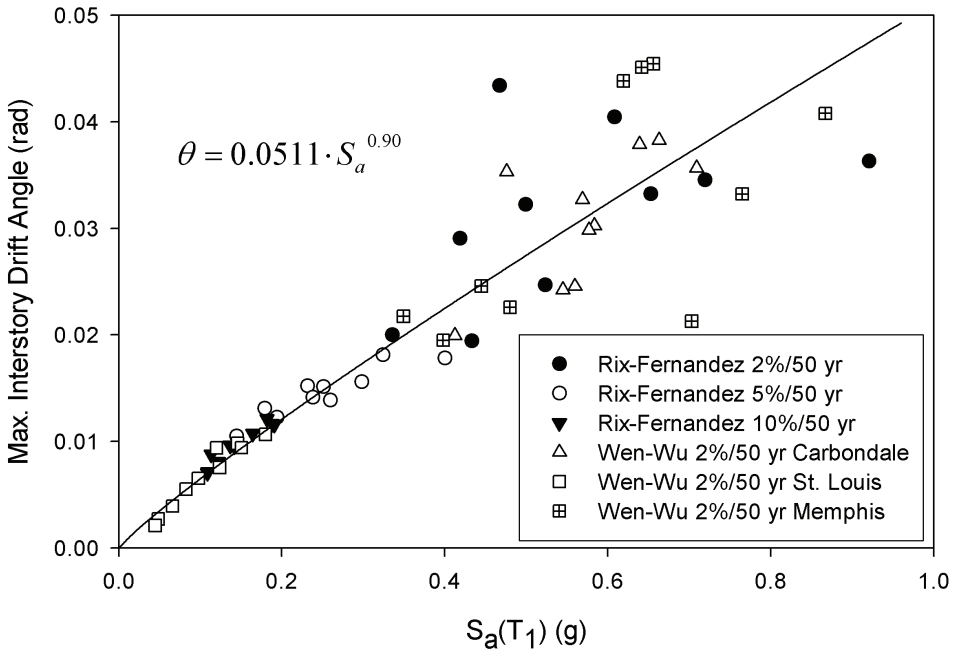

Figure 6.26 NTHA results for Frame R-2ST-PR.

The ultimate capacity of this frame was evaluated using three ensembles of 2%/50 yr Wen-Wu UHGMs in an IDA. All 30 IDA plots produced monotonically increasing deformations up to 10% ISDA without meeting any collapse criteria, so, the capacity was assumed to be 10% ISDA. Therefore, the three performance limits for the rehabilitated frame are 0.7%, 2.7% and 10% ISDA for IO, SD and CP levels, respectively.

The fragilities for this frame are illustrated in Figure 6.27. The performance state probabilities were calculated, as done for the previous frames, and compared with original case in Table 6.6. There is not a notable difference in the performance state probabilities as compared to the original case. This is because the structural modifications did not change either the demand relationship or the performance limits from the original model. In other words, the seismic performance of this low-rise PR frame is not enhanced by modifications to the connections that make it behave as a rigid frame. It is obvious from the earlier sections that the frame, as originally designed, behaved reasonably well under increasing levels of ground motion intensity mainly due to its low height. Thus, seismic rehabilitation of such low-rise frames through modification of their connections would provide little additional performance enhancement and likely would prove to be uneconomical.

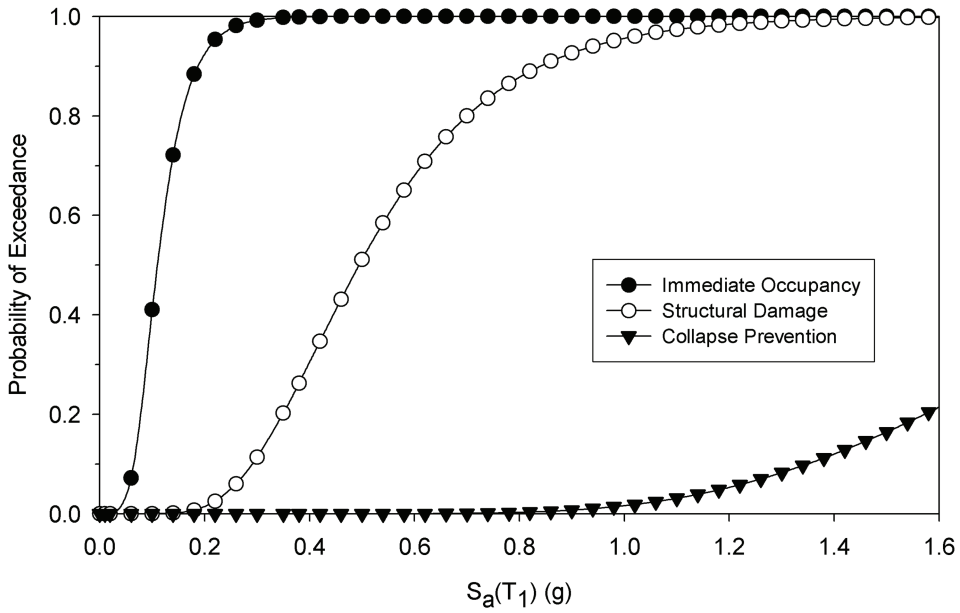

Figure 6.27 Seismic fragilities for Frame R-2ST-PR.

Table 6.6 Performance state probabilities for Frame 2ST-PR.

Perspective	Model	Spect. Accel. (g)	Continued Occupancy (%)	Impaired Occupancy (%)	Structural Damage (%)	Structural Collapse (%)
2%/50 yr UH	Original	0.34[a]	0	82	18	0
	Retrofitted	0.35[a]	0	80	20	0
M_w=7.5, R=20 km scenario	Original	0.91[b]	0	7	92	1
	Retrofitted	0.89[b]	0	8	91	1

[a] 2%/50yr mean spectral acceleration for Memphis, TN.
[b] Median spectral acceleration of M_W=7.5, R=20 km ensemble.

6.6 Rehabilitation of Frame 4ST-PR with Buckling-Restrained Braces

An alternative method of rehabilitation for PR moment frames is adding buckling-restrained brace members in one of the bays of these frames. This gives the frames a high initial stiffness and another source for energy dissipation with nearly perfect elastoplastic behavior. This procedure is applied to Frame 4ST-PR; the modified frame is designated as Frame BR-4ST-PR. Brace members were placed in the middle bay of Frame 2 (which represents the interior frame in the building plan) as seen in Figure 6.28. It is likely that such a building would be modified in the interior so that the exterior of the building is not affected. Square hollow brace members were selected such that under service loads, these brace members reach no more than 15% of their yield strength under compression. This value was selected after the analyses of other braced frames considered in this dissertation. The following brace members were chosen for this frame:

- First Story: TS6×6×5/16
- Second Story: TS5×5×3/8
- Third and Fourth Story: TS5×5×1/4.

The constitutive relationship used previously in the rehabilitation of braced-frames (Fig. 6.12) was utilized for buckling-restrained braces in Frame BR-4ST-PR, as well. For the PR connections in the system, the TS connection model was used. The dynamic properties of the frame changed considerably due to the addition of the braces. The frame got 4 times stiffer. The periods for the first three modes are calculated to be 0.68 s, 0.21 s, and 0.12 s, respectively. Modal participation factors are 83, 15 and 1% for the first three modes.

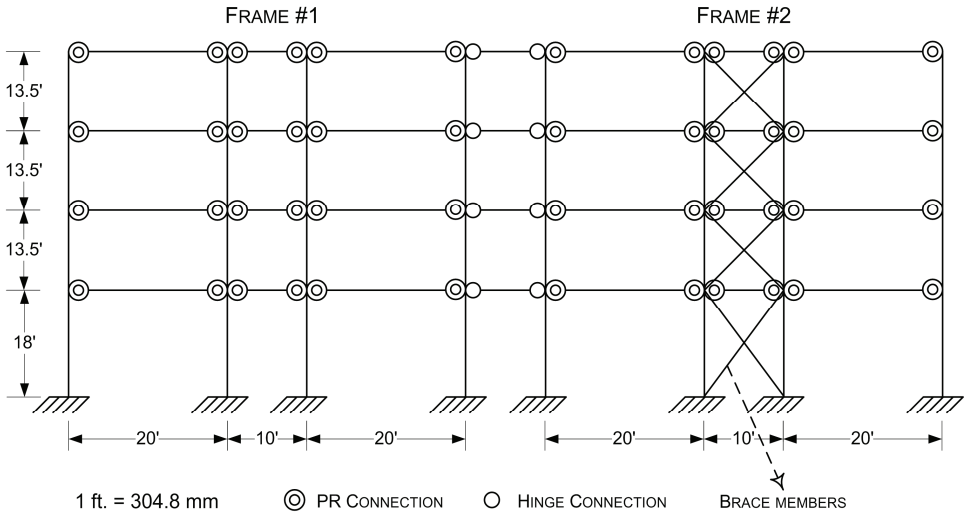

Figure 6.28 The analytical model for Frame BR-4ST-PR.

A NSPA was performed on the modified frame with three lateral load distributions; the load pattern corresponding to k=2 produced the least base shear capacity, as in the original case. These results are compared against the original frame in Figure 6.29. The base shear capacity of the modified frame is three times the capacity of the original frame. Moreover the frame remains stable up to 10% RDA without any decrease in capacity; in contrast, the original frame lost its integrity at around 6% RDA. Limits for

the IO and SD damage states were calculated to be 0.7% and 2.0%, respectively. The SD limit was governed by the ISDA at the 3rd story level.

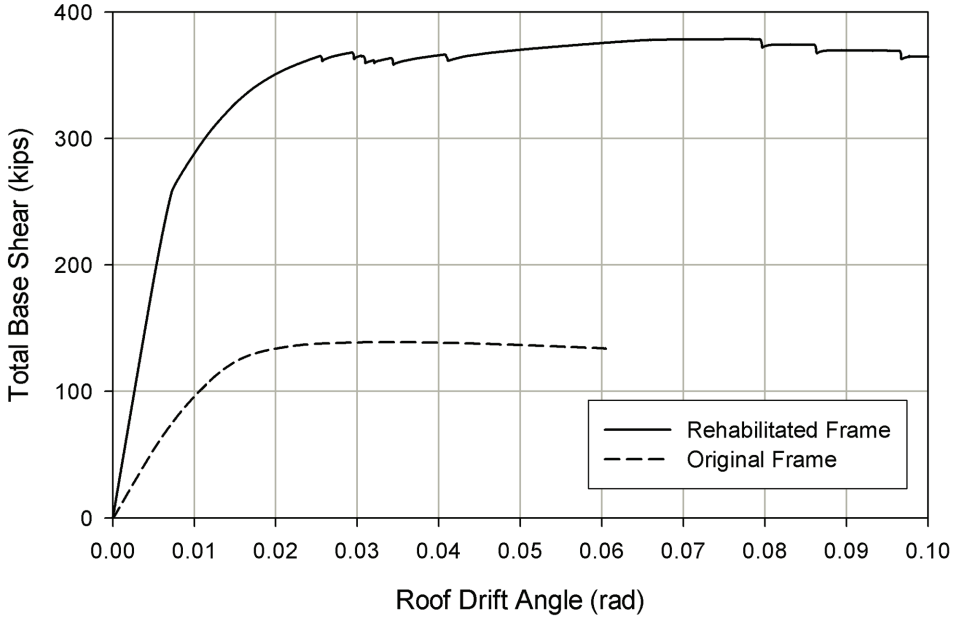

Figure 6.29 Comparison of the NSPA for original and rehabilitated Frame 4ST-PR.

The increase in capacity of Frame BR-4ST-PR against lateral loads was confirmed by a series of NTHAs. The seismic demand on the system was determined using the same ground motion ensembles (Wen-Wu Memphis) as the original frame, with the results shown in Figure 6.30. The median demand relationship obtained below clearly indicates that the seismic demand on the modified frame is substantially less than that on the original, as can be seen in Figure 6.31:

$$\hat{\theta}_{\max} = 0.0118 \cdot S_a^{\,0.83},\ \beta_{D|S_a} = 0.17\,. \tag{6.10}$$

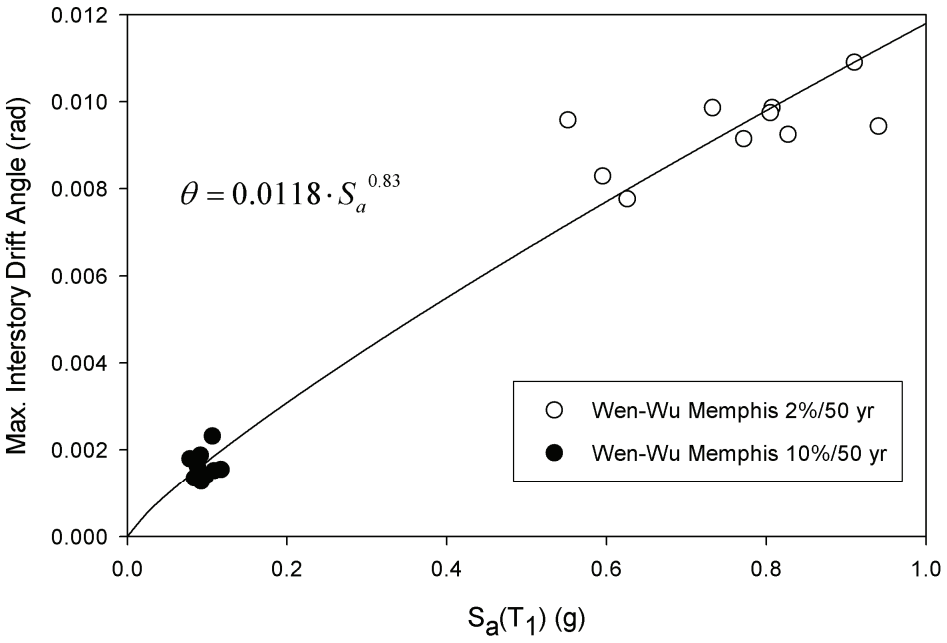

Figure 6.30 NTHA results for Frame BR-4ST-PR.

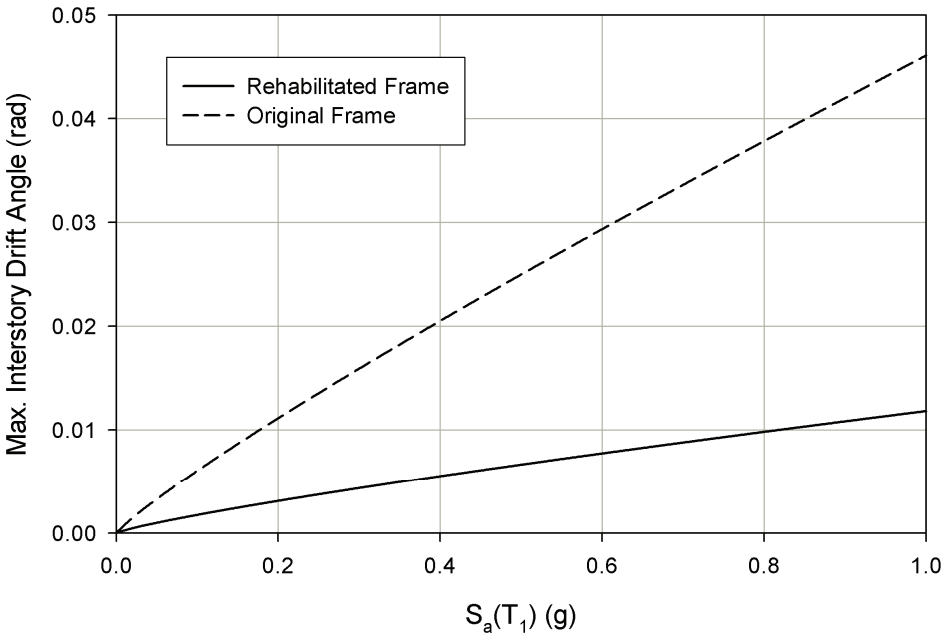

Figure 6.31 Comparison of seismic demand for original and rehabilitated Frame 4ST-PR.

However, it should also be mentioned that the significant shortening of the fundamental period of the system will cause the frame to attract more seismic force than the original frame. The effect of adding braces on the seismic performance of the frame will be determined later using fragility results. The capacity of this frame was investigated in an IDA using three Wen-Wu 2%/50 yr ground motion ensembles. It was seen that comparable ISDA values were experienced in the modified frame at much larger ground motion intensity levels than in the original frame. In other words, the ground motion records had to be scaled to higher values in order to cause collapse or numerical non-convergence in this frame. This might have been anticipated by Figure 6.31, which shows less ISDA for a given S_a. The mean ISDA capacity at collapse was found to be 5.70%, a smaller value than that for the original frame with TS connections. This lower CP limit does not necessarily mean that this frame will be more vulnerable than the original since the underlying demand relationship favors this frame.

The fragilities for Frame BR-4ST-PR are illustrated in Figure 6.32, and the performance state probabilities calculated from these fragilities are given and compared to original case in Table 6.7. The rehabilitated frame is very likely to stay in the continued occupancy state with no structural damage at all under 2%/50 yr event, which corresponds to the maximum considered earthquake level in *ASCE Standard 7-05*. This means an improvement in its seismic performance from the original case. For the high-intensity scenario event, the structural damage probability drops to 3% from 75% and the collapse probability drops to virtually zero from 6%. These results suggest that the seismic behavior and performance of the modified structural frame would be much improved under a possible future earthquake.

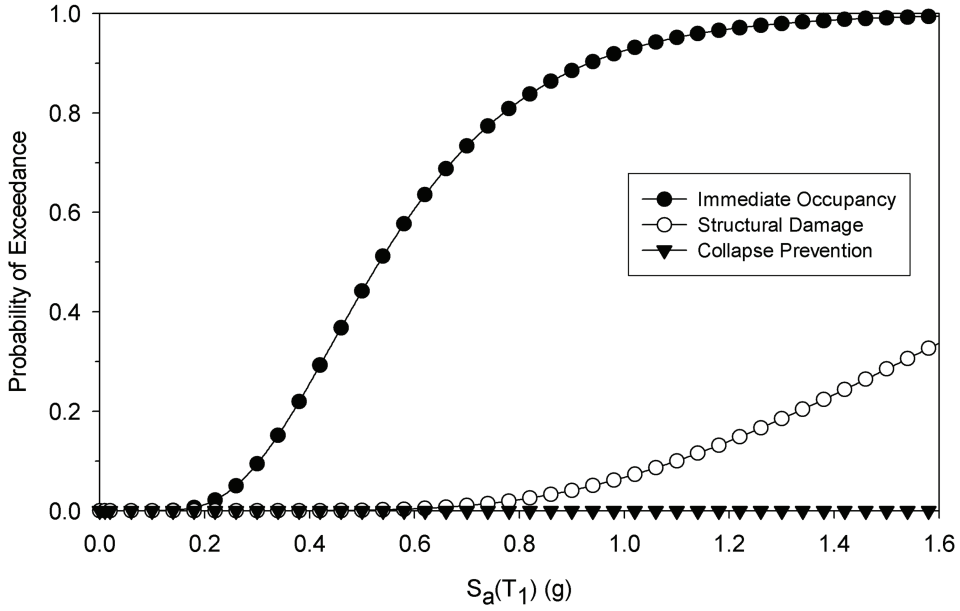

Figure 6.32 Fragilities for Frame BR-4ST-PR.

Table 6.7 Performance state probabilities for Frame 4ST-PR with TS connections.

Perspective	Model	Spect. Accel. (g)	Continued Occupancy (%)	Impaired Occupancy (%)	Structural Damage (%)	Structural Collapse (%)
2%/50 yr UH	Original	0.28[a]	2	95	3	0
	Retrofitted	0.50[a]	56	44	0	0
M_w=7.5, R=20 km scenario	Original	0.89[b]	0	19	75	6
	Retrofitted	0.83[b]	15	82	3	0

[a] 2%/50yr mean spectral acceleration for Memphis, TN.
[b] Median spectral acceleration of M_W=7.5, R=20 km ensemble.

To investigate the effects of connection strength on the effectiveness of this rehabilitation technique, the same buckling-restrained bracing was added to the original PR frame with CA connections. The fundamental period of the modified frame was calculated as 0.70 s. The results of the NSPA and NTHA indicated a similar strength gain in this model, as well. Seismic demand on the system was calculated using Wen-Wu

Memphis GMs as done in TS model earlier. The performance limits were found as 0.7%, 2.0%, and 5.2% ISDA for IO, SD, and CP levels, respectively. Details are not given for brevity. Following median seismic demand relationship was obtained:

$$\hat{\theta}_{\max} = 0.0120 \cdot S_a^{\,0.83}, \ \beta_{D|S_a} = 0.17 . \tag{6.11}$$

This is quite similar to what was observed previously. This, in a fact, shows that the effect of connection capacity on the dynamic performance of rehabilitated Frame 4ST-PR is minimal. In other words, this rehabilitation technique (adding buckling-restrained bracing to interior bays) is an effective method for enhancing seismic performance, regardless of the capacities of the existing PR connections. Due to the similarities in dynamic behavior and performance limits, the overall improvement in fragility assessment of this model is comparable to that of the TS model. This is verified in Table 6.8, where performance state probabilities are calculated in the same way as in the original case. The results are compared against the original case in the same table. In particular, the collapse probability drops from 37% to virtually zero for the scenario earthquake and structural damage, at 4% probability, also is very unlikely. The fragilities for this frame are given in Figure 6.33.

Table 6.8 Performance state probabilities of Frame BR-4ST-PR with CA connections.

Perspective	Model	Spect. Accel. (g)	Continued Occupancy (%)	Impaired Occupancy (%)	Structural Damage (%)	Structural Collapse (%)
2%/50 yr UH	Original	0.27[a]	2	95	3	0
	Retrofitted	0.49[a]	56	44	0	0
M_w=7.5, R=20 km scenario	Original	0.90[b]	0	19	44	37
	Retrofitted	0.86[b]	13	83	4	0

[a] 2%/50yr mean spectral acceleration for Memphis, TN.
[b] Median spectral acceleration of M_W=7.5, R=20 km ensemble.

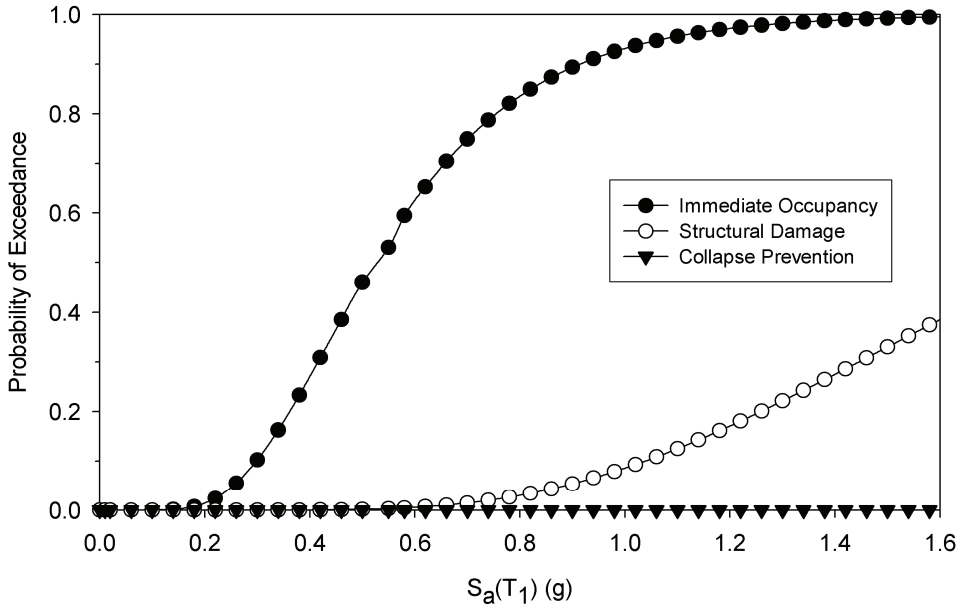

Figure 6.33 Fragilities for Frame BR-4ST-PR with CA connections.

6.7 Assessment of Residual Drifts Prior to and After Rehabilitation

Residual drifts sustained after a seismic event are directly related to future occupancy of a particular building. If the deformations (roof or interstory drifts) are not small enough, the building occupancy is endangered and the repair (if possible) or, demolition may be necessary. In general, steel frames have restoring capacity to reduce the residual deformations after the excitation ends. In particular, buckling-restrained braced-frames are thought to be lacking this characteristic. In other words, their residual deformations after large seismic events can be quite high if they are the only lateral force-resisting system.

In this section, all frames (both original and rehabilitated) were investigated in regard to residual drifts sustained after two levels of seismicity, i.e., 10%/50 yr and

2%/50 yr events. For this purpose, corresponding Wen-Wu Memphis GM ensembles were used. Maximum residual ISDA sustained after each record is calculated and mean value of these maxima after 10 GMs were tabulated in Tables 6.9 and 6.10.

Table 6.9 Residual ISDAs of original frames after seismic events.

Frame	Mean of maximum residual ISDAs (% rad)	
	10%/50 yr	2%/50 yr
2ST-PR	0.012	0.822
3ST-FR	0.046	1.575
4ST-PR(CA)	0.028	0.315
4ST-PR(TS)	0.028	0.367
5ST-CB	0.242	---[a]
6ST-XB	0.012	0.337

[a] Ensemble caused failure of the frame.

Table 6.10 Residual ISDAs of rehabilitated frames after seismic events.

Frame	Mean of maximum residual ISDAs (% rad)	
	10%/50 yr	2%/50 yr
BR-4ST-PR(CA)	0.007	0.082
BR-4ST-PR(TS)	0.011	0.070
BR-5ST-CB	0.252	0.755
BR-6ST-XB	0.012	0.716

Following conclusions can be drawn from these tables:

- 2-Story PR frame sustains negligible residual deformations under 10%/50 yr event; and experiences slightly larger deformations than its IO limit under 2%/50 yr event.
- 3-Story rigid frame sustains negligible residual deformations under 10%/50 yr event; and experiences deformations two times its IO limit under 2%/50 yr event.

- Original 4-Story PR frames with both connection types sustain negligible residual deformations under 10%/50 yr event; and experiences deformations about half of their IO limits under 2%/50 yr event.
- After rehabilitation, these 4-Story PR frames experience much less residual deformations, about 80% less than the original case under 2%/50 yr event.
- Original 5-Story chevron braced-frame sustains deformations less than its IO limit under 10%/50 yr event. It does not withstand any of the 2%/50 yr events.
- Rehabilitated 5-Story experiences same amount of residual deformations under 10%/50 yr events as the original case. Under 2%/50 yr event, it sustains deformations 50% larger than its IO limit.
- Both original and rehabilitated 6-Story X-braced frames experience negligible amount of residual deformations under 10%/50 yr event. For 2%/50 yr event, both frames sustain deformations slightly less than their respective IO limits.

6.8 Appraisal of the Rehabilitation Techniques and Results

Various rehabilitation strategies for partially-restrained and braced-frames were considered in this chapter from a seismic performance point of view. Braced-frames were rehabilitated using buckling-restrained brace members. Since the dynamic characteristics of the frames (fundamental period and mode shapes) are not altered by this approach, seismic forces on the frames remain unchanged after the rehabilitation. The seismic capacity of Frame 5ST-CB, a chevron-braced frame, was enhanced substantially by the addition of BRBs. This can be seen in Figure 6.34 in which the fragilities before and after

modification are compared. The same approach has also been utilized for Frame 6ST-XB, an X-braced frame. The seismic behavior of this frame also was improved by the addition of the braces, although not to the same degree as the chevron-braced frame. A comparison of seismic fragilities of the original and rehabilitated versions of this frame is given in Figure 6.35. In general, it can be concluded that this approach is quite effective for the seismic rehabilitation of braced frames.

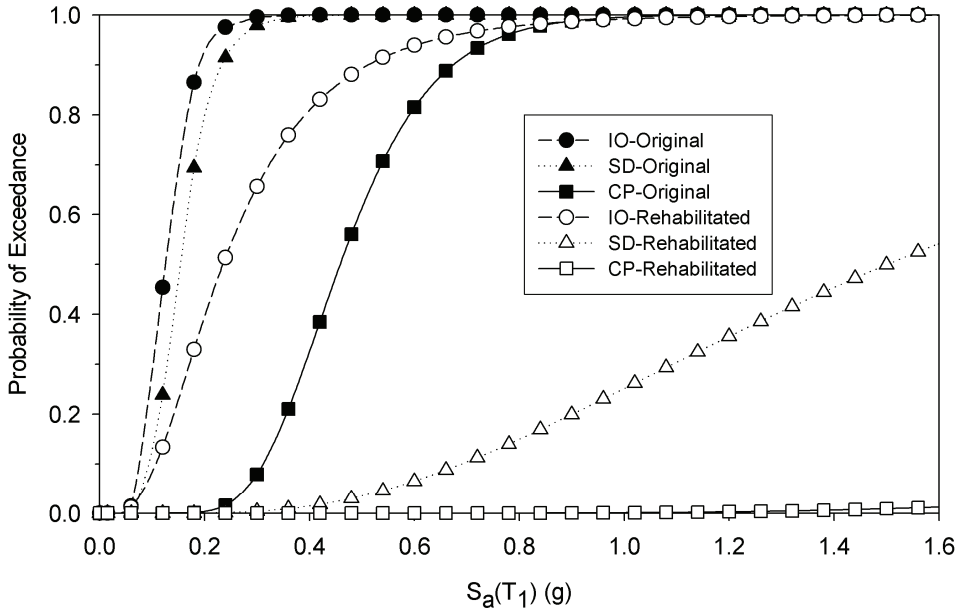

Figure 6.34 Comparison of fragilities for Frame 5ST-CB.

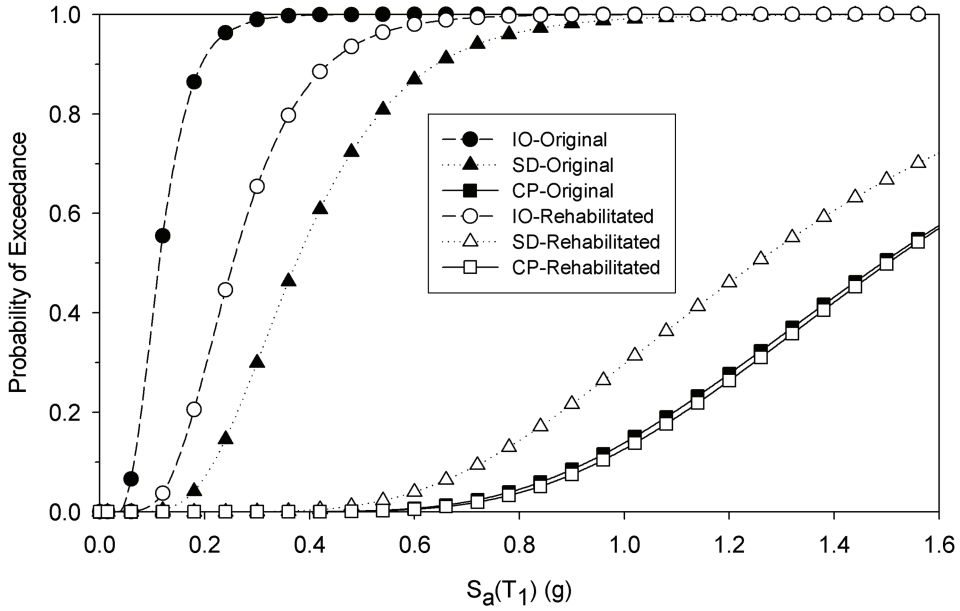

Figure 6.35 Comparison of fragilities for Frame 6ST-XB.

Partially restrained moment frames were rehabilitated using two different approaches. In the first approach, Frame 4ST-PR(TS) was modified by converting the PR connections to FR connections throughout the frame. This method resulted in a shorter fundamental period, an increase in the CP deformation limit, and a slight improvement in the median seismic demand relationship. However, the overall gain in seismic behavior of the system, as measured by its seismic fragilities, was limited as depicted in Figure 6.36; this approach does not appear to be effective improving seismic behavior. In the second approach, buckling-restrained X-braces were installed in the middle bay of the interior frame. This method produced a much shorter fundamental period, a slight decrease in the CP limit and a substantial improvement in the median seismic demand relationship. When all these effects are convolved in the seismic fragility assessment, the overall behavior is improved significantly, as seen in Figure 6.37. Thus, this method is quite effective as a technique for seismic rehabilitation of this PR moment frame.

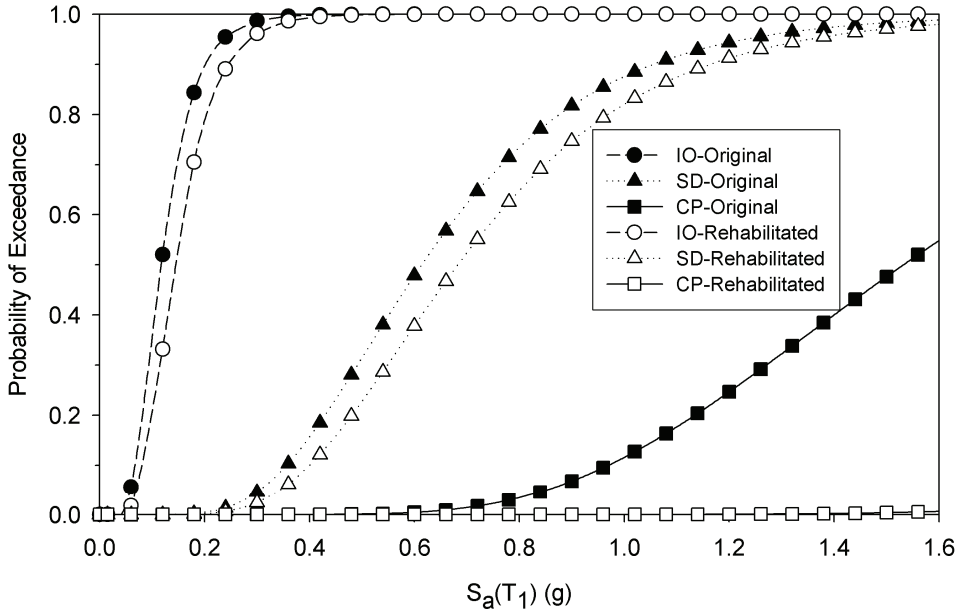

Figure 6.36 Comparison of fragilities for Frame 4ST-PR using FR connections.

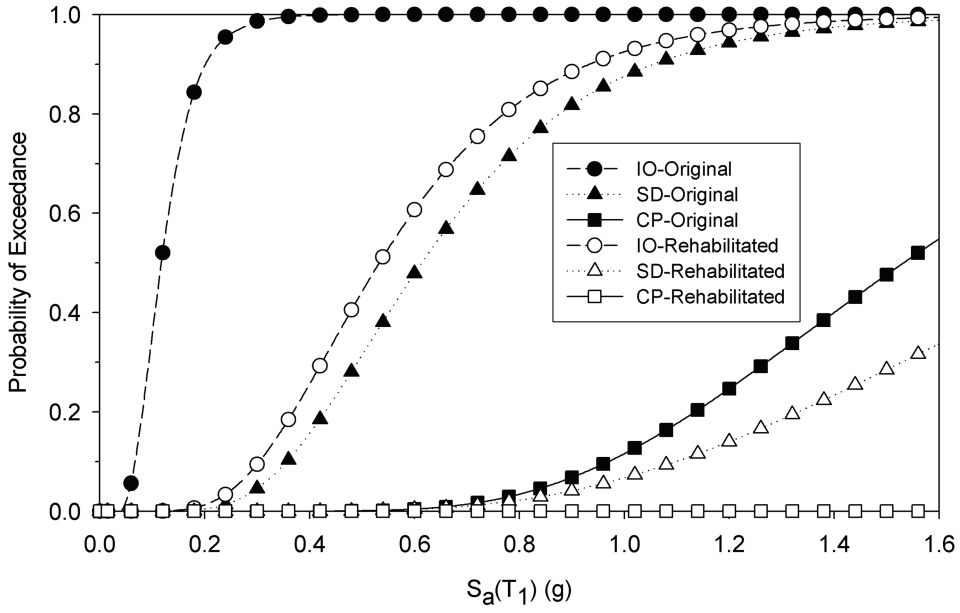

Figure 6.37 Comparison of fragilities for Frame 4ST-PR(TS) using brace members.

Similar conclusions were drawn from an analysis of the frame with the weaker connections, i.e., Frame 4ST-PR(CA) model, as summarized by the fragilities for this model in Figure 6.38. The PR connection capacity does not play a significant role in the effectiveness of this rehabilitation technique since the lateral response of the frame is determined to largely by the X-braces installed in its modification. Seismic rehabilitation of the two-story PR frame does not appear to enhance its performance significantly. Accordingly, such frames generally are poor candidates for rehabilitation.

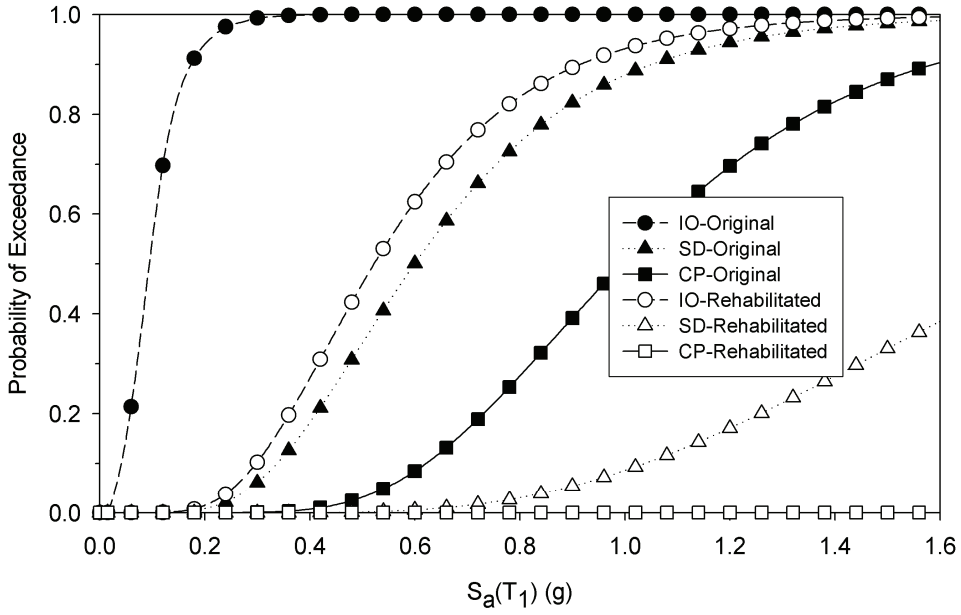

Figure 6.38 Comparison of fragilities for Frame 4ST-PR(CA) using brace members.

CHAPTER VII

PORTFOLIO RISK ASSESSMENT IN THE CEUS

Portfolio assessment of seismic risk is essential for assessing the likely performance of a building inventory under future seismicity in a region. The most accurate analysis method, NTHA, is time-consuming even with modern computational resources and would be impractical for inventories consisting of hundreds or thousands of distinct buildings. An efficient yet accurate rapid assessment procedure would reduce the computational burden on the engineer significantly and provide risk managers with the information needed for public planning. There have been several attempts in the past to develop such methods (Reitherman, 1985). Of these, the Capacity Spectrum Method (CSM) is the method that perhaps is used most frequently. In the mid to late 1990's, the Federal Emergency Management Agency (FEMA) sponsored the development of the portfolio loss estimation and assessment methodology HAZUS (Hazards U.S.), which was implemented initially for earthquake hazards and later extended to cover other natural hazards such as flood, fire, tornado, etc. The HAZUS software utilizes the CSM for assessing building performance. In the following section, both the HAZUS and the CSM are evaluated, and their advantages and shortcomings with regard to building performance assessment in the CEUS are discussed.

7.1 HAZUS

HAZUS is a multi-hazard loss estimation software package that is intended for use in loss assessment and disaster mitigation planning and response. HAZUS uses geographic

information systems technology to display and manipulate the available data on civil infrastructure in a region. It has been composed of separate modules giving it flexibility and making it easier to be implemented locally. HAZUS has a built-in general inventory of facilities, which includes 36 building types (in 28 occupancy classes), essential facilities, transportation networks and utility systems. There are three different levels of analysis possible in HAZUS. Level 1 analysis requires the least amount of information from the user and relies mainly on the built-in database. In this analysis, the region is defined in a simple way; a scenario event is identified and the results are gathered in either tabular or graphical form. Increasing the complexity of the analysis increases from Level 1 to Levels 2 or 3 requires more regional and portfolio-specific information from the analysis, but increases the level of confidence in the results.

HAZUS has a number of drawbacks and limitations at all levels, particularly if applied to individual facilities (Erberik and Elnashai, private communication; Whitman et al., 1997). First of all, HAZUS uses same soil conditions (class D) for all locations. For local site conditions, the user must provide the soil map in the desired format. Second, the public databases used by HAZUS often are not well-maintained. Damage estimates for earthquakes smaller than magnitude $M_w = 6$ and higher than $M_w = 7.5$ are not dependable and the effects of earthquake duration are not incorporated in the analyses. More importantly, HAZUS does not reflect dynamic response directly; it uses static response and predicts dynamic response from it. Third, there is high uncertainty related to the ground motion characteristics in the CEUS. Also, the structural response data in HAZUS do not reflect the practices in the CEUS. HAZUS mainly relies on the data available from

the WUS practices. Furthermore, HAZUS usually overestimates the damage and loss in the CEUS mostly due to lack of dependable ground motion data.

A parametric sensitivity study performed by Grossi (2000) showed that the largest source of uncertainty comes from the attenuation relationships. Fourth, HAZUS uses the capacity spectrum method to determine building response. The capacity curve in this method, in general, is a form of the nonlinear static pushover curve transformed into a relation between spectral acceleration and spectral displacement. Furthermore, HAZUS simplifies the NSPA approach further by defining the capacity curve with two points, i.e., the yield and the ultimate points. The intersection of this capacity curve with the nonlinear demand spectrum determines the peak building response.

Perhaps the most significant, HAZUS does not allow for analysis or propagation of uncertainty. The outcomes are mean values and the user cannot assess the confidence in the damage prediction. Whitman et al. (1997) argued that the products of HAZUS should be taken with caution since they may be off by a factor of two or even more. A further critique of HAZUS will be left for the end of this chapter following a thorough study of the CSM for assessing building performance in the CEUS.

7.2 Capacity Spectrum Method (CSM)

The CSM was first introduced by Freeman et al. (1975), and since has been adopted by ATC-40 (ATC, 1996) for evaluation and retrofit of reinforced concrete buildings and by HAZUS (FEMA, 2003) for portfolio assessment. It has also been the subject of many publications (Fajfar, 1999; Lin and Chang, 2003; Chopra and Goel, 1999; Freeman, 1998;

among others). In the CSM, the capacity of the structure is represented by a nonlinear pushover analysis and the demand on the structure is reflected by either an elastic response spectrum for an individual ground motion record or a smooth design spectrum. To show the demand and capacity on the same plot, both the pushover curve and response spectrum are transformed into acceleration-displacement (A-D) format (Chopra et al., 2000) and are plotted together. In order to reflect the nonlinear behavior in the structure, increased equivalent viscous damping was implemented to modify the elastic response spectrum. This approach is denoted the ATC Procedure-A in the following section.

7.2.1 Fundamentals of the CSM

The CSM requires that the earthquake-induced deformation of a non-linear SDOF system be estimated by that of a linear SDOF system through successive iterations (Lin and Chang, 2003). The intersection of the two curves gives the estimate of the response of the structure for that ground motion (termed the performance point). This performance point is determined by trial and error method using the damping ratio as a variable, graphically. If the capacity curve breaks through the demand curve, the building survives that earthquake (Freeman, 1998). However, finding the intersection of two nonlinear curves can be tedious, i.e., several "trial and error" steps usually must be taken to achieve the performance point. Even then, a converged solution cannot be obtained for some earthquake records. In an attempt at improvement, Lin and Chang used the absolute acceleration response spectrum instead of pseudo-acceleration response spectrum and the

WJE damping model (WJE, 1996) rather than the damping model recommended by ATC-40 and produced results that matched those of the NTHA more closely.

The ATC Procedure A is the most direct and easy to implement method. It requires successive iteration of the elastic spectrum using different levels of damping to achieve a match between assumed damping and elastic demand. Procedure A involves the following steps (Chopra and Goel, 2000):

1. Perform a NSPA of the system using an appropriate lateral load distribution (e.g., fundamental mode shape).

2. Idealize this pushover curve (V vs. Δ_{roof}) as bilinear and convert it to a capacity diagram (expressed in terms of S_a vs. S_d) using the following relationships:

$$S_a = \frac{V}{M_1^*} \tag{7.1a}$$

$$S_d = \frac{\Delta_{roof}}{\Gamma_1 \cdot \phi_{N1}} \tag{7.1b}$$

$$M_1^* = \frac{[\sum_{j=1}^{N} m_j \cdot \phi_{j1}]^2}{\sum_{j=1}^{N} m_j \cdot \phi_{j1}^2} \tag{7.1c}$$

$$\Gamma_1 = \frac{\sum_{j=1}^{N} m_j \cdot \phi_{j1}}{\sum_{j=1}^{N} m_j \cdot \phi_{j1}^2} \tag{7.1d}$$

where m_j = mass at jth floor level; ϕ_{j1} = jth element of the fundamental mode shape; M_1^* = effective modal mass of the fundamental mode.

3. Convert the traditional elastic response spectrum to seismic demand in terms of S_a vs. S_d.

4. Plot the capacity curve and demand diagram on the same plot.

5. Compute the damping value at the intersection point of these curves using the following relationship:

$$\zeta_{eq} = \frac{2}{\pi} \frac{(\mu - 1)(1 - \alpha)}{\mu(1 + \alpha\mu - \alpha)} < 0.45 \tag{7.2a}$$

$$\hat{\zeta}_{eq} = \zeta_{eq} + 0.05 \tag{7.2b}$$

where α = slope of the yielding branch of the bilinear force-deformation relationship; and μ = ductility factor.

6. If the damping factor of the demand diagram is not sufficiently close to the damping calculated from Equations (7.2a and 7.2b) update the demand diagram with the new damping factor and find the new intersection point.

7. Repeat step #6 until the required tolerance is achieved.

8. Calculate the roof displacement using the following formula:

$$\Delta_{roof} = S_d \cdot \Gamma_1 \tag{7.3}$$

This procedure is questionable in that it utilizes highly damped elastic spectra for the determination of seismic demand. Krawinkler (1994) noted that there is no clear relation between hysteretic energy dissipation and equivalent viscous damping, which plays a significant role in the CSM. There is also no obvious way to compute the elastic displacement from a de-amplified elastic spectrum based on damping alone. Fajfar (1999) and Chopra and Goel (1999) proposed an improved method that uses a constant-ductility

(inelastic) response spectrum. Inelastic spectra are expected to be more accurate than elastic spectra with equivalent damping, especially in the short-period range or when the ductility is high.

This method does not require successive iterations for the calculation of effective damping factor in steps 5 - 7 above. However, it requires iterations to determine the ductility demand on the system. The application of this procedure is same as the ATC Procedure A until step #4; at that step, the 5% damped elastic response spectrum is converted to a constant-ductility response spectrum via one of the methods in the literature (Newmark and Hall, 1982; Krawinkler and Nassar, 1992; Vidic et al., 1994). The inelastic spectrum is plotted for different values of ductility factor, μ. The capacity diagram intersects these spectra at different points and the performance point is obtained either by interpolation or by plotting the multiple spectra at finer increments of μ. To find this point, however, iterations are utilized. Because, the performance point should be on the response spectrum with appropriate ductility and in the meantime, it must intersect the capacity curve at a point of spectral displacement corresponding to that ductility ratio. An example is given in Figure 7.1 where the CSM was applied on Frame 3ST-FR with Wen-Wu Memphis 2%/50 yr GM #3, as described in more detail in the following section. Finally, this performance point is converted to roof displacement using Equation (7.7).

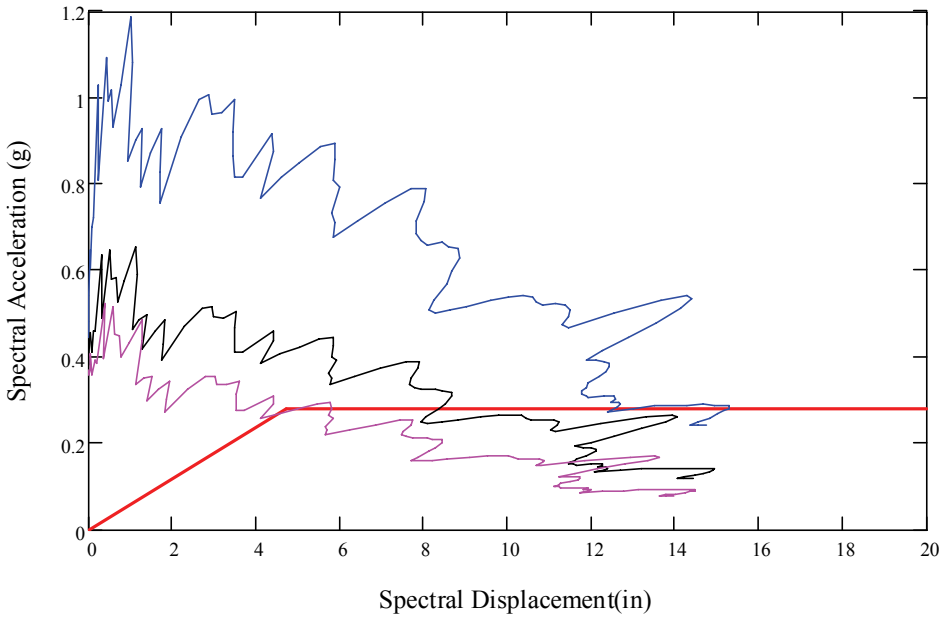

Figure 7.1 Application of the CSM on Frame 3ST-FR for μ=1, 2, 3.

This improved method was reported (Fajfar, 1999; Chopra and Goel, 1999) to produce more accurate results when the "exact" value of roof deformation was determined by NTHA. However, the results are not only sensitive to the ground motion record but also sensitive to the *R*-μ-*t* relationships used (discussed subsequently). One of the drawbacks of the CSM is the difficulty in determining the performance point, i.e., intersection point of the capacity and demand diagrams. Depending on the specific ground motion records, the irregularities in the demand diagram create multiple intersection points for a single plot of inelastic spectrum, as seen in Figure 7.1. In his excellent review of the applicability of the CSM to different shapes of response spectra, Yakut (2002) noted that if a ground motion record produces an atypical response spectrum (frequently seen in spectra of records from soft soil), no results can be obtained, while reasonable estimates of peak response can be obtained from typical response

spectrum shapes. Yakut also pointed out the need for understanding the physical meaning of multiple intersection points.

7.2.2 Inelastic Demand Diagram Calculations

An inelastic demand diagram can be obtained from an elastic response spectrum using certain *R*-μ-*t* relationships (described subsequently). For an elastic SDOF system, the following relationship holds:

$$S_{de} = \frac{T^2}{4\pi^2} S_{ae} \tag{7.4}$$

where S_{ae} and S_{de} are axes of 5% damped elastic spectrum. Assuming that an inelastic SDOF system has a bilinear force-deformation relationship, the corresponding axes of inelastic spectrum are calculated as follows (Fajfar, 1999):

$$S_a = \frac{S_{ae}}{R} \tag{7.5a}$$

$$S_d = \frac{\mu}{R} S_{de} = \mu \frac{T^2}{4\pi^2} S_a \tag{7.5b}$$

in which, μ = ductility factor (ratio of maximum displacement to yield displacement) and R_μ = reduction factor due to ductility only. The relationship between μ and R_μ depends on the period of interest, *T*. Several relationships have been proposed in the literature. Three of the most commonly used relationships are discussed herein. Newmark and Hall (1982) suggested that:

$$R_\mu = \begin{cases} 1 & T < T_a \\ (2\mu - 1)^{\beta/2} & T_a \le T < T_b \\ (2\mu - 1)^{1/2} & T_b \le T < 0.5 \\ \dfrac{T}{T_c}\mu & 0.5 \le T < T_c \\ \mu & T_c < T \end{cases} \tag{7.6a}$$

$$\beta = \frac{\ln(T / T_a)}{\ln(T_b / T_a)} \tag{7.6b}$$

where three period boundaries can be taken as T_a=1/33 s., T_b=0.125 s., and T_c=0.6s. Krawinkler and Nassar (1992) proposed that:

$$R_\mu = [c(\mu - 1) + 1]^{1/c} \tag{7.7a}$$

$$c(T, \alpha) = \frac{T^a}{1 + T^a} + \frac{b}{T} \tag{7.7b}$$

where constant a and b depend on the slope of the yielding branch of bilinear force-deformation curve. For elastoplastic systems, a = 1, and b = 0.42. Vidic, Fajfar and Fischinger (1994) proposed that:

$$R_\mu = \begin{cases} 1.35(\mu - 1)^{0.95} \dfrac{T}{T_o} + 1 & T \le T_o \\ 1.35(\mu - 1)^{0.95} + 1 & T > T_o \end{cases} \tag{7.8a}$$

$$T_o = 0.75\mu^{0.2} T_c \le T_c \tag{7.8b}$$

where T_c is the boundary between the acceleration and velocity sensitive regions.

Chopra and Goel (2000) concluded, after investigating the CSM applied to inelastic SDOF systems, that the ATC-40 procedure underestimates the peak deformations of inelastic systems by as much as 50%, stating that “the ATC-40 procedure

is deficient relative to even the elastic design spectrum in the velocity-sensitive and displacement-sensitive regions". They later argued that the results do not improve much by using the inelastic demand diagram.

To date, the CSM has been applied mainly to buildings in regions of high seismicity. In the remainder of this chapter, the CSM will be applied to the seismic assessment of non-seismically designed steel frames that are typical of the current steel building inventory in the CEUS, with a view toward evaluating its validity as a rapid assessment tool in that region.

7.3 Application of the CSM with Different Types of Response Spectra

The review above shows that the applicability of the CSM is highly dependent on the characteristics of the response spectra which, in turn, depend on the ground motion record. The CSM analysis may or may not converge to a performance point at which the ductility ratios of demand and capacity diagrams are equal. The achievement of such a performance point will be called "converged result" in the following text regardless of whether or not the record produced other intersection points as well. We will distinguish this from records resulting in only one converged performance point later in the following sections.

7.3.1 Type I Response Spectrum

This type consists of response spectra which have few peaks in the low-period range and which decrease with increasing period in a relatively smooth fashion. An example of this type is shown in Figure 7.2 where Wen-Wu 2%/50 yr Memphis GM #3 is used. The demand diagram calculated from this spectrum is given in Figure 7.3. Due to the continual decreasing nature of the demand diagram, records with spectra of this type produce one performance point which is the converged solution.

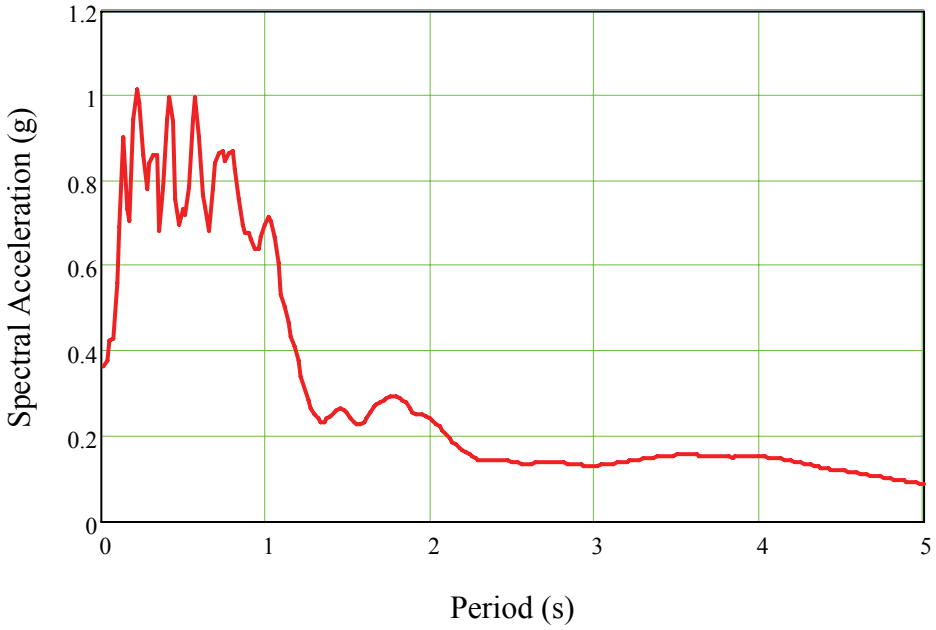

Figure 7.2 A typical Type I response spectrum.

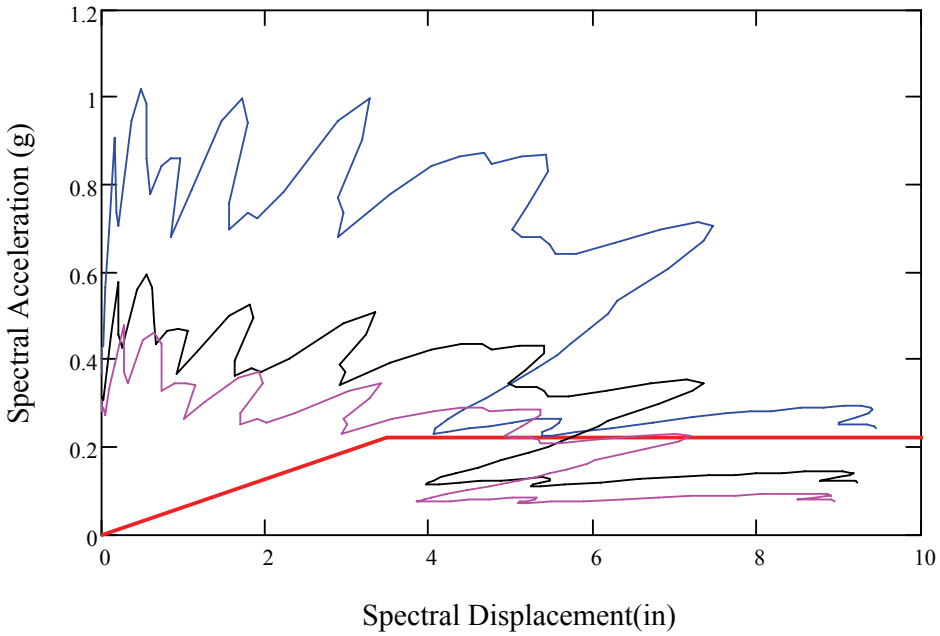

Figure 7.3 Application of CSM using a typical Type I response spectrum for μ=1, 2, 3.

7.3.2 Type II Response Spectrum

This type of spectra is generated by ground motions which produce response spectra with an essentially constant acceleration region over an extended period range. Unlike Type I spectra, the response spectra from these records do not decrease monotonically as the period lengthens. An example for this type of response spectra is given in Figure 7.4 where Wen-Wu 2%/50 yr Memphis GM #5 is used. It has an approximately constant spectral acceleration between periods of 0.5 and 1.7 seconds. The corresponding demand diagram is plotted in Figure 7.5; it is almost horizontal within the same period range. If, as in the case of Frame 2ST-PR, the post-yield region of the capacity diagram occurs in the same period range, then the application of the CSM is problematic, because the CSM may produce multiple performance points, none of which may converge.

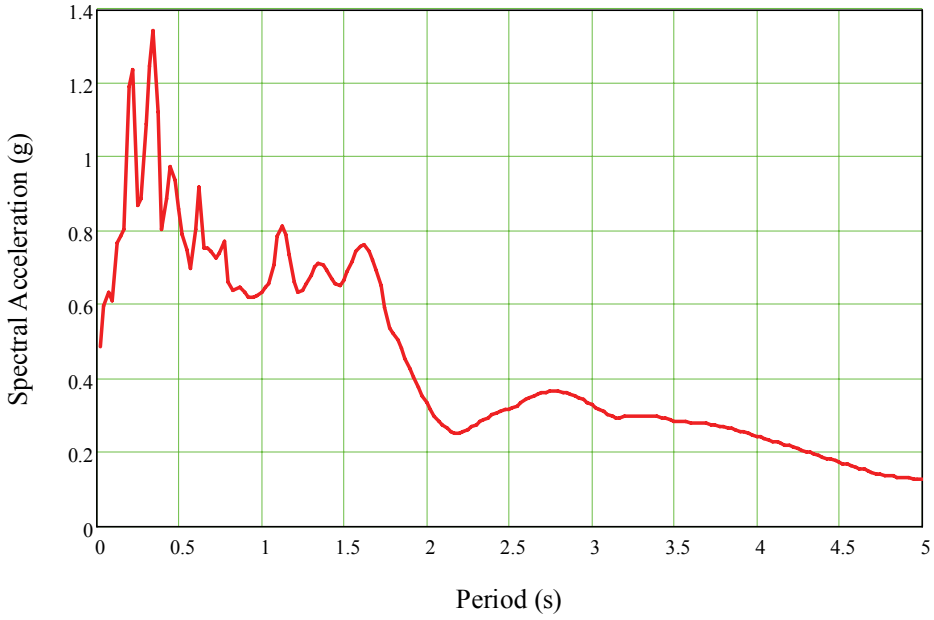

Figure 7.4 A typical Type II response spectrum.

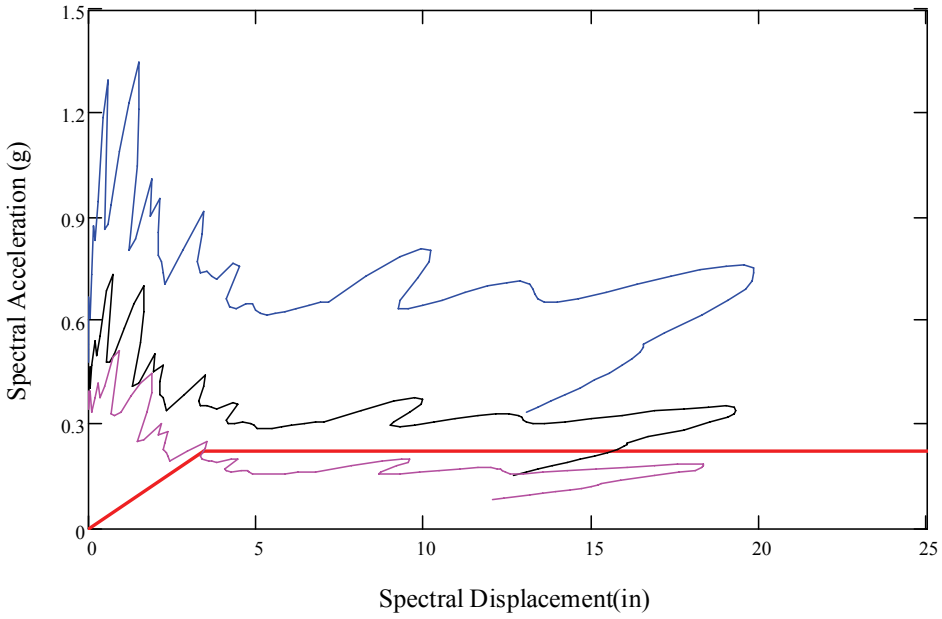

Figure 7.5 Application of CSM using a typical Type II response spectrum for μ=1, 2, 3.

7.3.3 Type III Response Spectrum

This type of response spectra is distinguished from the other two in the way that it has multiple local peaks at periods that are relatively far from each other. Such acceleration spectra typically contain a local peak in the high period range (T>1 sec) in addition to the peaks in the lower period range, which is typical for most hard rock ground motions. It is often seen in records from soil sites where the soil amplification factor is considerable. Figure 7.6 shows an example of this type of spectrum where Wen-Wu 2%/50 yr Memphis GM #2 is used. The relative peaks at periods of around 1 and 2 seconds create spikes in the demand diagrams after conversion, as shown in Figure 7.7. This causes multiple performance points and the one corresponding to the lowest spectral displacement converges.

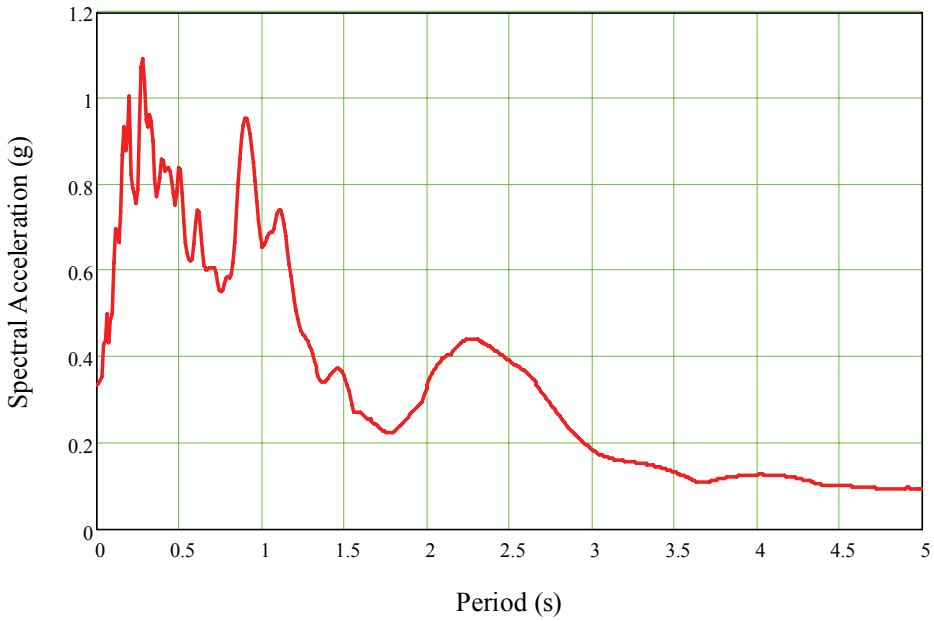

Figure 7.6 A typical Type III response spectrum.

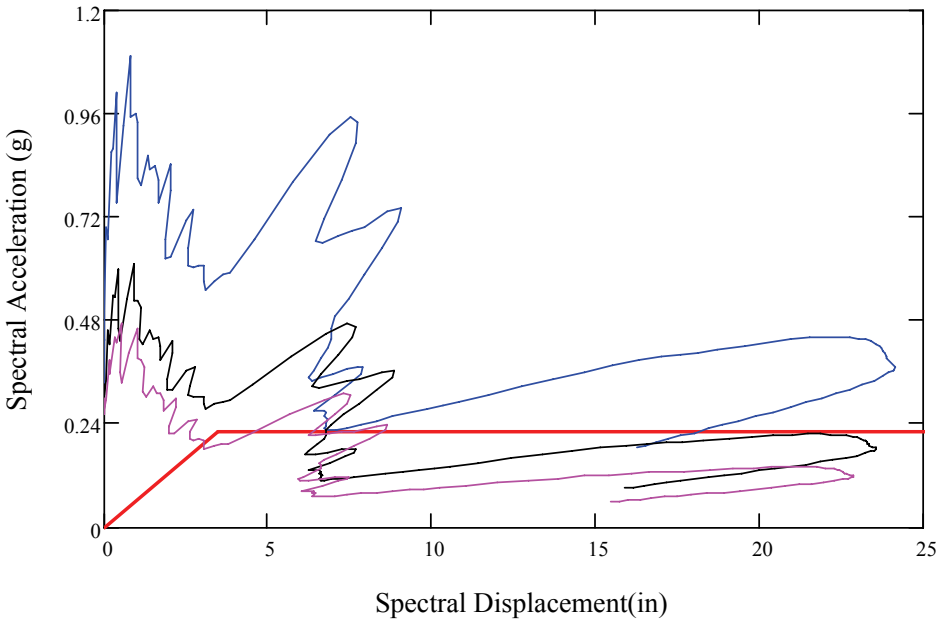

Figure 7.7 Application of CSM using a typical Type III response spectrum for μ=1, 2, 3.

7.4 Application of the CSM to Steel Frames in the CEUS

In this section, the CSM has been applied to three of the frames described in Chapter 4. Frame 2ST-PR is a first mode dominant frame; therefore, it might be expected that the CSM would predict the deformations with reasonable accuracy. Frames 3ST-FR and 6ST-XB also are assessed. These three frames reflect three different lateral force-resisting systems (PR, FR, and X-braced), with fundamental periods ranging between 1 and 2 seconds and first-mode participation factors ranging between 96% and 73%. In all cases, the roof deformations are compared against the roof deformations obtained from the NTHA.

7.4.1 Application of the CSM to Frame 2ST-PR

As a first step, the NSPA curve is approximated by a bilinear relationship. Inherent in the original formulation of the CSM is that the yielding slope of capacity curve can not be negative. For the case of Frame 2ST-PR, however, an elastoplastic approximation fits the pushover curve quite well, as seen in Figure 7.8. Following the steps described in the previous section, this pushover curve is converted into a capacity curve. The demand on the frame is represented by inelastic response spectrum approach described in Section 7.2.2. Three different R-μ-t relationships (Vidic et al., 1994; Krawinkler and Nassar, 1992; and Newmark and Hall, 1982) are plotted using Wen-Wu 2%/50 yr Memphis GM #1 in Figures 7.9, 7.10, and 7.11, respectively. Of these three, the last two are quite close to each other, while the first predicts slightly lower spectral accelerations than the other two.

The frame was analyzed using the Wen-Wu 2%/50 yr ensemble for Memphis using the three proposed R-μ-t relationships. The roof displacements are compared to the NTHA results in Table 7.1. The results which utilized the R-μ-t relationships of Krawinkler and Nassar (denoted KN hereafter) and those of Newmark and Hall (denoted NH) are in reasonably close agreement. The Vidic et al. (denoted VFF) model, however, produced somewhat different results. Neither the VFF nor KN models converged for 3 of the 10 GMs considered, while the NH model failed to converge in 4 cases out of 10.

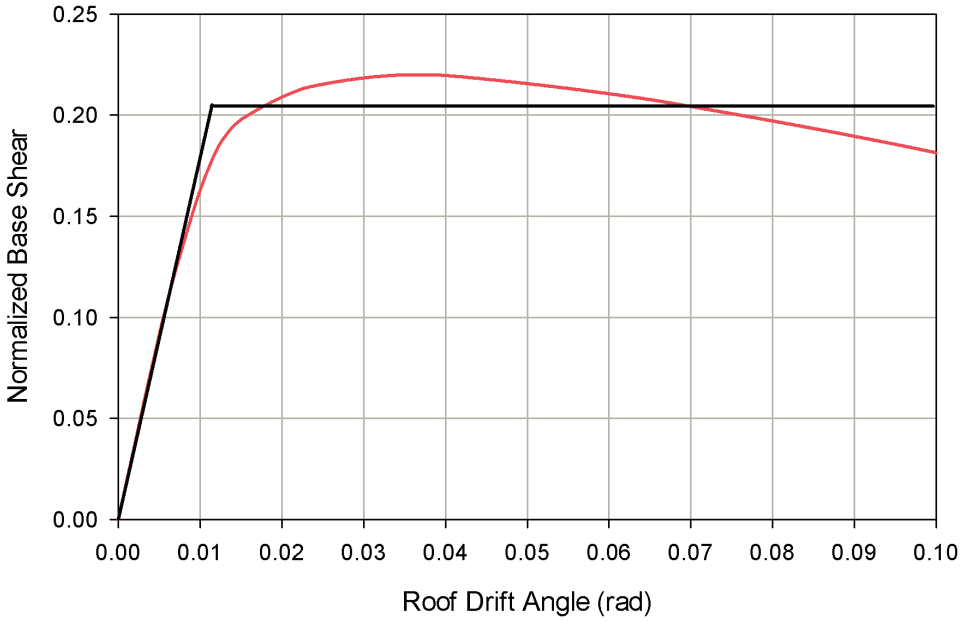

Figure 7.8 Approximation of pushover curve for Frame 2ST-PR by bilinear approach.

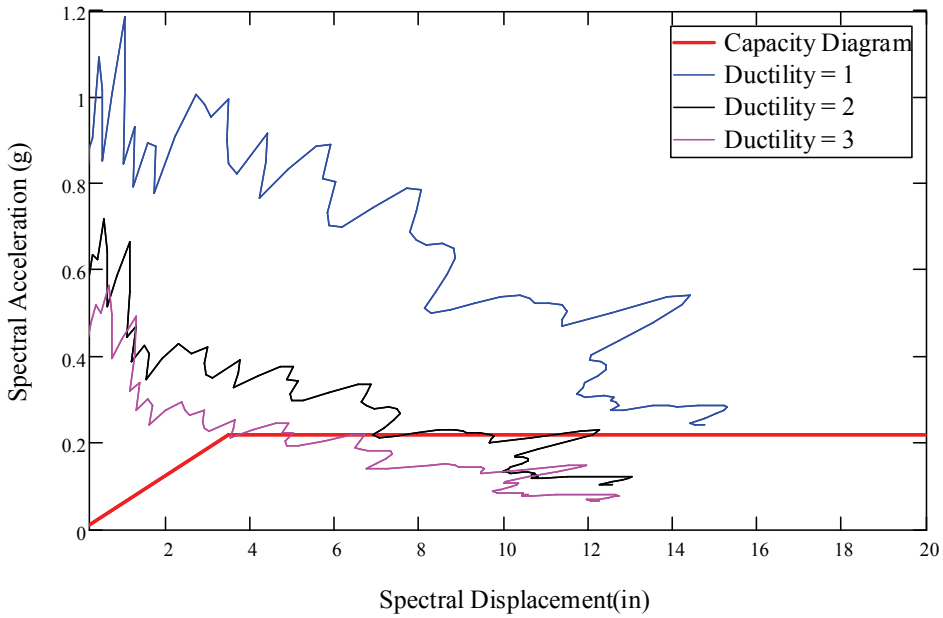

Figure 7.9 CSM plot for Frame 2ST-PR using VFF relationships.

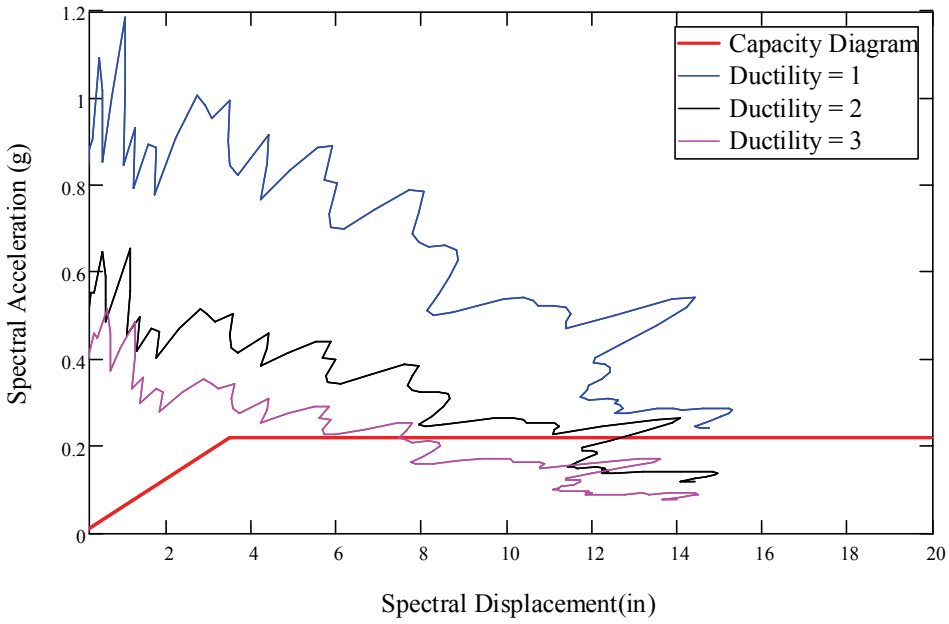

Figure 7.10 CSM plot for Frame 2ST-PR using KN relationships.

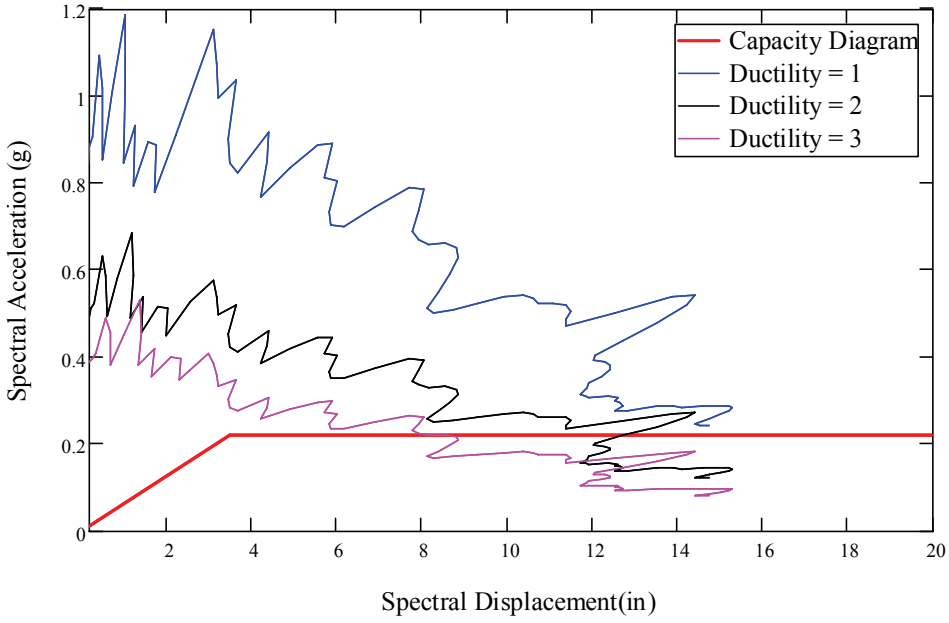

Figure 7.11 CSM plot for Frame 2ST-PR using NH relationships.

Table 7.1 Comparison of roof displacements produced by the CSM with NTHA for Frame 2ST-PR using original response spectra.

GM #	Roof Displacements (in)			
	NTHA	CSM(VFF)	CSM(KN)	CSM(NH)
1	8.41	9.36[a]	10.95[a]	10.95[a]
2	10.97	8.19[a]	9.17[a]	9.36[a]
3	6.26	5.38[b]	6.18[b]	6.55[b]
4	8.19	---[c]	---[c]	---[c]
5	10.57	---[c]	---[c]	---[c]
6	11.26	9.82[a]	11.23[a]	10.91[a]
7	5.11	---[c]	---[c]	---[c]
8	10.56	10.67[a]	---[c]	---[c]
9	6.33	6.46[a]	7.25[a]	7.25[a]
10	6.50	5.43[a]	5.62[a]	5.62[a]

[a] Produced multiple intersections; converged at the lowest spectral displacement.
[b] Produced single intersection; and converged.
[c] Produced multiple intersections; none converged.

The highly irregular nature of the response spectra hinders the feasibility of the CMS method for this frame. Irregularities observed during the application process are as follows:

- Multiple intersections of capacity and demand diagrams,
- Near-parallel behavior of some demand diagrams to the capacity diagram, which creates multiple intersections and non-convergence of the method.

To overcome the problems associated with the highly irregular nature of typical response spectra, the response spectra in their original format (S_a vs. T) were approximated using 6-order polynomial functions, as shown in Figure 7.12. The coefficients of the approximation to S_a for the 10 Wen-Wu 2%/50yr records for Memphis for powers of T are given in Table 7.2. The demand diagram calculated from these approximate response spectra becomes smoother (Fig. 7.13), and reduces the instances of

multiple roots or non-convergence of the CSM. The results obtained using these approximate response spectra are given in Table 7.3. All of the ground motion records except GM #5 produced a result. This indicates, at least for non-converging records, that the simplification of a response spectrum by a 6th order polynomial approximation to it facilitates solutions for ultimate displacement using the CSM. Solutions for all but one of the 10 records converged to a single performance point. This is mainly achieved by the smoothing of the local irregularities by the smooth polynomial functions.

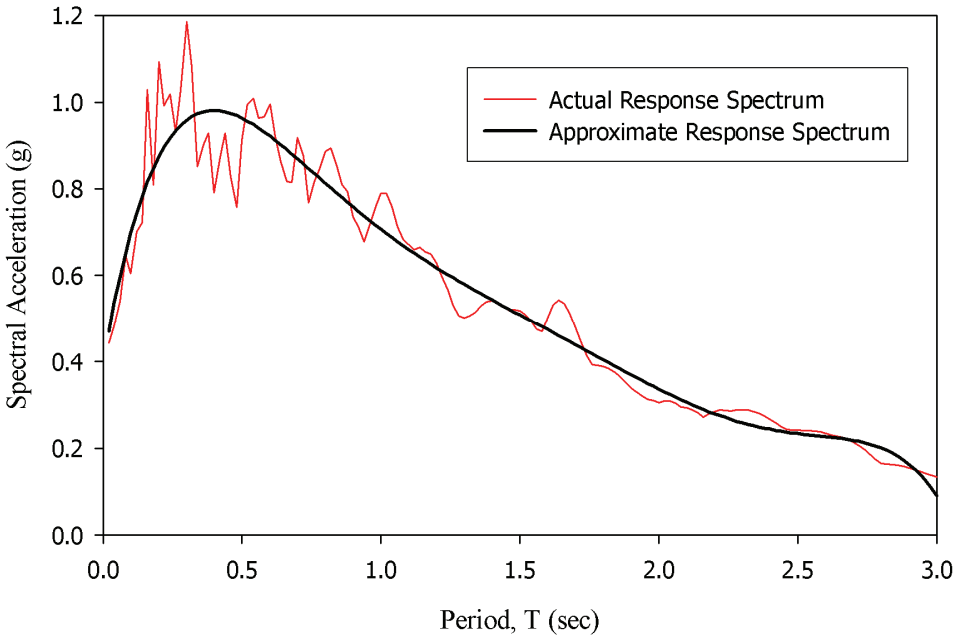

Figure 7.12 Response Spectrum and its simplification for Wen-Wu Memphis 2%/50 yr GM #01.

Table 7.2 Coefficients of polynomial approximation for 10 response spectra.

GM #	T^6	T^5	T^4	T^3	T^2	T^1	T^0
1	-41.784	415.08	-1631.2	3222.6	-3311.7	1466.6	153.52
2	1.1601	-11.079	-52.091	518.6	-1147.2	751.58	174.61
3	11.892	-56.066	-99.591	989.46	-1916.6	1163.8	130.22
4	-22.993	257.69	-1146	2547.5	-2876.7	1358	91.366
5	-161.9	1519.4	-5433.5	9234.8	-7568.3	2561.3	102.28
6	-40.981	475.16	-2132	4621.7	-4883	2084.5	118.24
7	-31.29	340.74	-1489.2	3259.2	-3576.5	1579.5	89.846
8	13.144	-108.35	265.59	-3.6948	-776.73	757.19	128.35
9	0.7684	48.248	-502.54	1777.3	-2641.9	1399.4	114.66
10	-40.855	429.91	-1832.9	3964.2	-4327.4	1904.7	97.075

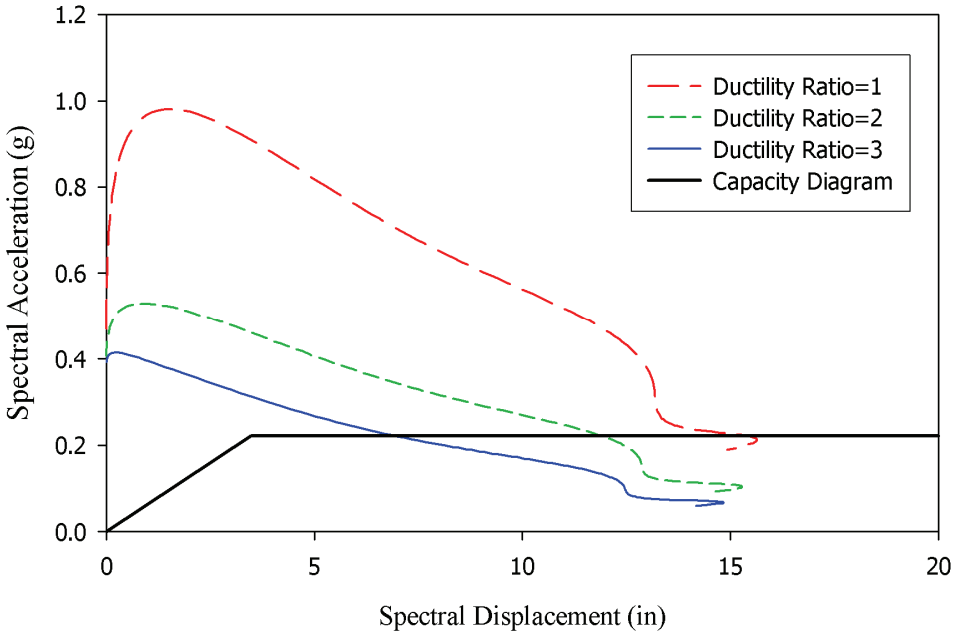

Figure 7.13 The CSM application using simplified response spectrum in Figure 7.12 for μ=1, 2, 3.

Table 7.3 Comparison of the CSM results with NTHA results for Frame 2ST-PR using polynomial representations for response spectra.

GM #	Roof Displacements (in)			
	NTHA	CSM(VFF)	CSM(KN)	CSM(NH)
1	8.41	10.57	12.00	12.47
2	10.97	8.25	9.33	9.47
3	6.26	5.38	6.18	6.55
4	8.19	7.99	9.07	9.10
5	10.57	---[a]	---[a]	---[a]
6	11.26	9.59	11.02	11.23
7	5.11	6.18	6.76	6.77
8	10.56	10.12	11.51	12.03
9	6.33	6.27	6.92	7.08
10	6.50	6.73	7.46	7.59

[a] Type II spectrum; produced multiple intersections, none converged.

The roof displacements produced by the CSM are comparable to those produced by NTHAs in most instances. The CSM predicts higher deformation demands than the NTHA most of the time. However, the roof displacements are also dependent on the *R*-μ-*t* relationships selected. As can be seen from Tables 7.1 and 7.3, the displacements produced by the KN and NH *R*-μ-*t* relationships are closer to each other than to those from the VFF relationship and in all cases predicted higher deformations than the latter. The ratio of predicted roof deflections to actual deflections calculated by NTHA is given in Figure 7.14.

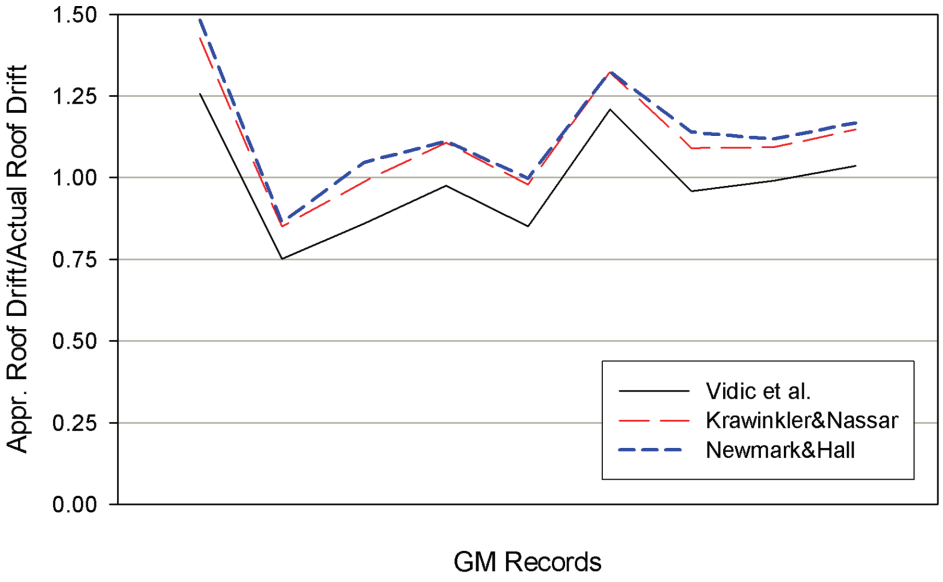

Figure 7.14 The ratio of the CSM results to NTHA results for Frame 2ST-PR.

7.4.2 Application of the CSM to Frame 3ST-FR

The same procedure was applied to Frame 3ST-FR, a three-story, fully-restrained moment frame whose pushover curve (Fig. 5.11) was represented by an elasto-plastic approximation. First the CSM was applied using the actual response spectra converted to the demand diagrams. Three *R*-μ-*t* relationships were used in this step. Six out of 10 Wen-Wu records produced multiple intersections of the demand and capacity spectra and neither of them converged to a performance point. Two of the remaining records resulted in multiple intersections, the one with lowest spectral displacement converged performance point. The final two converged to single performance points. Using the smooth approximations to the response spectra, 9 out of 10 records converged to a single point, as summarized in Table 7.4.

Table 7.4 Comparison of the CSM and NTHA results for Frame 3ST-FR.

GM #	Roof Displacements (in)			
	NTHA	CSM(VFF)	CSM(KN)	CSM(NH)
1	14.15	10.08	11.66	11.95
2	12.93	8.13	8.81	8.86
3	8.60	7.05	7.52	7.52
4	10.53	8.15	8.74	8.74
5	17.42	---[a]	---[a]	---[a]
6	18.07	9.49	10.84	10.84
7	16.55	6.64	6.35	6.35
8	18.55	9.72	10.96	11.19
9	15.64	6.23	6.41	6.41
10	19.09	6.66	7.11	7.11

[a] Type II spectrum; produced multiple intersections, none converged.

Overall, the agreement between the CSM and NTHA roof displacements for Frame 3ST-FR is not as good as that observed for Frame 2ST-PR. This can be attributed, to some extent, to the fact that the fundamental mode participation factor is lower for Frame 3ST-FR, i.e., 96% vs. 84%. The ratio of roof deflections predicted by the CSM to deflections calculated by NTHA is given in Figure 7.15. The KN and NH results are almost coincident and in general greater than the VFF results. Figure 7.15 indicates that the predicted results are always lower than the NTHA results.

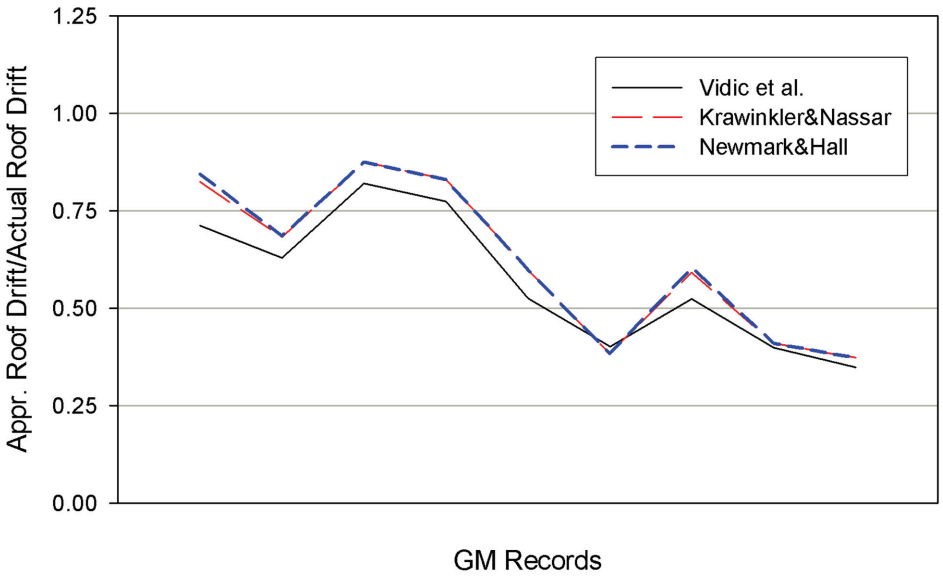

Figure 7.15 The ratio of the CSM results to NTHA results for Frame 3ST-FR.

7.4.3 Application of the CSM to Frame 6ST-XB

Frame 6ST-XB, a six-story, X-braced frame was analyzed using the CSM with the approximate response spectra converted to demand diagrams. Three *R*-μ-*t* relationships (VFF, KN and NH) were used. By using the smooth response spectra, solutions for the performance point were obtained for 9 out of 10 records, as summarized in Table 7.5. The overall agreement between the approximate and actual results is good especially for the KN and NH relationships. Again, these two models predict higher roof drifts than the VFF model. The ratio of predicted to actual roof deflections calculated by the NTHA is given in Figure 7.16. Although this frame has only 73% first mode participation factor, CSM results are quite close to the NTHA results.

Table 7.5 Comparison of the CSM and NTHA results for Frame 6ST-XB.

GM #	Roof Displacements (in)			
	NTHA	CSM(VFF)	CSM(KN)	CSM(NH)
1	10.89	8.26	9.52	9.79
2	9.07	7.18	8.21	8.41
3	6.61	6.80	7.80	7.91
4	7.71	6.45	7.34	7.41
5	12.74	---[a]	---[a]	---[a]
6	10.27	7.49	8.52	8.74
7	6.59	5.45	6.07	6.08
8	10.16	8.33	9.60	9.85
9	7.21	6.00	6.84	6.93
10	6.31	6.05	6.85	6.91

[a] Type II spectrum; produced multiple intersections, none converged.

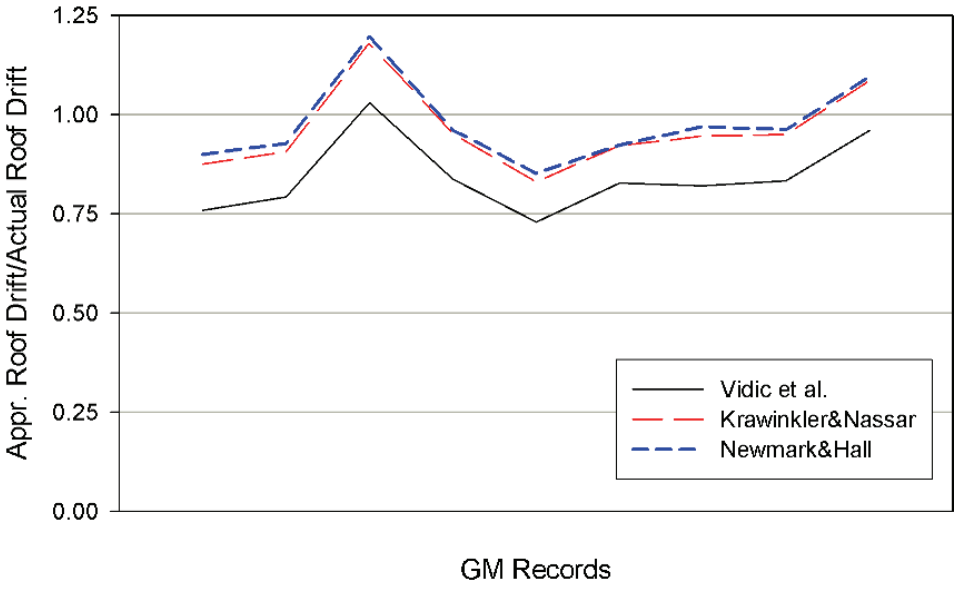

Figure 7.16 The ratio of the CSM results to NTHA results for Frame 6ST-XB.

7.5 Appraisal of the CSM and HAZUS

The Capacity Spectrum Method (CSM) was investigated with regard to its ability to predict roof displacements using actual ground motion records. It was shown that the agreement of its predictions with those from a NTHA depend on the characteristics of the particular ground motion selected and associated response spectrum. The differences resulting from the use of different R-μ-t relationships also were noted. In all cases, the KN and NH relationships produced roof displacements that were very close to one another. In contrast, VFF relationships estimated lower roof drifts in all cases than the other two.

The convergence and hence the applicability of the CSM depends on the shape of the response spectrum. The use of the actual response spectrum of a ground motion record has some drawbacks. The applicability of CSM is restricted by the local irregularities and extreme variations in some spectra, A method of smoothing the actual response spectra using polynomial functions to facilitate CSM solutions was proposed, and was shown to greatly improve the solution process and thus to extend the applicability of the CSM. The process of smoothing and the CSM analysis of an ensemble can be automated easily. However, even when the response spectra are smoothed by this process, some records may not produce a converged solution, e.g., GM #5 in Wen-Wu Memphis 2%/50 yr ensemble.

In general, it is expected that the CSM produces better results for first-mode dominant frames, and this was, in fact, observed in the analysis of Frame 2ST-PR. The CSM results are in good agreement with actual roof drifts for the 2-story frame. For the

3-story frame which has 84% first mode participation factor, however, roof drifts estimated using CSM are not close to actual results obtained using NTHA. For Frame 6ST-XB, the results are in good agreement, even though its first-mode participation factor is 73%. These show that the CSM predicts roof deformations better for stiffer frames and it tends to get biased in flexible frames irrespective of the first-mode participation factor (Kinali and Ellingwood, 2007b).

The results produced by the CSM in this chapter, in general, are off by about 30%, but the error can be either conservative or unconservative. Since HAZUS uses the CSM as the main analysis engine for predicting building deformations and the damage states are related to deformation levels, the damage state probabilities obtained from HAZUS may not be expected to be in good agreement with those obtained from NTHA.

The fragilities in HAZUS are modeled by the median structural capacity and the overall uncertainty term in the process. The fragilities are functions of spectral displacements at an effective period, T, at the performance point. Due to this peculiar way of determining building period, there is no simple relation between spectral acceleration and displacement values. Therefore, it is not practical to compare fragilities on the same plot. Also, the performance limits used in the HAZUS are mostly judgmental and therefore different from those used in this dissertation.

The resulting performance assessment can be quite pessimistic due to conservative performance limits and much higher logarithmic standard deviations, usually around 90% (Ellingwood et al., 2007).

CHAPTER VIII

SUMMARY AND CONCLUSIONS

8.1 Summary

The main objective of this dissertation has been to assess seismic vulnerability of steel building frames typical of construction practices in the Central and Eastern United States. Shelby Co., TN, which includes the city of Memphis and is a major urban population center near the New Madrid Seismic Zone (NMSZ), was selected to represent a region in the CEUS that is at substantial seismic risk. The Mid-America Earthquake (MAE) Center is currently engaged in a research program (the Memphis Testbed Project) to develop seismic risk reduction strategies for civil infrastructure in such regions. The research products of this dissertation contribute directly to that MAE Center program.

In a concurrent MAE Center project, the current building stock of Shelby County was surveyed. According to the results of that study, steel-framed buildings comprise the majority of commercial and industrial facilities in the region. Most of these buildings are 6 stories or less and were constructed before 1990 with little or no consideration of seismic resistance. Therefore, their performance during a future major earthquake may not be satisfactory. To represent the building stock in Shelby County, five code-compliant steel frames were identified. These frames had different lateral load resisting systems - rigid moment frame, partially-restrained moment frame and braced frame; ranged from 30 ft to 80 ft in height; and represented typical design and construction practice between 1950s and 1990s. The design of four out of five of these frames was governed by wind load requirements, which is typical of the practice in the CEUS. Two

concentrically-braced frames - a chevron braced frame and X-braced frame - represented typical braced-frames in the CEUS. Structure-specific performance limits were calculated and were used to define states of building performance, rather than using the general performance limits suggested in FEMA documents (FEMA 273/356).

Due to a lack of recorded accelerograms in the region of the NMSZ, seismicity was represented by two types of synthetic ground motions, e.g., uniform hazard and postulated scenario events. The frames were modeled using sophisticated modeling approaches and a finite element platform capable of nonlinear dynamic analysis. Using state-of-the-art performance assessment methods, building fragilities and performance state probabilities of all frames were evaluated for both a 2%/50 yr uniform hazard event (termed the maximum considered earthquake, or MCE, by the BSSC/NEHRP recommended provisions and by *ASCE Standard 7-05*) and a rare scenario event with M_w=7.5, R=20 km. Some of the frames behaved poorly under seismic events of this magnitude. The effect on building performance of seismic upgrades using feasible rehabilitation schemes also was considered. For one of the PR frames, the addition of brace members in one interior bay throughout the height of the frame was found to be sufficient. In the braced-frames, brace members were converted to buckling-restrained braces with nearly elasto-plastic cyclic behavior. After rehabilitation, seismic performances of these frames were improved considerably.

The Capacity Spectrum Method (CSM) was investigated in detail with regard to its applicability to assessing performance of frames using response spectra from CEUS ground motions. It was found that the CSM can produce a unique performance point for some of the ground motion records but not for others. Three types of response spectra

were identified, only one of which produces a consistent result for CSM applications. Smoothing of the actual response spectra using 6^{th} order polynomial functions greatly increased the convergence characteristics of the CSM solutions. When this approximation was applied to three of the frames, the estimated roof displacements were in good agreement with the results of NTHA for two of the three frames considered.

All in all, the steel building frames considered in this study performed better under seismic excitation than might be expected for frames designed without strict seismic criteria, with the exception of the 5-story chevron frame which performed poorly prior to rehabilitation with buckling-restrained braces; following rehabilitation, it performed quite well. This can be attributed to the fact that the PR frames considered in this dissertation possessed good energy dissipation characteristics and thus performed quite well in comparison with rigid frames. The frame with X-bracing revealed good load-redistribution characteristics and more ductile behavior than the chevron-braced frame.

8.2 Conclusions

Some of the specific conclusions that can be drawn from this dissertation for steel building frames in the CEUS follow:

- The performance limits in FEMA 273/356 were derived mainly from a consideration of frames designed in high-seismic regions. The Immediate Occupancy (IO) performance limits given in FEMA-273/356 for steel frames, i.e., 0.5% ISDA for braced-frames and 0.7% ISDA for moment frames, appear to be valid for building frames in the CEUS as well. The Collapse Prevention (CP) performance limit, i.e., 2% ISDA for braced frames, appears to be acceptable for ordinary concentrically braced frames (chevron frames where floor beams are weak) but is overly conservative for X-braced frames in which full truss action can develop. The CP limit of 5% ISDA for moment frames is also conservative for the FR and PR moment frames considered in this dissertation.
- There is good agreement between the most critical story found from the static nonlinear pushover analysis and the story identified from the NTHAs, i.e., the nonlinear pushover curve, if plotted for each interstory drift angle, can be used to identify the soft story in a frame.
- Seismic demand on the frames determined from the NTHA is less dependent on the particular ground motion ensemble selected than on the frame characteristics. Similarly, the structural capacity at the CP limit determined from the IDAs, measured in terms of the ISDA, appears to be virtually independent of the ground motion ensemble selected.

- Frame response becomes less sensitive to individual ground motion records as the frame approaches the point of incipient dynamic instability. The variability in seismic demand is higher at higher performance levels (IO, SD) than at the CP level.
- The 2-Story PR frame and the 3-Story rigid frame experienced similar damage levels under the 2%/50 yr event. The 2-Story PR frame has almost zero probability of collapse under both 2%/50 yr and the rare scenario event, mainly due to low P-Δ effects. Moreover, it sustains negligible residual deformations under the 10%/50 yr event; and experiences residual deformations that are only slightly larger than its IO limit under the 2%/50 yr event.
- The effect of connection capacity on frame behavior was found to be insignificant for the 4-Story PR frame at a level corresponding to the MCE (2%/50 yr uniform hazard). In contrast, at higher levels of ground motion associated with large scenario events, the behavior of the frame was dictated mainly by the capacity of connections. Strong connections decrease the collapse probability of this frame significantly (Kinali and Ellingwood, 2007c).
- The original 5-Story chevron-braced frame behaved poorly under the MCE, and it experienced almost certain collapse under rare scenario event. In contrast, the 6-Story X-braced frame performed quite favorably under both 2%/50 yr and rare scenario events. The braced frames considered in this dissertation possessed brace connections stronger than brace members, thus, the brace capacity governed. However, in some older braced frames, connections might be weaker and braces

do not reach their full capacity before connections fail. Consideration should be given to assess the capacity of braces and the connections.

- The addition of buckling-restrained brace members to the PR frames at all story levels appears to be an effective method of rehabilitation for such frames in the CEUS. Converting the existing braces to buckling-restrained braces enhances their seismic performance without excessive residual deformations. In fact, the technique decreased the residual drifts on Frame 4ST-PR by 80%.
- The performance points obtained from the CSM, in terms of roof displacements, are closer to the displacements from the NTHA for the 2-Story PR frame and 6-Story braced-frame than for the 3-Story rigid frame. The results produced by the CSM are, in general, off by about 30% for the frames considered, but they can err in either the conservative or unconservative direction. The CSM produces results that are closer to those of the NTHA for stiffer frames, irrespective of the first-mode participation factor. Smoothing the response spectra is effective in increasing chances of convergence of the CSM (Kinali and Ellingwood, 2007b).
- The performance assessment of individual building frames using HAZUS can be quite pessimistic due to median performance limits that are lower and logarithmic standard deviations that are higher (usually around 90%) than those supported by the NTHA-based fragility analyses conducted as part of this study. It should be noted that HAZUS was developed for the evaluation of portfolios of buildings rather than individual structures. However, it has been used for the latter purpose in the absence of alternative fragilities and damage state probabilities for construction in the CEUS. The current research fills that gap.

8.3 Future Research Suggestions

Most of the seismic performance assessment tools used in this dissertation have evolved in the last decade. Finite element platforms also have advanced in recent years. The increase in the computation power has made the application of methods that until recently were resource-intensive trivial. However, advances in computation have not eliminated the need for simplified models and simplifying assumptions in many common applications. Suggestions for future research follow:

- More accurate performance assessment can be made by using more refined modeling techniques, at the expense of additional cost. One of the assumptions of this dissertation – that the contribution of gravity frames and non-structural elements to lateral force resistance can be neglected – can be eliminated by using a different modeling approach. These contributions may be quite important, especially in older buildings where the redundancy in the structural system is larger than in modern building practices. Furthermore, the effect of building irregularities and torsional effects should be considered in a 3D analysis to determine the extent to which they affect the seismic fragilities. These effects may have a significant impact on the damage state probabilities.
- Although OpenSees has a wide library of elements and was found to be very robust, it has certain limitations. For example, there is no brace element in the library, either buckling-permitted or buckling-restrained. One must instead use a generic material model to define the axial stress-axial strain behavior and assign it

to a truss member. The generic material models, originally developed for defining moment-rotation behavior of connections, are not feasible for modeling brace cycling behavior. In addition, prismatic members in the element library do not take into account local buckling or lateral-torsional buckling. Since OpenSees is still under development and new elements or, materials are added all the time, it is likely that in the future, this platform will be capable of addressing the issues mentioned here.

- At the current state-of-the-art, seismic performance assessment of building frames in the CEUS must rely on synthetic ground motions. Most plausible synthetic ground motion modeling approaches in the literature (e.g., Atkinson and Boore, 1995; Frankel et al., 1996) are different in the way that they predict seismic intensity for a given region. The difference in the spectral accelerations at a given return period may be as large as 100%. These differences contribute considerably to the uncertainty in seismic performance assessment of building frames in the CEUS. A consensus on appropriate ground motion models for specific sites in the CEUS must evolve before analysts fully embark on seismic risk assessment using synthetic ground motions derived from these models.
- Current rapid assessment technologies (CSM, HAZUS) appear to be deficient when applied to buildings in the CEUS and when actual response spectra are used rather than smooth design spectra. Research should be undertaken to develop more robust damage prediction techniques for rapid assessment of both individual and portfolio of buildings.

REFERENCES

Abdalla, K.M., Chen, W.F. (1995) "Expanded Database of Semi-Rigid Steel Connections", Computers and Structures; 56(4), 553-564.

AISC. (1994) "Manual of Steel Construction, Load and Resistance Factor Design, Second Edition", American Institute of Steel Construction, Inc.

AISC. (2005) "Specification for Structural Steel Buildings", American Institute of Steel Construction, Inc., ANSI/AISC 360-05.

Altman, W.G., Azizinamini, A., Bradburn, J.H., Radziminski, J.B. (1982) "Moment-Rotation Characteristics of Semi-Rigid Steel Beam-Column Connections", Department of Civil Engineering, University of South Carolina, Columbia, SC.

ASCE. (2005) "Standard - Minimum Design Loads for Buildings and Other Structures, 7-05", American Society of Civil Engineers.

ATC. (1978) "Tentative Provisions for the Development of Seismic Regulations for Buildings, ATC 3-06", Applied Technology Council, Redwood City, CA, 1996.

ATC. (1996) "Seismic Evaluation and Retrofit of Concrete Buildings, ATC-40", Applied Technology Council, Redwood City, CA, 1996.

Atkinson, G.M, Boore, D.M. (1995) "New Ground Motion Relations for Eastern North America", Bull. Seism. Soc. Am.; 85: 17-30.

Atkinson, G.M, Boore, D.M. (1998) "Evaluation of Models for Earthquake Source Spectra in Eastern North America", Bull. Seism. Soc. Am.; 88(4), 917-934.

Azizinamini, A., Bradburn, J.H., Radziminski, J.B. (1985) "Static and Cyclic Behavior of Semi-Rigid Steel Beam-Column Connections", Department of Civil Engineering, University of South Carolina, Columbia, SC.

Barakat, M., Chen, W.F. (1991) "Design Analysis of Semi-Rigid Frames: Evaluation and Implementation", Engineering Journal, AISC; Second Quarter: 55-64.

Beavers, J.E. (2002) "A Review of Seismic Hazard Description in US Design Codes and Procedures", Progress in Structural Engineering and Materials; 4: 46-63.

Benjamin, J.R., Cornell, C.A. (1970) "Probability, Statistics and Decision for Civil Engineers", McGraw Hill Book Company, New York.

Beresnev, I.A., Atkinson, G.M. (1998) "FINSIM—a FORTRAN Program for Simulating Stochastic Acceleration Time Histories from Finite Faults", Seismological Research Letters; 69(1), 27–32.

Bertero, V.V., Krawinkler, H., Popov, E.P. (1973) "Further Studies on Seismic Behavior of Steel Beam-to-Column Subassemblages", EERC Rep. 73-27, University of California, Berkeley.

Bertero, V.V., Popov, E.P., Krawinkler, H. (1972) "Beam-Column Sub-Assemblages Under Repeated Loading", Journal of the Structural Division, ASCE; 98(5): 1137-59.

BSSC. (2003) "NEHRP Recommended Provisions for Seismic Regulations for New Buildings and Other Structures", Building Seismic Safety Council, Washington, D.C.

Chen, W.F., Kishi, N. (1989) "Semi-Rigid Steel Beam-To-Column Connections: Data Base and Modeling", Journal of Structural Engineering; 115(1), 105-119.

Chopra, A.K., Goel, R.K. (1999) "Capacity-Demand-Diagram Methods Based on Inelastic Design Spectrum", Earthquake Spectra; 15(4):637– 656.

Chopra, A.K., Goel, R.K. (2000) "Evaluation of NSP to Estimate Seismic Deformation: SDF Systems", Journal of Structural Engineering, ASCE; 126(4):482– 490.

Clark, P., Aiken, I., Kasai, K., Ko, E., Kimura, I. (1999) "Design Procedures for Buildings Incorporating Hysteretic Damping Devices", Proceedings of the 69th Convention of the SEAOC.

Cornell, C.A., Jalayer, F., Hamburger, R.O., Foutch, D.A. (2002) "Probabilistic Basis for 2000 SAC Federal Emergency Management Agency Steel Moment Frame Guidelines", Journal of Structural Engineering, 126(1); 127-136.

Ellingwood, B. (1990) "Validation Studies of Seismic PRAs", Nuclear Engineering and Design; 123(2):189–96.

Ellingwood, B.R., Celik, O., Kinali, K. (2007) "Fragility Assessment of Building Structural Systems in Mid-America", Earthquake Engineering and Structural Dynamics (submitted for publication).

Ellingwood, B.R., Wen, Y.K. (2005) "Risk-Benefit Based Design Decisions for Low Probability/High Consequence Earthquake Events in Mid-America", Progress in Structural Engineering and Materials; 7(2):56–70.

Elnashai, A.S., Elghazouli, A.Y., Denesh-Ashtiani, F.A. (1998) "Response of Semirigid Steel Frames to Cyclic and Earthquake Loads" Journal of Structural Engineering; 124(8), 857-67.

Fajfar, P. (1999) "Capacity Spectrum Method Based on Inelastic Demand Spectra", Earthquake Engineering and Structural Dynamics; 28, 979-993.

FEMA. (2003) "Multi Hazard Loss Estimation Methodology", HAZUS Technical Manual, Washington, D.C.

FEMA 273/356. (1997/2000) "NEHRP Guidelines for the Seismic Rehabilitation of Buildings." Prepared by the Applied Technology Council for the Building Seismic Safety Council, Published by the Federal Emergency Management Agency, Washington, DC.

FEMA 302. (1997) "NEHRP Recommended Provisions for Seismic Regulations for New Buildings", Federal Emergency Management Agency, Washington, DC.

FEMA 351. (2000) "Recommended Seismic Evaluation and Upgrade Criteria for Existing Welded Steel Moment-Frame Buildings", Federal Emergency Management Agency, Washington, DC.

FEMA 355-C. (2000) "State of the Art Report on Systems Performance of Steel Moment Frames Subject to Earthquake Ground Shaking", Federal Emergency Management Agency Washington, DC.

FEMA 355-F. (2000) "State of the Art Report on Performance Prediction and Evaluation of Steel Moment-Frame Structures", Federal Emergency Management Agency, Washington, DC.

Fernandez, J.A., Rix, G.J. (2006) "Soil Attenuation Relationships and Seismic Hazard Analyses in the Upper Mississippi Embayment", Eighth U.S. National Conference on Earthquake Engineering, 8NCEE, San Francisco, California.

Foley, C.M., Vinnakota, S. (1997) "Inelastic Analysis of Partially Restrained Unbraced Steel Frames", Engineering Structures; 19(11), 891-902.

Forcier, G.P. (1994) "Seismic Performance of Older Steel Frames", Ph.D. Dissertation, Department of Civil and Environmental Engineering, University of Minnesota.

Foutch, D.A., Yun. S.Y. (2002) "Modeling of steel moment frames for seismic loads", Journal of Constructional Steel Research; 58:529-64.

Frankel, A., Mueller, C., Barnhard, T., Perkins, D., Leyendecker, E., Dickman, N. (1996) "National Seismic Hazard Maps: Documentation", U.S. Geological Survey Open-File Report 96-532.

Freeman, S.A, Nicoletti J.P, Tyrell J.V. (1975) "Evaluations of Existing Buildings for Seismic Risk—A Case Study of Puget Sound Naval Shipyard, Bremerton, Washington." Proceedings of the 1st U.S. National Conference on Earthquake Engineering; 113–122.

Freeman, S.A. (1998) "Development and Use of Capacity Spectrum Method." Paper No. 269. The 6th U.S. National Conference on Earthquake Engineering, EERI, Seattle, Washington.

French, S.P., Olshansky, R. (2001) "Inventory of Essential Facilities in Mid-America", Project SE-1 Report, Mid-America Earthquake Center, Champaign-Urbana, IL.

Galambos, T.V., Ravindra, M.K. (1978) "Properties of Steel for Use in LRFD", Journal of the Structural Division, ASCE; 104(9), 1459-68.

Gao, L., Haldar, A. (1995) "Safety Evaluation of Frames with PR Connections" Journal of Structural Engineering; 121(7), 1101-18.

Giovenale, P., Cornell, C.A., Esteva, L. (2004) "Comparing the Adequacy of Alternative Ground Motion Intensity Measures for the Estimation of Structural Responses", Earthquake Engineering and Structural Dynamics; 33(8), 951-79.

Goggins, J.M., Broderick, B.M., Elghazouli, A.Y., Lucas, A.S. (2006) "Behavior of Tubular Steel Members under Cyclic Axial Loading", Journal of Constructional Steel Research, 62, 121-31.

Goverdhan, A.V. (1984) "A Collection of Experimental Moment-Rotation Curves and Evaluation of Prediction Equations for Semi-Rigid Connections", Ph.D. Thesis, Vanderbilt University, Nashville, TN.

Grossi, P. (2000) "Quantifying the Uncertainty in Seismic Risk and Loss Estimation." Ph.D Dissertation, University of Pennsylvania.

Gupta, A., Krawinkler, H. (2000) "Behavior of Ductile SMRFs at Various Seismic Hazard Levels", Journal of Structural Engineering; 126(1): 98-107.

IBC. (2003) "International Building Code", International Code Council.

Jain, A.K., Goel, S.C. (1978) "Inelastic Cyclic Behavior of Bracing Members and Seismic Response of Braced Frames of Different Proportions", Report No. UMEE78R3, Department of Civil Engineering, University of Michigan, Ann Arbor.

Jain, A.K., Goel, S.C. (1979) "Cyclic End Moments and Buckling in Steel Members", Proc. Of the Second U.S. Nat. Conf. Earthquake Eng., Stanford, CA.

Jain, A.K., Goel, S.C., Hanson, R.D. (1980) "Hysteretic Cycles of Axially-Loaded Steel Members", Journal of the Structural Division, ASCE; 106(ST8), 1777-1794.

Johnson, A.C. (1982) "A Major Earthquake Zone on the Mississippi" Scientific American, 246(4), 60-68.

Jones, S.W., Kirby, P.A., Nethercot, D.A. (1980) "Effect of Semi-Rigid Connections on Steel Column Strength", Journal of Constructional Steel Research, Vol. 1, 38-46.

Kim, D-H. (2003) "Seismic Performance of PR Frames in Areas of Infrequent Seismicity", Ph.D. Dissertation, School of Civil&Environmental Engineering, Georgia Institute of Technology, Atlanta, GA.

Kim, J., Choi, H. (2005) "Response Modification Factors of Chevron-Braced Frames", Engineering Structures; 27:285-300.

Kinali, K., Ellingwood, B.R. (2007a) "Seismic Fragility Assessment of Steel Frames for Consequence-Based Engineering: A Case Study for Memphis, TN", Engineering Structures (in press).

Kinali, K., Ellingwood, B.R. (2007b) "Application of the Capacity Spectrum Method to Steel Frames in the Central and Eastern United States", Proceedings of the Thematic Conference on Computational Methods in Structural Dynamics and Earthquake Engineering, ECCOMAS, June 13-16, 2007, Rethymno, Crete, Greece.

Kinali, K., Ellingwood, B.R. (2007c) "Performance of Non-Seismically Designed PR Moment Frames under Earthquake Loading", Proceedings of the 10th International Conference on Applications of Statistics and Probability in Civil Engineering, ICASP10, July31-August 3, 2007, Tokyo, Japan.

Kishi, N., Chen, W.F. (1986) "Database of Steel Beam-to-Column Connections, Vols. I and II", Structural Engineering Report No. CE-STR-86-26, School of Civil Engineering, Purdue University, West Lafayette, IN.

Krawinkler, H. (1994) "New Trends in Seismic Design Methodology", Proc. 10th European Conference in Earthquake Engineering., Vol. 2, pp. 821-830, Balkema, Rotterdam.

Krawinkler, H. (1978) "Shear in Beam-Column Joints in Seismic Design of Steel Frames", Engineering Journal, AISC; 15(3): 82-91.

Krawinkler, H., Bertero, V.V., Popov, E.P. (1975) "Shear Behavior of Steel Frame Joints", Journal of the Structural Division, ASCE; 101(11): 2317-36.

Krawinkler, H., Nassar, A.A. (1992) "Seismic Demand Based on Ductility and Cumulative Damage Demands and Capacities", Nonlinear Seismic Analysis and Design of Reinforced Concrete Buildings, Elsevier Applied Science, New York.

Krawinkler, H., Seneviratna, G.D.P.K. (1998) "Pros and Cons of a Pushover Analysis of Seismic Performance Evaluation." Engineering Structures, Vol.20, 452-464.

Lee, K., Foutch, D.A. (2002) "Seismic Performance Evaluation of Pre-Northridge Steel Frame Buildings with Brittle Connections", Journal of Structural Engineering; 128(4), 546-555.

Leon, R.T., Kim, D-H. (2004) "Seismic Performance of Older PR Frames in Areas of Infrequent Seismicity", 13th World Conference on Earthquake Engineering 2004; Paper No. 2696. Vancouver, B.C., Canada.

Lin, Y.Y., Chang, K.C. (2003) "An Improved Capacity Spectrum Method for ATC-40", Earthquake Engineering and Structural Dynamics: 32:2013-2025.

Lindsey, S.D. (1987) "Design of Frames with PR Connections", Journal of Constructional Research; 8: 251-260.

Luco, N., Cornell, C.A. (2001) "Structure-Specific Scalar Intensity Measures for Near-Source and Ordinary Earthquake Ground Motions", Submitted for Publication: Earthquake Spectra.

Lui, E.M., Chen, W.F. (1986) "Analysis and Behavior of Flexibly Jointed Frames", Engineering Structures; 8(2), 107-118.

Maison, B., Bonowitz, D. (1999) "How Safe Are Pre-Northridge WSMFs? A Case Study of the Sac Los Angeles Nine-Story Building", Earthquake Spectra, 15(4): 765-789.

Maison, B.F., Kasai, K. (1999) "Seismic Performance of 3 and 9 Story PR Moment Frame Buildings", SAC Joint Venture Background Document; SAC/BD-99/16.

Martinelli, L., Mulas, M.G., Perotti, F. (1998) "The Seismic Behavior of Steel Moment-Resisting Frames with Stiffening Braces", Engineering Structures; 20(12), 1045-62.

Mazzoni, S., McKenna, F., Fenves, G.L. (2005) "OpenSees Command Language Manual" Pacific Earthquake Engineering Center; University of California, Berkeley.

McGuire, R.K (2004) "Seismic Hazard and Risk Analysis", Earthquake Engineering Research Institute, Second Monograph Series, MNO-10.

Mwafy, A.M., Elnashai, A.S. (2001) "Static Pushover versus Dynamic Collapse Analysis of RC Buildings", Engineering Structures, 23(5), 407-24.

Nader, M.N., Astaneh-Asl, A. (1996) "Shaking Table Tests of Rigid, Semirigid, and Flexible Steel Frames", Journal of Structural Engineering; 122(6), 589-96.

Naeim, F., Skliros, K., Reinhorn, A.M., Sivaselvan, M.V. (2000) "Effects of Hysteretic Deterioration Characteristics on Seismic Response of Moment Resisting Steel Structures", SAC-BD/99-18.

Newmark, N. M., Hall, W. J. (1982) "Earthquake Spectra and Design", Engineering Monographs on Earthquake Criteria, Structural Design, and Strong Motion Records, Vol. 3, Earthquake Engineering Research Institute, Oakland, CA.

Popov, E.P., Amin, N.R., Louie, J.J., Stephen, R.M. (1986) "Cyclic Behavior of Large Beam-Column Assemblies", Engineering Journal; 23(1):9-23.

Popov, E.P., Pinkney, R.B. (1969) "Cyclic Yield Reversals in Steel Building Connections", Journal of Structural Division, ASCE; 95(3), 327-53.

Popov, E.P., Stephen, R.M. (1970) "Cyclic Loading of Full-Size Steel Connections", EERC Rep. 70-3, University of California, Berkeley, CA.

Rathbun, J.C. (1936) "Elastic Properties of Riveted Connections", ASCE Paper No. 1933, Vol. 101.

Razzaq, Z. (1983) "End Restraint Effect on Steel Column Strength", Journal of Structural Division, ASCE; 109(ST2), 314-334.

Reitherman, R. (1985) "A Review of Earthquake Damage Estimation Methods", Earthquake Spectra, Vol 1. No. 4, 805-847.

Richard, R.M., Abbott, B.J. (1975) "Versatile Elastic Plastic Stress-Strain Formula", Journal of Engineering Mechanics, ASCE; 101: 511-515.

Roeder, C.W. (2002) "Connection Performance for Seismic Design of Steel Moment Frames", Journal of Structural Engineering; 128(4), 517-25.

Roeder, C.W., Foutch, D.A. (1996) "Experimental Results for Seismic Resistant Steel Moment Frame Connections", Journal of Structural Engineering; 122(6), 581-88.

Sabelli, R., Mahin, S., Chang, C. (2003) "Seismic Demands on Steel Braced Frame Buildings with Buckling-Restrained Braces", Engineering Structures; 25, 655-666.

Salazar, A.R., Haldar, A. (2001) "Energy Dissipation at PR Frames Under Seismic Loading", Journal of Structural Engineering; 127(5), 588-92.

Schneider, S.P., Amidi, A. (1998) "Seismic Behavior of Steel Frames with Deformable Panel Zones", Journal of Structural Engineering, ASCE; 124(1): 35-42.

SEAOC Blue Book (1999) "Recommended Lateral Force Requirements and Commentary", 7th edition, Structural Engineers Association of California, Sacramento, CA.

Shinozuka, M., Feng, N.Q., Lee, J., Naganuma, T. (2000) "Statistical Analysis of Fragility Curves", Journal of Structural Engineering ASCE 126(12):1224-31.

Shome, N., Cornell, C.A. (1998) "Normalization and Scaling Accelerograms for Nonlinear Structural Analysis", 6th U.S. National Conference on Earthquake Engineering.

Shome, N., Cornell, C.A. (1999) "Probabilistic Seismic Demand Analysis of Non-linear Structures", Report No. RMS-35, RMS Program, Stanford University.

Shome, N., Cornell, C.A., Bazzurro, P., Carballo, J. (1998) "Earthquake, Records and Nonlinear MDOF Responses." Earthquake Spectra, 14(3); 469-500.

Silva, W., Gregor, N., Darragh, R. (2003) "Development of Regional Hard Rock Attenuation Relations for Central and Eastern North America, Mid-Continent and Gulf Coast Areas", Pacific Engineering and Analysis, El Cerrito, CA.

Singhal, A., Kiremidjian, A.S. (1996) "Method for Probabilistic Evaluation of Seismic Structural Damage", Journal of Structural Engineering, ASCE; 122(12):1459–67.

Somerville, P., Smith, N., Punyamurthula, S., Sun, J. (1997) "Development of Ground Motion Time Histories for Phase 2 of FEMA/SAC Steel Project", SAC-BD/97-04.

Song, J., Ellingwood, B.R. (1999) "Probabilistic Modeling of Steel Moment Frames with Welded Connections", Engineering Journal, AISC; 36(3), 129-137.

Swanson, J.A., Leon, R.T. (2000) "Bolted Steel Connections: Tests on T-Stub Components", Journal of Structural Engineering; 126(1), 50-56.

Tremblay, R. (2002) "Inelastic Seismic Response of Steel Bracing Members", Journal of Constructional Steel Research; 58: 665-701.

Tremblay, R. (2005) "Fundamental Periods of Vibration of Braced Steel Frames for Seismic Design", Earthquake Spectra; 21(3): 833-860.

Uang, C-H., Kiggins, S. (2003) "Reducing Residual Drift of Buckling-Restrained Braced Frames as a Dual System", Proceedings of the International Workshop on Steel and Concrete Composite Constructions, 189-198.

UBC. (1994) "Uniform Building Code", International Conference of Building Officials.

USGS. (2002a) "U.S. Geological Survey Fact Sheet FS-131-02", United States Geological Survey.

USGS. (2002b) "United States Geological Survey, National Seismic Hazard Mapping Project", http://eqint.cr.usgs.gov/eq-men/html/deaggint2002-06.html (03/07).

Vamvatsikos, D., Cornell, C.A. (2002) "Incremental Dynamic Analysis", Earthquake Engineering and Structural Dynamics; 31:491-514.

Veletsos, A.S., Newmark, N.M. (1960) "Effect of Inelastic Behavior on the Response of Simple Systems to Earthquake Motions", Proceedings of the 2nd World Conference on Earthquake Engineering; Japan, 895–912.

Vidic, T., Fajfar, P., Fischinger, M. (1994) "Consistent Inelastic Design Spectra: Strength and Displacement", Earthquake Engineering and Structural Dynamics; 23:502-521.

Wen, Y.K., Ellingwood, B.R., Veneziano, D., Bracci, J. (2003) "Uncertainty Modeling in Earthquake Engineering", MAE Center Project FD-2 Report.

Wen, Y.K., Wu, C.L. (2001) "Uniform Hazard Ground Motions for Mid-America Cities", Earthquake Spectra; 17(2), 359-384.

Whitman, R.V., Anagnos, T., Kircher, C.A., Lagorio, H.J., Lawson, R.S., Schneider, P. (1997) "Development of a National Earthquake Loss Estimation Methodology." Earthquake Spectra, Vol.13, No.4.

WJE. (1996) "Seismic Dynamic Analysis for Buildings." Final manuscript prepared for the U.S. Army Engineering Division by Wiss, Janney, Elstner Associates, Inc., Emeryville, CA.

Yakut, A. (2002) "Evaluation of Capacity Spectrum Method for Various Shapes of Response Spectra", 7th National Conference on Earthquake Engineering, Boston, MA.

Yun, S.Y., Hamburger, R.O., Cornell, C.A., Foutch, D.A. (2002) "Seismic Performance Evaluation for Steel Moment Frames", Journal of Structural Engineering; 128(4), 534-545.